MANY-BODY EFFECTS IN BOSE-EINSTEIN CONDENSATES OF DILUTE ATOMIC GASES

by

BRETT DANIEL ESRY

B.S., Kansas State University, 1993

M.S., University of Colorado, 1996

A thesis submitted to the

Faculty of the Graduate School of the

University of Colorado in partial fulfillment

of the requirements for the degree of

Doctor of Philosophy

Department of Physics

1997

This thesis for the Doctor of Philosophy degree by

Brett Daniel Esry

has been approved for the

Department of

Physics

by

Chris H. Greene

Eric Cornell

Date

The final copy of this thesis has been examined by the signators, and we find that both the content and the form meet acceptable presentation standards of scholarly work in the above mentioned discipline.

Esry, Brett Daniel (Ph. D., Physics)

Many-body Effects in Bose-Einstein Condensates of Dilute Atomic Gases

Thesis directed by Professor Chris H. Greene

The recent experimental achievement of Bose-Einstein condensation in a dilute alkali gas has spurred a great deal of interest among physicists from many fields. Dilute atomic gas experiments are particularly attractive, compared to experiments on the closely related phenomena of superfluidity and superconductivity, because a dilute gas is a weakly interacting system which is far more amenable to theoretical description. Experimentally, dilute gas experiments are advantageous because relatively straightforward and convenient diagnostics exist, using laser excitation of atomic transitions. As a result, dilute atomic gas experiments can be more completely understood using first principles theoretical treatments.

I have adapted the Hartree-Fock, random phase, and configuration interaction approximations to describe systems of interacting bosons, and have shown that such systems can be treated accurately and efficiently within a particle number conserving approximation. In fact, the resulting approximations are remarkably similar to those made in the standard Bogoliubov approach and lead to largely the same equations. A key conclusion is that a system of interacting bosons can be treated in a manner analogous to that used to describe the electronic states of atoms. The hope is that the knowledge and intuition that have been gained from the extensive study of the atomic structure problem will ultimately lead to a deeper understanding of the quantum mechanical states of interacting, trapped atoms.

In the course of this work, several phenomena are studied using both the Hartree-Fock approximation and the random phase approximation. The resulting analysis of the stability criteria for single and double condensates improves on results available in the literature in both cases. The double condensate ground state is explored for various hyperfine and isotopic combinations of rubidium in fully three-dimensional configurations for realistic numbers of atoms. Random phase approximation excitation spectra are also calculated for both single and double

condensates. Many of these predictions have not yet been tested experimentally, nor is there any other theoretical treatment with which comparisons can be made. A systematic study of spatial symmetry breaking at the Hartree-Fock level of approximation for the ground state of double condensates is also presented.

ACKNOWLEDGEMENTS

I would first like to thank my advisor Chris Greene for his guidance and support during my years at JILA. I have gained both greater physics knowledge and a broader perspective on the field under his supervision. This bulk of this work, in fact, grew from his suggestion a little less than two years ago that the atom trapping experiments underway at JILA could be modeled using techniques from atomic structure. Since then, we have come a long way not only in our understanding of systems of interacting bosons but also in our understanding of the subtle differences between our approach and conventional approaches. Many outstanding issues remain on both fronts, however, that I hope can be resolved through our continued collaboration.

Second, I would like to acknowledge the benefits of working in JILA where active atomic physics programs — especially Bose-Einstein condensation — are being pursued. Within Chris' group, I have had many useful conversations with Jim Burke and John Bohn both on two-body scattering and the many-boson problem. From the greater Bose-Einstein condensation effort here at JILA, many people have posed questions or offered suggestions that have deepened my understanding of the field. I would like to mention a few here with whom I have had the most interaction: Jinx Cooper, Eric Cornell, Carl Wieman, Murray Holland, Jason Ensher, Mike Matthews, and Debbie Jin. In particular, I would like to recognize the many constructive criticisms of the manuscript of this thesis by Eric Cornell and Carl Wieman.

Third, I would like to acknowledge initial discussions on this project with Mike Cavagnero and discussions on the basics of some of the methods presented here with Jim Shepard. I want to acknowledge the constructive comments of Peter Zoller on a portion of this manuscript as well as the many helpful suggestions of Leo Radzihovsky on the entire manuscript.

Finally, I would like to acknowledge the financial support of this research by the Department of Energy, Office of Basic Energy Sciences.

CONTENTS

FIGURES

FIGURE

TABLES

TABLE

CHAPTER 1

INTRODUCTION

The field of Bose-Einstein condensation (BEC) in a dilute alkali atom gas has emerged in the last few years as a rich and exciting commingling of several disciplines within physics. While this can often lead to conflict and confusion stemming from disparate viewpoints, it also adds to the level of excitement in the field and the variety of physics discussed. The rise of BEC has been fueled largely by the experimental observation of the phenomena first at JILA by Anderson *et al.* [1], then by Davis *et al.* at MIT [2] and Bradley *et al.* at Rice [3]. Since the flurry of initial observations in the summer of 1995, four more groups have reported observing BEC in an alkali gas [4, 5, 6, 7]. With several concrete experimental observations already published and the prospect of a continuous and growing stream of results emerging for the foreseeable future, theorists with backgrounds in quantum optics, atomic physics, nuclear physics, and condensed matter physics are tackling the problem with a wide variety of theoretical tools. This dissertation develops a theoretical description of a zero temperature system of interacting bosons, combining some of the viewpoints and techniques of atomic and nuclear physics.

Bose-Einstein condensation, a phenomenon in which a substantial fraction of the particles in a system of bosons suddenly and spontaneously occupies the lowest quantum state as the temperature approaches absolute zero, was theoretically predicted 73 years ago [8]. Dilute atomic gas experiments have not only achieved BEC, but have also performed detailed and revealing experiments [9, 10] which have motivated several groups to develop BEC experiments and have guided other groups already actively seeking BEC.

Experiments using a dilute atomic gas to study Bose-Einstein condensation are particularly attractive, compared to experiments on the closely related phenomena of superfluidity

and superconductivity, because a dilute gas is a weakly interacting system which is far more amenable to theoretical description. A dilute gas experiment is also advantageous because relatively straightforward and convenient diagnostics exist, using laser excitation of atomic transitions. As a result, dilute atomic gas experiments can be more completely understood using first principles theoretical treatments. Comparisons between theoretical and experimental results for single species condensates have shown quite good agreement for both ground and excited state properties [11, 12]. The first principles treatment of multiple component condensates can also be expected to provide good agreement with experiment. Multiple component condensates are intrinsically interesting as macroscopically occupied interacting and interpenetrating quantum states and have long been sought in low temperature physics, primarily in the ^{3}He-^{4}He system [13]. Dilute atomic gas experiments have the advantage — in addition to those already mentioned — that nearly all aspects can be independently controlled to some extent. The numbers of particles present of each species, for instance, can be varied as can the amount of overlap between the condensates. The interatomic interactions can also, in principle, be varied with additional external light, magnetic, or RF fields.

Theoretically, the problem of computing the zero temperature ground and excited state properties of an interacting boson system is conventionally carried out within the Bogoliubov approximation [14]. The Bogoliubov approximation abandons the strict number conservation inherent in a many-body Hamiltonian from the outset and introduces both a chemical potential and the "phase" of the condensate. Such analyses proceed *via* field theoretic methods and lead to a definition of the condensate which requires the condensate wave function to be a coherent state in the number of particles. That is, the condensate wave function is a linear combination of many "ordinary" Schrödinger states, each corresponding to a different number of particles. The chemical potential enters the treatment to fix the average number of particles in this mixed state. The condensate phase enters as the variable canonically conjugate to the particle number [15]. When applied to the strongly interacting system of liquid ^{4}He, the standard example of Bose-Einstein condensation prior to the success of dilute atomic gas experiments, this approach

leads to the concepts of phonons, maxons, and rotons [16].

In this work, I take the very different point of view that the system of bosons can be described by a strictly number conserving Schrödinger equation. A number conserving approach has been developed also by Gardiner [17], although from a very different starting point. Mann [18] also briefly investigated a number conserving approach to superfluidity using methods developed for nuclear structure. I take my cue from atomic structure methods such as Hartree-Fock and configuration interaction, and borrow techniques such as the random phase approximation from nuclear structure. Of course, both atomic and nuclear structure are concerned with systems of interacting fermions. My task, then, has been to generalize these methods to bosonic systems. A system of interacting bosons differs from a system of interacting fermions such as an atom or molecule by more than the permutation symmetry requirement. In typical experiments, an atom is essentially always in or near its ground state electronic configuration since the first excitation energy is large compared to background thermal energies. A system of bosons, on the other hand, is almost *never* near its true ground state configuration since background thermal energies are many orders of magnitude larger than the critical temperature of condensation. Nevertheless, experiments can now be performed in which the fractional occupation of the ground state is near unity, making the theoretical description of their zero temperature behavior worthwhile.

In a strictly number conserving theory, there is a fundamental difficulty in defining the "condensate". The calculated ground state is the lowest energy eigenstate of a system with exactly N bodies. As such, it is also an eigenstate of the number operator; in other words, it is a number state. As stated above, however, the standard definition of a condensate implies that the condensate is a superposition of number states for different numbers of particles. To the extent that the condensate is ordinarily defined as a coherent state, one cannot claim to calculate a "condensate wave function" in the number conserving scheme adopted for this dissertation. The methods developed here will, however, provide a means to calculate approximate energy eigenstates that are equally applicable or even more applicable to describe current dilute atomic

gas experiments. Of course, the thermodynamics of the system can, in principle, be wholly described given a complete knowledge of the energy spectrum. In this picture, however, at T=0 there is no "depletion" of the ground state. One can define quantities analogous to the ground state depletion introduced in other theories which roughly measures the strength of interparticle interactions. The difference between unity and the absolute square of the projection of the ground energy eigenstate onto the Hartree-Fock ground state, for instance, is negligible in the weakly interacting limit and large in the strongly interacting limit. For liquid ^{4}He, a strongly interacting system, the ground state depletion is typically reported as being on the order of 90%, meaning that 10% of the atoms are in the zero momentum state (which is not the ground energy eigenstate) at T=0 [16].

A complete construction of the energy spectrum is not a feasible task, given that condensates in the present incarnations of atomic BEC experiments contain anywhere from thousands to millions of atoms. Yet the lower lying excitations, for which the energy eigenfunctions differ little from the Hartree-Fock solution, can be calculated. Approaches such as the random phase approximation (which I develop here) and the conventional Bogoliubov transformation describe precisely these types of excitations. Both employ the familiar physical notion that approximately reduces a complex multidimensional problem to a set of uncoupled harmonic oscillators. The approximation of hopelessly complex systems by uncoupled oscillators has a long and distinguished history. It is used routinely to describe small oscillations in classical systems. The classical normal modes form the basis for classifying and analyzing nuclear vibrations in polyatomic molecules. A phonon or a photon can be regarded as an excitation quantum of a single normal mode in a system of noninteracting harmonic oscillators. The major reason for the proliferation of this approach is that it is usually the most sophisticated approximation that can be solved exactly.

Despite the relative simplicity of the decoupled oscillator approach, the resulting equations are not trivial to solve for atoms in a trapping potential. Nonetheless, several groups have developed techniques for solving them. The zero temperature Thomas-Fermi or hydrodynamic

model has been developed by Stringari and coworkers [19, 20] and by Griffin and coworkers [21]. Both groups have applied this model to study the ground and excited state properties of trapped atoms. Fliesser *et al.* [22] and Öhberg *et al.* [23] were even able to completely determine the entire excited state spectrum for an anisotropic trap in the hydrodynamic limit. The Thomas-Fermi model has also been applied recently to two component condensates by Ho and Shenoy [13] to determine the ground state density and by Graham and Walls [24] to study the excitations.

Variational treatments of the Gross-Pitaevskii equation have also proven informative in studies of the stability of both one and two component condensates. In particular, one component condensates have been examined by Stoof and coworkers [25, 26], by Zoller and coworkers [27], and by Fetter [28]. Zoller *et al.* also used their variational wave function to study the lowest few excitations [27]. More recently, they have extended their analysis to the ground and low-lying excited states of two component condensates [29].

The Gross-Pitaevskii equation has also been solved numerically by several groups for both isotropic and anisotropic traps. The first group to do so — Edwards, Burnett, Clark, and coworkers [11] — found that the approximate Bogoliubov transformation to a set of uncoupled harmonic oscillators yields excitation frequencies in good agreement with experiment [9]. This same group has also solved the Gross-Pitaevskii equation numerically to examine the stability of the condensate for negative scattering lengths [30] and to examine the spectroscopy of vortices [31]. You *et al.* [32] and Dalfovo *et al.* [20] have also solved the Gross-Pitaevskii equation for the low-lying excitation spectrum.

The mean field approach has also been generalized to finite temperatures and the resulting equations has been solved by several groups. Öhberg *et al.* [33] calculated the ground state properties for temperatures below the critical temperature. Griffin *et al.* [34] and Dodd *et al.* [35] have calculated the excitation spectrum as well as the ground state properties for temperatures below the critical temperature, while Stoof *et al.* [36] and Stringari *et al.* [37] have studied how the mean field affects the critical temperature. A finite temperature mean field

study of the ground state of the two component system has even been conducted by Öhberg and Stenholm [38]. They found evidence for the interesting case of spatial symmetry breaking for a configuration of concentric trapping potentials.

Of course, many aspects of BEC experiments are not described by the Gross-Pitaevskii equation. Holland, Cooper, and coworkers have studied the kinetic evolution of a dilute cloud of alkali atoms from the evaporative cooling stage through the formation of the condensate [39]. Zoller, Gardiner, and coworkers have also actively investigated the kinetic aspects of condensate formation [40]. Other groups — notably Castin *et al.* [41], Javanainen *et al.* [42], and Walls *et al.* [43] — have applied techniques borrowed from quantum optics to describe both the phase of a condensate and the interference of two condensates.

In Chap. 2, I review the conventional procedure for obtaining both the equilibrium solution and the normal modes of a system of interacting bosons. The former is found by solving the Gross-Pitaevskii equation; and the latter, by solving the Bogoliubov normal mode equations. Also in Chap. 2 is a short section dealing with the notation of second quantization needed in later chapters and a short section describing the basic results of the Thomas-Fermi approximation for the ground state of identical, trapped, bosonic atoms.

The next chapter, Chap. 3, develops the number conserving Hartree-Fock and random phase approximations employed throughout this work. Different derivations of each are included to make more clear the differences between and similarities with the more conventional approach in Sec. 2.2. Also included are first quantized derivations of the equations for these approximations that highlight the simplicity of the approximations. In Sec. 3.4, the configuration interaction method is generalized to bosons, and its connection to the random phase approximation is sketched and discussed. The remainder of the chapter is devoted to selected results for isotropic and anisotropic harmonically trapped atoms. Among the results presented is a discussion of the stability of the Hartree-Fock solution and the excitation spectrum in several regimes.

Chap. 4 generalizes the treatment of Chap. 3 to the case in which more than one

species is present in the trap, and obtains Hartree-Fock and random phase approximation equations. One point that may be of particular interest is the resolution of a fundamental question about a factor of two appearing in the interspecies interaction term of the Hartree-Fock equations. Stability issues relevant to the two component system are also addressed. In the second half of the chapter, I show some of the rich varieties of phenomena that can occur in two component systems. A number of these systems are experimentally relevant. In particular, calculations are presented for the Myatt *et al.* [87] experimental configuration, and for a proposed experiment on mixed isotopes of rubidium (*i.e.* with ^{85}Rb and ^{87}Rb) that could be performed with the same apparatus. Other aspects addressed include the ground and excited state properties of a rubidium double condensate in a TOP trap. Finally, Chap. 4 concludes with a discussion of the possibility of spatial symmetry breaking in a two component system.

Chap. 5 provides a brief summary and discusses possible studies for the future.

CHAPTER 2

STANDARD APPROACHES FOR BOSE-EINSTEIN CONDENSATES

This chapter introduces the notation needed in following chapters and explains the conventional method for treating Bose-Einstein condensates. The second-quantized notation presented in Sec. 2.1 can be found in many sources, some of which are Refs. [44, 45, 46, 47, 48]. In addition, the Thomas-Fermi approximation presented in Sec. 2.3 is a simple approximation that has been used quite successfully [19, 22, 49].

The method commonly applied to zero temperature systems of bosons is developed in Sec. 2.2 for arbitrary two-body interactions. It begins with the grand canonical Hamiltonian and makes the Bogoliubov approximation for the boson field operator. This approximation breaks the particle number conserving symmetry. In fact, the solution of the Gross-Pitaevskii equation [Eq. (6) below] can be viewed as a coherent state in the total number of particles in the ground state such that the expectation value of the ground state number operator is N_0. The deviation from this number, however, is nonzero. In other words, $\Delta N_0 = \sqrt{\langle \hat{N}_0^2 \rangle - \langle \hat{N}_0 \rangle^2} \neq 0$. It is precisely this indeterminacy in the number that leads to the concept of the "phase" of the condensate and is, in fact, the variable conjugate to the number. As such, their uncertainties obey a Heisenberg uncertainty principle. The approach I will present in Chap. 3, on the other hand, conserves the number of particles exactly leading to the interpretation of the solution of the Hartree-Fock equation, Eq. (18) or (25), as a number state (or Fock state). Further, in this number conserving approach, there are no physical consequences of the phase of the ground state of the bosonic system, and the expectation value of the ground state number operator is exactly N with no fluctuations. Since a coherent state can be constructed from number states, however, the solution to the Gross-Pitaevskii equation can be constructed from the Hartree-Fock

solutions for different numbers of particles.

2.1 Review of second quantization

In the formalism of second quantization [44], the many-body wave function is transformed from configuration space to occupation number space. This transformation is accomplished *via* the independent particle representation and simplifies the construction of properly symmetrized many-body states within the independent particle approximation. This simplification is especially useful for keeping track of the combinatorial factors arising in the calculation of matrix elements for bosonic systems. Within this independent particle representation, a basis function in a many boson Hilbert space is specified by a set of occupation numbers $\mathbf{n}=\{n_\alpha\}$ where α represents all of the quantum numbers needed to label a single particle state from some single particle basis $\{\psi_\alpha(\mathbf{x})\}$. For instance,

$$|\mathbf{n}\rangle = |n_0, 0, \ldots, 0, n_i, 0, \ldots\rangle \tag{1}$$

is a many boson basis function with n_0 bosons in the 0-*th* single particle state, n_i bosons in the *i-th* single particle state, and no bosons in any other single particle state. It is orthogonal to all other many-body basis states having different sets of occupation numbers, and it is normalized. In other words, $\langle \mathbf{n'} \mid \mathbf{n}\rangle = \delta_{\mathbf{n'},\mathbf{n}}$. An additional consequence of this condition is that states with a different total number of particles are orthogonal. Taken together, all such many-body states form a complete expansion basis which spans the many-body Hilbert space for a given total number of particles. Of course, the sum of occupation numbers for any single many-body basis state necessarily equals the total number of particles, *i.e.* $\sum_i n_i = N$. The above basis state can also be written as

$$|\mathbf{n}\rangle = \frac{(\hat{c}_0^\dagger)^{n_0}}{\sqrt{n_0!}} \frac{(\hat{c}_i^\dagger)^{n_i}}{\sqrt{n_i!}} |0\rangle \, .$$

Here, $|0\rangle$ is the state with no bosons present in any single particle state. The creation, $\hat{c}_\alpha^\dagger$, and annihilation, $\hat{c}_\alpha$, operators create and annihilate a boson in the α-*th* single particle state in the

following sense:

$$\begin{aligned}\hat{c}_\alpha^\dagger \left|\ldots, n_\alpha, \ldots\right\rangle &= \sqrt{n_\alpha + 1}\left|\ldots, n_\alpha + 1, \ldots\right\rangle \\ \hat{c}_\alpha \left|\ldots, n_\alpha, \ldots\right\rangle &= \sqrt{n_\alpha}\left|\ldots, n_\alpha - 1, \ldots\right\rangle .\end{aligned}$$

Further, the $\hat{c}$'s satisfy the boson commutation relations

$$\left[\hat{c}_\alpha, \hat{c}_\beta^\dagger\right] = \delta_{\alpha\beta} \text{ and } \left[\hat{c}_\alpha^\dagger, \hat{c}_\beta^\dagger\right] = [\hat{c}_\alpha, \hat{c}_\beta] = 0.$$

Yet another way to write the basis state in Eq. (1), adopting now the coordinate representation, is

$$\Psi_{\mathbf{n}}(\mathbf{x}_1, \ldots, \mathbf{x}_N) = \sqrt{\frac{n_0! n_i!}{N!}}\, \mathcal{S}\left[\psi_0(\mathbf{x}_1) \cdots \psi_0(\mathbf{x}_{n_0}) \psi_i(\mathbf{x}_{n_0+1}) \cdots \psi_i(\mathbf{x}_N)\right],$$

with $\mathcal{S}$ the symmetrization operator. This form explicitly utilizes the configuration space viewpoint that is more commonly adopted in the context of atomic structure calculations.

The Hamiltonian for a system of bosons interacting *via* two-body forces can be written in second quantization as

$$\hat{H} = \sum_{\alpha\beta} \hat{c}_\alpha^\dagger \left\langle \alpha \left| H_0 \right| \beta \right\rangle \hat{c}_\beta + \frac{1}{2} \sum_{\alpha\beta\gamma\delta} \hat{c}_\alpha^\dagger \hat{c}_\beta^\dagger \left\langle \alpha\beta \left| V \right| \gamma\delta \right\rangle \hat{c}_\delta \hat{c}_\gamma. \tag{2}$$

In this expression, all indices are summed over the complete set of single particle states and

$$\left\langle \alpha \left| H_0 \right| \beta \right\rangle = \int d^3x\; \psi_\alpha^*(\mathbf{x})\, H_0(\mathbf{x})\, \psi_\beta(\mathbf{x})$$

is the matrix element of $H_0(\mathbf{x})$ between single particle orbitals. All one-body operators such as the kinetic energy are included in $H_0(\mathbf{x})$ (see, for example, Eq. (16) in the next chapter). The two particle interaction matrix element in Eq. (2) is given by

$$\left\langle \alpha\beta \right| V \left| \gamma\delta \right\rangle = \int d^3x \int d^3x'\, \psi_\alpha^*(\mathbf{x})\, \psi_\beta^*(\mathbf{x}')\, V(\mathbf{x} - \mathbf{x}')\, \psi_\gamma(\mathbf{x})\, \psi_\delta(\mathbf{x}').$$

The factor of 1/2 preceding the two-body interaction energy in Eq. (2) eliminates double counting of interacting pairs [50, 51]. The $\psi_\alpha(\mathbf{x})$ in these matrix elements are (arbitrary) single particle orbitals that form a complete orthonormal basis:

$$\int d^3x\; \psi_\alpha^*(\mathbf{x})\, \psi_\beta(\mathbf{x}) = \delta_{\alpha\beta}.$$

2.2 Bogoliubov approximation

To better understand the differences and similarities between my formulation of Hartree-Fock and the random phase approximation (RPA) for bosons and the Bogoliubov approach more commonly used for boson systems, I reproduce here the basics of the conventional Bogoliubov derivation for a general two-body interaction. The essence of the Bogoliubov approximation lies in treating the condensate (*i.e.* the ground state configuration) separately from the rest of the system, an approximation justified by the comparatively small occupation of the excited configurations relative to the condensate configuration. In the limit $N\rightarrow\infty$, the Bogoliubov approximation is exact as it is for noninteracting particles in the low temperature limit. For finite interacting systems, the assumption is that the condensate has on the order of N particles while the excited states collectively have on the order of 1 particle. Having made this approximation, an effective Hamiltonian is derived which has a quadratic dependence on excitation — or fluctuation — operators. This quadratic form can be diagonalized through the use of a canonical transformation [44].

Conventional approaches for bosons describe the state of the system in terms of fields rather than sets of occupation numbers [44]. The field operator $\hat{\psi}(\mathbf{x})$ ($\hat{\psi}^\dagger(\mathbf{x})$) is defined as

$$\hat{\psi}(\mathbf{x}) = \sum_\alpha \phi_\alpha(\mathbf{x})\hat{c}_\alpha$$

where $\hat{c}$ ($\hat{c}^\dagger$) is as before and $\phi_\alpha(\mathbf{x})$ is an arbitrary single particle basis function. The field operator $\hat{\psi}(\mathbf{x})$ ($\hat{\psi}^\dagger(\mathbf{x})$) is interpreted as destroying (creating) a particle at a point $\mathbf{x}$. Inverting the above relation and substituting it into Eq. (2) yields the following form for the Hamiltonian in terms of the field operators [44]:

$$\hat{H} = \int d^3x\ \hat{\psi}^\dagger(\mathbf{x})\, H_0(\mathbf{x})\, \hat{\psi}(\mathbf{x}) + \frac{1}{2}\int d^3x \int d^3x'\ \hat{\psi}^\dagger(\mathbf{x})\, \hat{\psi}^\dagger(\mathbf{x}')\, V(\mathbf{x}-\mathbf{x}')\, \hat{\psi}(\mathbf{x})\, \hat{\psi}(\mathbf{x}'). \tag{3}$$

The standard Bogoliubov approach [44] separates the condensate from the excited states in the field operator (and its adjoint),

$$\hat{\psi}(\mathbf{x}) = \phi_0(\mathbf{x})\hat{c}_0 + \sum_{\alpha\neq 0} \phi_\alpha(\mathbf{x})\hat{c}_\alpha,$$

replaces the operators $\hat{c}_0$ ($\hat{c}_0^\dagger$) by the c-number $\sqrt{N_0}$, and collects the sum over excited states into a fluctuation operator $\hat{\varphi}(\mathbf{x})$ ($\hat{\varphi}^\dagger(\mathbf{x})$),

$$\hat{\varphi}(\mathbf{x}) = \sum_{\alpha \neq 0} \phi_\alpha(\mathbf{x}) \hat{c}_\alpha.$$

Physically, this operator annihilates (creates) a particle in a singly excited state at position $\mathbf{x}$ and must be small, in some sense, compared to the condensate wave function in order to justify the expansion of the Hamiltonian only through quadratic terms in $\hat{\varphi}$. The total field operator is then just

$$\hat{\psi}(\mathbf{x}) \approx \sqrt{N_0}\, \phi_0(\mathbf{x}) + \hat{\varphi}(\mathbf{x}). \tag{4}$$

The consequence of this replacement is that the number operator,

$$\begin{aligned} \hat{N} &= \int d^3x\, \hat{\psi}^\dagger(\mathbf{x})\, \hat{\psi}(\mathbf{x}) \\ &= N_0 + \sqrt{N_0} \int d^3x \left(\phi_0^*(\mathbf{x}) \hat{\varphi}(\mathbf{x}) + \hat{\varphi}^\dagger(\mathbf{x}) \phi_0(\mathbf{x}) \right) + \int d^3x\, \hat{\varphi}^\dagger(\mathbf{x})\, \hat{\varphi}(\mathbf{x}), \end{aligned}$$

no longer commutes with the Hamiltonian so that the number of particles is not conserved. This shortcoming can be approximately overcome by instead using the grand canonical Hamiltonian, $\hat{K} = \hat{H} - \mu \hat{N}$ [44]. In this expression, μ is the chemical potential which is chosen to fix the average number of particles. Excitation energies can be computed directly within this approach, but it has recently been pointed out [52] that the fact that the number of particles is not conserved implies the existence of a solution of the normal mode equations with a vanishing excitation energy — the Goldstone mode [14, 54] — that restores the lost symmetry. Such symmetry-restoring modes are common in RPA analyses and arise whenever a continuous symmetry present in the Hamiltonian is broken for any reason in the mean field solution [45, 53, 66].

After the field operator from Eq. (4) is substituted into $\hat{K}$ and terms through $\mathcal{O}(\hat{\varphi}^2)$ are retained, $\hat{K}$ can be diagonalized with the canonical transformation [84, 44]

$$\hat{\varphi}(\mathbf{x}) = \sum_\lambda u_\lambda(\mathbf{x}) \hat{\beta}_\lambda + v_\lambda^*(\mathbf{x}) \hat{\beta}_\lambda^\dagger. \tag{5}$$

The $\hat{\beta}_\lambda$ ($\hat{\beta}^\dagger_\lambda$) are interpreted as annihilation (creation) operators for quasi-particles. Diagonalizing $\hat{K}$ in this approximation is thus equivalent to transforming to a system of non-interacting quasi-particles [see Eq. (50)]. $\hat{K}$ can only be diagonalized, however, provided the condensate wave function $\phi_0(\mathbf{x})$ satisfies the self-consistent equation

$$\left[H_0(\mathbf{x})+N_0\int d^3x'\phi_0^*(\mathbf{x}')V(\mathbf{x}-\mathbf{x}')\phi_0(\mathbf{x}')\right]\phi_0(\mathbf{x})=\mu\phi_0(\mathbf{x}). \tag{6}$$

This condition eliminates terms linear in $\hat{\varphi}(\mathbf{x})$ from $\hat{K}$ defining its minimum with respect to small fluctuations. Equation 6 is known as the nonlinear Schrödinger equation or the Gross-Pitaevskii equation [55]. Given the interpretation of $\hat{\varphi}(\mathbf{x})$, it is evident that the elimination of linear terms in $\hat{\varphi}$ from $\hat{K}$ builds single particle excitations into the condensate wave function. Keeping terms through $\mathcal{O}(\hat{\varphi}^2)$ in $\hat{K}$ allows for only single and double excitations of the system state ket. In the next chapter, I will present a number conserving theory that includes much the same physics, but which starts from a very different point of view. For instance, the Hartree-Fock approximation (see Sec. 3.1) includes single particle excitations and results in an equation similar to Eq. (6). The RPA (see Sec. 3.3) encompasses essentially the same physics of double excitations as the expansion of $\hat{K}$ to second order in $\hat{\varphi}$.

After the Bogoliubov transformation, the grand canonical Hamiltonian takes the simple form

$$\hat{K} = E_0 - \mu N_0 - \sum_\lambda \hbar\Omega_\lambda \int d^3x\, v_\lambda^*(\mathbf{x})v_\lambda(\mathbf{x}) + \sum_\lambda \hbar\Omega_\lambda \hat{\beta}^\dagger_\lambda\hat{\beta}_\lambda \tag{7}$$

provided $u_\lambda(\mathbf{x})$ and $v_\lambda(\mathbf{x})$ satisfy the normal mode equations

$$\begin{aligned}
&\left[H_0(\mathbf{x}) - \mu + N_0\int d^3x'\,\phi_0^*(\mathbf{x}')\,V(\mathbf{x}-\mathbf{x}')\,\phi_0(\mathbf{x}')\right]u_\lambda(\mathbf{x}) + \\
&\qquad N_0\int d^3x'\,\phi_0^*(\mathbf{x}')\,V(\mathbf{x}-\mathbf{x}')\,u_\lambda(\mathbf{x}')\;\phi_0(\mathbf{x}) + \\
&\qquad N_0\int d^3x'\,\phi_0(\mathbf{x}')\,V(\mathbf{x}-\mathbf{x}')\,v_\lambda(\mathbf{x}')\;\phi_0(\mathbf{x}) = \hbar\Omega_\lambda u_\lambda(\mathbf{x}) \\
&\left[H_0(\mathbf{x}) - \mu + N_0\int d^3x'\,\phi_0^*(\mathbf{x}')\,V(\mathbf{x}-\mathbf{x}')\,\phi_0(\mathbf{x}')\right]v_\lambda(\mathbf{x}) + \\
&\qquad N_0\int d^3x'\,\phi_0(\mathbf{x}')\,V(\mathbf{x}-\mathbf{x}')\,v_\lambda(\mathbf{x}')\;\phi_0^*(\mathbf{x}) + \\
&\qquad N_0\int d^3x'\,\phi_0^*(\mathbf{x}')\,V(\mathbf{x}-\mathbf{x}')\,u_\lambda(\mathbf{x}')\;\phi_0^*(\mathbf{x}) = -\hbar\Omega_\lambda v_\lambda(\mathbf{x}).
\end{aligned} \tag{8}$$

In these equations, $\hbar\Omega_\lambda$ is the excitation energy, and the solutions $u_\lambda(\mathbf{x})$ and $v_\lambda(\mathbf{x})$ are normalized as

$$\int d^3x\, u^*_{\lambda'}(\mathbf{x})u_\lambda(\mathbf{x}) - v^*_{\lambda'}(\mathbf{x})v_\lambda(\mathbf{x}) = \delta_{\lambda'\lambda}$$

in order to preserve the bosonic commutation relations of $\hat{\beta}$ and $\hat{\varphi}$.

The normal mode equations can be additionally transformed into algebraic eigenvalue equations by expanding $u(\mathbf{x})$ and $v(\mathbf{x})$ on a single particle basis. Specifically,

$$\begin{aligned} u_\lambda(\mathbf{x}) &= \sum_{p\neq 0} U_{\lambda p}\phi_p(\mathbf{x}) \\ v_\lambda(\mathbf{x}) &= \sum_{p\neq 0} V_{\lambda p}\phi_p(\mathbf{x}). \end{aligned}$$

A convenient and physical choice for the single particle basis is the set of states that satisfy

$$H_0(\mathbf{x})\phi_i(\mathbf{x}) + \frac{N_0}{2}\left[\int d^3x'\, \phi^*_0(\mathbf{x}')\, V(\mathbf{x}-\mathbf{x}')\, \phi_0(\mathbf{x}')\, \phi_i(\mathbf{x}) + \int d^3x'\, \phi^*_0(\mathbf{x}')\, V(\mathbf{x}-\mathbf{x}')\, \phi_i(\mathbf{x}')\, \phi_0(\mathbf{x})\right] = \epsilon_i\phi_i(\mathbf{x}).$$

where $\epsilon_0{=}\mu$. This basis is physically sensible since it includes the mean field effects of the condensate. Using such a basis to solve the normal mode equations usually requires fewer — often far fewer — states than would be needed if $u_\lambda(\mathbf{x})$ and $v_\lambda(\mathbf{x})$ were expanded in terms of a harmonic oscillator basis as is one common method of solution [11].

$$\begin{aligned} \frac{N_0}{2}\sum_{p\neq 0}\left[\, U_{\lambda p}\left\langle q0\left|\overline{V}\right|p0\right\rangle + V_{\lambda p}\left\langle qp\left|\overline{V}\right|00\right\rangle\right] + (\epsilon_q-\mu)\, U_{\lambda q} &= \hbar\Omega_\lambda\, U_{\lambda q} \\ \frac{N_0}{2}\sum_{p\neq 0}\left[\, U_{\lambda p}\left\langle qp\left|\overline{V}\right|00\right\rangle + V_{\lambda p}\left\langle q0\left|\overline{V}\right|p0\right\rangle\right] + (\epsilon_q-\mu)\, V_{\lambda q} &= -\hbar\Omega_\lambda\, V_{\lambda q}. \end{aligned} \tag{9}$$

The shift in the ground state energy [see Eq. (7)] can now be written in the $\{\phi_i(\mathbf{x})\}$ representation as

$$\sum_\lambda \hbar\Omega_\lambda \int d^3x\, v^*_\lambda(\mathbf{x})v_\lambda(\mathbf{x}) = \sum_\lambda \hbar\Omega_\lambda \sum_{p\neq 0} |V_{\lambda p}|^2\,. \tag{10}$$

2.3 Thomas-Fermi approximation

The Thomas-Fermi approximation greatly simplifies the solution of the Gross-Pitaevskii equation, Eq. (6), by reducing it to an algebraic one. This reduction is accomplished by neglecting the kinetic energy and retaining the trapping potential and the mean field interaction. It follows that this approximation is valid in the limit that the mean field term dominates.

To make the approximation more concrete, consider the Gross-Pitaevskii equation in the shape independent approximation (see Sec. 3.5) scaled by the harmonic oscillator energy, $\hbar\omega$, and length, $\beta{=}\sqrt{\hbar/m\omega}$:

$$\left[-\frac{1}{2}\tilde{\nabla}^2+\frac{1}{2}\left(\tilde{\omega}_x^2\tilde{x}^2+\tilde{\omega}_y^2\tilde{y}^2+\tilde{\omega}_z^2\tilde{z}^2\right)+\alpha\left|\phi_0(\tilde{\mathbf{x}})\right|^2\right]\phi_0(\tilde{\mathbf{x}})=\tilde{\mu}\phi_0(\tilde{\mathbf{x}}). \tag{11}$$

In this expression, $\alpha{=}4\pi N_0\tilde{a}_{sc}$ with a_{sc} the scattering length, and the tildes denote rescaled quantities, *i.e.* $\mu{=}\hbar\omega\tilde{\mu}$ and $\mathbf{x}{=}\beta\tilde{\mathbf{x}}$. The reference frequency ω entering the scaling is chosen to be some convenient value. Note that the two-body scattering information and the number dependence enter only through the parameter α. The validity condition for the Thomas-Fermi approximation can now be written as $\alpha{\gg}1$. This condition must be supplemented by the caveat that the local kinetic energy (which has been neglected) should also be small compared to the mean field energy.

For simplicity, I consider an isotropic oscillator. The method can, of course, be applied to anisotropic systems and even multiple component systems [13, 24], but the additional algebraic complication is not particularly enlightening. So, neglecting kinetic energy, Eq. 11 can be rearranged to give the Thomas-Fermi approximation to the probability density,

$$\left|\phi_0(\mathbf{x})\right|^2=\begin{cases}\left(\tilde{\mu}-\frac{1}{2}\tilde{r}^2\right)/\alpha, & 0\le\tilde{r}\le\sqrt{2\tilde{\mu}}\\ 0, & \tilde{r}>\sqrt{2\tilde{\mu}}\end{cases} \tag{12}$$

The limit in $\tilde{r}$ arises from the requirement that the probability density be a non-negative number. It is in the region of this upper limit in $\tilde{r}$ that the Thomas-Fermi approximation will break down since the local kinetic energy dominates the mean field. In practice, however, this failure is not

a significant drawback. The remaining free parameter, $\tilde{\mu}$, is chosen so that the wave function is normalized. The result is

$$\tilde{\mu} = \left(\frac{15\alpha}{4\sqrt{2}}\right)^{\frac{2}{5}} \tag{13}$$

The Thomas-Fermi approximation for bosons in a trap has a simple interpretation in the sense that the bosons can be imagined to be a "liquid" filling the bottom of the trap up to the level $\tilde{\mu}$. The resulting effective potential — the combination of the trapping potential and the mean field — is thus a flat bottomed version of the potential. The analogy to liquid drops has been pursued with considerable success to calculate, for instance, the low-lying excitation spectrum of a condensate [19, 22]. An especially attractive feature of the approximation is that nearly all quantities can be calculated analytically, which yields useful scaling laws in the limit $\alpha \gg 1$.

CHAPTER 3

ZERO TEMPERATURE THEORY FOR SINGLE COMPONENT CONDENSATES

The recent experimental observations of Bose-Einstein condensates [1, 2, 3, 4, 5, 6, 7] and the successful experiments [9, 10] on condensate properties have increased the desirability of a comprehensive theoretical formulation. Several groups [11, 19, 32, 52, 56, 57, 58, 59] have made progress in this direction by adopting the standard Bogoliubov approach for many interacting bosons [44]. This is an approach that treats the condensate as a reservoir which can exchange both particles and energy with the rest of the system. This approximation, however, does not inherently conserve the number of particles, although the chemical potential μ can be introduced to enforce this condition on average.

In order to connect to many-body approaches such as those used in atomic structure calculations, I formulate the theory for trapped atoms using standard Schrödinger quantum mechanics [60]. This, of course, automatically conserves the number of interacting particles. This methodology pursues the analogy of atoms in a trap to electrons trapped by the Coulomb field of a nucleus. A fundamental difference between these cases is, of course, the character of the particles: the atoms experimentally studied in such traps to date are bosons, whose exchange properties differ simply yet profoundly from the fermionic electrons in an atom. This viewpoint allows concepts such as quasi-particles to be discussed in terms of *configurations* and *orbitals*, and permits the language of condensed matter physics to be linked to that of atomic physics and nuclear physics. As I will show below, this formulation leads to results which are *largely* equivalent to those obtained in the Bogoliubov approach, aside from very minor differences that should be unimportant for current experimental conditions. A key byproduct of this approach is that it permits the application of standard tools of atomic theory, such as configuration

interaction [61], which transcend Hartree-Fock theory in order to describe new phenomena such as multiple particle excitations that are not encompassed by Bogoliubov theory.

3.1 Hartree-Fock approximation

With the Hartree-Fock approximation, one seeks the best independent particle wave function given the occupancy of each single particle orbital. In the present case, I concentrate on the ground state of a system of bosons (*i.e.* all particles occupy the lowest orbital) although more general occupation schemes can be used. In such cases, however, basic properties of the single particle states such as orthogonality must be explicitly addressed. Considerable freedom exists in the choice of a single particle basis set. This flexibility is used to derive an equation that determines those single particle states which variationally minimize the total energy. In other words, the Hamiltonian is approximately diagonalized, including as much of the interparticle interactions as is possible given that the trial wave function is constrained to independent particle form.

The Hartree-Fock equation can be derived from either first- or second-quantized formalisms. Each provides separate and useful insights. The first-quantized derivation provides a simple picture that can be easily understood in terms of basic quantum mechanics. The second-quantized derivation, on the other hand, provides greater insight into the physics included in the trial wave function. Both approaches, of course, yield identical results and will be described below.

3.1.1 First-quantized approach. The derivation here is first-quantized in that the many-body wave function is expressed directly in terms of spatial coordinates, although it is written in the independent particle approximation. In many respects, the first-quantized derivation presented here parallels the first-quantized derivation of the Hartree-Fock equations for fermions (see Cowan [61], for example). The *ansatz* for the total ground state wave function Φ in the independent particle approximation is expressed as

$$\Phi(\mathbf{x_1}, \ldots, \mathbf{x_N}) \approx \psi_0(\mathbf{x_1}) \ldots \psi_0(\mathbf{x_N}) \tag{14}$$

where the single particle orbitals ψ_0 are to be determined. The spin part of the wave function is similarly a product of the spin kets for each atom and otherwise does not enter the calculation. The equation for ψ_0 is obtained by applying the variational principle to the Hamiltonian

$$H = \sum_{i=1}^{N} H_0(\mathbf{x}_i) + \sum_{i<j}^{N} V(\mathbf{x}_i - \mathbf{x}_j). \tag{15}$$

In this expression, the one particle operator $H_0(\mathbf{x})$ includes any external trapping potential $V_{\rm ext}(\mathbf{x})$ and is given by

$$H_0(\mathbf{x}) = -\frac{\hbar^2}{2m}\nabla^2 + V_{\rm ext}(\mathbf{x}) \tag{16}$$

For typical magnetic traps $V_{\rm ext}(\mathbf{x})$ is a cylindrically symmetric harmonic trapping potential; in atomic structure calculations, $V_{\rm ext}(\mathbf{x})$ is the electron-nucleus Coulomb interaction. The two particle operator $V(\mathbf{x}_i - \mathbf{x}_j)$ in Eq. (15) is the particle-particle interaction. In the case of neutral trapped atoms, it is a potential with a strongly repulsive core at distances of roughly a few atomic units, a well at a few tens of atomic units, and a van der Waals tail. In atomic structure calculations, the particle-particle interaction is just the electronic Coulomb repulsion.

Given the trial wave function in Eq. (14), the expectation value of the Hamiltonian [Eq. (15)] — the total energy for this system of N particles — is then

$$E_0^{\rm HF} = N\frac{\langle \psi_0 \,|H_0|\, \psi_0\rangle}{\langle \psi_0 \mid \psi_0\rangle} + \frac{N(N-1)}{2}\frac{\langle \psi_0\psi_0 \,|V|\, \psi_0\psi_0\rangle}{\langle \psi_0 \mid \psi_0\rangle^2}. \tag{17}$$

This notation for the one particle matrix element is interpreted as

$$\langle \psi_0 \,|H_0|\, \psi_0\rangle = \int d^3x\; \psi_0^*(\mathbf{x})\, H_0(\mathbf{x})\, \psi_0(\mathbf{x})$$

while the notation for the two particle matrix element implies a double integral over all coordinates of two particles:

$$\langle \psi_0\psi_0 \,|V|\, \psi_0\psi_0\rangle = \int d^3x \int d^3x'\, \psi_0^*(\mathbf{x})\, \psi_0^*(\mathbf{x}')\, V(\mathbf{x}-\mathbf{x}')\, \psi_0(\mathbf{x})\, \psi_0(\mathbf{x}').$$

Taking the variation of E with respect to ψ_0^* gives, after some algebra,

$$\delta E_0^{\rm HF} = N\frac{\langle \delta\psi_0 \,|H_0|\, \psi_0\rangle}{\langle \psi_0 \mid \psi_0\rangle} + \frac{N(N-1)}{2}\frac{\langle \delta\psi_0\psi_0 + \psi_0\delta\psi_0 \,|V|\, \psi_0\psi_0\rangle}{\langle \psi_0 \mid \psi_0\rangle^2}$$

$$- N \left(\frac{E_0^{\rm HF}}{N} - \frac{(N-1)}{2} \frac{\langle \psi_0 \psi_0 \left| V \right| \psi_0 \psi_0 \rangle}{\langle \psi_0 \mid \psi_0 \rangle^2} \right) \frac{\langle \delta\psi_0 \mid \psi_0 \rangle}{\langle \psi_0 \mid \psi_0 \rangle}.$$

If arbitrary variations $\delta\psi_0^*$ are allowed, the first variation $\delta E_0^{\rm HF}$=0 subject to $\langle \psi_0 \mid \psi_0 \rangle$=1 is satisfied when

$$\left[H_0(\mathbf{x}) + (N-1) \int d^3x' \, \psi_0^*(\mathbf{x}') \, V(\mathbf{x}-\mathbf{x}') \, \psi_0(\mathbf{x}') \right] \psi_0(\mathbf{x}) = \varepsilon_0 \psi_0(\mathbf{x}). \tag{18}$$

For a system of only one boson, Eq. (18) reduces to the appropriate noninteracting Schrödinger equation. Moreover, this equation is the number conserving analogue of the nonlinear Schrödinger equation for the condensate wave function (see Ref. [44, 55, 62] and Eq. (6) in Sec. 2.2). The eigenenergy ε_0 in Eq. (18) is defined as

$$\varepsilon_0 = \frac{E_0^{\rm HF}}{N} + \frac{(N-1)}{2} \langle \psi_0 \psi_0 \left| V \right| \psi_0 \psi_0 \rangle . \tag{19}$$

Being the eigenvalue of the equation for the ground state orbital, ε_0 is the ground state orbital energy. Interestingly, ε_0 obeys Koopmans theorem [63] as do the orbital energies for fermions. The statement of Koopmans theorem applicable to a system of bosons is that the orbital energy represents the difference between the Hartree-Fock ground state energy for N particles and $N-1$ particles provided the difference between the ground state orbital for N particles and the ground state orbital for $N-1$ orbitals can be neglected. In the limit $N \gg 1$, the latter approximation is physically reasonable given the order N^{-1} effect of a single additional particle on the orbital. In fact, this approximation holds quite well for as few as 10 particles. From the above statement, it can also be recognized that Koopmans theorem is essentially a statement of the definition of the chemical potential encountered in the Bogoliubov approach (see Sec. 2.2).

From Eq. (19), the total energy for a system of N particles can be written as

$$E_0^{\rm HF} = N \langle \psi_0 \left| H_0 \right| \psi_0 \rangle + \frac{N(N-1)}{2} \langle \psi_0 \psi_0 \left| V \right| \psi_0 \psi_0 \rangle .$$

The energy difference between a system with N particles and one with $N-1$ is thus

$$E_0^{\rm HF}(N) - E_0^{\rm HF}(N-1) = \langle \psi_0 \left| H_0 \right| \psi_0 \rangle + (N-1) \langle \psi_0 \psi_0 \left| V \right| \psi_0 \psi_0 \rangle = \varepsilon_0.$$

Thus, Koopmans theorem is also satisfied by bosons.

3.1.2 Second-quantized approach. To the extent that the potential energy of the system is described completely by a pairwise sum of two-body interactions and a sum of one-body trap potentials — an assumption made throughout this work — Eq. (2) is an exact representation of the Hamiltonian for *any* choice of single particle basis. Only when the composite nature of the particles is taken into account do three or more particle interactions enter. In this case, the Hamiltonian can again be made exact by adding the appropriate multi-particle generalization of the interaction term. These multi-particle interactions are typically weak and of much shorter range than the two-body interactions and, therefore, are usually neglected.

To proceed, I solve the Schrödinger equation variationally, using for a trial function the completely symmetric product wave function

$$\Phi(\mathbf{x}_1, \ldots, \mathbf{x}_N) \approx \phi(\mathbf{x}_1) \cdots \phi(\mathbf{x}_N) \tag{20}$$

just as in the first-quantized approach of Sec. 3.1.1. The orbital $\phi(\mathbf{x})$ can, in turn, be expanded on a single particle basis $\{\psi_\alpha(\mathbf{x})\}$,

$$\phi(\mathbf{x}) = \mathcal{N}\left[\psi_0(\mathbf{x}) + \sum_{p\neq 0} a_p \psi_p(\mathbf{x})\right]$$

with $\mathcal{N}$ an overall normalization constant. I will choose the single particle basis such that $\psi_0(\mathbf{x})$ alone is sufficient to minimize the total ground state energy.

The first few terms obtained when Eq. (20) is expanded using $\phi(\mathbf{x})$ can be written in second quantization as

$$|\Phi\rangle \approx \mathcal{N}^N\big(1 + \sum_{p\neq 0} a_p \frac{\hat{c}_p^\dagger \hat{c}_0}{\sqrt{N}} + \frac{1}{2}\sum_{p,p'\neq 0} a_p a_{p'} \frac{\hat{c}_p^\dagger \hat{c}_0}{\sqrt{N-1}} \frac{\hat{c}_{p'}^\dagger \hat{c}_0}{\sqrt{N}} + \ldots\big) \left|\Phi_0^{\mathrm{HF}}\right\rangle \tag{21}$$

where $\left|\Phi_0^{\mathrm{HF}}\right\rangle$ is the Hartree-Fock ground state of the system,

$$\left|\Phi_0^{\mathrm{HF}}\right\rangle = \frac{(\hat{c}_0^\dagger)^N}{\sqrt{N!}}|0\rangle = |N, 0, \ldots\rangle$$

or

$$\left\langle \mathbf{x}_1, \ldots, \mathbf{x}_N \right| \left.\Phi_0^{\mathrm{HF}}\right\rangle \quad = \quad \Phi_0^{\mathrm{HF}}(\mathbf{x}_1, \ldots, \mathbf{x}_N)$$

$$= \quad \psi_0(\mathbf{x}_1) \cdots \psi_0(\mathbf{x}_N).$$

Thus, the trial function $|\Phi\rangle$ includes multiple excitations of the Hartree-Fock ground state: the second term of Eq. (21) involves one creation operator $\hat{c}^\dagger$ representing a singly excited state, the third term of Eq. (21) involves two creation operators $\hat{c}^\dagger$ representing a doubly excited state, and so on. One can regard the Hartree-Fock ground state as a first approximation to the ground energy eigenstate of the many boson system, but it is only an approximation since it does not exactly diagonalize the many-body Hamiltonian, Eq. (2). The residual interparticle interaction couples the Hartree-Fock ground and excited states so that the exact ground state can only be represented as a linear combination of all of the Hartree-Fock many-body states. Further, in this dissertation, I will often use the term "condensate" interchangeably with "ground energy eigenstate" even though this does not conform with the standard usage of the term.

The derivation of the Hartree-Fock equation for bosons parallels the more familiar Hartree-Fock derivation for fermions [44, 45, 53, 61]. The procedure requires variations of the total energy E to be stationary with respect to single particle excitations. This requirement is equivalent to minimizing E, the expectation value of the Hamiltonian Eq. (2) for the trial wave function Eq. (21), with respect to the coefficients a_p,

$$\delta E = \frac{\delta}{\delta a_p} \frac{\left\langle \Phi \left| \hat{H} \right| \Phi \right\rangle}{\langle \Phi \mid \Phi \rangle} \bigg|_{a_p=0} = 0,$$

which leads to the condition

$$\left\langle \Phi_0^{\mathrm{HF}} \left| \frac{\hat{c}_0^\dagger \hat{c}_p}{\sqrt{N}} \hat{H} \right| \Phi_0^{\mathrm{HF}} \right\rangle = \left\langle \Phi_p^{\mathrm{HF}} \left| \hat{H} \right| \Phi_0^{\mathrm{HF}} \right\rangle = 0 \tag{22}$$

also known as Brillouin's theorem [64]. This condition ensures that the Hartree-Fock basis is chosen so that the Hamiltonian cannot produce single particle excitations of $\left|\Phi_0^{\mathrm{HF}}\right\rangle$ to first order. Also, $\left|\Phi_0^{\mathrm{HF}}\right\rangle$ is variationally the best completely symmetric, single configuration, independent particle, ground state wave function as was shown previously in Sec. 3.1.1. The analogous and possibly more familiar statement for a fermion system is that the Hartree-Fock ground

state is the best single Slater determinant wave function. Equation (22) leads to the following "quasi-Hartree-Fock" equation:

$$H_0(\mathbf{x})\,\psi_\alpha(\mathbf{x}) + \frac{N-1}{2}\Bigg[\int d^3x'\,\psi_0^*(\mathbf{x}')\,V(\mathbf{x}-\mathbf{x}')\,\psi_0(\mathbf{x}')\,\psi_\alpha(\mathbf{x}) + \int d^3x'\,\psi_0^*(\mathbf{x}')\,V(\mathbf{x}-\mathbf{x}')\,\psi_\alpha(\mathbf{x}')\,\psi_0(\mathbf{x})\Bigg] = \varepsilon_\alpha\psi_\alpha(\mathbf{x}). \tag{23}$$

This equation holds not only for the ground state orbital but also for excited state orbitals. I label this a *quasi*-Hartree-Fock equation for the *excited* orbitals since it does not yield the best completely symmetric, single configuration, independent particle wave function for a singly excited state. A Hartree-Fock treatment of a singly excited state leads to an equation for the excited orbitals in which the mean field is larger than the mean field in Eq. (23) by a factor of two. Neglecting the effects of the excited orbital mean field on the ground state orbital, the true Hartree-Fock equations consist of Eq. (23) for the ground state, α=0, plus

$$H_0(\mathbf{x})\,\psi_\alpha(\mathbf{x}) + (N-1)\Bigg[\int d^3x'\,\psi_0^*(\mathbf{x}')\,V(\mathbf{x}-\mathbf{x}')\,\psi_0(\mathbf{x}')\,\psi_\alpha(\mathbf{x}) + \int d^3x'\,\psi_0^*(\mathbf{x}')\,V(\mathbf{x}-\mathbf{x}')\,\psi_\alpha(\mathbf{x}')\,\psi_0(\mathbf{x})\Bigg] = \varepsilon_\alpha\psi_\alpha(\mathbf{x}) + \lambda_\alpha\psi_0(\mathbf{x}) \tag{24}$$

for the excited states, $\alpha\neq0$. This treatment is, in fact, the boson equivalent of the "frozen core" approximation [61]. The additional term on the right hand side ensures orthogonality of the excited state orbitals to the ground state orbital, with λ_α the associated Lagrange multiplier. The first term in the square brackets in either equation is the direct contribution to the interaction energy and behaves as a local potential arising from the mean field due to the ground state orbital. The second term is the nonlocal exchange contribution to the interaction energy. Thus, the ground state orbital in both approximations satisfies the same Hartree-Fock equation that simplifies to [*c.f.* Eq. (18)],

$$\left[H_0(\mathbf{x}) + (N-1)\int d^3x'\,\psi_0^*(\mathbf{x}')\,V(\mathbf{x}-\mathbf{x}')\,\psi_0(\mathbf{x}')\right]\psi_0(\mathbf{x}) = \varepsilon_0\psi_0(\mathbf{x}). \tag{25}$$

The overall normalization of the Hartree-Fock ground state is again ensured by normalizing $\psi_0(\mathbf{x})$ to unity.

As noted in Sec. 3.1.1, the total energy of the ground state $E_0^{\rm HF}$ in the Hartree-Fock approximation is not $N\varepsilon_0$ as might be expected but rather

$$\begin{aligned} E_0^{\rm HF} &= \left\langle \Phi_0^{\rm HF} \left| \hat{H} \right| \Phi_0^{\rm HF} \right\rangle \\ &= N\varepsilon_0 - \frac{N(N-1)}{2} \left\langle 00 \left| V \right| 00 \right\rangle . \end{aligned} \tag{26}$$

The "additional" term can be understood as eliminating the double counting of pairs of particles included in $N\varepsilon_0$. In other words, $N\varepsilon_0$ includes the energy for each particle interacting with every other particle and so counts the contribution from a given pair twice. Double counting considerations arise for any system of particles interacting by pairwise forces [50, 51]. Similarly, the single excitation energy in the quasi-Hartree-Fock approximation (QHF) is not simply the difference of quasi-Hartree-Fock single particle energies $\varepsilon_p - \varepsilon_0$, but rather

$$\begin{aligned} E_p^{\rm QHF} - E_0^{\rm HF} &= \left\langle \Phi_p^{\rm QHF} \left| \hat{H} \right| \Phi_p^{\rm QHF} \right\rangle - \left\langle \Phi_0^{\rm HF} \left| \hat{H} \right| \Phi_0^{\rm HF} \right\rangle \\ &= (\varepsilon_p - \varepsilon_0) + \frac{N-1}{2} \left\langle p0 \left| \overline{V} \right| p0 \right\rangle \end{aligned} \tag{27}$$

since $E_0^{\rm QHF} = E_0^{\rm HF}$. In the Hartree-Fock approximation, however, the single excitation energy is precisely the difference of the orbital energies —

$$E_p^{\rm HF} - E_0^{\rm HF} = \varepsilon_p - \varepsilon_0 .$$

In Eq. (27), I have used the shorthand notation

$$\left\langle q0 \left| \overline{V} \right| p0 \right\rangle \equiv \left\langle q0 \left| V \right| p0 \right\rangle + \left\langle q0 \left| V \right| 0p \right\rangle \tag{28}$$

for the direct plus exchange contributions to the interparticle interaction matrix element. Note that the plus sign in this expression results from the requirement of symmetry upon permutation of the identical bosons (the requirement of antisymmetry for fermions would yield a minus sign instead).

3.1.3 Time-dependent Hartree-Fock equation. In some cases it is useful to consider the time evolution of a Hartree-Fock state. For instance, the expansion of a condensate

after it has been released from a trap has been modeled in this way using the time-dependent nonlinear Schrödinger equation [65]. In a first-quantized approach, the time-dependent Hartree-Fock equation can be obtained from the time-dependent Schrödinger equation for the system

$$\left(H - i\hbar\frac{\partial}{\partial t}\right)\Phi\left(\mathbf{x}_1,\ldots,\mathbf{x}_N,t\right) = 0 \tag{29}$$

using the *ansatz*

$$\Phi\left(\mathbf{x}_1,\ldots,\mathbf{x}_N,t\right) \approx \phi(\mathbf{x}_1,t)\cdots\phi(\mathbf{x}_N,t). \tag{30}$$

Projecting out the coordinates of all but one particle, say the Nth one, gives

$$\left(H_0(\mathbf{x}_N) - i\hbar\frac{\partial}{\partial t} + (N-1)\int d^3x_1\,\phi^*(\mathbf{x}_1,t)\,V(\mathbf{x}_1-\mathbf{x}_N)\,\phi(\mathbf{x}_1,t)\right)\phi(\mathbf{x}_N,t) = F(t)\,\phi(\mathbf{x}_N,t). \tag{31}$$

The time-dependent coefficient $F(t)$ is given by

$$F(t) = -\left(N-1\right)\left\langle\phi(t)\left|H_0 - i\hbar\frac{\partial}{\partial t}\right|\phi(t)\right\rangle - \frac{\left(N-1\right)\left(N-2\right)}{2}\left\langle\phi(t)\phi(t)\left|V\right|\phi(t)\phi(t)\right\rangle$$

which can be simplified using the Schrödinger equation, Eq. (29), to write the total energy per particle E/N as

$$\begin{aligned}\frac{E}{N} &= \left\langle\phi(t)\left|H_0\right|\phi(t)\right\rangle + \frac{N-1}{2}\left\langle\phi(t)\phi(t)\left|V\right|\phi(t)\phi(t)\right\rangle \\ &= \left\langle\phi(t)\left|i\hbar\frac{\partial}{\partial t}\right|\phi(t)\right\rangle.\end{aligned}$$

The simplified expression for $F(t)$ is then

$$F(t) = \frac{N-1}{2}\left\langle\phi(t)\phi(t)\left|V\right|\phi(t)\phi(t)\right\rangle.$$

In any case, the time-dependent orbital can be redefined such that the right hand side of Eq. (31) vanishes. This is accomplished by factoring out the phase

$$\varphi(t) = \int^t dt' F(t'),$$

i.e. $\phi(\mathbf{x},t)$=$\exp(\frac{i}{\hbar}\varphi(t))\phi'(\mathbf{x},t)$, and writing a new time-dependent Hartree-Fock equation for $\phi'(\mathbf{x},t)$.

The time-independent Hartree-Fock equation is recovered by writing a stationary solution as

$$\phi(\mathbf{x}, t) = e^{-\frac{i}{\hbar}\frac{E}{N}t}\psi(\mathbf{x}).$$

In deriving the equation for $\psi(\mathbf{x})$, one is again led to define an orbital energy as in Eq. (19). This form for the stationary solution is consistent with the *ansatz* for the full wave function [Eq. (30)] as it leads to the phase evolving in time according to the total energy of the system. That is,

$$\Phi\left(\mathbf{x}_1, \ldots, \mathbf{x}_N\right) = e^{-\frac{i}{\hbar}Et}\psi(\mathbf{x}_1)\cdots\psi(\mathbf{x}_N),$$

c.f. Eq. (30). Thus, it is clear that it is the total energy, or equivalently the total energy per particle, that is conserved during the time-evolution rather than the orbital energy.

3.2 Stability of the Hartree-Fock solution

In Sec. 3.1, I constructed an energy functional corresponding to the total energy of the system in a parameter space constrained by the independent particle approximation and the requisite symmetry of the trial wave function. The Hartree-Fock solution is the set of parameters which minimizes this functional, and the Hartree-Fock energy is its minimum value. The most direct route to investigate the stability of the Hartree-Fock solution is to expand the energy functional to second order about the extremum in parameter space defined by the Hartree-Fock solution, recalling that the first order terms are guaranteed to vanish by the Hartree-Fock condition. This procedure allows one to obtain the curvature of the energy functional in the neighborhood of the Hartree-Fock solution, revealing whether the Hartree-Fock solution is stable, metastable, or unstable. In the latter case, the only information gained is that the Hartree-Fock solution is not a local minimum of the energy. Physically, an unstable Hartree-Fock solution is simply a poor approximation to the true ground state wave function.

Specifically, I repeat the second-quantized derivation of Sec. 3.1.2, now including terms up to *second* order in a_p — that is, double excitations of the Hartree-Fock ground state. In addition to being the next largest nonvanishing terms in the energy functional, the second order

terms lead to equations that are linear and thus readily solvable. Higher order terms, on the other hand, lead to systems of nonlinear equations. This truncation to second order implies, for instance, that Hamiltonian matrix elements between doubly excited states are neglected as are the matrix elements between singly and double excited states. Explicitly, the energy functional in the Hartree-Fock or quasi-Hartree-Fock basis to second order in a_p is

$$E_n = \frac{E_0 + \sum_{pp'\neq 0}\left[\frac{1}{2}a^*_{pn}a^*_{p'n}C^*_{pp'} + a^*_{pn}a_{p'n}\left(E_0\delta_{pp'}+B_{pp'}\right) + \frac{1}{2}a_{pn}a_{p'n}C_{pp'}\right]}{1+\sum_{pp'\neq 0}a^*_{pn}a_{p'n}}. \tag{32}$$

The coupling that is retained links the ground state to doubly excited states and singly excited states to singly excited states through the coefficients $B_{pp'}$ and $C_{pp'}$ (written in the quasi-Hartree-Fock basis):

$$\begin{aligned} B_{pp'} &= \frac{N-1}{2}\left\langle p0\left|\overline{V}\right|p'0\right\rangle + \left(\varepsilon_p-\varepsilon_0\right)\delta_{pp'} \\ C_{pp'} &= \frac{N-1}{2}\left\langle 00\left|\overline{V}\right|pp'\right\rangle . \end{aligned} \tag{33}$$

Variation of E_n with respect to a^*_{qn} (a_{qn}) leads to the equations

$$\begin{aligned} \sum_{p\neq 0}\left[\, a_{pn}B_{qp} + a^*_{pn}C^*_{qp}\right] &= \hbar\omega_n\, a_{qn} \\ \sum_{p\neq 0}\left[\, a_{pn}C_{qp} + a^*_{pn}B^*_{qp}\right] &= \hbar\omega_n\, a^*_{qn} \end{aligned} \tag{34}$$

where $\hbar\omega_n{=}E_n - E_0$. Diagonalizing this system of equations yields the principal axes of the quadratic energy surface and the curvature along each axis in the eigenvectors and eigenvalues, respectively. It is clear, then, that for the Hartree-Fock solution to be stable all of the eigenvalues must be positive. A negative eigenvalue indicates that the Hartree-Fock extrema is at best a saddle point in the many dimensional parameter space and that lower energies are possible for any deviation along the corresponding principal axis. Rewriting Eq. (34) as

$$E_n = E_0 + \hbar\omega_n$$

makes this clear. A negative frequency indicates that the excited state energy is lower than the energy of the approximate ground state. In this case, the solution assumed to be the ground state clearly is not.

An exactly zero excitation frequency implies that a continuous symmetry present in the many-body Hamiltonian has been broken in the ground state Hartree-Fock solution [45, 66]. It is worth noting that the mode described by Lewenstein and You [52] corresponds to exactly this situation, although they obtained it from the solution of the Bogoliubov normal mode equations, Eq. (8). The symmetry broken there is, of course, particle number conservation and is broken in the derivation of the Gross-Pitaevskii equation.

The stability of the ground state can also be studied variationally using a trial wave function in the expression for the total energy per particle, Eq. (17), [25, 27]. For a harmonic trapping potential, the common choice for the trial wave function is a Gaussian with a variable width, although a more sophisticated trial function has been studied by Fetter [28]. Besides being the exact solution in the noninteracting limit, a Gaussian has the advantage that the energy can be evaluated analytically. It cannot, however, be minimized in the general case analytically. Nonetheless, the variational analysis with a Gaussian trial wave function is much easier to carry out for an arbitrary harmonic trap than the exact solution of the Hartree-Fock equation; and, since it is acceptably accurate for the present purpose, I will devote the remainder of this section to a discussion of its application to the stability of the ground state.

For a system of interacting bosons in a cylindrically symmetric harmonic trap, two parameters are needed after scaling the Hamiltonian Eq. (15) to describe the system: the anisotropy, ω_z/ω_ρ, given by λ; and the interaction strength, $(N-1)a_{sc}/\beta$, given by α. The length scale β is the harmonic oscillator length $\sqrt{\hbar/m\omega_\rho}$. The scaled one-body operator $H_0(\mathbf{x})$ in Eq. (17), expressed in units of $\hbar\omega_\rho$, is then given by

$$H_0(\mathbf{x}) = -\frac{1}{2\xi}\frac{\partial}{\partial\xi}\left(\xi\frac{\partial}{\partial\xi}\right) - \frac{1}{2}\frac{\partial^2}{\partial\eta^2} + \frac{1}{2}\left(\xi^2 + \lambda^2\eta^2\right)$$

where $\rho{=}\beta\xi$ and $z{=}\beta\xi$ are the scaled coordinates. The normalized Gaussian trial wave function, with b and c the variational parameters, is given by

$$\psi(\xi,\eta,\phi) = \left(\frac{8b^4c^2}{\pi^3}\right)^{\frac{1}{4}} e^{-b^2\xi^2 - c^2\eta^2}$$

so that the expectation value of $H_0(\mathbf{x})$ is

$$\langle H_0 \rangle = b^2 + \frac{1}{2}c^2 + \frac{2c^2 + \lambda^2 b^2}{8b^2 c^2}.$$

and the expectation value of the two-body interaction is

$$\langle V \rangle = 2\alpha \frac{b^2 c}{\sqrt{\pi}}.$$

The optimal values of the variational parameters b and c are the solutions of

$$\begin{aligned} \frac{\partial}{\partial b}\frac{E_0}{N} &= 0 \\ \frac{\partial}{\partial c}\frac{E_0}{N} &= 0 \end{aligned} \tag{35}$$

where the total energy per particle E_0/N is just $\langle H_0 \rangle + \langle V \rangle$. An orbital energy can also be calculated given the solution to these equations and is given by

$$\varepsilon_0 = b^2 + \frac{1}{2}c^2 + \frac{2c^2 + \lambda^2 b^2}{8b^2 c^2} + 4\alpha \frac{b^2 c}{\sqrt{\pi}}. \tag{36}$$

In Sec. 3.6 below, the variational orbital energy for an isotropic trap is compared to both the Thomas-Fermi and Hartree-Fock results.

For an isotropic trap, the parameters are equal so that

$$\frac{E_0}{N} = \frac{3b^2}{2} + \frac{3}{8b^2} + \frac{2\alpha b^3}{\sqrt{\pi}}. \tag{37}$$

For positive α (*i.e.* positive a_{sc}), this equation always has a global minimum. For negative α (negative a_{sc}), however, no matter how small, the b^3 term dominates for large b and this equation has at most only a local minimum. Figure 1 shows the total energy per particle as a function of the variational parameter b for several values of α, both positive and negative. The thick solid line denotes the noninteracting case, and all curves above it are for positive α. Each curve below it corresponds to increasingly negative α. It can be seen that the local maximum in the curve gradually approaches the local minimum until at some negative value of α, α_c, no minimum exists for finite b. The curve corresponding to α_c is indicated in the figure by a dashed

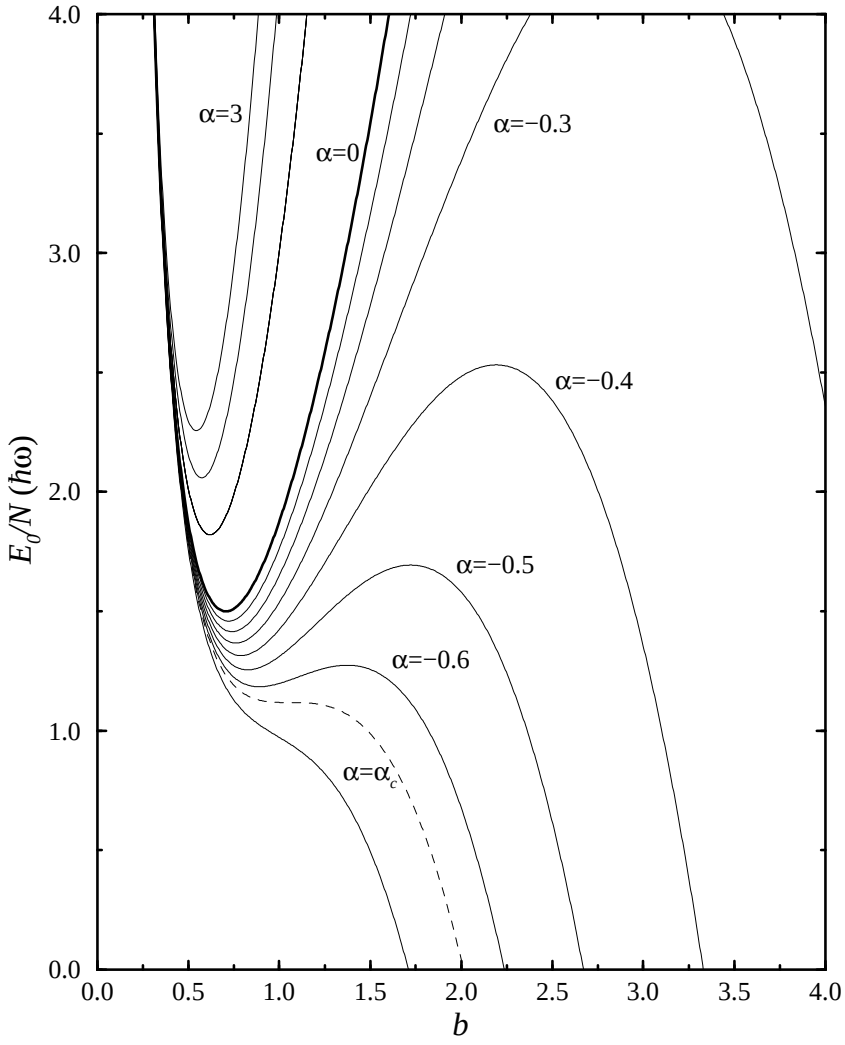

Figure 1. The total energy per particle, Eq. (37), as a function of the variational parameter b for several values of α. The thick solid line corresponds to the noninteracting case α=0, and the dashed line to α=α_c.

line. Since the minimization of Eq. (37) reduces to finding the roots of a quintic polynomial, the value of α_c can be determined using Sturm's theorem [25, 67] to be

$$\alpha_c = -\frac{2\sqrt{2\pi}}{5^{5/4}} \approx -0.670513.$$

This value compares well with the result obtained by direct numerical solution of the Hartree-Fock equation, $\alpha_c \approx -0.57497$, (for details see Sec. 3.6 and Ref. [30]).

To determine α_c for $\lambda \neq 1$, Eq. (35) must be solved numerically, although Baym and Pethick have obtained the approximate analytical solution [68]

$$\alpha_c = -\sqrt{\frac{\pi}{2\lambda}}.$$

Figure 2 shows α_c as a function of λ for λ between 0.1 and 10. The dashed line is the Baym and Pethick result, and the solid line is the numerical solution of Eq. (35). The circle included in this figure is determined from direct numerical solution of the Hartree-Fock equation. The fact that the variational solution overestimates the critical value of α is not surprising given that the Gaussian trial wave function tends to underestimate the density as α grows more negative. Further, since the Baym and Pethick result overestimates the critical value relative to the variational calculation, it is clear that any estimates based upon the Baym and Pethick result will be overly optimistic. In Sec. 3.6, I will discuss in more detail the stability of the ground state for an isotropic trap and compare the variational and numerical solution of the Hartree-Fock equation.

3.3 Random phase approximation

I showed in Eq. (22) that the Hartree-Fock approximation accounts for single particle excitations in the ground state. This approximation can be improved by including two or more particle excitations in the trial wave function. One approach that includes some of the physics of two particle excitations is the random phase approximation (RPA) [44, 45, 53]. This method amounts to replacing the Hamiltonian, Eq. (2), by an effective Hamiltonian which accounts for up to two particle excitations of the ground state. (The full Hamiltonian allows for single

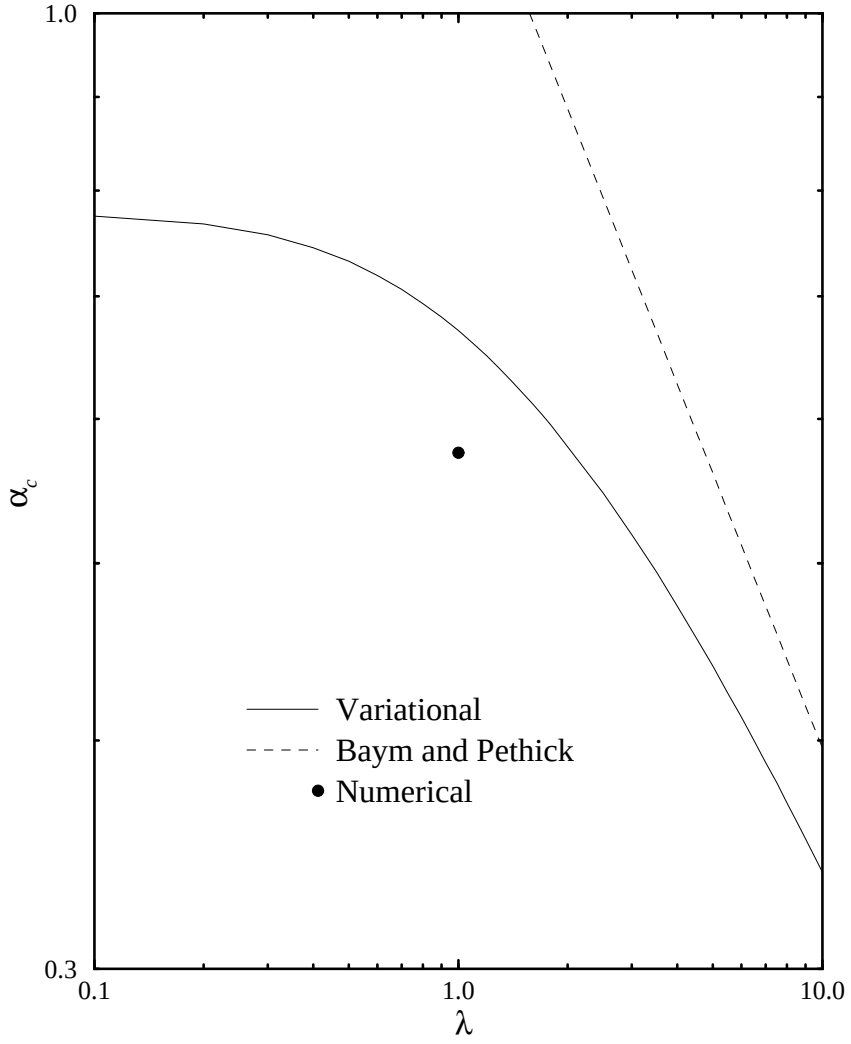

Figure 2. The critical value of α, α_c, as determined by a variational analysis as a function of trap anisotropy, λ=ω_z/ω_ρ. The solid line is the result of numerically solving Eq. (35), and the dashed line is the approximate analytical solution of Baym and Pethick [68]. The circle marks the result, α_c=-0.57497, of numerically solving the Hartree-Fock equation for an isotropic trap (see Sec. 3.6 and Ref. [30]).

and double excitations of *excited* states as well.) The RPA equations or their equivalent can be derived in a number of ways. I will present in the next section two derivations based on the time-independent Schrödinger equation which make the connection to the Bogoliubov approach most transparent. In the following section, I will present a derivation based on the time-dependent Schrödinger equation which makes a transparent connection to the stability analysis in Sec. 3.2 [45, 53].

3.3.1 Time-independent derivation. I begin with the exact solutions to the time-independent many-body Schrödinger equation,

$$\hat{H}\left|\nu\right\rangle = E_\nu \left|\nu\right\rangle,$$

and define operators $\hat{Q}_\nu$ such that

$$\hat{Q}_\nu \left|0\right\rangle = 0 \text{ and } \hat{Q}_\nu^\dagger \left|0\right\rangle = \left|\nu\right\rangle \tag{38}$$

where $|0\rangle$ is the exact many-body ground state. The energy of the ν-*th* excited state is written as

$$E_\nu = \frac{\left\langle \nu \left| \hat{H} \right| \nu \right\rangle}{\left\langle \nu \mid \nu \right\rangle}$$

or, using Eq. (38), as

$$E_\nu - E_0 = \frac{\left\langle 0 \left| \left[\hat{Q}_\nu, \left[\hat{H}, \hat{Q}_\nu^\dagger \right] \right] \right| 0 \right\rangle}{\left\langle 0 \left| \left[\hat{Q}_\nu, \hat{Q}_\nu^\dagger \right] \right| 0 \right\rangle}. \tag{39}$$

This is an equation for the energy difference — which is the experimentally measurable quantity — between the exact many-body excited state and the exact many-body ground state. One must, however, approximate the solution to Eq. (39). One approximation is the RPA [44, 45, 53] which consists of restricting $\hat{Q}$ to single particle excitations

$$\hat{Q}_\nu^\dagger = \frac{1}{\sqrt{N}} \sum_{p \neq 0} X_{p\nu} \hat{c}_p^\dagger \hat{c}_0 - Y_{p\nu} \hat{c}_0^\dagger \hat{c}_p \tag{40}$$

where p refers to the quasi-Hartree-Fock (or Hartree-Fock) single particle basis. The first term removes a particle from the lowest quasi-Hartree-Fock orbital and places it in an excited orbital

while the second term does the opposite. To consistently treat Eq. (39) in this approximation, both the eigenstates and eigenenergies must be approximated by their RPA equivalent. In particular, for $\hat{Q}$ defined by Eq. (40) I define the RPA ground state by

$$\hat{Q}_\nu \left|\Phi_0^{\mathrm{RPA}}\right\rangle = 0$$

and the RPA excited states by

$$\left|\Phi_\nu^{\mathrm{RPA}}\right\rangle = \hat{Q}_\nu^\dagger \left|\Phi_0^{\mathrm{RPA}}\right\rangle .$$

With these definitions, the RPA version of Eq. (39) is written as

$$E_\nu^{\mathrm{RPA}} - E_0^{\mathrm{RPA}} = \frac{\left\langle \Phi_0^{\mathrm{RPA}} \left| \left[\hat{Q}_\nu, \left[\hat{H}, \hat{Q}_\nu^\dagger\right]\right] \right| \Phi_0^{\mathrm{RPA}} \right\rangle}{\left\langle \Phi_0^{\mathrm{RPA}} \left| \left[\hat{Q}_\nu, \hat{Q}_\nu^\dagger\right] \right| \Phi_0^{\mathrm{RPA}} \right\rangle}. \tag{41}$$

While Eq. (39) is exact, Eq. (41) is only approximate since the approximation $\hat{H}\left|\Phi_\nu^{\mathrm{RPA}}\right\rangle \approx E_\nu^{\mathrm{RPA}}\left|\Phi_\nu^{\mathrm{RPA}}\right\rangle$ was used in its derivation. Further, since the RPA ground state remains unknown, I make the additional approximation of replacing $\left|\Phi_0^{\mathrm{RPA}}\right\rangle$ by $\left|\Phi_0^{\mathrm{HF}}\right\rangle$ in order to evaluate the matrix elements in Eq. (41). With this replacement, the numerator of the right hand side of Eq. (41) can be written as

$$\left\langle \Phi_0^{\mathrm{HF}} \left| \left[\hat{Q}_\nu, \left[\hat{H}, \hat{Q}_\nu^\dagger\right]\right] \right| \Phi_0^{\mathrm{HF}} \right\rangle = \sum_{pp'\neq 0} X_{p\nu}^* \left[B_{pp'} X_{p'\nu} + C_{pp'}^* Y_{p'\nu}\right] + Y_{p\nu}^* \left[C_{pp'} X_{p'\nu} + B_{pp'}^* Y_{p'\nu}\right]$$

where $B_{pp'}$ and $C_{pp'}$ are defined in Eq. (33) of Sec. 3.2. Similarly, the denominator of the right hand side of Eq. (41) can be written as

$$\left\langle \Phi_0^{\mathrm{HF}} \left| \left[\hat{Q}_\nu, \hat{Q}_\nu^\dagger\right] \right| \Phi_0^{\mathrm{HF}} \right\rangle = \sum_{p\neq 0} X_{p\nu}^* X_{p\nu} - Y_{p\nu}^* Y_{p\nu}.$$

Minimizing E_ν^{RPA} in Eq. (41) with respect to $X_{q\nu}^*$ and $Y_{q\nu}^*$ yields the RPA equations

$$\begin{aligned} \sum_{p\neq 0} \left[B_{qp} X_{p\nu} + C_{qp}^* Y_{p\nu}\right] &= \hbar\omega_\nu^{\mathrm{RPA}} X_{q\nu} \\ \sum_{p\neq 0} \left[C_{qp} X_{p\nu} + B_{qp}^* Y_{p\nu}\right] &= -\hbar\omega_\nu^{\mathrm{RPA}} Y_{q\nu} \end{aligned} \tag{42}$$

where $\hbar\omega_{q0} = \varepsilon_q - \varepsilon_0$ and $\hbar\omega_\nu^{\mathrm{RPA}} = E_\nu^{\mathrm{RPA}} - E_0^{\mathrm{RPA}}$. I should emphasize that the RPA is *not* a variational approximation. In other words, the total energies $E_\nu^{\mathrm{RPA}} = E_0^{\mathrm{RPA}} + \hbar\omega_\nu^{\mathrm{RPA}}$ computed

from Eq. (42) are not upper bounds to the true energies of the system. This property was lost when the matrix elements in Eq. (41) were evaluated only approximately. In addition, because of the minus sign in the second of the RPA equations, the excitation energies are not guaranteed to be real. In fact, it was shown Sec. 3.2 (see also Refs. [45, 53]) that an imaginary energy indicates an instability of the Hartree-Fock solution. The interesting and important question of the stability of a condensate for negative scattering lengths could, for instance, be studied by searching for imaginary excitation energies as N is increased (see Sec. 3.6 for a discussion of such a study). The only differences between Eq. (42) and the RPA equations for fermions [44, 45, 53] are the factor of $(N-1)/2$ and the plus sign noted in Eq. (28) above given that there is only one "hole" for a boson system — the ground state orbital alone.

Notice that the RPA equations are very similar to the Bogoliubov normal mode equations, Eq. (8); the only difference in form is the presence of $N-1$ rather than N_0. For large N and low lying excitations, this difference is negligible to within the order N^{-1} errors already introduced at various points in each approximation. However, there is also a more subtle difference. Where the Hartree-Fock single particle basis functions strictly conserve particle number, the single particle basis functions to which the labels refer in Eq. (9) have built into them the order N^{-1} error present in the nonlinear Schrödinger equation, Eq. (6). The most significant difference, then, between the Bogoliubov approximation and the RPA is the exclusion of terms of order N^{-1} from the self-consistent ground state in the Bogoliubov approximation and the consequent loss of particle number conservation. In the RPA, both the quasi-boson approximation and the RPA ground state conserve particle number.

The normalization of the eigenvectors of the RPA equations is determined by requiring the excited states to be orthonormal

$$\langle \nu' \mid \nu \rangle = \left\langle \Phi_0^{\mathrm{RPA}} \left| \left[\hat{Q}_{\nu'}, \hat{Q}_{\nu}^{\dagger} \right] \right| \Phi_0^{\mathrm{RPA}} \right\rangle = \delta_{\nu'\nu}. \tag{43}$$

But, approximating the RPA ground state by the Hartree-Fock ground state $\left|\Phi_0^{\mathrm{HF}}\right\rangle$ gives

$$\left\langle \Phi_0^{\mathrm{RPA}} \left| \left[\hat{Q}_{\nu'}, \hat{Q}_{\nu}^{\dagger} \right] \right| \Phi_0^{\mathrm{RPA}} \right\rangle \approx \left\langle \Phi_0^{\mathrm{HF}} \left| \left[\hat{Q}_{\nu'}, \hat{Q}_{\nu}^{\dagger} \right] \right| \Phi_0^{\mathrm{HF}} \right\rangle$$

$$= \sum_{pp' \neq 0} \left(X^*_{\nu' p} X_{\nu p'} - Y^*_{\nu' p} Y_{\nu p'} \right) \delta_{pp'}. \tag{44}$$

When combined with Eq. (43) this gives the normalization condition

$$\sum_{p \neq 0} \left(X^*_{p\nu'} X_{p\nu} - Y^*_{p\nu'} Y_{p\nu} \right) = \delta_{\nu'\nu}. \tag{45}$$

The substitution of the Hartree-Fock ground state for the RPA ground state here and in Eq. (39) is known as the quasi-boson approximation [44, 45]. It has been studied as an approximation to the interacting boson model in the study of nuclear structure [45]. In the nuclear structure problem, the interacting boson model replaces the pair of fermion operators that create a single particle excitation of the ground state by an expansion on boson operators; the quasi-boson approximation truncates this expansion at the first term. In the present problem, the quasi-boson approximation replaces the pair of boson operators which create a single particle excitation of the ground state by a single operator which also obeys boson commutation relations. That is, the quasi-boson approximation effects the replacement

$$\frac{\hat{c}^\dagger_p \hat{c}_0}{\sqrt{N}} \longrightarrow \hat{A}^\dagger_p;$$

the exact commutator is

$$\left[\frac{\hat{c}^\dagger_0 \hat{c}_p}{\sqrt{N}}, \frac{\hat{c}^\dagger_{p'} \hat{c}_0}{\sqrt{N}} \right] = \frac{\hat{c}^\dagger_0 \hat{c}_0}{N} \delta_{pp'} - \frac{\hat{c}^\dagger_{p'} \hat{c}_p}{N}, \tag{46}$$

but the quasi-boson approximation gives

$$\left[\hat{A}_p, \hat{A}^\dagger_{p'} \right] = \delta_{pp'}. \tag{47}$$

The relation of this replacement to the approximation of the RPA ground state by the Hartree-Fock ground state is made more clear by comparing the matrix elements of Eq. (46) and Eq. (47):

$$\begin{aligned} \frac{1}{N} \left\langle \Phi^{\mathrm{RPA}}_0 \left| \left[\hat{c}^\dagger_0 \hat{c}_p, \hat{c}^\dagger_{p'} \hat{c}_0 \right] \right| \Phi^{\mathrm{RPA}}_0 \right\rangle &\approx \frac{1}{N} \left\langle \Phi^{\mathrm{HF}}_0 \left| \left[\hat{c}^\dagger_0 \hat{c}_p, \hat{c}^\dagger_{p'} \hat{c}_0 \right] \right| \Phi^{\mathrm{HF}}_0 \right\rangle \\ &= \left\langle \Phi^{\mathrm{HF}}_0 \left| \left[\hat{A}_p, \hat{A}^\dagger_{p'} \right] \right| \Phi^{\mathrm{HF}}_0 \right\rangle = \delta_{pp'}. \end{aligned}$$

The quasi-boson approximation is thus valid only when the occupation of the quasi-Hartree-Fock excited states in the RPA ground state is small [44, 45], and the error introduced in this case is on the order of N^{-1} due to the second term of the commutator in Eq. (46) above.

Within the quasi-boson approximation, solving the RPA equations is equivalent to diagonalizing the quasi-boson representation of the Hamiltonian $\hat{H}_{\mathrm{B}}$ to second order in $\hat{A}$. $\hat{H}_{\mathrm{B}}$ is defined by requiring that the matrix elements of the quasi-boson representation operators be the same as the matrix elements of the corresponding operators in the original representation [45]. Explicitly, the definitions needed for the RPA are

$$\begin{aligned}
\left\langle \Phi_0^{\mathrm{HF}} \middle| \hat{H}_{\mathrm{B}} \middle| \Phi_0^{\mathrm{HF}} \right\rangle &= \left\langle \Phi_0^{\mathrm{HF}} \middle| \hat{H} \middle| \Phi_0^{\mathrm{HF}} \right\rangle = E_0^{\mathrm{HF}} \\
\left\langle \Phi_0^{\mathrm{HF}} \middle| \left[\hat{A}_p, \left[\hat{H}_{\mathrm{B}}, \hat{A}_{p'}^\dagger \right] \right] \middle| \Phi_0^{\mathrm{HF}} \right\rangle &= \frac{1}{N} \left\langle \Phi_0^{\mathrm{HF}} \middle| \left[\hat{c}_0^\dagger \hat{c}_p, \left[\hat{H}, \hat{c}_{p'}^\dagger \hat{c}_0 \right] \right] \middle| \Phi_0^{\mathrm{HF}} \right\rangle = B_{pp'} \\
\left\langle \Phi_0^{\mathrm{HF}} \middle| \left[\hat{A}_p, \left[\hat{H}_{\mathrm{B}}, \hat{A}_{p'} \right] \right] \middle| \Phi_0^{\mathrm{HF}} \right\rangle &= \frac{1}{N} \left\langle \Phi_0^{\mathrm{HF}} \middle| \left[\hat{c}_0^\dagger \hat{c}_p, \left[\hat{H}, \hat{c}_0^\dagger \hat{c}_{p'} \right] \right] \middle| \Phi_0^{\mathrm{HF}} \right\rangle = -C_{pp'}
\end{aligned}$$

with $B_{pp'}$ and $C_{pp'}$ defined by Eq. (33). The quasi-boson Hamiltonian is then written as

$$\hat{H}_{\mathrm{B}} = E_0^{\mathrm{HF}} + \sum_{pp' \neq 0} B_{pp'} \hat{A}_p^\dagger \hat{A}_{p'} + \frac{1}{2} \sum_{pp' \neq 0} C_{pp'} \hat{A}_p^\dagger \hat{A}_{p'}^\dagger + C_{pp'}^* \hat{A}_{p'} \hat{A}_p. \tag{48}$$

The terms linear in $\hat{A}$ and $\hat{A}^\dagger$ vanish identically by the Hartree-Fock condition, Eq. (22). Since it has a quadratic form, $\hat{H}_{\mathrm{B}}$ can be diagonalized by a canonical (or Bogoliubov) transformation from the set of operators $\hat{A}$ to another set $\hat{O}$. In other words, I transform from the set of boson operators $\hat{A}$ for which the Hamiltonian is given by Eq. (48) and which satisfy

$$\hat{A}_p \left| \Phi_0^{\mathrm{HF}} \right\rangle = 0 \text{ and } \hat{A}_p^\dagger \left| \Phi_0^{\mathrm{HF}} \right\rangle = \left| \Phi_p^{\mathrm{HF}} \right\rangle$$

to a set $\hat{O}$ such that

$$\hat{O}_\nu \left| \Phi_0^{\mathrm{RPA}} \right\rangle = 0 \text{ and } \hat{O}_\nu^\dagger \left| \Phi_0^{\mathrm{RPA}} \right\rangle = \left| \Phi_\nu^{\mathrm{RPA}} \right\rangle.$$

The transformation which connects these two sets of operators is given by

$$\begin{aligned}
\hat{O}_\nu^\dagger &= \sum_{p \neq 0} X_{p\nu} \hat{A}_p^\dagger - Y_{p\nu} \hat{A}_p \\
\hat{O}_\nu &= \sum_{p \neq 0} X_{p\nu}^* \hat{A}_p - Y_{p\nu}^* \hat{A}_p^\dagger.
\end{aligned} \tag{49}$$

The operators $\hat{O}$ are the quasi-boson approximations to the $\hat{Q}$ operators defined in Eq. (40). Further, for the transformation to be canonical, the $\hat{O}$'s must satisfy boson commutation relations just as the $\hat{A}$'s do. This requirement leads directly to the normalization condition Eq. (45) and places an additional constraint on the coefficients X and Y:

$$\sum_{p\neq 0} X_{p\nu'}Y_{p\nu} - X_{p\nu}Y_{p\nu'} = 0.$$

In order to construct an approximate eigenstate within the RPA, the ground state must first be known. Using the Thouless theorem [69], the RPA ground state can be related to the Hartree-Fock ground state by

$$\left|\Phi_0^{\mathrm{RPA}}\right\rangle = \mathcal{N}e^{\hat{Z}}\left|\Phi_0^{\mathrm{HF}}\right\rangle.$$

In this expression, $\mathcal{N}$ is a normalization constant and

$$\hat{Z} = \frac{1}{2}\sum_{pp'\neq 0} Z_{pp'}\hat{A}_p^\dagger \hat{A}_{p'}^\dagger$$

with the coefficient matrix $\mathbf{Z}$ given by

$$\mathbf{Z}^* = \mathbf{Y}\mathbf{X}^{-\mathbf{1}} = \mathbf{Z}^\dagger.$$

Thus, because a product of two $\hat{A}^\dagger$'s is present in $\hat{Z}$, the exponential of $\hat{Z}$ will have only even powers of $\hat{A}^\dagger$. It follows that the RPA ground state contains only even numbers of particle excitations of the Hartree-Fock ground state. A direct calculation of the RPA ground state would then provide a means of checking the validity of the quasi-boson approximation. If the coefficient, $\mathcal{N}$, of the Hartree-Fock ground state in the expansion of the RPA ground state is near unity, then replacing the RPA ground state by the Hartree-Fock ground state is valid and the RPA ground state is a better approximation to the physical ground state. Conversely, if $\mathcal{N}$ is not nearly unity, the quasi-boson RPA is not valid. In this case, a self-consistent RPA [45] might be used instead (see Sec. 3.3.2 below). That is, the RPA ground state calculated as described here could be used directly in Eq. (41) to derive new equations which could then be

solved for a new set of X's and Y's. A new ground state could be calculated from these and the procedure iterated until some convergence criteria is met.

To bring the quasi-boson Hamiltonian to an uncoupled oscillator form, *i.e.*

$$\hat{H}_{\mathrm{B}} = E_0^{\mathrm{RPA}} + \sum_{\nu \neq 0} \hbar\omega_\nu^{\mathrm{RPA}} \hat{O}_\nu^\dagger \hat{O}_\nu, \tag{50}$$

the RPA equations are precisely the necessary constraints on X and Y needed to cancel the $\hat{O}\hat{O}$ and $\hat{O}^\dagger\hat{O}^\dagger$ terms. The RPA equations could thus have been derived using such a condition. The total energy of the ground state in the RPA, E_0^{RPA}, can be related to the Hartree-Fock ground state energy Eq. (26) by

$$E_0^{\mathrm{RPA}} = E_0^{\mathrm{HF}} - \sum_\nu \hbar\omega_\nu^{\mathrm{RPA}} \sum_{p \neq 0} |Y_{p\nu}|^2 . \tag{51}$$

The RPA ground state energy is lower than the Hartree-Fock energy, but as there is no variational bound on the RPA result, it can be lower than the true ground state energy. In fact, it is not uncommon to find that this is the case for fermionic systems [45]; it results from the fact that the RPA can overestimate ground state correlations. The similarity between the combination of Eqs. (50) and (51) and their Bogoliubov equivalents, Eqs. (7) and (10), is no accident. Besides the fundamental question of particle number conservation, the physics included in both approximations is nearly identical. The mapping between the two can be made even more complete by identifying the operators $\hat{O}$ and $\hat{O}^\dagger$ with the quasi-particle operators $\hat{\beta}$ and $\hat{\beta}^\dagger$, Eq. (5).

I should point out that both the Hartree-Fock approximation and the RPA strictly conserve particle number. For Hartree-Fock, this follows from the fact that the number of particles is conserved in the Hartree-Fock equation, Eq. (25); and for the RPA, it can be seen that this is the case from the quasi-boson Hamiltonian in Eq. (50). The $\hat{A}$ operators are defined to create single particle excitations with the same total number of particles and so cannot change the total number of particles in any combination. This is in contrast to the Bogoliubov approximation in which the conservation of particle number is abandoned from the beginning.

I should point out that a modified form of the Bogoliubov treatment that strictly conserves particle number has been presented recently by Gardiner [17].

3.3.2 Time-dependent derivation. The RPA equations can also be derived from the time-dependent Schrödinger equation using a small oscillations normal mode analysis just as in classical mechanics [51]. The "equilibrium" about which the oscillations take place is just the extremum in a_p space defined by the Hartree-Fock solution. For this reason, the connection of the RPA to the stability analysis of Sec. 3.2 is somewhat more clearly seen in the time-dependent derivation.

The starting point for this derivation is the time-dependent Schrödinger equation. A wave function of the form

$$|\Phi(t)\rangle \approx e^{-\frac{i}{\hbar}E_0^{\mathrm{HF}}t}\Big(1+\sum_{p\neq 0}a_p(t)\frac{\hat{c}_p^\dagger\hat{c}_0}{\sqrt{N}}+\frac{1}{2}\sum_{p,p'\neq 0}a_p(t)a_{p'}(t)\frac{\hat{c}_p^\dagger\hat{c}_0}{\sqrt{N-1}}\frac{\hat{c}_{p'}^\dagger\hat{c}_0}{\sqrt{N}}+\dots\Big)\left|\Phi_0^{\mathrm{HF}}\right\rangle$$

is substituted into the equation

$$\frac{\delta}{\delta a_p^*}\left\langle\Phi(t)\left|i\hbar\frac{d}{dt}-\hat{H}\right|\Phi(t)\right\rangle=0$$

where the matrix element is evaluated to second order in the $a_p(t)$'s [see Eq. (32)]. The result is the following set of first order differential equations for $a_p(t)$:

$$i\hbar\frac{d}{dt}a_q(t)=\left(E_q^{\mathrm{HF}}-E_0^{\mathrm{HF}}\right)a_q(t)+\frac{N-1}{2}\sum_{p\neq 0}\left[a_p(t)\left\langle q0\left|\overline{V}\right|p0\right\rangle+a_p^*(t)\left\langle qp\left|\overline{V}\right|00\right\rangle\right]. \qquad (52)$$

These equations may be solved as in classical small oscillation theory by assuming

$$a_q(t)=X_qe^{-i\omega t}+Y_q^*e^{i\omega^* t}.$$

Substituted into Eq. (52) and equating coefficients of $e^{-i\omega t}$ and $e^{i\omega^* t}$, the RPA equations, Eq. (42), are immediately obtained. Should an ω be imaginary, it is clear that $a_q(t)$ will have an exponentially growing piece indicating that the small oscillation is unstable.

To make the connection of imaginary RPA frequencies to the stability of the Hartree-Fock ground state (see Sec. 3.2) formally complete, consider the argument of Thouless [66, 70].

Recall that it was shown in Sec. 3.2 that the necessary condition for the stability of the Hartree-Fock ground state is that the RPA coefficient matrix [see Eq. (42)]

$$\begin{pmatrix} B & C^* \\ C & B^* \end{pmatrix}$$

be positive definite for B and C defined in Eq. (33). If we suppose that there is a solution of the RPA equations with a complex, non-zero excitation energy $\hbar\omega$, then Eq. (42) implies

$$\begin{pmatrix} X^\dagger & Y^\dagger \end{pmatrix} \begin{pmatrix} B & C^* \\ C & B^* \end{pmatrix} \begin{pmatrix} X \\ Y \end{pmatrix} = \hbar\omega \begin{pmatrix} X^\dagger & Y^\dagger \end{pmatrix} \begin{pmatrix} X \\ -Y \end{pmatrix}. \tag{53}$$

The left hand side must be a real non-negative number since it is the expectation value of a positive definite Hermitian matrix. The coefficient of $\hbar\omega$ on the right hand side is similarly a real non-negative number. Since $\hbar\omega$ is assumed to be complex, however, this coefficient must vanish. But, the expectation value of a positive definite Hermitian matrix can only be identically zero for an eigenvector. If this is so, then $\hbar\omega$, the corresponding eigenvalue, must also be zero. This contradicts our initial assumption that $\hbar\omega$ is complex. It follows that if the Hartree-Fock ground state is stable, then $\hbar\omega$ cannot be complex.

An alternate derivation of the RPA equations from a time-dependent point of view is possible starting with the time-dependent Hartree-Fock equation Eq. (31),

$$i\hbar\frac{\partial}{\partial t}\phi(\mathbf{x},t) = \left(H_0(\mathbf{x}) + (N-1)\int d^3x'\,\phi^*(\mathbf{x}',t)\,V(\mathbf{x}'-\mathbf{x})\,\phi(\mathbf{x}',t)\right)\phi(\mathbf{x},t). \tag{54}$$

To obtain the RPA equations, a Floquet-like *ansatz* is made for the orbital

$$\phi(\mathbf{x},t) = e^{-\frac{i}{\hbar}\varepsilon t}\sum_{m=-\infty}^{\infty}\psi_m(\mathbf{x})e^{-im\omega t}$$

and substituted into Eq. (54). Projecting out the time-dependence $\exp(-\frac{i}{\hbar}(\varepsilon + n\hbar\omega)t)$ gives the following system of equations:

$$n\hbar\omega\psi_n(\mathbf{x}) = (H_0(\mathbf{x})-\varepsilon)\,\psi_n(\mathbf{x}) + \sum_{n'-m+m'=n}(N-1)\int d^3x'\,\psi_m^*(\mathbf{x}')\,V(\mathbf{x}'-\mathbf{x})\,\psi_{m'}(\mathbf{x}')\,\psi_{n'}(\mathbf{x}).$$

These equations should be regarded as a set of nonlinear eigenvalue equations for the ground and excited single particle states. The ground state corresponds to n=0 with the ladder of excited states given by n=1, 2, 3, ... The orthonormalization of $\phi_\nu(\mathbf{x},t)$ comes from the usual requirement

$$\int d^3x\, \phi_\nu(\mathbf{x},t)\phi_\nu(\mathbf{x},t) = \delta_{\nu\nu'}$$

or

$$\sum_{nn'} \int d^3x\, \psi_{\nu n}(\mathbf{x})\psi_{\nu' n'}(\mathbf{x},t) = \delta_{\nu\nu'}.$$

In the limit that $\psi_n(\mathbf{x})$ for $n\neq 0$ is in some sense small compared to $\psi_0(\mathbf{x})$ and limiting the expansion to single excitations n=$\pm$1, the infinite set of nonlinear eigenvalue equations above reduces to

$$0 = (H_0(\mathbf{x})-\varepsilon)\,\psi_0(\mathbf{x}) + (N-1)\int d^3x'\,\psi_0^*(\mathbf{x}')\,V(\mathbf{x}'-\mathbf{x})\,\psi_{0'}(\mathbf{x}')\,\psi_{0'}(\mathbf{x})$$

for the ground state and

$$\begin{aligned}
+\hbar\omega\psi_{+1}(\mathbf{x}) = (H_0(\mathbf{x})-\varepsilon)\,\psi_{+1}(\mathbf{x}) &+ (N-1)\int d^3x'\,\psi_0^*(\mathbf{x}')\,V(\mathbf{x}'-\mathbf{x})\,\psi_0(\mathbf{x}')\,\psi_{+1}(\mathbf{x}) \\
&+ (N-1)\int d^3x'\,\psi_0^*(\mathbf{x}')\,V(\mathbf{x}'-\mathbf{x})\,\psi_{+1}(\mathbf{x}')\,\psi_0(\mathbf{x}) \\
&+ (N-1)\int d^3x'\,\psi_{-1}^*(\mathbf{x}')\,V(\mathbf{x}'-\mathbf{x})\,\psi_0(\mathbf{x}')\,\psi_0(\mathbf{x}) \\
-\hbar\omega\psi_{-1}(\mathbf{x}) = (H_0(\mathbf{x})-\varepsilon)\,\psi_{-1}(\mathbf{x}) &+ (N-1)\int d^3x'\,\psi_0^*(\mathbf{x}')\,V(\mathbf{x}'-\mathbf{x})\,\psi_0(\mathbf{x}')\,\psi_{-1}(\mathbf{x}) \\
&+ (N-1)\int d^3x'\,\psi_0^*(\mathbf{x}')\,V(\mathbf{x}'-\mathbf{x})\,\psi_{-1}(\mathbf{x}')\,\psi_0(\mathbf{x}) \\
&+ (N-1)\int d^3x'\,\psi_{+1}^*(\mathbf{x}')\,V(\mathbf{x}'-\mathbf{x})\,\psi_0(\mathbf{x}')\,\psi_0(\mathbf{x}) \qquad (55)
\end{aligned}$$

for the excited states. The ground state equation is the usual Hartree-Fock equation while the excited state equations are just the configuration space version of the RPA equations, Eqs. (42), derived in Sec. 3.3.1. Expanding $\psi_{+1}(\mathbf{x})$ and $\psi_{-1}(\mathbf{x})$ on either of the Hartree-Fock bases brings the excited state equations into the form presented there. Equations (55) make yet another connection to the Bogoliubov approach presented in Chap. 2.

This approach also makes clear the fact that the random phase approximation for the excited states retains the simple product form of the total wave function. Further, it provides a relatively simple prescription for improving upon the linear approximation made in both the Bogoliubov approximation and the RPA. Such a possibility was considered above as a "self-consistent RPA", although its practical realization was much more difficult in that formulation. Here, though, the linear eigenvalue equations can be solved to provide an initial guess to an iterative scheme to solve the nonlinear equations. The higher harmonics can also be included to account for the frequencies generated by the nonlinear mean field term.

3.4 Configuration Interaction

A connection to standard atomic structure methods can be made by applying configuration interaction (CI) [61] to the system of bosons. The term "configuration" in this context means a given set of occupation numbers $\{n_i\}$ corresponding to the set of single particle orbitals $\{\psi_i(\mathbf{x})\}$ defined in Secs. 3.1.1 or 3.1.2. Configuration interaction, then, is the variational approach in which the trial wave function is expanded on a complete basis of many-body wave functions — or configurations — including the ground state and singly to multiply excited configurations. Since this is a complete many-body basis, the exact, time-independent, many-body energy eigenstates can in principle be calculated. In practice, of course, one must limit the expansion to a finite number of basis functions.

Explicitly, I assume a trial wave function of the form

$$\begin{aligned} |\Psi\rangle = a_0 \, |N, 0, \ldots\rangle \quad &+ \quad \sum_{p \neq 0} a_p \, |N-1, 0, \ldots, 0, 1_p, 0, \ldots\rangle \\ &+ \quad \sum_{p,p' \neq 0} b_{pp'} \, |N-2, 0, \ldots, 0, 1_p, 0, \ldots, 0, 1_{p'}, 0, \ldots\rangle + \cdots \end{aligned} \tag{56}$$

where the notation 1_p indicates that the *p-th* quasi-Hartree-Fock (or Hartree-Fock) orbital is occupied by one boson. This trial function includes the same basis functions as Eq. (21), the trial function used to derive the Hartree-Fock equation, but it is not constrained to be a product form. Specifically, the coefficients for multiple excitations do not factor into products

as they did in Eq. (21). Thus, this wave function is the most general completely symmetric wave function as opposed to the most general completely symmetric *product* wave function as in the Hartree-Fock approximation and the RPA. Upon truncation, the variational principle for the total energy yields the matrix eigenvalue problem

$$\mathbf{H}\Psi_\nu = E_\nu \Psi_\nu,$$

where Ψ_ν is the vector of expansion coefficients. Since neither the RPA nor the Bogoliubov equations are variational approximations, one cannot expect to derive them from CI. To obtain a similar approximation, however, it is only necessary to include up to doubly excited configurations [that is, truncate the trial function $|\Psi\rangle$ to those terms explicitly written in Eq. (56)]. It is possible to go beyond the RPA and the Bogoliubov approximation within the CI framework with the inclusion of triple and higher excitations. In fact, the inclusion of all double excitation matrix elements (*i.e.* those that involve one and two particle excitations of *excited* states as well as of the ground state) improves upon both the RPA and the Bogoliubov approximations. This improvement stems from the fact that CI is a variational approximation based upon an expansion on a complete set of states, and the inclusion of higher and more varied excitations not included in the RPA or the Bogoliubov approximation must yield better approximations to the exact energy eigenstates. Physically, this improvement can be described as incorporating correlations beyond both the RPA and the Bogoliubov approximation.

The Hamiltonian matrix for this RPA-like truncated CI expansion can then be partitioned into submatrices according to the states that are coupled: the ground state G, singly excited states S, or doubly excited states D. Explicitly,

$$\mathbf{H} = \begin{pmatrix} H_{GG} & H_{GS} & H_{GD} \\ H_{SG} & H_{SS} & H_{SD} \\ H_{DG} & H_{DS} & H_{DD} \end{pmatrix}.$$

For example, the submatrix H_{GS}=H_{SG}^{T} contains the coupling between the ground state and singly excited states. For both the quasi-Hartree-Fock and the Hartree-Fock single particle

orbitals, all of the elements of this submatrix are identically zero by the Hartree-Fock condition, Eq. (22). The full CI matrix equation is then

$$\begin{pmatrix} H_{GG} & 0 & H_{GD} \\ 0 & H_{SS} & H_{SD} \\ H_{DG} & H_{DS} & H_{DD} \end{pmatrix} \begin{pmatrix} a_G \\ a_S \\ b_D \end{pmatrix}_\nu = E_\nu \begin{pmatrix} a_G \\ a_S \\ b_D \end{pmatrix}_\nu \tag{57}$$

with E_ν the total energy of the ν-*th* state. In order to connect this set of equations as closely as possible to the RPA and Bogoliubov equations, recall that in both the RPA and Bogoliubov approaches only those matrix elements coupling single particle excitations to single particle excitations and two particle excitations to the ground state are retained. Keeping only these matrix elements in the CI matrix, or equivalently keeping terms proportional to N^2 and N while neglecting terms proportional to $\sqrt{N}$ and 1, results in setting H_{SD} and H_{DS} to zero and approximating H_{DD} by its diagonal elements H'_{DD}. The RPA-like approximation to CI reads:

$$\begin{pmatrix} H_{GG} & 0 & H_{GD} \\ 0 & H_{SS} & 0 \\ H_{DS} & 0 & H'_{DD} \end{pmatrix} \begin{pmatrix} a_G \\ a_S \\ b_D \end{pmatrix}_\nu = E_\nu \begin{pmatrix} a_G \\ a_S \\ b_D \end{pmatrix}_\nu . \tag{58}$$

In this approximation, single excitations are decoupled from double excitations as well as from the ground state. Because the submatrices decouple, I can permute the rows and columns to bring **H** to block diagonal form and diagonalize within the subspace of single particle excitations separately to find the low lying excited state energies,

$$H_{SS} a_S^\nu = E_\nu a_S^\nu . \tag{59}$$

Diagonalizing the remainder of the matrix gives corrections to the ground state and higher lying excited states. H_{SS} can be written as

$$(H_{SS})_{qp} = E_0^{\mathrm{HF}} \delta_{qp} + B_{qp}$$

with B_{qp} from Eq. (33). (The general form of the Hamiltonian matrix elements is explicitly

shown in App. B.) Combined with Eq. (59), this gives

$$Ba_S^\nu = \hbar\omega_\nu^{\mathrm{TDA}} a_S^\nu$$

after rearranging. This is a special case of the RPA equations with $Y_{q\nu}$ set to zero and $X_{q\nu}$ replaced by a_S^ν. It is, in fact, the true Hartree-Fock approximation for the singly excited states (in a frozen core approximation) and is completely equivalent to Eq. (24). It is also known as the Tamm-Dancoff approximation [44, 45, 53], and, unlike the RPA, *is* variational (with the constraint that the ground state is the Hartree-Fock ground state). This is readily understood since it is just a more severely truncated ($b_{pp'}$=0) CI expansion.

So, while I have evaluated the CI Hamiltonian in Eq. (58) to the same order in N as the RPA, the RPA-like CI spectrum is presumably less accurate than the RPA spectrum since the coupling between single and double excitations is neglected. However, with the further modifications $a_0 \to 1$ and $b_{pp'} \to a_p a_{p'}$, the CI equation Eq. (58) becomes qualitatively more like the RPA equations: the submatrix H_{GG} drops out; H_{GD}, H_{SS}, and H_{DG} become coupled; and H_{DD} is neglected as it is then of order a_p^4 (in other words, it includes terms like two particle excitations of excited states which are neglected in the RPA). This approach does lead to a set of equations much like the RPA equations, Eq. (42), [45, 53]. In fact, they coincide with the equations derived in the context of stability analysis for the Hartree-Fock ground state, Eq. (34) in Sec. 3.2.

3.5 Pseudopotential approximation

The calculation of observables for experimental systems is greatly facilitated by the disparity in the length scales of the atomic interactions and the trapping potential. For the former, the s wave scattering length a_{sc} for the atom-atom interaction, typically on the order of several tens to a hundred atomic units for alkali atoms, characterizes the scale on which the interaction is effective. For the latter, the length scale can roughly be taken to be the classical turning point of the lowest oscillator state, typically on the order of a few microns.

The wavelength of the atomic motion is thus three to four orders of magnitude larger than the interaction length scale, and the shape independent approximation can be effectively employed for the atom-atom interaction potential. In using just the s wave scattering length, it is also assumed that since the average interparticle spacing is much larger than a_{sc} the effects of other particles can be neglected in obtaining the effective two-body interaction. This assumption is typically stated as $na_{sc}^3 \ll 1$ where n is a characteristic number density in the trap.

The shape independent approximation amounts to replacing the atom-atom interaction potential by a delta function whose strength is chosen so that the two-body scattering wave function is reproduced asymptotically. For the very low energy collisions taking place in the condensate, the coefficient of the delta function is simply proportional to the s wave scattering length. Corrections for higher energies and higher partial waves can also be made [47, 71]. In order to account for two-body collision energies different from zero, I could use for the interparticle interaction the configuration space scattering T-matrix instead of a delta function [53]. However, the energy dependence of the T-matrix over the energy range of importance should be negligible. At the level of reproducing only the zero energy s wave scattering wave function, however, the approximation can be loosely thought of as replacing the physical atom-atom interaction by a hard sphere whose radius is just equal to the s wave scattering length. This point of view seems to have been taken as early as 1929 when Lenz used an excluded volume argument to modify the kinetic energy in a gas [72]. One of the first instances in which the shape independent approximation was used in essentially the same spirit that I use it here was in a 1935 article by Fermi [73]. He introduced his contact potential and used it to obtain a simple formula for the energy levels of a Rydberg atom in the presence of a neutral perturbing rare gas atom. In the context of a weakly interacting gas, the pseudopotential was first used by Huang to derive the low-lying energy spectrum for bosons in the perturbative limit.

Using the pseudopotential plus s wave scattering length to reproduce the two-body scattering wave function is a physically intuitive approach, but it can also be viewed from the rather different and more mathematical perspective of many-body perturbation theory. In this

language, a many-body problem is written in terms of some independent particle basis and the interactions accounted for in a perturbation expansion. Each term of the expansion can then be represented diagrammatically. The general goal of theoretical many-body techniques is to include as many of these diagrams as possible in a given calculation. Several techniques have been devised, in fact, to include particular classes of diagrams to infinite order in the interaction. The Hartree-Fock and random phase approximations introduced in previous sections are two such techniques which sum different classes of diagrams to all orders. For two-body interactions with a very strongly repulsive core, however, an additional class of diagrams must be taken into account. These diagrams represent repeated two-body interactions and correspond to the usual Born series in scattering theory. In the first Born approximation, the s wave scattering length is

$$a_{\rm B} = \frac{\mu}{2\pi\hbar^2}\int d^3x\, V(\mathbf{x})$$

where μ is the reduced mass and $V(\mathbf{x})$ is the two-body interaction. Summing this class of diagrams essentially amounts to replacing the first Born scattering length above by the scattering length obtained in a two-body scattering calculation since the full calculation must in some sense correspond to summing the Born series (neglecting questions of convergence of the series). This issue has recently been explored more carefully by Proukakis *et al.* [74] specifically for harmonically trapped alkali gases. A more general effective interaction theory has been developed by Brueckner and others to handle strongly repulsive two-body interactions including the effects of the mean field [75, 76, 77].

The relevance to the Hartree-Fock equation can be seen more directly by considering the mean field term from the Hartree-Fock equation, Eq. (18) or Eq. (25):

$$V_{\rm HF}(\mathbf{x}) = \int d^3x'\, \psi_0^*(\mathbf{x}')\, V(\mathbf{x}-\mathbf{x}')\, \psi_0(\mathbf{x}').$$

The orbital $\psi_0(\mathbf{x})$ varies slowly on the scale of $V(\mathbf{x})$, whereby $V_{\rm HF}(\mathbf{x})$ can be approximately

rewritten as

$$\begin{aligned} V_{\rm HF}(\mathbf{x}) &\approx |\psi_0(\mathbf{x})|^2 \int d^3x' \, V(\mathbf{x}-\mathbf{x}') \\ &= \frac{2\pi\hbar^2 a_{\rm B}}{\mu} |\psi_0(\mathbf{x})|^2 . \end{aligned}$$

Since a typical molecular interaction potential has a large repulsive core, $a_{\rm B}$ is a large positive number regardless of the details of the potential. From this perspective, it is not only convenient to make the shape independent approximation but actually imperative in order to obtain quantitatively correct results. Whether the approximation is motivated by physical intuition as in the Fermi contact potential approach or by the more mathematical treatment of many-body perturbation theory, the approximation is well justified.

To illustrate the importance of including the correct two-body scattering physics, I compare three calculations of the ground state energy of three atoms in a harmonic trap. The first calculation is the direct solution of the three-body Schrödinger equation with realistic two-body interactions in the adiabatic hyperspherical approximation (see App. A for details of this approach). The second calculation is a "direct" solution of the Hartree-Fock equation using the same interaction potential. The third calculation is the Hartree-Fock solution using the shape independent approximation with a scattering length corresponding to the interaction potential of the other two approaches. For the purposes of comparison, I take the adiabatic hyperspherical results to be exact since they should be the most accurate of the three approximations.

The example system is three interacting bosons in an isotropic harmonic trap. I use the mass for ^{87}Rb in a trap with frequency ν=133 Hz. For the interaction potential in the adiabatic hyperspherical approximation and the "direct" Hartree-Fock solution, I have chosen the Morse potential [78],

$$V(r) = De^{-\alpha(r-r_0)} \left(e^{-\alpha(r-r_0)} - 2 \right) . \tag{60}$$

The constants D, α, and r_0 are chosen to set the dissociation limit, width of the potential well, and location of the well minimum, respectively. The Morse potential is a standard choice

Table 1. Comparison of the calculated total ground state energies for three bosons in a harmonic trap in three different approximations.

	Energies ($\hbar\omega$)	
Method	a_{sc}=3.11915 a.u.	a_{sc}=−26.8031 a.u.
Adiabatic hyperspherical	4.5004	4.4964
Morse Hartree-Fock	4.5038	4.5445
Shape independent Hartree-Fock	4.5004	4.4964

for a model molecular interaction [79] and is a convenient choice since the angular integrals in the mean field term of the Hartree-Fock equation can be evaluated analytically (see Sec. 3.5.2 below). The only significant difference from a real neutral atom-atom interaction is the absence of a van der Waal's r^{-6} tail. This poses no real difficulty since both can be considered short range interactions for the purposes of scattering calculations and since I consider physics which is controlled essentially by only the scattering length. Further, I have fixed the constants α and r_0 to approximate the Rb+Rb interaction potential, α=0.35 a.u.$^{-1}$ and r_0=11.65 a.u. (a.u. indicating here atomic units of length, 1 a.u.= 0.529177×10^{-10} m=a_0=the Bohr radius in hydrogen). I have left the constant D free to vary in order to generate different scattering lengths. Below, I will discuss the results for two values of D, D=1.2×10^{-8} a.u. and D=1.42×10^{-7} a.u. (where a.u. now indicates atomic units of energy, 1 a.u. = 27.2116 eV = twice the binding energy of hydrogen), corresponding to scattering lengths a_{sc} of 3.11915 a.u. and −26.8031 a.u. and summarize the results in Table 1. Further, for these values of D there are no two-body bound states. This is a convenient choice rather than an essential one.

3.5.1 Adiabatic hyperspherical approximation. The details of this approach are presented in App. A, so I will only briefly discuss it here. For three particles in a trap there are nine coordinates needed to fully specify their wave function. I first use the fact that the center of mass separates completely for particles in a confining harmonic potential

so that the center of mass wave function is simply a harmonic oscillator eigenfunction. This leaves only six relative coordinates which I choose to be the Jacobi coordinates. For zero total angular momentum (*i.e.* for the ground state) a transformation to the body frame completely separates the internal motion from the rotational motion in the Schrödinger equation. The rotational degrees of freedom are thus accounted for by a rotation matrix depending on the Euler angles, which is simply a constant for J=0. Only the three internal coordinates remain: the length of each Jacobi vector, ρ_1 and ρ_2, and the angle between them, θ. At this point, the transformation to hyperspherical coordinates is made, taking the pair (ρ_1,ρ_2) into (R,ϕ) much like the standard transformation from Cartesian to polar coordinates in two dimensions. The Schrödinger equation, now a function of (R,ϕ,θ), is approximately solved adiabatically (in R) by fixing R and solving the remaining adiabatic eigenvalue equation. The eigenvalues form adiabatic hyperradial potential curves which can be interpreted physically just as for any potential curves. The Schrödinger equation can also be solved "exactly" by including the coupling between the potential curves although the adiabatic approximation is often quite accurate.

Using Morse two-body potentials $V(r)$, I write the interaction for three bodies as the pairwise sum

$$V(R,\phi,\theta) = V(r_{12}) + V(r_{23}) + V(r_{31}).$$

In principle, for three interacting atoms there are also pure three-body terms due to the composite nature of the atoms. The lowest such term appearing in perturbation theory was found by Axilrod and Teller [80] (see also Ref. [81]) and is essentially the three-body analogue of the van der Waal's interaction. This Axilrod-Teller interaction depends on the interparticle distance r as r^{-9} asymptotically, however, so I neglect it here and in the Hartree-Fock equations.

For the two comparison cases, I have calculated the total ground state energy within the adiabatic hyperspherical approximation. For a trap frequency of 133 Hz, the classical turning point is at approximately 17700 a.u. It is both difficult and unnecessary to calculate the potential

curves to such a large distance. The difficulty lies in the fact that the interaction region in the (ϕ,θ) plane shrinks roughly as R^{-1} so that the numerical solution of the adiabatic eigenvalue equation becomes an increasingly intensive problem as R increases. But, for the hyperradial potential of interest here that correlates to three free atoms at $R\to\infty$, the asymptotic form of the hyperspherical potentials for short range two-body interactions is known [82] to be

$$U_0(R) \to \frac{15}{8\mu R^2} + \frac{\alpha a_{sc}}{R^3} + \frac{\beta}{R^4} + \dots$$

for finite a_{sc}. Thus, the potentials can be fit at some reasonably asymptotic distance (400-500 a.u. for these examples) and extrapolated to distances on the trap scale. The total energies are 4.5004 $\hbar\omega$ and 4.4964 $\hbar\omega$ for a_{sc}=3.11915 a.u. and -26.8031 a.u., respectively. Nonadiabatic corrections do not effect the energies to the precision shown.

3.5.2 Hartree-Fock with Morse interactions. On first thought, direct solution of the Hartree-Fock equation,

$$\left[H_0(\mathbf{x}) + (N-1)\int d^3x'\, \psi_0^*(\mathbf{x}')\, V(\mathbf{x}-\mathbf{x}')\, \psi_0(\mathbf{x}')\right] \psi_0(\mathbf{x}) = \varepsilon_0 \psi_0(\mathbf{x}), \tag{61}$$

with no approximation for $V(\mathbf{x})$ would seem to be an improvement over the seemingly severe approximation $V(\mathbf{x})\to\gamma\delta(\mathbf{x})$ with γ some strength parameter. The Morse potential Eq. (60) is ideal for testing this proposition since the mean field interaction integral can be performed in part analytically. When the radius is rescaled as $r=\beta x$, the energies as $\varepsilon=\hbar\omega\tilde{\varepsilon}$, and the orbital as $R(r)=\beta^{-\frac{3}{2}}\chi(x)$ with $\beta=\sqrt{\hbar/m\omega}$ the oscillator length scale, the Hartree-Fock equation becomes

$$\left[-\frac{1}{2}\frac{1}{x^2}\frac{d}{dx}\left(x^2\frac{d}{dx}\right) + \frac{1}{2}x^2 + V_{\rm HF}(\mathbf{x})\right] \chi_0(x) = \tilde{\varepsilon}_0 \chi_0(x). \tag{62}$$

The scaled orbital $\chi_0(x)$ is related to $\psi_0(\mathbf{x})$ by

$$\psi_0(\mathbf{x}) = \beta^{-\frac{3}{2}}\chi_0(x) Y_{00}(\Omega) = \beta^{-\frac{3}{2}}\frac{\chi_0(x)}{\sqrt{4\pi}}.$$

The mean field term in Eq. (62) is defined as

$$V_{\rm HF}(\mathbf{x}) = (N-1)\int dx' x'^2\, |\chi_0(x')|^2 \int \frac{d\Omega'}{4\pi}\frac{V(|\mathbf{x}-\mathbf{x}'|)}{\hbar\omega}.$$

As stated above, the angular integrals in $V_{\rm HF}(\mathbf{x})$ can be evaluated analytically. After rescaling, the result is

$$V_{\rm HF}(x) = (N-1)\,\frac{D}{\hbar\omega}\frac{1}{\alpha^2}\int_0^\infty dx'\,\frac{x'^2\,|\chi_0(x')|^2}{x_> x_<}\times \\ \left[\frac{1}{8}\left\{e^{-2\alpha(x_>-x_<-x_0)}\,(1+2\alpha(x_>-x_<))-e^{-2\alpha(x_>+x_<-x_0)}\,(1+2\alpha(x_>+x_<))\right\}\right. \\ \left.-\left\{e^{-\alpha(x_>-x_<-x_0)}\,(1+\alpha(x_>-x_<))-e^{-\alpha(x_>+x_<-x_0)}\,(1+\alpha(x_>+x_<))\right\}\right].$$

In this expression, $x_>$ ($x_<$) indicate that the larger (smaller) of x and x' is to be used. Equation (62) can now be readily solved numerically. Its solution for a typical trap, however, is identical to the solution of the Hartree-Fock equation with the approximation $V(\mathbf{x})\approx 4\pi\hbar^2 m^{-1} a_{\rm B}\delta(\mathbf{x})$ again because of the disparity in length scales. The first Born approximation to the scattering length for a Morse potential is given by

$$a_{\rm B} = \frac{D}{4a_0\beta^2\alpha^3\hbar\omega}e^{\alpha r_0}\left(e^{\alpha r_0}-16\right). \tag{63}$$

With all quantities on the right hand side in SI units, $a_{\rm B}$ will be in atomic units.

From Eq. (63), it is clear that using a realistic potential directly in the Hartree-Fock equations will give quantitatively poor results since as a function of D, $a_{\rm B}$ is monotonic. The physical scattering length shows a tangent-like pole structure as in Fig. 3. The shortcoming is especially evident for negative scattering lengths since $a_{\rm B}$ will most likely remain positive even in this case. This is true for the present negative scattering length example. For a_{sc}=−26.8031 a.u., $a_{\rm B}$=332.616 a.u. and the total energy is 4.5445 $\hbar\omega$. The energy shift from three noninteracting particles for a_{sc}=3.11915 a.u. is in the right direction, but is overestimated since $a_{\rm B}$=28.1083 a.u.; the total energy in this case is 4.5038 $\hbar\omega$.

3.5.3 Hartree-Fock in the shape independent approximation. The details of solving the Hartree-Fock equation in this approximation are explained at length in Secs. 3.6 and 3.7 and App. D. The total energies are 4.5004 $\hbar\omega$ for a_{sc}=3.11915 a.u. and 4.4964 $\hbar\omega$ for a_{sc}=−26.8031 a.u. Both results are identical to the hyperspherical to the five digits shown. The deviation from the noninteracting energy of 4.5 $\hbar\omega$, however, is small. I expect that as this shift

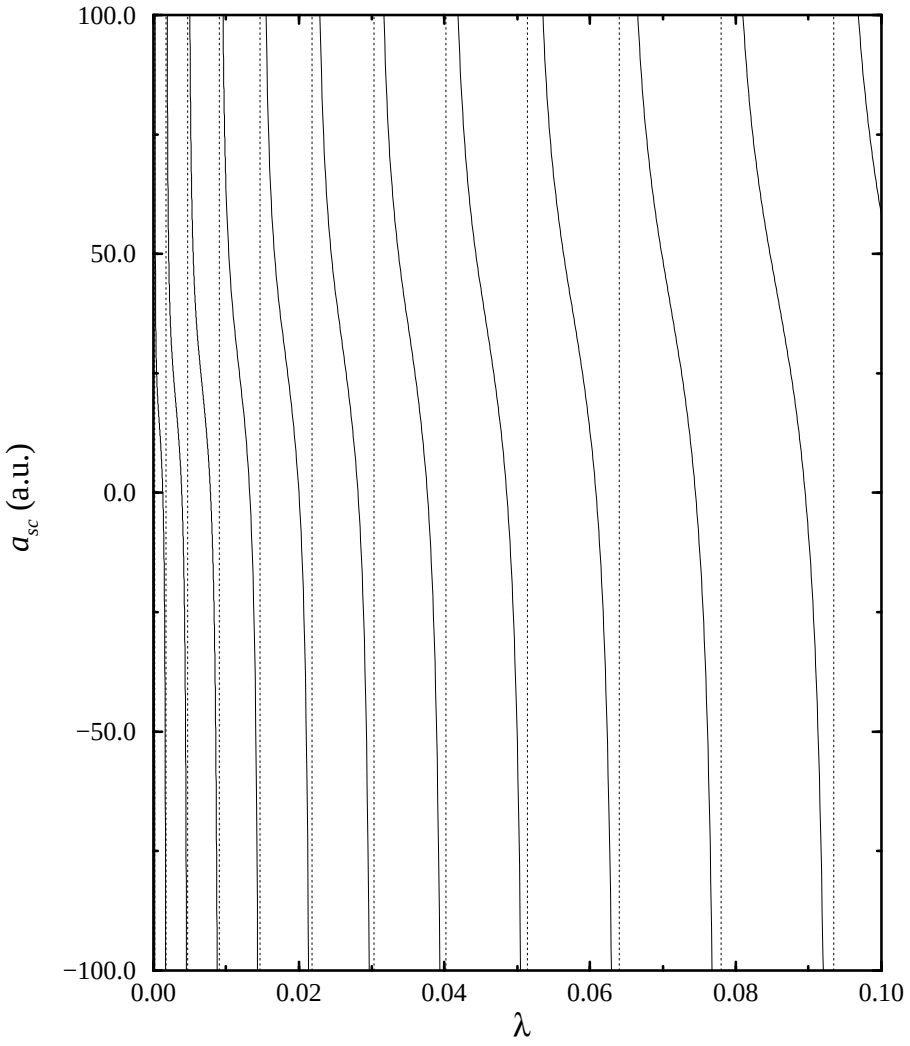

Figure 3. The two-body ^{87}Rb+^{87}Rb triplet scattering length as a function of the depth of the potential λ. The shape of the potential is fixed. The solid lines are the scattering length itself, and the dotted lines mark the values of λ at which a new two-body bound state is added.

increases — through increasing the number of particles, the trap frequency, or the scattering length — that the shape independent Hartree-Fock approximation will deteriorate compared to the hyperspherical results. The basis for this expectation is that correlation between particles will grow increasingly important as the mean interparticle spacing approaches the magnitude of the scattering length and that the hyperspherical approach incorporates correlation much more naturally than any independent particle approximation.

3.6 Isotropic trap results

In nearly all of the traps in which BEC has been observed to date, the aspect ratio of the trapping frequencies is not unity. In fact, most are cylindrically symmetric with the ratio of trapping frequency in the z direction to that in the ρ direction ranging from a pancake-like $\sqrt{8}$ for the TOP trap to a cigar-like 0.05 for the MIT Ioffe trap. Notable exceptions are the Rice permanent magnet trap which is nearly isotropic and, again, the MIT Ioffe trap. The aspect ratio of the MIT Ioffe trap can be adjusted from a highly asymmetric configuration to one that is isotropic.

Since there has been only one experiment to date in an isotropic trap [83], most theoretical work has been carried out for the more experimentally relevant cylindrically symmetric case. Nevertheless, for many purposes the spherically symmetric trap is attractive theoretically largely because it reduces to a one dimensional problem in the independent particle approximation. Numerical solution of the Hartree-Fock equation is thus greatly simplified and much less time consuming. Additionally, the solution of the Hartree-Fock equation for both the ground and excited states depends on only one parameter, making general and exhaustive studies of the available parameter space much simpler. The physics of condensates with negative scattering lengths, for instance, can be well characterized within the Hartree-Fock approximation by a single critical parameter. I will present in this section a selection of results for the isotropic case, discussing in particular the case of negative scattering lengths and the role of the critical parameter.

For a spherically symmetric harmonic trapping potential, the Hartree-Fock equation, Eq. (25), in the shape independent approximation simplifies to

$$\left[-\frac{\hbar^2}{2m}\nabla^2+\frac{1}{2}m\omega\, r^2+\frac{4\pi\hbar^2 a_{sc}}{m}\,(N-1)\,|\psi_0(r,\theta,\phi)|^2\right]\psi_0(r,\theta,\phi)=\varepsilon_0\psi_0(r,\theta,\phi). \qquad (64)$$

As in Sec. 3.5.2, I scale the wave function as

$$\psi_0(r,\theta,\phi)=\beta^{-\frac{3}{2}}\chi_0(x)Y_{00}(\theta,\phi)=\beta^{-\frac{3}{2}}\frac{\chi_0(x)}{\sqrt{4\pi}}$$

where $\beta=\sqrt{\hbar/m\omega}$ is the oscillator length scale and $r=\beta x$. The scaled equation for $\chi_0(x)$ is then

$$\left[-\frac{1}{2}\frac{1}{x^2}\frac{d}{dx}\left(x^2\frac{d}{dx}\right)+\frac{1}{2}x^2+(N-1)\,\tilde{a}_{sc}\,|\chi_0(x)|^2\right]\chi_0(x)=\tilde{\varepsilon}_0\chi_0(x). \qquad (65)$$

In this equation, a quantity with a tilde is the scaled counterparts of the same quantity without a tilde in Eq. (64), *i.e.* $a_{sc}=\beta\tilde{a}_{sc}$ and $\varepsilon_0=\hbar\omega\tilde{\varepsilon}_0$. Note that the only dependence upon trap and scattering parameters and the number of atoms enters in the combination $(N-1)\,\tilde{a}_{sc}$. Labeling this combination α, it is clear that the solutions of the Hartree-Fock equation for an isotropic trap are completely characterized by α. For instance, I show in Fig. 4 the scaled ground state orbital energy as a function of α, for α between the critical value of -0.57497 and about 70. For the largest positive α and parameters roughly corresponding to ^{87}Rb (a_{sc}=100 a.u. and m=86.909188 amu) in a trap with $\omega=2\pi\,200$ Hz, this corresponds to about 10^4 atoms. The critical value for negative scattering lengths corresponds to about 22 ^{85}Rb atoms ($a_{sc}=-400$ a.u. and m=84.911794 amu) in a trap with the same frequency. An α of zero corresponds to the noninteracting case or N=1. The dashed line in the figure is the Thomas-Fermi result [see Sec. 2.3, Eq. (13)]. It is in good semi-quantitative agreement with the Hartree-Fock result for nearly all α, and is low by a few percent at α=60. Negative scattering lengths cannot, of course, be treated in the simple Thomas-Fermi approximation since it results in a negative semi-definite probability density. The long dashed line in the figure is the orbital energy obtained from a variational approximation (see Eq. (36) in Sec. 3.2). Since the trial wave function in the variational calculation is the exact solution in the noninteracting limit, α=0, it stands to reason

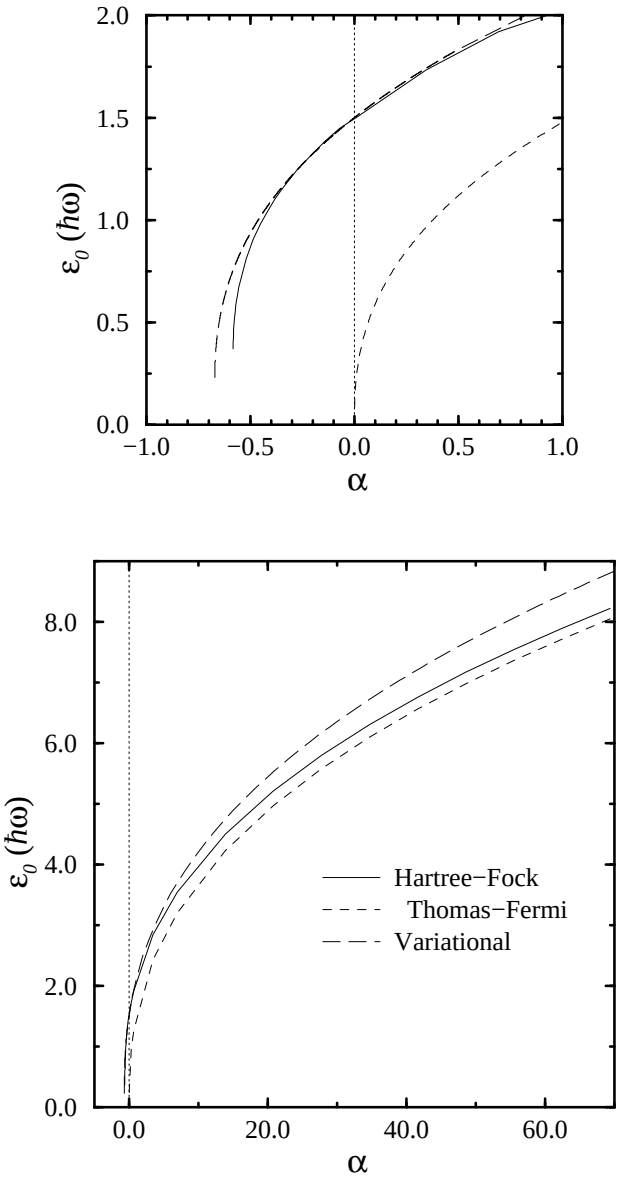

Figure 4. The ground state orbital energy $\tilde{\varepsilon}_0$ for an isotropic trap as a function of $\alpha=(N-1)\,\tilde{a}_{sc}$ for both positive and negative scattering lengths. The solid line is the result of solving the Hartree-Fock equation, Eq. (65); the dashed line is the Thomas-Fermi approximation, Eq. (13); the long-dashed line is the variational result, Eq. (36); and the dotted line marks the location α=0. The upper plot shows an enlargement of the region near α=0.

that the orbital energy agrees well in that region, but for increasing α, the agreement steadily worsens. It is the negative α region, however, that is of interest here, and the agreement there is reasonably good. For negative scattering lengths (*i.e.* negative α), the ground state orbital energy $\tilde{\varepsilon}_0(\alpha)$ is rapidly decreasing as α decreases until $\tilde{\varepsilon}_0(\alpha)$ reaches a point of infinite slope. The point at which this occurs is the critical value of α, α_c=−0.57497. As α approaches α_c from above, the orbital energy changes from positive to negative indicating that the total energy decreases with the addition of one more atom. The solution of the Hartree-Fock equation in the region of this sign change is difficult to obtain numerically and so negative orbital energies are not actually obtained.

Figure 5 shows the total energy of the Hartree-Fock ground state for the approximate ^{87}Rb parameters listed above. Notice that the total energy computed from Eq. (26) depends on N as well as on α. Equation (26) can be rearranged, however, to show that the total energy per particle *is* a function of only α. The lower plot shows the total energy as a function of $N\text{sign}(\alpha)$ over the whole range of N while the upper plot shows an expanded view around N_c. From the upper plot, it is clear that the total energy displays no abrupt behavior near N_c.

In terms of the ground state Hartree-Fock equation, the physics of the ground state behavior including the instability near α_c can be understood from the effective one-body potential

$$V_{eff}(x) = \frac{1}{2}x^2 + \alpha\left|\chi_0(x)\right|^2.$$

Figure 6 shows $\chi_0(x)$ for several values of α both positive and negative; and in Fig. 7, the corresponding effective potentials $V_{eff}(x)$. For positive α, the mean field — $\alpha\left|\chi_0(x)\right|^2$ — is repulsive resulting in a much broader ground state orbital. In Fig. 6, the broadest wave function at the bottom of the plot is for $\alpha\approx 7\times 10^4$ or $N\approx 10^7$ ^{87}Rb atoms. The uppermost curve of the lower plot in Fig. 7 is the corresponding effective one-body potential. It is quite solidly in the Thomas-Fermi limit with the Thomas-Fermi orbital energy in error by only about 0.01%. This can also be seen from the fact that the effective potential has essentially reached

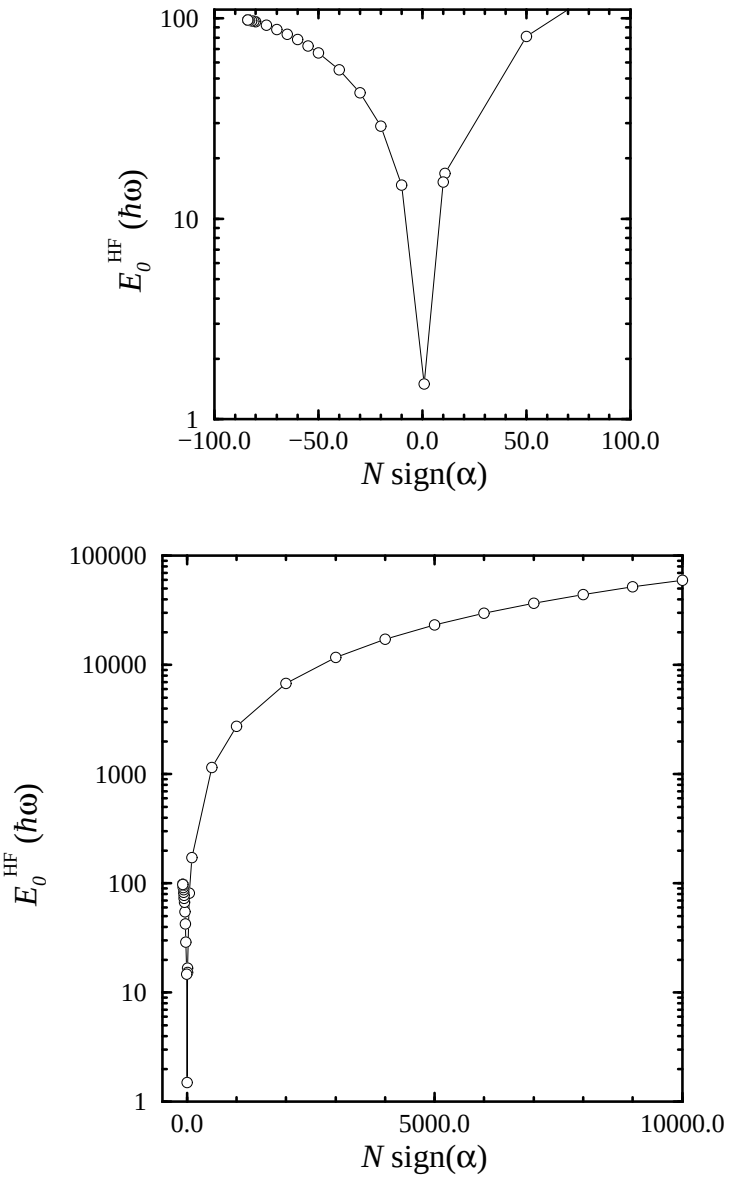

Figure 5. The total ground state energy $E_0^{\rm HF}$ for ^{87}Rb in an isotropic trap as a function of N for the approximate ^{87}Rb parameters noted in the text. The lower plot shows the energy over the range of N corresponding to Fig. 4; the upper plot focuses on the negative scattering length region.

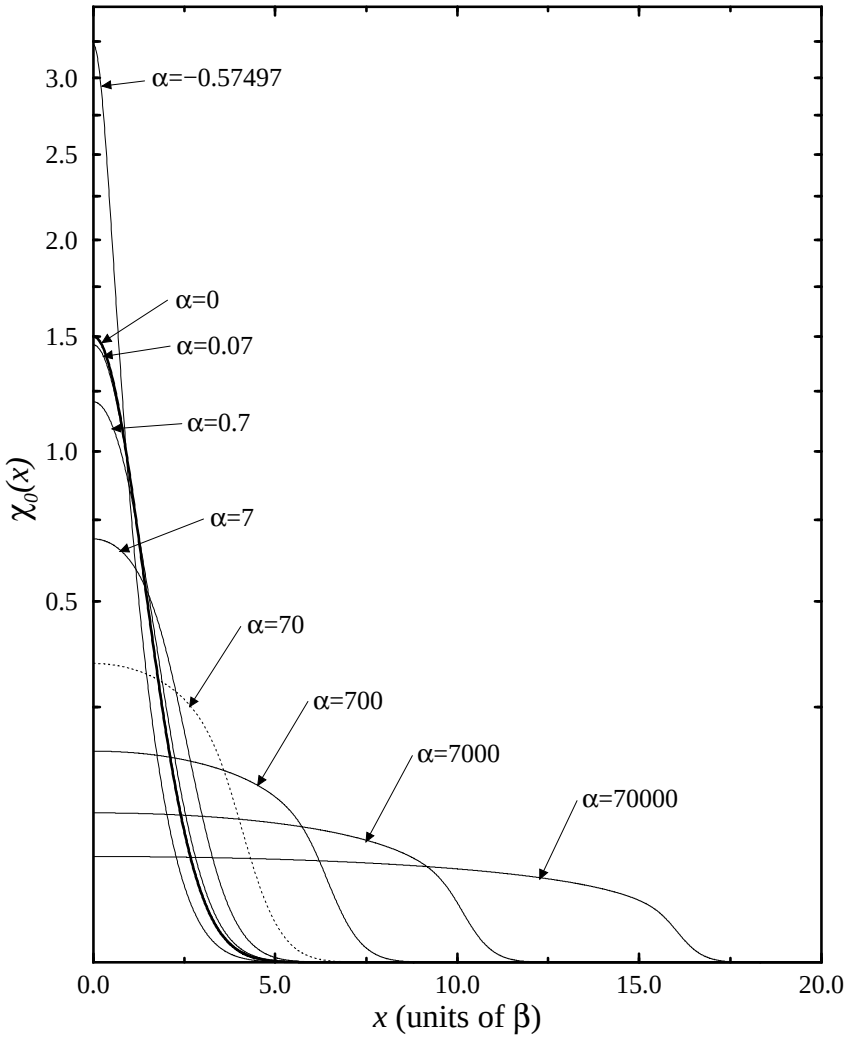

Figure 6. Solutions of the Hartree-Fock equation for several values of α. The thick line marks the α=0 solution. The first wave function below it corresponds to $\alpha\approx$0.07 with α for each subsequent curve below it increasing by roughly an order of magnitude. The broadest curve has an α of approximately 7×10^4, and the dotted curve has $\alpha\approx$70 corresponding to the dotted curves in Fig. 7. The wave function above the α=0 solution has α=−0.57497. Notice that the vertical scale is a square root scale.

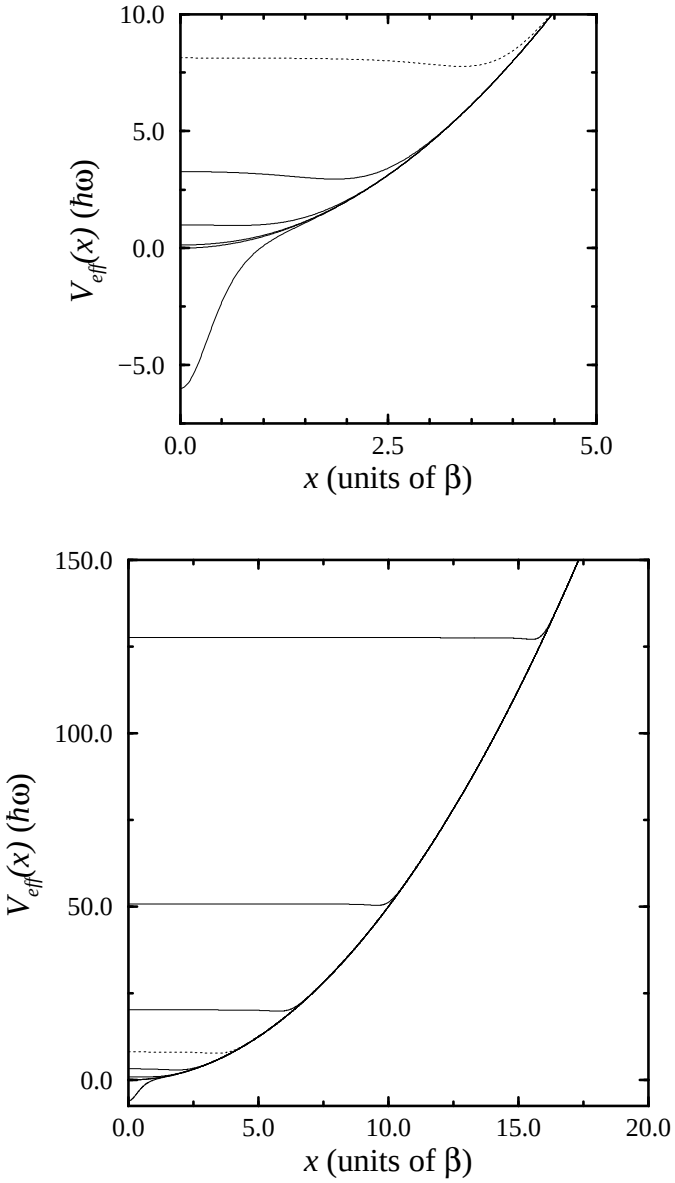

Figure 7. The effective ground state orbital one-body potentials corresponding to the wave functions in Fig. 6. The lower plot shows all of the effective potentials; and the upper plot, an expanded view of the smaller α curves. The dotted line in both upper and lower plots marks the effective potential for the dotted wave function of Fig. 6. The lowest curve in each plot is the effective potential for α=−0.57497.

the liquid model limit (as discussed in Sec. 2.3) except for a small region near the turning point where the Thomas-Fermi approximation always breaks down. The dotted line in both figures is the wave function for $\alpha \approx 70$ or $N \approx 10^4$ ^{87}Rb atoms. This is the largest α shown in the other figures of this section and is less accurately modeled by the Thomas-Fermi approximation since the ground state orbital energy differs by about 2% from the Hartree-Fock result. The thick line in Fig. 6 marks the wave function for the noninteracting limit ($N=1$) while the much narrower wave function is the result for $\alpha \approx \alpha_c$. The effective potential for the latter case is the lowest curve in each plot of Fig. 7. These curves partially reveal the nature of the instability in that the mean field leads to an effective potential which is attractive. At some point, this attraction overwhelms the kinetic energy, and the ground state orbital is drawn wholly into the well at which point the orbital energy becomes negative.

The effective one-body potentials are also useful for understanding the various approximations to the low lying excitation spectrum. Recall from the discussion following the quasi-Hartree-Fock equation, Eq. (23), that the mean field due to the ground state orbital that the excited states "see" is a factor of two larger in the Hartree-Fock equation than in the quasi-Hartree-Fock equation. This difference leads to drastically different behavior of the first several excited state orbitals. To illustrate this point, Fig. 8 shows the effective potentials and lowest six excited state orbitals for the quasi-Hartree-Fock and Hartree-Fock approximations for $\alpha \approx 70$. In the lower plot, the effective one-body potential in the Hartree-Fock approximation clearly shows a barrier — the result of the larger mean field. In fact, the barrier is high enough (approximately $\tilde{\varepsilon}_0$ high) in this example that three of the six states lie below the top of the barrier and are localized in the well. The energies and orbital wave functions are distinctly different than for the quasi-Hartree-Fock results in the upper plot. The effective potential in the quasi-Hartree-Fock approximation is exactly the same as for the ground state orbital calculation and thus is essentially flat across the bottom. Being wider and flatter than the Hartree-Fock potential, the first few quasi-Hartree-Fock orbital energies are more closely spaced. Since the Hartree-Fock approximation diagonalizes the many-body Hamiltonian in the space of single

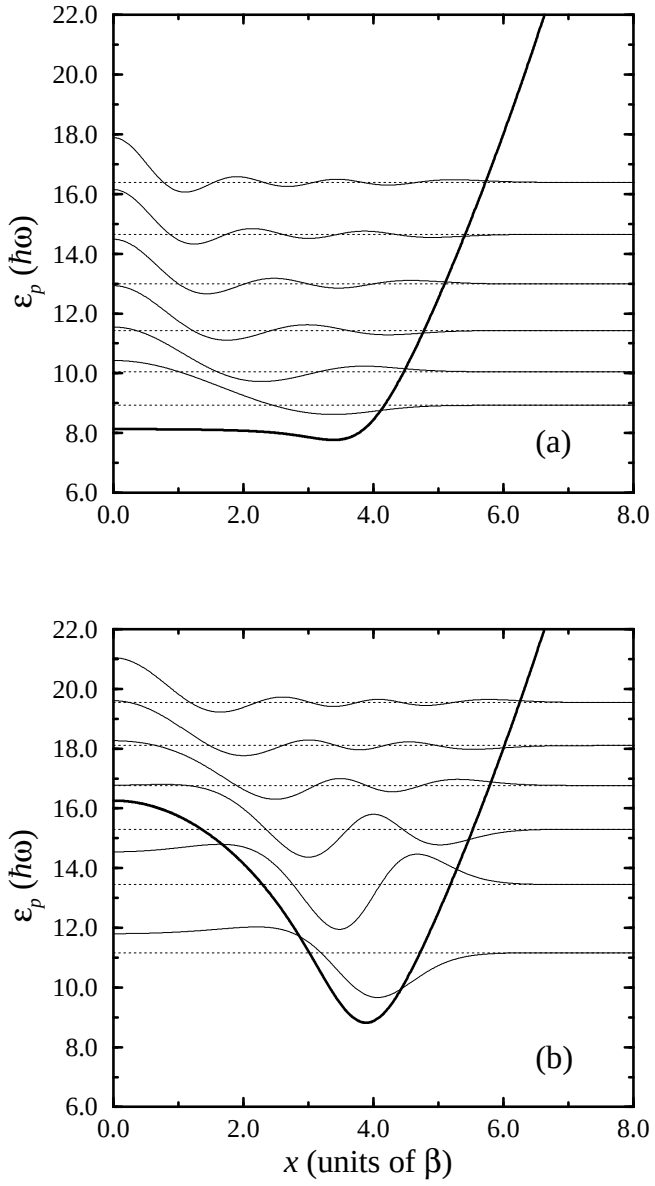

Figure 8. The effective one-body potential and six lowest ℓ=0 excited state orbital wave functions in the quasi-Hartree-Fock and Hartree-Fock approximations for $\alpha\approx 70$. The lower plot shows the Hartree-Fock approximation results. The thick line is the effective one-body potential, the thin solid lines the six lowest excited state orbitals, and the thin solid lines the excited state orbital energies. The same notation applies to the quasi-Hartree-Fock results in the upper plot. The scale on the left of each plot measures the energy for the effective potential and the orbital energies.

particle excitations and the quasi-Hartree-Fock does not, the Hartree-Fock spectrum should be more accurate. It is, in fact, and the comparison will be explored in more detail in the next section. Here, I will focus more on the question of whether the barrier in the Hartree-Fock approximation is physical or has any observable consequences.

Since the Hartree-Fock approximation is the best effective one-body — or mean field — theory, the effective potential cannot be directly compared with one from a more sophisticated theory. Instead, the effect of the barrier, or lack thereof, must be inferred from the spectrum. The lower plot of Fig. 9 shows the spectrum for zero total orbital angular momentum in both the Hartree-Fock and random phase approximations. The thin solid lines denote the results of solving the scaled RPA equations in the pseudopotential approximation:

$$\sum_{p\neq 0}\Big[\,\tilde{B}_{qp}X_{p\nu}+\tilde{C}^{*}_{qp}Y_{p\nu}\Big]=\,\tilde{\omega}^{\rm RPA}_{\nu}\,X_{q\nu}$$
$$\sum_{p\neq 0}\Big[\,\tilde{C}_{qp}X_{p\nu}+\tilde{B}^{*}_{qp}Y_{p\nu}\Big]=-\tilde{\omega}^{\rm RPA}_{\nu}\,Y_{q\nu}.$$

In these equations, $\tilde{B}_{qp}$ and $\tilde{C}_{qp}$ are given by

$$\tilde{B}_{qp}=\alpha\mathcal{V}_{q0,p0}+\tilde{\omega}_{q0}\delta_{qp}$$
$$\tilde{C}_{qp}=\alpha\mathcal{V}_{qp,00},$$

since in the pseudopotential approximation a dimensionless matrix element $\mathcal{V}$ can be defined

$$\mathcal{V}_{p'0,p0}\,=\,\delta_{\ell,\ell'}\delta_{m,m'}V_{p'p}$$
$$\mathcal{V}_{p'p,00}\,=\,\delta_{\ell,\ell'}\delta_{m,-m'}V_{p'p}.$$

The quantity $V_{p'p}$ entering these equations is just the radial integral

$$V_{p'p}=\int\!x^{2}dx\,\chi_{n'\ell}(x)\,|\chi_{0}(x)|^{2}\,\chi_{n\ell}(x).$$

Notice that these expressions have been written in the quasi-Hartree-Fock basis. That is, the orbital wave functions $\chi_{n\ell}(x)$ are solutions of

$$\left[-\frac{1}{2}\frac{1}{x^{2}}\frac{d}{dx}\left(x^{2}\frac{d}{dx}\right)+\frac{\ell\,(\ell+1)}{2\,x^{2}}+\frac{1}{2}x^{2}+\alpha\,|\chi_{0}(x)|^{2}\right]\chi_{n\ell}(x)=\tilde{\varepsilon}_{n\ell}\chi_{n\ell}(x).$$

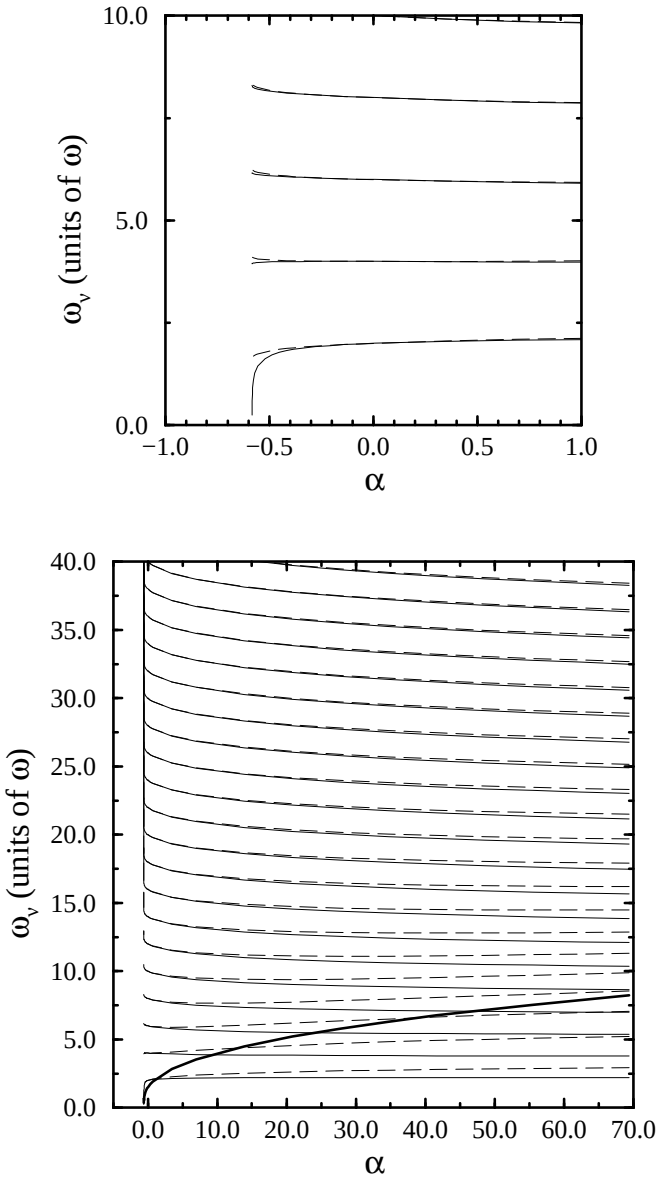

Figure 9. The L=0 excitation spectrum in the random phase and Hartree-Fock approximations for $\alpha \approx 70$. The lower plot shows the lowest twenty zero total angular momentum excited states, and the upper plot shows an expanded view around α_c. The solid lines are the RPA results and the long dashed are the Hartree-Fock results.

The orbital energy depends on both n and ℓ since the mean field breaks the ℓ-degeneracy. If the Hartree-Fock basis had been used instead, the matrix $\tilde{B}$ would simply be the diagonal matrix with entries $\tilde{\omega}_{q0}$ and $\chi_{n\ell}(x)$ would be the solution of the same equation with α replaced by 2α. In Fig. 9, the long dashed lines are the Hartree-Fock excitation energies which are just the difference of the orbital energies [see Eq. (27)]. The first feature that is relevant is the relatively good agreement between Hartree-Fock and RPA for higher lying excitations [20]. "Higher lying" in this case being a few to several times the barrier height (approximately the orbital energy) which is indicated in the figure by the thick solid line. The second feature that is relevant is the poor agreement of the Hartree-Fock and the RPA for excitations on the order of the barrier height. Such poor agreement would seem to indicate that the barrier is not physical and that much of the improvement of RPA over Hartree-Fock comes in removing its artifacts.

This figure is also interesting in that it displays the symptoms of instability described in Sec. 3.2. The upper plot enlarges the region around α=0 showing that the lowest RPA excitation frequency is diving to zero just at α_c. As discussed in Sec. 3.2, this indicates that the Hartree-Fock ground state is no longer a good zeroth order approximation to the true ground state. That is, the true ground state has a large admixture of Hartree-Fock excited states in addition to the ground state. It is also instructive to note that the Hartree-Fock approximation agrees with the RPA quite well for negative α. This agreement is less than impressive given that both approximations agree for similar magnitude positive α's as well. Somewhat surprising, though, is that the lowest Hartree-Fock state turns over towards zero just as the RPA result does near α_c. In this wholly uncorrelated approximation, the effective one-body potential is not attractive enough.

3.7 Anisotropic trap results

To make a closer connection to experiment, I consider in this section a system of atoms trapped by a cylindrically symmetric harmonic potential. This is the applicable symmetry for all of the traps in which BEC has been observed [1, 2, 3, 4, 5, 6, 7, 87].

With a delta function interaction and a harmonic trapping potential, the Hartree-Fock equation, Eq. (25), simplifies to

$$\left[-\frac{\hbar^2}{2M}\nabla^2+\frac{1}{2}M\left(\omega_\rho^2\rho^2+\omega_z^2z^2\right)+\frac{4\pi\hbar^2a_{sc}}{M}\left(N-1\right)\left|\psi_0(\rho,\phi,z)\right|^2\right]\psi_i(\rho,\phi,z)=\varepsilon_i\psi_i(\rho,\phi,z). \tag{66}$$

I assume that the single particle orbitals have the same symmetries as the trapping potential. Specifically, I take them to be eigenstates of L_z and Π_z which are the projection of orbital angular momentum on the z-axis and the parity with respect to the xy-plane, respectively. Each single particle orbital is thus labeled by an energy quantum number n and the quantum numbers m and π_z for L_z and Π_z, respectively. These symmetry considerations lead to the following choice for $\psi_i(\mathbf{x})$:

$$\psi_i(\rho,\phi,z)=\beta^{-\frac{3}{2}}\,\chi^{\pi_z}_{n|m|}(\xi,\eta)\,\frac{e^{im\phi}}{\sqrt{2\pi}}.$$

In this expression, β is the length scale for a harmonic oscillator of frequency ω,

$$\beta=\sqrt{\frac{\hbar}{M\omega}}.$$

The scaled coordinates ξ and η are related to the physical coordinates by

$$\rho=\beta\xi \text{ and } z=\beta\eta.$$

The specific form of $\psi_i(\mathbf{x})$ is chosen so that

$$\int\xi d\xi\int d\eta\ \left|\chi_i(\xi,\eta)\right|^2=1$$

gives

$$\int\rho d\rho\int dz\int d\phi\ \left|\psi_i(\rho,z,\phi)\right|^2=1.$$

The rescaled Hartree-Fock equation for $\chi_i(\xi,\eta)$ now reads

$$\left[-\frac{1}{2\xi}\frac{\partial}{\partial\xi}\left(\xi\frac{\partial}{\partial\xi}\right)-\frac{1}{2}\frac{\partial^2}{\partial\eta^2}+\frac{m^2}{2\xi^2}+\frac{1}{2}\left(\omega_\xi^2\xi^2+\omega_\eta^2\eta^2\right)+2\alpha\left|\chi_0(\xi,\eta)\right|^2\right]\chi_i(\xi,\eta)=\tilde{\varepsilon}_i\chi_i(\xi,\eta) \tag{67}$$

where the dimensionless trap frequencies are ω_ξ=ω_ρ/ω, ω_η=ω_z/ω, the scaled single particle energy is $\tilde{\varepsilon}_i$=$\varepsilon_i/\hbar\omega$, and the dimensionless nonlinear parameter that characterizes the interaction strength is still

$$\alpha = (N-1)\frac{a_{sc}}{\beta}.$$

From Eq. (67) one can show that all energies with m>0 are doubly degenerate. For the ground state, Eq. (67) is a self-consistent equation. Having obtained the self-consistent ground state, it becomes straightforward to solve for the excited orbitals, since the equation is then a linear Schrödinger equation with a static potential comprised of the trapping potential plus the mean field contribution of the ground state. The resulting set of single particle orbitals thus forms a complete, orthonormal basis.

Now that a set of single particle orbitals has been determined, I can set up and solve the RPA equations. To do this, I first need the interaction matrix elements. As in Eq. (66), for delta function interactions the direct and exchange contributions to the potential matrix elements are identical. In other words, $\langle q0\,|V|\,p0\rangle$=$\langle q0\,|V|\,0p\rangle$. With $p\equiv\{n, m, \pi_z\}$,

$$\langle p'0\,|V|\,p0\rangle = \frac{2\hbar^2 a_{sc}}{M\beta^3}\,\mathcal{V}_{p'0,p0}$$

with the dimensionless matrix element defined by

$$\mathcal{V}_{p'0,p0} = \delta_{m,m'}\delta_{\pi_z,\pi'_z}V_{p'p} \tag{68}$$

where

$$V_{p'p} = \int\xi d\xi\int d\eta\,\chi^{\pi_z}_{n'|m|}(\xi,\eta)\left|\chi^{+}_{00}(\xi,\eta)\right|^2\chi^{\pi_z}_{n|m|}(\xi,\eta).$$

In the same notation,

$$\mathcal{V}_{p'p,00} = \delta_{m,-m'}\delta_{\pi_z,\pi'_z}V_{p'p}. \tag{69}$$

The only difference between the matrix elements in Eqs. (68) and (69) — the delta function in m — arises physically from conservation of total L_z. Thus, only states with the same total projection M_L are coupled. The parity delta function is also readily understood since both

matrix elements are integrated over all z and contain χ_0^2, which is an even function of z. The RPA equations then reduce to

$$\begin{pmatrix} \tilde{B} & \tilde{C} \\ \tilde{C} & \tilde{B} \end{pmatrix} \begin{pmatrix} X \\ Y \end{pmatrix} = \tilde{\omega} \begin{pmatrix} X \\ -Y \end{pmatrix} \tag{70}$$

where $\tilde{\omega}_\nu/\omega$ is the rescaled excitation frequency and

$$\begin{aligned} \tilde{B}_{qp} &= 2\alpha \mathcal{V}_{q0,p0} + \tilde{\omega}_{q0}\delta_{qp} \\ \tilde{C}_{qp} &= 2\alpha \mathcal{V}_{qp,00} \end{aligned}$$

are the rescaled matrices from Eq. (33).

The delta functions in the expressions for the integrals reduce the computational burden of solving the RPA equations significantly. Specifically, the RPA equations can be diagonalized separately for each π_z and $|m|$. Moreover, the structure of the RPA matrix yields automatically that all excitation energies for each positive m are degenerate with the excitation energies for $-m$.

I have solved the Hartree-Fock and RPA equations for parameters appropriate to the JILA experiment, ν_ρ=$\nu_z/\sqrt{8}$=133 Hz [1, 9] and a_{sc}=110 a.u. [85]. Note that in all of my numerical calculations I choose the frequency scale ω to be ω_ρ. Figure 10 shows the Hartree-Fock energies for the ground state as a function of the number N of trapped atoms. The lower plot of Fig. 10 shows the total Hartree-Fock ground state energy $E_0^{\rm HF}$ from Eq. (26); and the upper plot, the Hartree-Fock ground state orbital energy ε_0. The N dependence of the two is quite different as is, of course, their physical interpretation. The total energy sets the absolute scale for the excitation spectrum while the orbital energy is the energy necessary to remove one atom completely from the ground state. For N=5000, I have also calculated the RPA shift in the ground state energy ΔE_0=$\left|E_0^{\rm RPA} - E_0^{\rm HF}\right|$ to be 162.10 $\hbar\omega$. This lowers the Hartree-Fock ground state energy of 33492 $\hbar\omega$ by only 0.5% which is a good indication that the quasi-boson approximation, replacing the RPA ground state by the Hartree-Fock ground state, is valid.

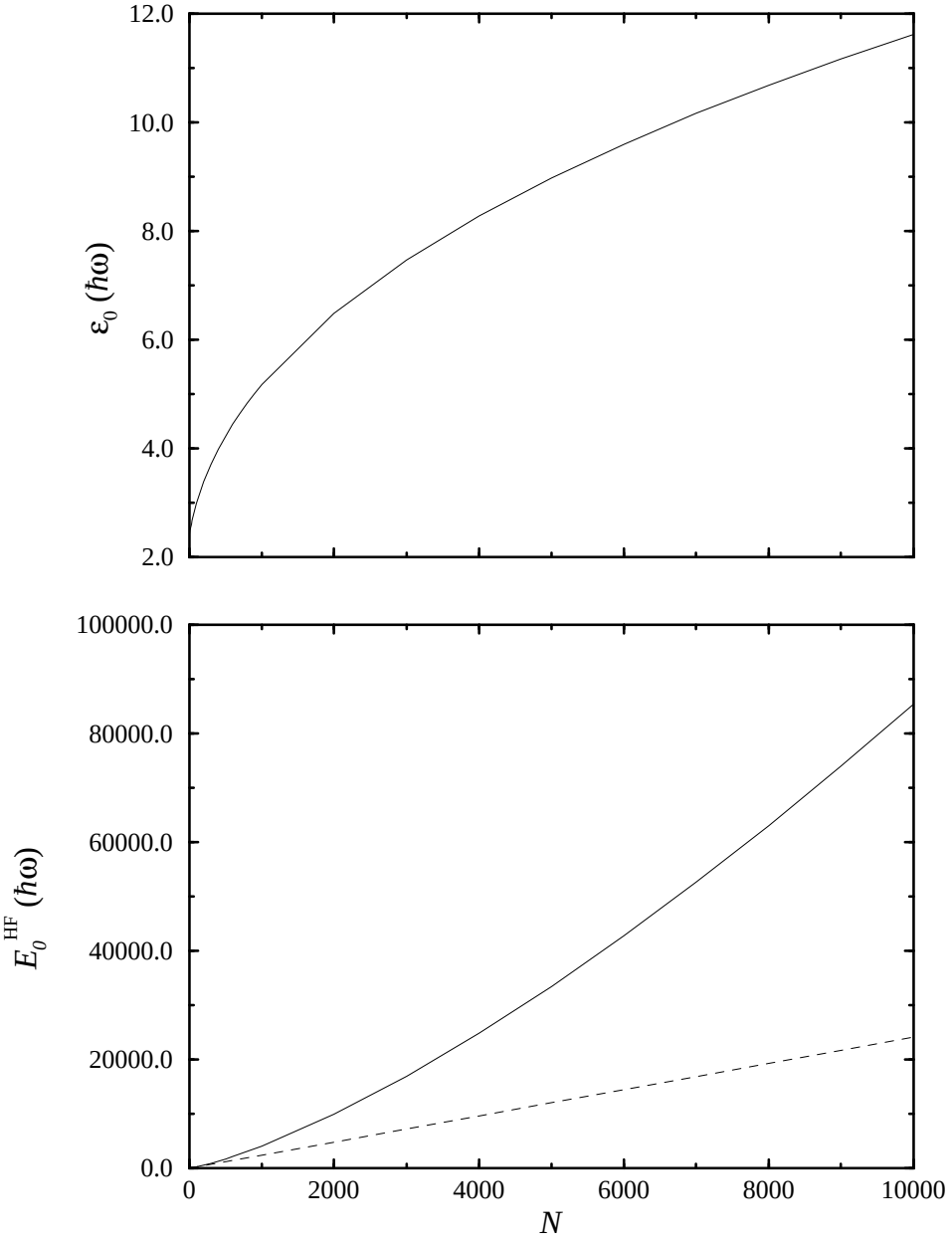

Figure 10. The Hartree-Fock ground state orbital and total energies. The lower plot shows the total energy, $E_0^{\rm HF}$ from Eq. (26), as a solid line. The dashed line is the total energy for a system of N noninteracting atoms. The upper plot shows the orbital energy $\tilde{\varepsilon}_0$. This figure adapted from Ref. [12].

From the expression for the RPA ground state energy, Eq. (51), the excitation spectrum and transformation coefficients for all m and π_z must in principle be calculated in order to evaluate the ground state energy shift. To approximately compute the energy shift, however, I solved the RPA equations for $m \leq 10$ and both z-parities, then constructed the scaled sum

$$\Delta\tilde{E}_0^{m\pi_z} = \sum_\nu \tilde{\omega}_\nu \left|Y_{m\pi_z\nu}\right|^2, \tag{71}$$

and extrapolated $\Delta\tilde{E}_0^{m\pi_z}$ to $m \to \infty$ using the empirical expression

$$\Delta\tilde{E}_0^{m\pi_z} = \tilde{\epsilon}_{\pi_z} e^{-\delta_{\pi_z} m}.$$

The coefficients $\tilde{\epsilon}_{\pi_z}$ and δ_{π_z} are the parameters for the fit. As shown in Fig. 11, this form fits the calculated points for both parities quite well for over the approximately order of magnitude decrease in $\Delta\tilde{E}_0^{m\pi_z}$ between m=0 and m=10. Including the degeneracy in m, the full ground state shift is then

$$\Delta\tilde{E}_0 = \sum_{\pi_z} \left(\Delta\tilde{E}_0^{0\pi_z} + 2\sum_{m=1}^{10} \Delta\tilde{E}_0^{m\pi_z} + 2\tilde{\epsilon}_{\pi_z} \sum_{m=11}^{\infty} e^{-\delta_{\pi_z} m} \right).$$

The last sum over m involves a geometric series and therefore is easily evaluated. I find that when summed over both parities it contributes approximately 14% to the total energy shift. It follows that the errors introduced through the empirical fit will lead to only small errors in the total energy shift.

To solve the RPA equations, it is only necessary to expand into a small number of quasi-Hartree-Fock single particle orbitals in order to obtain few percent accuracies in the low lying excitation energies. For example, with N=5000 atoms and m=0, a basis set of ten quasi-Hartree-Fock orbitals gives the lowest excitation energy to an accuracy of 0.7% compared to the converged result. Table 2 shows the convergence behavior for the lowest five excitation energies for N=5000 and m=0. For instance, when 60 orbitals are used the lowest excitation energy is converged to six significant figures. For comparison, the number of harmonic oscillator states necessary to obtain the same convergence can be estimated by expanding the highest energy

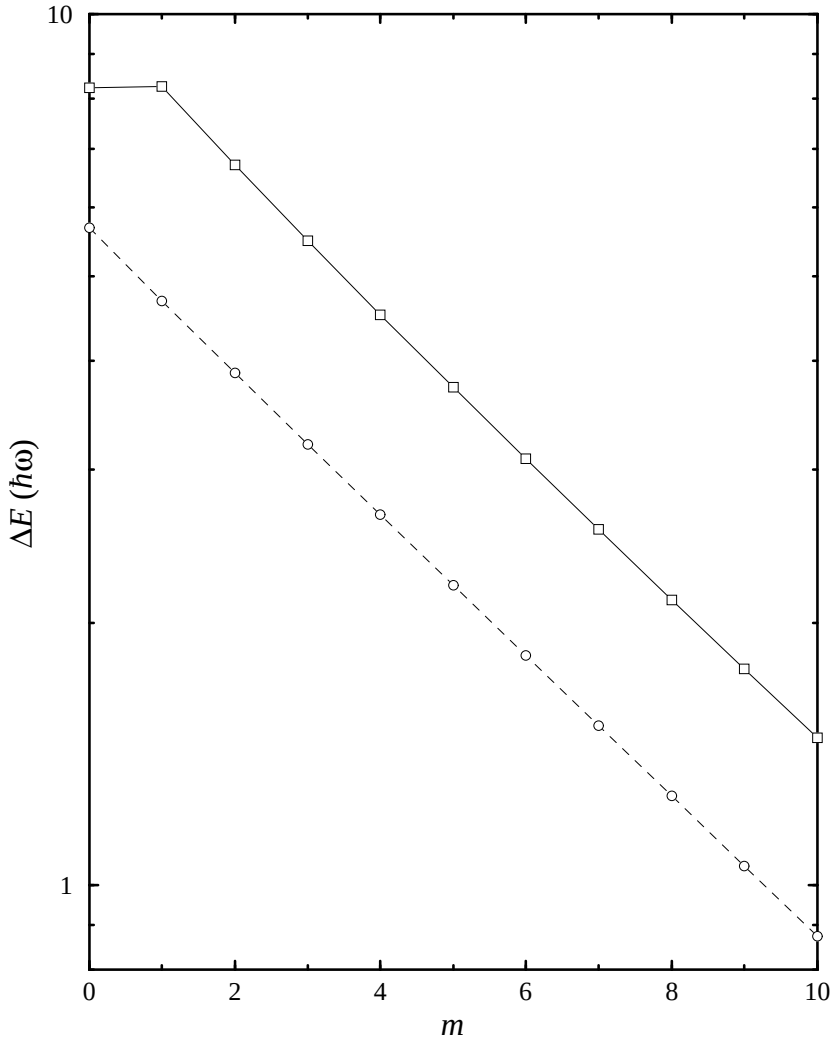

Figure 11. The shift in the total ground state energy, Eq. (71), for each z-parity as a function of m. The solid line is even z-parity and the dashed is odd. Notice that both follow an exponential decay quite closely (the vertical axis is logarithmic).

Table 2. The convergence of the RPA spectrum with respect to the size of the quasi-Hartree-Fock single particle orbital basis for N=5000 ^{87}Rb atoms and the JILA trap parameters. The frequencies $\tilde{\omega}_\nu$ are the scaled frequencies ω_ν/ω. This figure adapted from Ref. [12].

N_{basis}	$\tilde{\omega}_1$	$\tilde{\omega}_2$	$\tilde{\omega}_3$	$\tilde{\omega}_4$	$\tilde{\omega}_5$
10	1.87193	3.29129	4.77010	5.50449	6.21153
20	1.86003	3.26675	4.71695	5.15355	5.98377
40	1.85963	3.26573	4.71530	5.14483	5.97368
60	1.85958	3.26562	4.71512	5.14438	5.97331
80	1.85958	3.26562	4.71510	5.14432	5.97322

quasi-Hartree-Fock orbital in terms of harmonic oscillator states. Restricting the harmonic oscillator expansion using both m and π_z, it takes approximately 80 oscillator states to represent the 60-th quasi-Hartree-Fock orbital. In addition, as the nonlinear parameter α increases, the number of oscillator states needed to achieve a given level of convergence increases whereas the number of quasi-Hartree-Fock orbitals remains essentially constant.

In order to better understand whether excited state and ground state correlations make significant contributions to the excitation spectrum, I have calculated the spectrum in three of the approximations discussed above: the quasi-Hartree-Fock (QHF) approximation, the (frozen core) Hartree-Fock (HF) approximation or Tamm-Dancoff approximation (TDA), and the random phase approximation (RPA). The QHF approximation includes no correlation effects beyond those implied by identical particle statistics. Each of the QHF many-body states is thus simply a symmetrized product state (or a single configuration). The HF approximation is based upon an expansion on QHF single particle orbitals and allows correlations only among the singly excited QHF states. In other words, the HF approximation excited states are linear combinations of the QHF singly excited states. The ground state in the HF approximation, however, is just the QHF ground state. The RPA improves upon HF approximation by allowing correlations in the ground state as well as the excited states. As a result, both the ground state and the excited states in the RPA will be linear combinations of the QHF ground and excited states.

Figures 12-13 show the results of these calculations for both z-parities and M=0, 1, and 2. The RPA spectrum should be the most accurate of the three approximations as it includes the most correlation among the QHF states. Given this expectation, one sees from the dashed lines in Figs. 12 and 13 that the QHF excitation spectrum [calculated from $\hbar\omega_\nu^{\rm HF}=E_p^{\rm HF}-E_0^{\rm HF}$ and Eq. (27)] is in reasonable agreement with the RPA energies only for the higher lying states for N less than a few hundred to a thousand. This agreement suggests that the excitation is adequately described by the simple picture of a single particle being excited out of the ground state to a higher lying QHF state. Arguing on the basis of the nodal structure of the single

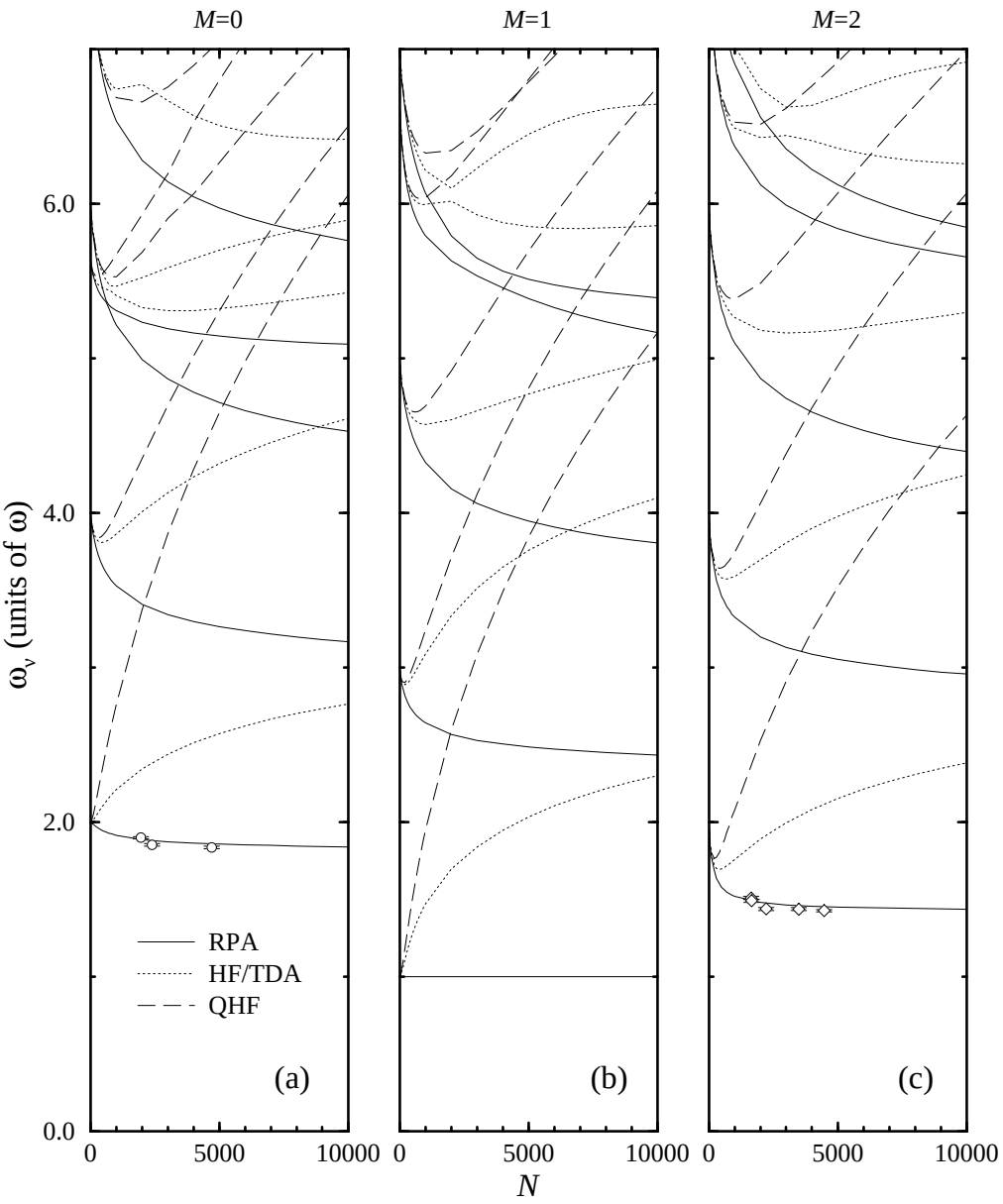

Figure 12. The even z-parity excitation spectra for ^{87}Rb atoms in a TOP trap in three different approximations: quasi-Hartree-Fock (QHF), dashed lines; Hartree-Fock (HF) or Tamm-Dancoff approximation (TDA), dotted lines; random phase approximation (RPA), solid lines. The points shown for M=0 and M=2 are those measured by Jin *et al.* [9]. This figure adapted from Ref. [12].

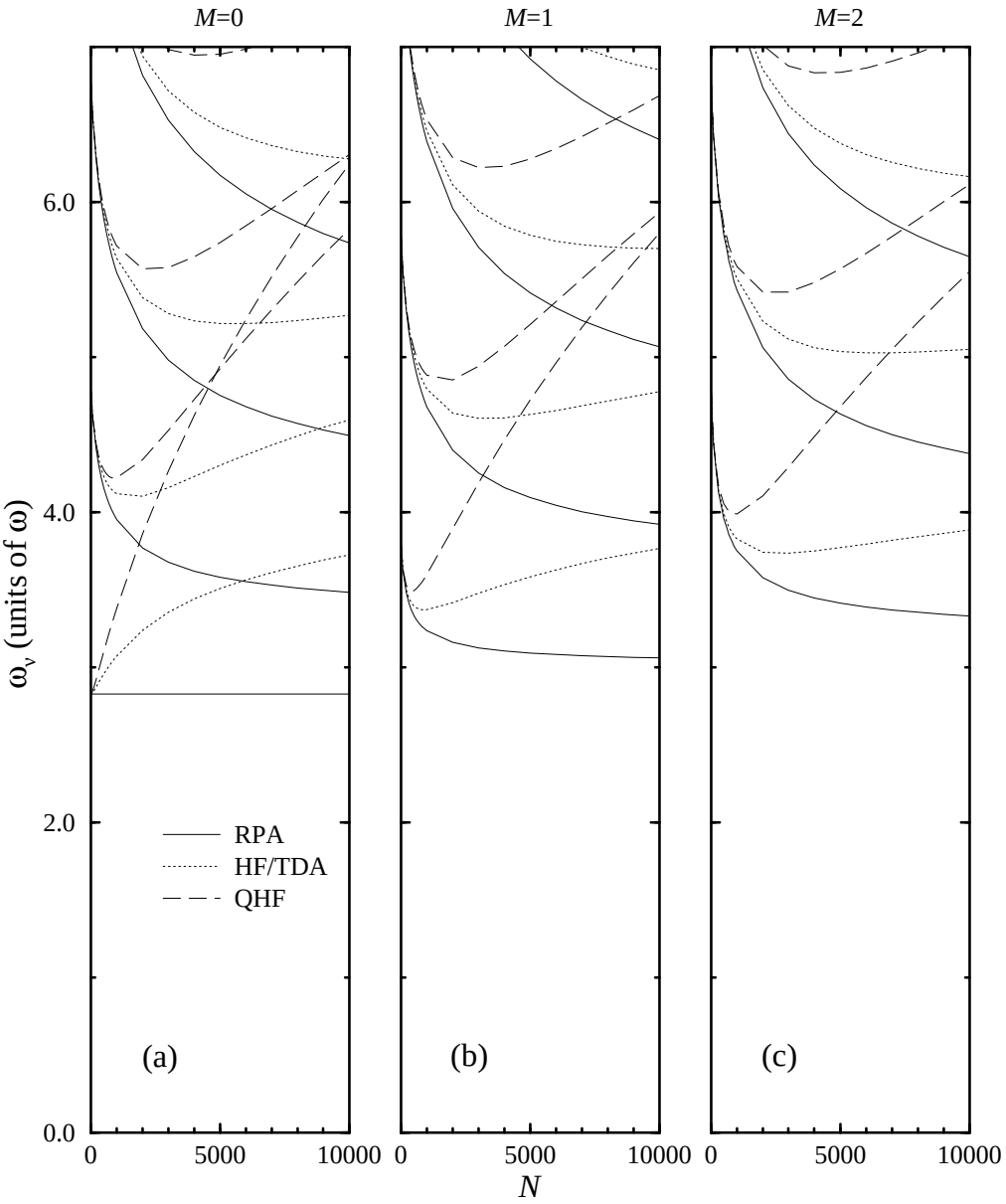

Figure 13. The odd z-parity excitation spectra for ^{87}Rb atoms in a TOP trap in three different approximations: quasi-Hartree-Fock (QHF), dashed lines; Hartree-Fock (HF) or Tamm-Dancoff approximation (TDA), dotted lines; random phase approximation (RPA), solid lines. This figure adapted from Ref. [12].

particle orbitals and Eq. (27), the agreement for higher lying excitations and odd z-parity seems reasonable since the mean field due to the ground state has less overlap with higher lying excited states which have an increasing number of nodes in the region of the mean field. Since the difference in QHF single particle orbital energies, $\varepsilon_p - \varepsilon_0$, decreases as N increases due to the flattening and widening of the bottom of the harmonic trapping potential by the mean field, the overlap of the single particle orbital and the mean field must be responsible for the increase in the QHF excitation energies with increasing N [see Eq. (27)]. By a similar argument, odd z-parity states will have less overlap with the ground state mean field than even z-parity states with a similar energy since they have a node at z=0 rather than an antinode. This is also the reason that the QHF spectrum for odd z-parity states is qualitatively closer to the RPA spectrum for larger N than the even z-parity states.

The Hartree-Fock spectrum, the dotted lines in Figs. 12 and 13, is an improvement on the QHF spectrum although the close agreement with the RPA spectrum is over essentially the same region of small N. However, for larger N the Hartree-Fock spectrum is quite a large improvement over the QHF spectrum. I can conclude that excited state correlations are important, but that the ground state correlations included in the RPA calculation are essential for accurate excitation energies. The solid lines in Figs. 12 and 13 are the RPA excitation spectra, and the points in Fig. 12 are the experimental points from the JILA measurement [9]. The agreement of the experimental points with the RPA spectrum — and disagreement with the other two spectra — bears out the expectation that the RPA is the more accurate approximation. However, the agreement is not perfect as Fig. 14 shows. Further, as shown in Ref. [9], the agreement of the RPA spectrum with the excitation spectrum obtained by Edwards *et al.* [11] from the Bogoliubov approximation is quite good over the range of N they computed.

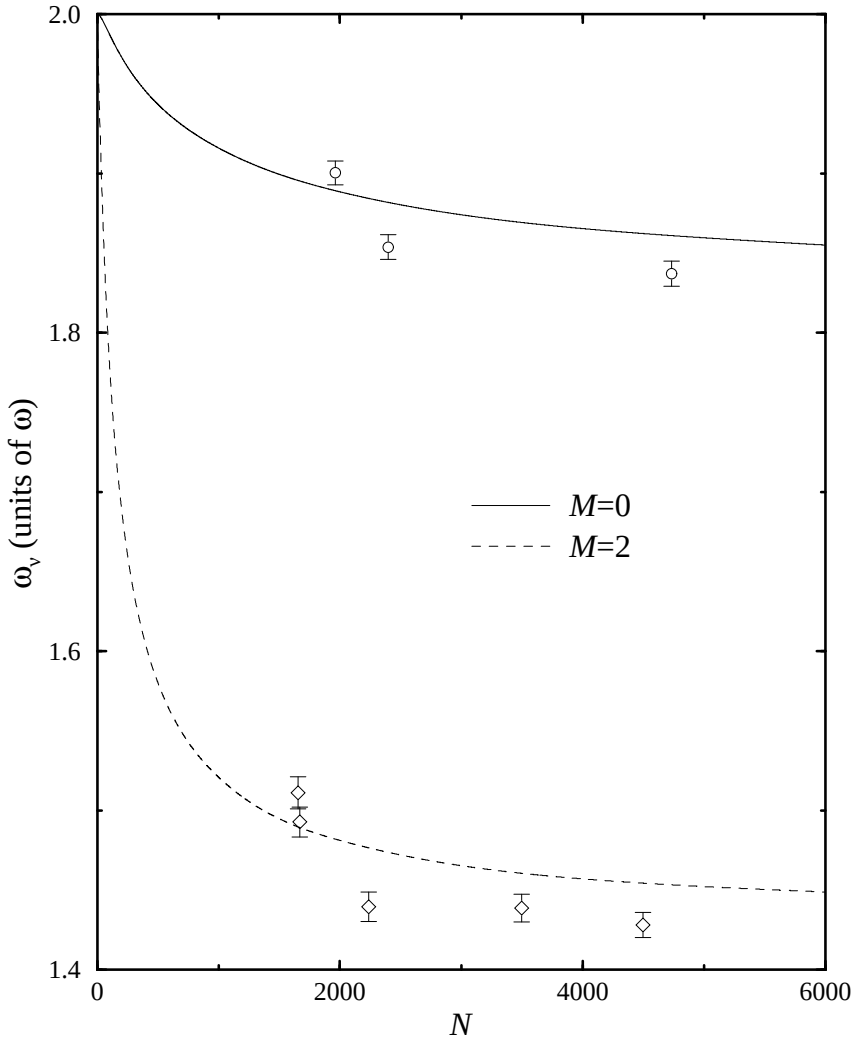

Figure 14. Comparison of the lowest M=0 (solid line) and M=2 (dashed line) random phase approximation (RPA) excitation frequencies with the JILA measurements [9]. This figure adapted from Ref. [12].

CHAPTER 4

ZERO TEMPERATURE THEORY FOR MULTIPLE COMPONENT CONDENSATES

In a recent experiment, Myatt *et al.* [87] observed Bose-Einstein condensation (BEC) of ^{87}Rb atoms in a new dynamical regime. Two *interacting* condensates of atoms in different hyperfine spin states, $|F, M_F\rangle$=$|1, -1\rangle$ and $|2, 2\rangle$, were formed using evaporative cooling in a magneto-optical trap (MOT) to cool only the $|1, -1\rangle$ state. Sympathetic cooling reduced the temperature of atoms in the other hyperfine state $|2, 2\rangle$ to form a second condensate of atoms that were "effectively distinguishable" from those in the $|1, -1\rangle$ condensate. Once condensed, the atoms were observed to separate into two distinct clouds with small spatial overlap. By reducing the opportunity for inelastic interspecies (spin exchange) collisions, this separation makes possible the observed lifetime of seconds for the condensed phase.

This chapter shows how the properties of this remarkable "double condensate" emerge from joint considerations of the identical particle collisions and the distinguishable particle collisions. The very existence of a metastable pair of interacting condensates was far from evident, *a priori*. In the s-wave domain that characterizes these collisions, spin exchange between unlike atoms can produce untrapped atomic hyperfine substates. There is now theoretical evidence for a remarkably low spin exchange loss rate of condensed trapped atoms due to these two-body collisions [86, 91]. Additionally, I find that the loss is slow in part because the condensates repel each other rather than intermingle. Other predicted features of interacting condensates also hinge on the values of the three relevant scattering lengths. It may be that two component condensate experiments can provide a means of measuring the s-wave scattering lengths, making greater refinements of the two-body interaction potentials possible.

There have been many theoretical studies of multiple condensates in the context of

Josephson junction-like experiments and the coherence properties of condensates. Most, however, have considered two spatially separated condensates of the *same* species that are allowed to interfere. Only a handful have considered the case of two different species present in the same trap. Most of these two component studies have considered a simplified geometry either for lack of a definite experiment or because of the inherent technical numerical difficulty of solving the coupled nonlinear Hartree-Fock equations for a more complicated geometry. The experiment of Myatt *et al.*, for instance, requires the solution of a fully three dimensional set of two coupled nonlinear partial differential equations. The complication in modeling this experiment stems from the fact that the resultant of the gravitational and trapping forces differentially affects the two spin states and, since the symmetry axis of the trap was aligned perpendicular to gravity, destroyed the symmetry in the problem. Specifically, the $|1,-1\rangle$ state, less strongly confined than the $|2,2\rangle$ state because of its smaller magnetic moment, experiences a comparatively larger "sag" due to gravity. So, while each cloud individually remains in a cylindrically symmetric trap, the symmetry axes of the effective trapping potentials for each spin state do not coincide. This circumstance wrecks even the cylindrical symmetry of the individual clouds due to the interaction between the two species, as will become evident below in Sec. 4.4.2.

Section 4.1 presents several derivations of the Hartree-Fock equations for multicomponent condensates and discusses a factor of two in the coupling term of the resulting equations that has been the source of some confusion in the literature. Errors in this factor of two can greatly affect the calculated overlap of the Hartree-Fock wave functions which, in turn, can greatly affect such experimentally measurable quantities as the lifetimes of the condensates and their excitation frequencies. To characterize the low-energy intraspecies and interspecies interactions, I have used scattering lengths calculated from the full multichannel S-matrix [86]. Strictly speaking, scattering lengths obtained in this way possess an imaginary part which accounts for inelastic scattering processes. Here, only its real part is retained with the assumption that the fractional loss of atoms will be minimal over the time scale of the experiment, although consider loss due to inelastic processes will be considered in Sec. 4.4.2. Both Sec. 4.4.1 and

Sec. 4.4.2 present studies of the Hartree-Fock equation for various parameter combinations, considering in particular the possibility of stabilizing the metastable condensate of an atomic sample with an attractive two-body interaction.

Section 4.2 examines the conditions for the stability of the Hartree-Fock ground state. As in Sec. 3.2, I will make use of the connection to the RPA frequencies and apply a variational analysis with simple Gaussian trial wave functions. For double condensates, it is also possible to obtain an approximate stability condition within the Thomas-Fermi approximation for the case of repulsive intraspecies interactions and attractive interspecies interactions. Section 4.3 shows the derivation of the random phase approximation equations for multi-component condensates. One of the intriguing possibilities multi-component condensates offer is the simultaneous excitation of collective modes of several species. To probe these dynamics, I have calculated the excitation spectrum of a TOP trap double condensate for a wide range of parameters in the random phase approximation and present the results in Sec. 4.5. The excitation spectrum is rich and has states for which both condensates respond equally to the driving field. There are also states, however, for which one condensate responds much more strongly than the other. With the use of nondestructive imaging techniques, it is entirely feasible that both types of excitations can be experimentally observed in real time.

The concluding section of this chapter, Sec. 4.6, investigates the interesting phenomena of spatial symmetry breaking [38, 88] in a two component condensate. A detailed and systematic study based on both the Hartree-Fock and random phase approximations is presented for the particular case of a cylindrically symmetric trapping potential. The symmetry of the system is increased by the choice of identical intraspecies interactions and equal numbers of each species. Additional examples are included in which the symmetry of the system is somewhat lower.

4.1 Hartree-Fock approximation

The Hartree-Fock approximation for a multi-component condensate is the variational approximation in which the trial function is a suitably symmetrized independent particle wave

function. To be clear, the wave function for a two component condensate can satisfy the boson permutation requirement of being "completely symmetric" in two ways: (*i*) the two species can be distinguishable as for ^{23}Na+^{87}Rb; or (*ii*) the two species can be indistinguishable, differing only in their internal state, as for the experiment of Myatt *et al.* [87]. In the former case, the many-body wave function should be separately symmetric for permutations of atoms of each species thus consisting of only one term; in the latter, it should be symmetric under permutation of any two particles regardless of species and so consists of $(N_1+N_2)!/N_1!N_2!$ terms. Unless stated otherwise, I assume that case (*ii*) holds throughout this chapter although the generalization for case (*i*) is straightforward and is briefly discussed in Sec. 4.1.2. In the limit that interconversion (*i.e.* the exchange term) is neglected in case (*ii*), the two cases are in fact identical. While generally small compared to the contribution of the direct term, the exchange contribution is typically included in the scattering lengths obtained from multichannel scattering calculations.

Just as for single condensates, there are two distinct and subtly different approximations made in calculating the zero temperature properties of a system of bosons. The Bogoliubov approximation (discussed in Sec. 2.2) conserves the number of particles only on average leading to a factor of N_0 in the mean field interaction term in the Gross-Pitaevskii equation, Eq. (6). The approach I presented in Chap. 3, on the other hand, conserves the number of particles exactly leading to a factor of $N-1$ in the mean field interaction term of the Hartree-Fock equation, Eq. (18) or (25).

For multiple condensates, both approaches can still, of course, be written down. But, in addition to questions of the conservation of the total number of particles, there arises an additional question: are the numbers of each species separately conserved? I will again choose the Hartree-Fock approach in which the total number of particles is exactly conserved, but will allow for the possibility of varying the number of each species within this constraint. Modeling experiments in which the atoms are driven from one hyperfine state to another, for instance, would generally require such an approach. Such experiments have been discussed, and one

has even been performed by Ketterle *et al.* in creating the so-called atom laser [89]. In this instance atoms were driven from a trapped hyperfine state to an untrapped hyperfine state to form an output coupler for the atoms. Such experiments have also been discussed in which both hyperfine states are trapped and driven from one state to the other in analogy to standard two-level quantum optics experiments. In Secs. 4.1.1 and 4.1.3, I present time-independent and time-dependent derivations in which the number in each state may vary while maintaining a constant total number. In Sec. 4.1.2, I present derivations from the alternative viewpoint in which the number of particles of each species is separately conserved. The difference between the two will again essentially reduce to a difference between $N_i - 1$ and N_i.

4.1.1 First-quantized approach. In this section, I present a derivation of the two component condensate Hartree-Fock equations from a first-quantized formulation. The method can be generalized to multiple components in a straightforward manner. As mentioned above, the many-body state constructed from the solution of the Hartree-Fock presented here will *not* be an eigenstate of the number operator for each species. The total number of atoms N will be strictly conserved, but the number in each component, say N_1 and N_2, will be conserved only on average.

Hartree-Fock equations in which the number in each species *is* separately conserved can also be derived from a first quantized formulation. The necessary starting point is the many body Hamiltonian and a completely symmetric trial wave function built from N_1 orbitals $\psi_0(\mathbf{x})$ and N_2 orbitals $\phi_0(\mathbf{x})$. The derivation then follows just as in Sec. 3.1.1.

When the number in each species is not separately conserved, then the derivation can proceed starting from the single component expression for the total energy per particle, Eq. (17) or

$$\frac{E}{N} = \int d^3x\ \psi^*(\mathbf{x})\, H_0(\mathbf{x})\, \psi(\mathbf{x}) + \frac{N-1}{2} \int d^3x \int d^3x' \psi^*(\mathbf{x})\, \psi^*(\mathbf{x}')\, V(\mathbf{x}-\mathbf{x}')\, \psi(\mathbf{x})\, \psi(\mathbf{x}'), \qquad (72)$$

I assume that each particle is in a superposition of both components. Explicitly,

$$\psi(\mathbf{x}) = \phi_1(\mathbf{x})\, |1\rangle + \phi_2(\mathbf{x})\, |2\rangle$$

where $|1\rangle$ and $|2\rangle$ denote the spinors associated with internal atomic degrees of freedom of otherwise indistinguishable atoms. Notice that this assumption leads to a many-body wave function which is totally symmetric under any permutation of two particles, including permutations of particles in different spin states [90, 89]. In the spin basis, the one- and two-body operators in Eq. (72) are as follows:

$$H_0(\mathbf{x}) = |1\rangle\, h_1(\mathbf{x})\, \langle 1| + |2\rangle\, h_2(\mathbf{x})\, \langle 2| \tag{73}$$

and

$$\begin{aligned} V(\mathbf{x}-\mathbf{x}') = {} & |1\rangle\,|1\rangle\, V_{11}(\mathbf{x}-\mathbf{x}')\, \langle 1|\,\langle 1| + |2\rangle\,|2\rangle\, V_{22}(\mathbf{x}-\mathbf{x}')\, \langle 2|\,\langle 2| + \\ & |1\rangle\,|2\rangle\, V_{12}^{\mathrm{D}}(\mathbf{x}-\mathbf{x}')\, \langle 1|\,\langle 2| + |2\rangle\,|1\rangle\, V_{12}^{\mathrm{D}}(\mathbf{x}-\mathbf{x}')\, \langle 2|\,\langle 1| + \\ & |1\rangle\,|2\rangle\, V_{12}^{\mathrm{Ex}}(\mathbf{x}-\mathbf{x}')\, \langle 2|\,\langle 1| + |2\rangle\,|1\rangle\, V_{12}^{\mathrm{Ex}}(\mathbf{x}-\mathbf{x}')\, \langle 1|\,\langle 2|\,. \end{aligned} \tag{74}$$

The interspecies interactions $V_{12}^{\mathrm{D}}(\mathbf{x}-\mathbf{x}')$ and $V_{12}^{\mathrm{Ex}}(\mathbf{x}-\mathbf{x}')$ are the direct and exchange contributions, respectively. In terms of $\phi_1(\mathbf{x})$ and $\phi_2(\mathbf{x})$ the total energy per particle is then

$$\begin{aligned} \frac{E}{N} = {} & \langle \phi_1\, |h_1|\, \phi_1\rangle + \frac{N-1}{2}\, \langle \phi_1\phi_1\, |V_{11}|\, \phi_1\phi_1\rangle + \\ & \langle \phi_2\, |h_2|\, \phi_2\rangle + \frac{N-1}{2}\, \langle \phi_2\phi_2\, |V_{22}|\, \phi_2\phi_2\rangle + \\ & (N-1)\, \left\langle \phi_1\phi_2\, \left|\overline{V}_{12}\right|\, \phi_1\phi_2\right\rangle \end{aligned} \tag{75}$$

where the matrix elements with one ϕ are integrated over $\mathbf{x}$, the matrix elements with two ϕ's are integrated over $\mathbf{x}$ and $\mathbf{x}'$, and the bar indicates that both the direct and exchange terms are to be included (with the appropriate reordering of ϕ_1 and ϕ_2). Explicit forms for this notation are given in Eq. (28). In writing Eq. (72), I have assumed that the wave function $\psi(\mathbf{x})$ is normalized to unity. This condition translates into the following constraint on $\phi_1(\mathbf{x})$ and $\phi_2(\mathbf{x})$:

$$\int d^3x\ \left(|\phi_1(\mathbf{x})|^2 + |\phi_2(\mathbf{x})|^2\right) = 1.$$

If the average number of particles in each spin state is to be N_1 and N_2, then the following constraints must also be satisfied:

$$\int d^3x\ |\phi_1(\mathbf{x})|^2 = \frac{N_1}{N} \quad \text{and} \quad \int d^3x\ |\phi_2(\mathbf{x})|^2 = \frac{N_2}{N}$$

with $N_1+N_2=N$. Taking variations of Eq. (75) with respect to $\phi_1^*(\mathbf{x})$ and $\phi_2^*(\mathbf{x})$ gives the Hartree-Fock equations for the two component condensate,

$$\begin{aligned}
&\left[h_1(\mathbf{x})+(N-1)\left(\mathcal{I}_1(\mathbf{x})+\mathcal{J}_{22}(\mathbf{x})\right)\right]\phi_1(\mathbf{x})+\mathcal{K}_{21}(\mathbf{x})\phi_2(\mathbf{x})=\varepsilon_1\phi_1(\mathbf{x})\\
&\left[h_2(\mathbf{x})+(N-1)\left(\mathcal{I}_2(\mathbf{x})+\mathcal{J}_{11}(\mathbf{x})\right)\right]\phi_2(\mathbf{x})+\mathcal{K}_{12}(\mathbf{x})\phi_1(\mathbf{x})=\varepsilon_2\phi_2(\mathbf{x})
\end{aligned} \tag{76}$$

where the mean field terms $\mathcal{I}(\mathbf{x})$, $\mathcal{J}(\mathbf{x})$, and $\mathcal{K}(\mathbf{x})$ are defined as

$$\begin{aligned}
\mathcal{I}_i(\mathbf{x}) &= \int d^3x'\,\phi_i^*(\mathbf{x}')\,V_{ii}(\mathbf{x}-\mathbf{x}')\,\phi_i(\mathbf{x}')\\
\mathcal{J}_{ij}(\mathbf{x}) &= \int d^3x'\,\phi_i^*(\mathbf{x}')\,V_{12}^{\mathrm{D}}(\mathbf{x}-\mathbf{x}')\,\phi_j(\mathbf{x}')\\
\mathcal{K}_{ij}(\mathbf{x}) &= \int d^3x'\,\phi_i^*(\mathbf{x}')\,V_{12}^{\mathrm{Ex}}(\mathbf{x}-\mathbf{x}')\,\phi_j(\mathbf{x}')
\end{aligned}$$

The constants ε_1 and ε_2 in Eq. (76) originated as Lagrange multipliers associated with the normalization constraints and are interpreted as the orbital energies. Defining the new wave functions

$$\tilde{\phi}_1(\mathbf{x})=\sqrt{\frac{N}{N_1}}\,\phi_1(\mathbf{x}) \quad \text{and} \quad \tilde{\phi}_2(\mathbf{x})=\sqrt{\frac{N}{N_2}}\,\phi_2(\mathbf{x})$$

gives, in the limit $N\gg 1$,

$$\begin{aligned}
&\left[h_1(\mathbf{x})+N_1\mathcal{I}_1(\mathbf{x})+N_2\mathcal{J}_{22}(\mathbf{x})\right]\tilde{\phi}(\mathbf{x})+N_2\mathcal{K}_{21}(\mathbf{x})\tilde{\phi}(\mathbf{x})=\varepsilon_1\tilde{\phi}(\mathbf{x})\\
&\left[h_2(\mathbf{x})+N_2\mathcal{I}_2(\mathbf{x})+N_1\mathcal{J}_{11}(\mathbf{x})\right]\tilde{\phi}(\mathbf{x})+N_1\mathcal{K}_{12}(\mathbf{x})\tilde{\phi}(\mathbf{x})=\varepsilon_2\tilde{\phi}(\mathbf{x})
\end{aligned}$$

provided the mean field terms are defined in terms of $\tilde{\phi}_i(\mathbf{x})$ instead of $\phi_i(\mathbf{x})$.

It is important to note that in this approach N_1 is the *average* number of particles in state $|1\rangle$ and N_2 is the *average* number of particles in state $|2\rangle$. Consideration of the many-body wave function makes this point clear. The many body wave function, including spin degrees of freedom as $\chi_i(\mathbf{x})=\phi_i(\mathbf{x})\,|i\rangle$, is

$$\begin{aligned}
\Psi(\mathbf{x}_1,\ldots,\mathbf{x}_N) &= \left(\chi_1(\mathbf{x}_1)+\chi_2(\mathbf{x}_1)\right)\cdots\left(\chi_1(\mathbf{x}_N)+\chi_2(\mathbf{x}_N)\right)\\
&= \chi_1(\mathbf{x}_1)\cdots\chi_1(\mathbf{x}_N)+\\
&\quad \mathcal{S}\left[\chi_1(\mathbf{x}_1)\cdots\chi_1(\mathbf{x}_{N-1})\chi_2(\mathbf{x}_N)\right]+\ldots+
\end{aligned}$$

$$\mathcal{S}\left[\chi_1(\mathbf{x}_1)\chi_2(\mathbf{x}_2)\cdots\chi_2(\mathbf{x}_N)\right] +$$

$$\chi_2(\mathbf{x}_1)\cdots\chi_2(\mathbf{x}_N)$$

where $\mathcal{S}$ is the symmetrization operator. The many-body wave function thus includes terms describing all N particles in state $|1\rangle$, all particles save one in state $|1\rangle$, and so on. The mean value of the operator $\hat{N}_1$

$$\hat{N}_1 = \sum_{i=1}^{N}\sum_{\{\alpha\}=1}^{2} |\alpha_1\rangle\cdots|1_i\rangle\cdots|\alpha_{N-1}\rangle\langle\alpha_1|\cdots\langle 1_i|\cdots\langle\alpha_{N-1}|$$

is N_1, however. This result is relatively straightforward to show and proceeds as follows:

$$\begin{aligned}
\left\langle \hat{N}_1 \right\rangle &= \int d^3x_1\cdots d^3x_N\ \Psi^*(\mathbf{x}_1,\ldots,\mathbf{x}_N)\hat{N}_1\Psi(\mathbf{x}_1,\ldots,\mathbf{x}_N) \\
&= \langle\phi_1\,|\,\phi_1\rangle^N N\binom{N}{0} + \\
&\quad \langle\phi_1\,|\,\phi_1\rangle^{N-1}\langle\phi_2\,|\,\phi_2\rangle(N-1)\binom{N}{1} + \ldots + \\
&\quad \langle\phi_1\,|\,\phi_1\rangle^{2}\langle\phi_2\,|\,\phi_2\rangle^{N-2}2\binom{N}{N-2} + \\
&\quad \langle\phi_1\,|\,\phi_1\rangle\langle\phi_2\,|\,\phi_2\rangle^{N-1}1\binom{N}{N-1} \\
&= \frac{N_1}{N^{N-1}}(N_1+N_2)^{N-1} \\
&= N_1
\end{aligned}$$

I have used the relations $\langle\phi_1\,|\,\phi_1\rangle{=}N_1$ and $\langle\phi_2\,|\,\phi_2\rangle{=}N_2$ as well as the binomial theorem to obtain this result. But, the many-body wave function Ψ is a superposition of many-body basis functions that includes a state in which all atoms are in species $|1\rangle$ and a state in which all atoms are in species $|2\rangle$. It follows that there must be a nonzero deviation in the number N_1 from its mean, *i.e.* $\Delta N_1 = \sqrt{\langle\hat{N}_1^2\rangle - \langle\hat{N}_1\rangle^2} \neq 0$. In fact, N_1 and N_2 are distributed among their possible values according to the binomial distribution. The variation in the number of particles in state $|1\rangle$ (or the number in state $|2\rangle$) is thus $\sqrt{N_1N_2/N}$.

4.1.2 Second-quantized approach. I briefly outline the derivation of the Hartree-Fock equations for the double condensate system, following closely the development in Ref. [12] for single condensates. I make the independent particle approximation and assume

that the numbers of atoms N_1 and N_2 in each species are separately conserved. The states of the system are then described in terms of symmetrized products of the single particle states $\{\psi_i\}$ and $\{\phi_j\}$ for each species, respectively. The Hamiltonian can then be written as

$$\hat{H} = \hat{H}_1 + \hat{H}_2 + \hat{V}_{12} \tag{77}$$

where $\hat{H}_1$ and $\hat{H}_2$ are the intraspecies Hamiltonians and $\hat{V}_{12}$ is the interspecies interaction term. Explicitly, in second-quantized form,

$$\begin{aligned} \hat{H}_1 &= \sum_{\alpha\beta} \hat{c}_\alpha^\dagger \langle \psi_\alpha | h_1 | \psi_\beta \rangle \hat{c}_\beta + \frac{1}{2} \sum_{\alpha\beta\gamma\delta} \hat{c}_\alpha^\dagger \hat{c}_\beta^\dagger \langle \psi_\alpha \psi_\beta | V_{11} | \psi_\gamma \psi_\delta \rangle \hat{c}_\delta \hat{c}_\gamma, \\ \hat{H}_2 &= \sum_{\alpha\beta} \hat{d}_\alpha^\dagger \langle \phi_\alpha | h_2 | \phi_\beta \rangle \hat{d}_\beta + \frac{1}{2} \sum_{\alpha\beta\gamma\delta} \hat{d}_\alpha^\dagger \hat{d}_\beta^\dagger \langle \phi_\alpha \phi_\beta | V_{22} | \phi_\gamma \phi_\delta \rangle \hat{d}_\delta \hat{d}_\gamma \end{aligned} \tag{78}$$

where $h_i(\mathbf{x})$ includes the kinetic energy and any external potential $V_i(\mathbf{x})$

$$h_i(\mathbf{x}) = -\frac{\hbar^2}{2m_i}\nabla^2 + V_i(\mathbf{x}).$$

with m_i the mass of the i-th species atom. The creation and annihilation operators, $\hat{c}$ and $\hat{d}$, for each species are defined in terms of their effect on a number state of the system. That is, $\hat{c}_\alpha^\dagger$ ($\hat{c}_\alpha$) creates (annihilates) an atom of species 1 in the state ψ_α with the prefactor $\sqrt{n_\alpha + 1}$ ($\sqrt{n_\alpha}$) while leaving all atoms of species 2 unaffected; $\hat{d}_\beta^\dagger$ ($\hat{d}_\beta$) is the analogous operator for species 2. The operators $\hat{c}$ and $\hat{d}$ obey boson commutation relations $[\hat{c}_\alpha, \hat{c}_\beta^\dagger] = [\hat{d}_\alpha, \hat{d}_\beta^\dagger] = \delta_{\alpha\beta}$ with all other commutators, including the mixed commutators of $\hat{c}$ and $\hat{d}$, equal to zero.

For indistinguishable atoms — case (*ii*) above — the interspecies interaction term is given by

$$\hat{V}_{12} = \sum_{\alpha\beta\gamma\delta} \hat{c}_\alpha^\dagger \hat{d}_\beta^\dagger \left\langle \psi_\alpha \phi_\beta \left| \overline{V}_{12} \right| \psi_\gamma \phi_\delta \right\rangle \hat{c}_\delta \hat{d}_\gamma \tag{79}$$

using the shorthand notation

$$\left\langle \psi_\alpha \phi_\beta \left| \overline{V}_{12} \right| \psi_\gamma \phi_\delta \right\rangle = \left\langle \psi_\alpha \phi_\beta \left| V_{12}^{\mathrm{D}} \right| \psi_\gamma \phi_\delta \right\rangle + \left\langle \psi_\alpha \phi_\beta \left| V_{12}^{\mathrm{Ex}} \right| \phi_\delta \psi_\gamma \right\rangle \tag{80}$$

for the direct and exchange contributions. Note that this interaction differs from the intraspecies interaction terms in Eq. (78) by a factor of 1/2. This factor is not needed since there is no

double counting in the sum over all α and β, *i.e.* $\hat{c}^\dagger_\alpha \hat{d}^\dagger_\beta \neq \hat{c}^\dagger_\beta \hat{d}^\dagger_\alpha$. Additionally, because this symmetry under index exchange is absent, the direct and exchange terms must be explicitly built into the interspecies interaction.

For distinguishable atoms — case (*i*) above — the construction of direct and exchange matrix elements is, of course, not relevant. Thus, the matrix element in Eq. (79) is replaced by the unsymmetrized version

$$\left\langle \psi_\alpha \phi_\beta \left| \overline{V}_{12} \right| \psi_\gamma \phi_\delta \right\rangle \rightarrow \left\langle \psi_\alpha \phi_\beta \left| V_{12} \right| \psi_\gamma \phi_\delta \right\rangle .$$

The connection between the second-quantized many-body Hamiltonian in Eq. (77) and the first-quantized treatment using Eqs. (73) and (74) can be made explicit for the familiar case of a two-body system. Consider the second-quantized wave function for one atom in each spin state, $|1;1\rangle$. The expectation value of the Hamiltonian is

$$\left\langle 1;1 \left| \hat{H} \right| 1;1 \right\rangle = \left\langle \psi_0 \left| h_1 \right| \psi_0 \right\rangle + \left\langle \phi_0 \left| h_2 \right| \phi_0 \right\rangle + \left\langle \psi_0 \phi_0 \left| \overline{V}_{12} \right| \psi_0 \phi_0 \right\rangle . \tag{81}$$

The corresponding first-quantized wave function is written

$$\Psi(\mathbf{x}_1, \mathbf{x}_2) = \frac{1}{\sqrt{2}} \left(\psi_0(\mathbf{x}_1) \left| 1 \right\rangle \phi_0(\mathbf{x}_2) \left| 2 \right\rangle + \phi_0(\mathbf{x}_1) \left| 2 \right\rangle \psi_0(\mathbf{x}_2) \left| 1 \right\rangle \right) .$$

The expectation value of the Hamiltonian $H_0 + V$ for H_0 and V from Eqs. (73) and (74) is

$$\begin{aligned} \left\langle \Psi \mid \Psi \right\rangle = \frac{1}{2} \Big[& 2 \left\langle \psi_0 \left| h_1 \right| \psi_0 \right\rangle + 2 \left\langle \phi_0 \left| h_2 \right| \phi_0 \right\rangle + \left\langle \psi_0 \phi_0 \left| V_{12}^{\mathrm{D}} \right| \psi_0 \phi_0 \right\rangle + \left\langle \psi_0 \phi_0 \left| V_{12}^{\mathrm{Ex}} \right| \phi_0 \psi_0 \right\rangle + \\ & \left\langle \phi_0 \psi_0 \left| V_{12}^{\mathrm{D}} \right| \phi_0 \psi_0 \right\rangle + \left\langle \phi_0 \psi_0 \left| V_{12}^{\mathrm{Ex}} \right| \psi_0 \phi_0 \right\rangle \Big] \\ = \quad & \left\langle \psi_0 \left| h_1 \right| \psi_0 \right\rangle + \left\langle \phi_0 \left| h_2 \right| \phi_0 \right\rangle + \left\langle \psi_0 \phi_0 \left| \overline{V}_{12} \right| \psi_0 \phi_0 \right\rangle \end{aligned}$$

which is identical to Eq. (81).

I approximate all interatomic interactions V_{ij} by a Dirac delta function pseudopotential, V_{ij}=$U_{ij}\delta(r_{ij})$, whose coefficient is given by

$$U_{ij} = \frac{2\pi\hbar^2 a_{ij}}{\mu_{ij}}$$

where a_{ij} is the s-wave scattering length between an i species atom and a j species atom and $\mu_{ij} = m_i m_j/(m_i + m_j)$ is the reduced mass. The justification for this approximation was discussed in Sec. 3.5 although its validity has been more rigorously examined recently by Stoof *et al.* [74]. In this approximation, the interaction matrix elements reduce to

$$\langle \psi_\alpha \psi_\beta \left| V_{ij} \right| \psi_\gamma \psi_\delta \rangle = U_{ij} \int d^3x \, \psi_\alpha^*(\mathbf{x}) \psi_\beta^*(\mathbf{x}) \psi_\gamma(\mathbf{x}) \psi_\delta(\mathbf{x}) \tag{82}$$

save for the interspecies interaction, Eq. (80), for indistinguishable atoms which instead is

$$\left\langle \psi_\alpha \phi_\beta \left| \overline{V}_{12} \right| \psi_\gamma \phi_\delta \right\rangle = U_{12} \int d^3x \, \psi_\alpha^*(\mathbf{x}) \phi_\beta^*(\mathbf{x}) \psi_\gamma(\mathbf{x}) \phi_\delta(\mathbf{x}). \tag{83}$$

The difference between Eq. (82) and Eq. (83) is that Eq. (83) includes the contribution of both the direct and exchange terms while Eq. (82) does not. This difference is the source of a factor of two discrepancy in the interspecies interaction term between Hartree-Fock equations in the literature: Ho and Shenoy [13] have a 1/2; Ballagh, *et al.* [90] have a 2; and Graham and Walls [24] have a 1, in agreement with the above expression. That the correct factor is unity can be understood from a consideration of the multichannel T-matrix for two-body scattering. First, recall from Sec. 3.5 that in the shape independent approximation the replacement of the two-body interaction potential by a pseudopotential whose strength is given by the scattering length in effect replaces the interaction matrix element by the corresponding T matrix element. In addition, the T-matrix (or S-matrix) from which the scattering lengths are extracted in multichannel calculations (see Refs. [86, 91, 92]) are obtained using symmetrized two-body wave functions, while the matrix elements required in Eqs. (80) and (83) are unsymmetrized. Thus, it is the sum of the direct and exchange terms that should be replaced in the shape independent approximation by a_{12} not each term separately.

The Hartree-Fock equations are obtained by minimizing the total energy [compare Eq. (75)]

$$E_0 = N_1 \left[\langle \psi_0 \left| h_1 \right| \psi_0 \rangle + \frac{N_1 - 1}{2} \langle \psi_0 \psi_0 \left| V_{11} \right| \psi_0 \psi_0 \rangle \right] +$$

$$N_2\left[\langle\phi_0\left|h_2\right|\phi_0\rangle+\frac{N_2-1}{2}\left\langle\phi_0\phi_0\left|V_{22}\right|\phi_0\phi_0\right\rangle\right]+$$
$$N_1N_2\left\langle\psi_0\phi_0\left|\overline{V}_{12}\right|\psi_0\phi_0\right\rangle \tag{84}$$

with respect to the orbitals ψ_0^* and ϕ_0^*,

$$\frac{\delta}{\delta\psi_0^*}\left\langle N_1;N_2\left|\hat{H}\right|N_1;N_2\right\rangle=0$$
$$\frac{\delta}{\delta\phi_0^*}\left\langle N_1;N_2\left|\hat{H}\right|N_1;N_2\right\rangle=0.$$

The minimization is constrained by requiring ψ_0 and ϕ_0 to be normalized to unity. The orthogonality of ψ_0 to ϕ_0 is generally ensured by the orthogonality of the spin states. The Hartree-Fock equations are then

$$\left(h_1+(N_1-1)U_{11}\left|\psi_0\right|^2+N_2U_{12}\left|\phi_0\right|^2\right)\psi_0=\varepsilon_{10}\psi_0$$
$$\left(h_2+N_1U_{12}\left|\psi_0\right|^2+(N_2-1)U_{22}\left|\phi_0\right|^2\right)\phi_0=\varepsilon_{20}\phi_0. \tag{85}$$

Their structure closely resembles the Hartree-Fock (or Gross-Pitaevskii or nonlinear Schrödinger) equation for a single condensate, Eq. (6) or Eq. (25); and, up to factors of two in the interspecies interaction term discussed above [93], these are a relatively straightforward generalization of the single condensate result. The two component generalization of the quasi-Hartree-Fock single particle basis can be obtained using an argument very similar to the one preceding Eq. (22) in Sec. 3.1.2. Brillouin's theorem, Eq. (22), for a two component system can be written as

$$\left\langle\Phi_0^{\mathrm{HF}}\left|\frac{\hat{c}_0^\dagger\hat{c}_p}{\sqrt{N_1}}\hat{H}\right|\Phi_0^{\mathrm{HF}}\right\rangle=0$$
$$\left\langle\Phi_0^{\mathrm{HF}}\left|\frac{\hat{d}_0^\dagger\hat{d}_p}{\sqrt{N_2}}\hat{H}\right|\Phi_0^{\mathrm{HF}}\right\rangle=0.$$

These conditions lead directly to the uncoupled linear equations for the quasi-Hartree-Fock single particle basis states $\{\psi_i\}$ and $\{\phi_j\}$,

$$\left(h_1+(N_1-1)U_{11}\left|\psi_0\right|^2+N_2U_{12}\left|\phi_0\right|^2\right)\psi_i=\varepsilon_{1i}\psi_i$$
$$\left(h_2+N_1U_{12}\left|\psi_0\right|^2+(N_2-1)U_{22}\left|\phi_0\right|^2\right)\phi_j=\varepsilon_{2j}\phi_j.$$

It should be noted that this is not the only choice for the single particle basis, but it is convenient and includes many of the mean field effects due to the condensate.

Another possible single particle basis is the Hartree-Fock (or frozen core Hartree-Fock) basis (see Sec. 3.1.2). This basis is obtained variationally by assuming the many-body singly excited state has the form $|N_1-1, 1_p; N_2\rangle$ or $|N_1; N_2-1, 1_q\rangle$ for excitations of species $|1\rangle$ or $|2\rangle$, respectively. Except for the ground state orbital, the single particle bases to which the labels p and q refer are not yet determined. The equations they satisfy are precisely the relations that will be obtained from the application of the variational method.

The expectation value of the Hamiltonian for the state $|N_1-1, 1_p; N_2\rangle$ is

$$E_p = \langle \psi_p | h_1 | \psi_p \rangle + (N_1-1) \left\langle \psi_p \psi_0 \left| \overline{V}_{11} \right| \psi_p \psi_0 \right\rangle + N_2 \left\langle \psi_p \phi_0 \left| \overline{V}_{12} \right| \psi_p \phi_0 \right\rangle$$

up to a constant that is essentially the ground state Hartree-Fock energy of $|N_1-1; N_2\rangle$. The energy E_q has the same form as E_p and can be obtained from this expression with the interchanges $1 \leftrightarrow 2$, $\psi \leftrightarrow \phi$, and $p \leftrightarrow q$. The equations satisfied by $\psi_p(\mathbf{x})$ ($\phi_q(\mathbf{x})$) are determined by taking variations of E_p (E_q) with respect to $\psi_p^*(\mathbf{x})$ ($\phi_q^*(\mathbf{x})$) with the constraint that they be normalized to unity and orthogonal to $\psi_0(\mathbf{x})$ ($\phi_0(\mathbf{x})$). The resulting equations, including the Lagrange multipliers λ_{ip} to ensure orthogonality to the ground state orbital, are as follows:

$$\begin{aligned}
\left(h_1(\mathbf{x}) + 2\,(N_1-1)\,U_{11}\,|\psi_0(\mathbf{x})|^2 + N_2 U_{12}\,|\phi_0(\mathbf{x})|^2 \right) \psi_p(\mathbf{x}) &= \varepsilon_{1p}\psi_p(\mathbf{x}) + \lambda_{1p}\psi_0(\mathbf{x}) \\
\left(h_2(\mathbf{x}) + N_1 U_{12}\,|\psi_0(\mathbf{x})|^2 + 2\,(N_2-1)\,U_{22}\,|\phi_0(\mathbf{x})|^2 \right) \phi_p(\mathbf{x}) &= \varepsilon_{2p}\phi_p(\mathbf{x}) + \lambda_{2p}\phi_0(\mathbf{x}). \qquad (86)
\end{aligned}$$

Note the additional factor of two preceding the intraspecies interaction terms just as for a single component system, Eq. (24), and the absence of a similar factor of two for the interspecies interaction. Since variations of $\psi_0(\mathbf{x})$ were not allowed, this is the frozen core Hartree-Fock approximation for the excited states, or simply just the Hartree-Fock approximation. Interestingly, the Hartree-Fock approximation for the excited states of a two component system is *not* the same as the Tamm-Dancoff approximation as it was for a single component system (see Sec. 3.4). In particular, the Tamm-Dancoff approximation mixes the single excitations of both

species. I will discuss this further in Sec. 4.3 below.

4.1.3 Time-dependent Hartree-Fock equations. The multi-component time-dependent Hartree-Fock equations can be useful for modeling many interesting experiments. They have been studied in one dimension by Ballagh *et al.* [90], who theoretically investigated the properties of an output coupler — the necessary first step in making an "atom laser". A method very similar to the one Ballagh *et al.* studied was implemented by Mewes *et al.* [89]. In their method, atoms are driven by radio frequency transitions from a trapped hyperfine spin state, in which a condensed sample waits, into an untrapped spin state that accelerates the atoms out of the trap. The time-dependent equations could also be used, for instance, to model the decay of the condensates *via* two- or three-body loss mechanisms.

The time-dependent version of the two component Hartree-Fock equations can be derived from the single component equation,

$$i\hbar\frac{\partial}{\partial t}\phi(\mathbf{x},t) = \left[H_0(\mathbf{x}) + (N-1)\int d^3x'\ \phi^*(\mathbf{x}',t)V(\mathbf{x}-\mathbf{x}')\phi(\mathbf{x}',t)\right]\phi(\mathbf{x},t), \tag{87}$$

just as the time-independent equation was in Sec. 4.1.1. Setting the time-dependent wave function $\phi(\mathbf{x},t)$ to

$$\phi(\mathbf{x},t) = \phi_1(\mathbf{x},t)\,|1\rangle + \phi_2(\mathbf{x},t)\,|2\rangle\,,$$

using the expressions for $H_0(\mathbf{x})$ and $V(\mathbf{x}–\mathbf{x}')$ in the spin basis, Eqs. (73) and (74), and projecting out the spin components, gives the coupled time-dependent Hartree-Fock equations:

$$\begin{aligned}
i\hbar\frac{\partial}{\partial t}\phi_1(\mathbf{x},t) &= \left[h_1(\mathbf{x}) + (N-1)\left(\mathcal{I}_1(\mathbf{x},t) + \mathcal{J}_{22}(\mathbf{x},t)\right)\right]\phi_1(\mathbf{x},t) + \mathcal{K}_{21}(\mathbf{x},t)\phi_2(\mathbf{x},t)\\
i\hbar\frac{\partial}{\partial t}\phi_2(\mathbf{x},t) &= \left[h_2(\mathbf{x}) + (N-1)\left(\mathcal{I}_2(\mathbf{x},t) + \mathcal{J}_{11}(\mathbf{x},t)\right)\right]\phi_2(\mathbf{x},t) + \mathcal{K}_{12}(\mathbf{x},t)\phi_1(\mathbf{x},t).
\end{aligned}$$

To model transitions driven by an external field $F(\mathbf{x},t)$ from one spin state to the other, a term such as

$$U(\mathbf{x},t) = |1\rangle\,F(\mathbf{x},t)\,\langle 2| + |2\rangle\,F^*(\mathbf{x},t)\,\langle 1|$$

could be included in Eq. (87). The resulting time-dependent equations could then be propagated

with the initial condition $\phi_2(\mathbf{x}, t = 0)$=0, and the populations $\langle \phi_i(t) \mid \phi_i(t) \rangle$ monitored as a function of time.

4.2 Stability of the Hartree-Fock solution

Just as for a single component condensate, the stability of the Hartree-Fock solution for multi-component condensates can be addressed by examining the curvature of the energy surface in the neighborhood of the minimum defined by the Hartree-Fock solution itself. The analysis proceeds in an entirely analogous manner to that presented in Sec. 3.2 and leads to the same conclusions. That is, if the RPA frequencies at some point become imaginary, then the Hartree-Fock solution is no longer an adequate zeroth order approximation to the true ground state of the system. The details of the RPA for a two component system (which are generalizable to the multi-component case) are presented in the next section.

An additional stability question arises in the case of multi-component condensates, however. For a single component, the essential property governing the stability is the degree to which the particles attract each other. If they are too attractive, there is no physical solution to the ground state Hartree-Fock equation in the shape independent approximation, and the ground state is said to be unstable. In all other cases, a stable solution can be found. If more than one species is present, then the role of the *intra*species interaction and the consequences for an overly attractive interaction is largely unchanged from the single component case. The *inter*species interaction, however, can also lead to an instability. Consider the case in which the intraspecies interactions are repulsive, but the interspecies interaction is attractive. It is not difficult to imagine making the attraction between species so large as to overwhelm their own repulsive interaction leading to a collapse of the wave function for the system. This can be seen in a simple case from the two component Hartree-Fock equations, Eqs. (76), replacing the two-body interactions with the s-wave pseudopotential. In an isotropic trapping potential, let the scattering lengths a_{11} and a_{22} be equal, and let the numbers of each type of atom N_1 and N_2 be equal. In this case, the orbital wave functions $\phi_1(\mathbf{x})$ and $\phi_2(\mathbf{x})$ and the orbital energies

ε_1 and ε_2 are equal as well so that the coupled equations reduce to the single equation

$$\left[-\frac{1}{2}\frac{1}{x^2}\frac{d}{dx}\left(x^2\frac{d}{dx}\right)+\frac{1}{2}x^2+(N-1)\left(\tilde{a}_{11}+\tilde{a}_{12}\right)\left|\chi(x)\right|^2\right]\chi(x)=\tilde{\varepsilon}\chi(x)$$

in scaled units [compare Eq. (62)]. The two component system thus mimics the single component system with an effective scaled scattering length $\tilde{a}_{\text{eff}}=\tilde{a}_{11}+\tilde{a}_{12}$. The stability criteria for the attractive isotropic case is well characterized by the critical parameter $\alpha_c=(N-1)\,\tilde{a}_{sc}=-0.57497$ (see Sec. 3.6). It follows that in this case the interspecies scattering length must satisfy

$$\tilde{a}_{12}\geq\frac{\alpha_c}{N-1}-\tilde{a}_{11} \tag{88}$$

in order for the two component Hartree-Fock ground state to be a good zeroth order approximation to the true ground state. Another way to approach this same question is to consider the Thomas-Fermi approximation to the ground state wave function for the two component system. Recall from Sec. 2.3 that the kinetic energy is neglected from the outset in the Thomas-Fermi approximation. For the two component system, this leads to coupled linear equations for the probability density in the region where the densities overlap. Specifically, in the shape independent approximation,

$$\begin{aligned}\alpha_{11}\left|\phi_1(\mathbf{x})\right|^2+\alpha_{12}\left|\phi_2(\mathbf{x})\right|^2&=\varepsilon_1-V_1(\mathbf{x})\\ \alpha_{21}\left|\phi_1(\mathbf{x})\right|^2+\alpha_{22}\left|\phi_2(\mathbf{x})\right|^2&=\varepsilon_2-V_2(\mathbf{x}),\end{aligned}$$

where, given the mass of each particle m_1 and m_2 and their reduced mass μ,

$$\begin{aligned}\alpha_{11}&=\frac{4\pi\hbar^2}{m_1}\left(N_1-1\right)a_{11} & \alpha_{12}&=\frac{2\pi\hbar^2}{\mu}N_2a_{12}\\ \alpha_{21}&=\frac{2\pi\hbar^2}{\mu}N_1a_{12} & \alpha_{22}&=\frac{4\pi\hbar^2}{m_2}\left(N_2-1\right)a_{22}.\end{aligned}$$

This 2×2 set of equations can be solved for $\left|\phi_1(\mathbf{x})\right|^2$ and $\left|\phi_2(\mathbf{x})\right|^2$ which must be non-negative. For this to be true, $|a_{12}|$ must be less than some critical value a_{12}^c, where the critical scattering length a_{12}^c is defined as [94, 95]

$$|a_{12}^c|=\left(\frac{4\mu^2}{m_1m_2}\frac{N_1-1}{N_1}\frac{N_2-1}{N_2}a_{11}a_{22}\right)^{1/2}\approx\sqrt{\frac{4\mu^2}{m_1m_2}a_{11}a_{22}}. \tag{89}$$

For a_{12} less than $-a_{12}^c$, no physical solution of the Hartree-Fock equation in the shape independent approximation is possible; for a_{12} greater than $+a_{12}^c$, the two species do not overlap. Note that in the limit a_{11}=a_{22} and m_1=m_2, this result does not reduce to Eq. (88) above, but rather to $a_{12}\geq -a_{11}$. The difference can be traced to the neglect of the kinetic energy in obtaining the latter result. Its inclusion thus tends to stabilize the two component system and can be expected to similarly contribute for more general sets of parameters and geometries. A general statement of the exact requirement for a_{12} is difficult, however, given the strong dependence upon the overlap of the two density distributions which, in turn, depend strongly upon the geometry of the system.

It is possible to study a specific case in order to gain some insight to the quality of the Thomas-Fermi stability condition. As for a single component condensate, the variational method with Gaussian trial wave functions proves to be a convenient approach to use. For the two component system, a Gaussian will generally not even qualitatively reproduce the exact solutions of the Hartree-Fock equation. Near $-a_{12}^c$, however, the interspecies interaction is sufficient to virtually "lock" the shape of wave functions to each other [93]. Further, near the critical point, the attractive interaction will tend to localize the wave function and, in some sense, cancel the intraspecies interaction. To improve the approximation further, I will take the trapping potentials to be concentric, and to simplify the analysis, I will take them to be isotropic with the same spring constant. For N_1 and N_2 separately conserved, the total energy of the system is in the general case

$$\begin{aligned} E = N_1 \left[\langle \phi_1 \left| h_1 \right| \phi_1 \rangle + \frac{N_1 - 1}{2} \langle \phi_1 \phi_1 \left| V_{11} \right| \phi_1 \phi_1 \rangle \right] + \\ N_2 \left[\langle \phi_2 \left| h_2 \right| \phi_2 \rangle + \frac{N_2 - 1}{2} \langle \phi_2 \phi_2 \left| V_{22} \right| \phi_2 \phi_2 \rangle \right] + \\ N_1 N_2 \left\langle \phi_1 \phi_2 \left| \overline{V}_{12} \right| \phi_1 \phi_2 \right\rangle \end{aligned}$$

[compare Eq. (75)]. Substituting into this equation the trial wave functions

$$\phi_i(\mathbf{x}) = \left(\frac{8 b_i^6}{\pi^3} \right)^{\frac{1}{4}} e^{-b_i^2 x^2} \quad i = 1, 2$$

gives

$$E = N_1 \left(\frac{3b_1^2}{2} + \frac{3}{8b_1^2} + \frac{2}{\sqrt{\pi}} \left(N_1 - 1\right) \tilde{a}_{11} b_1^3 \right) + N_2 \left(\frac{3b_2^2}{2} + \frac{3}{8b_2^2} + \frac{2}{\sqrt{\pi}} \left(N_2 - 1\right) \tilde{a}_{22} b_2^3 \right) + 8\sqrt{\frac{2}{\pi}} N_1 N_2 \tilde{a}_{12} b_1^3 b_2^3 \left(b_1^2 + b_2^2\right)^{-3/2}. \quad (90)$$

Equation (90) has been expressed in terms of the oscillator units of energy $\hbar\omega$ and length $\beta = \sqrt{\hbar/m\omega}$. That is, $r = \beta x$ in the trial wave function and $a_{ij} = \beta \tilde{a}_{ij}$. The total energy must be minimized with respect to b_1 and b_2 which, in turn, reduces to a numerical problem. Even with the geometric simplifications of this example there remain four parameters upon which the critical value of $\tilde{a}_{12}$ depends: N_1, N_2, $\tilde{a}_{11}$, and $\tilde{a}_{22}$. Noting that Eq. (90) is symmetric under the interchange of the labels 1 and 2, it is sufficient to fix N_1 and $\tilde{a}_{11}$, say, and vary N_2 and $\tilde{a}_{22}$. Figure 89 shows the variational critical $\tilde{a}_{12}$ as a function of N_2 and $\tilde{a}_{22}$ for $N_1 = 5000$ and $\tilde{a}_{11} = 0.005$. In the figure, $\tilde{a}_{12}$ is scaled by the Thomas-Fermi result, $\tilde{a}_{12}^c = \sqrt{\tilde{a}_{11}\tilde{a}_{22}}$, Eq. (89) with $m_1 = m_2$. The filled circle marks the point at which $N_2 = N_1$ and $\tilde{a}_{22} = \tilde{a}_{11}$. At this point, the ratio of the variational result to the Thomas-Fermi result is 1.02 as given by Eq. (88) above. From the figure, it is clear that the Thomas-Fermi result is worse than the variational result by up to an order of magnitude in the regions where the product of N_2 and $\tilde{a}_{22}$ is small. This failure is to be expected since the Thomas-Fermi approximation should not yield an accurate representation of ϕ_2 in these regions (see the discussion in Sec. 3.2 and Fig. 4). The agreement improves for values of $N_2\tilde{a}_{22}$ on the order of unity although the variational treatment should still be the more accurate of the two. For values of $N_2\tilde{a}_{22}$ on the order of 10 or larger, the agreement worsens again. In this region, however, it is likely the variational treatment breaking down rather than the Thomas-Fermi.

4.3 Random phase approximation

In Sec. 3.3, the random phase approximation was considered in detail for single component condensates. In this section, I discuss the generalization to the two component system,

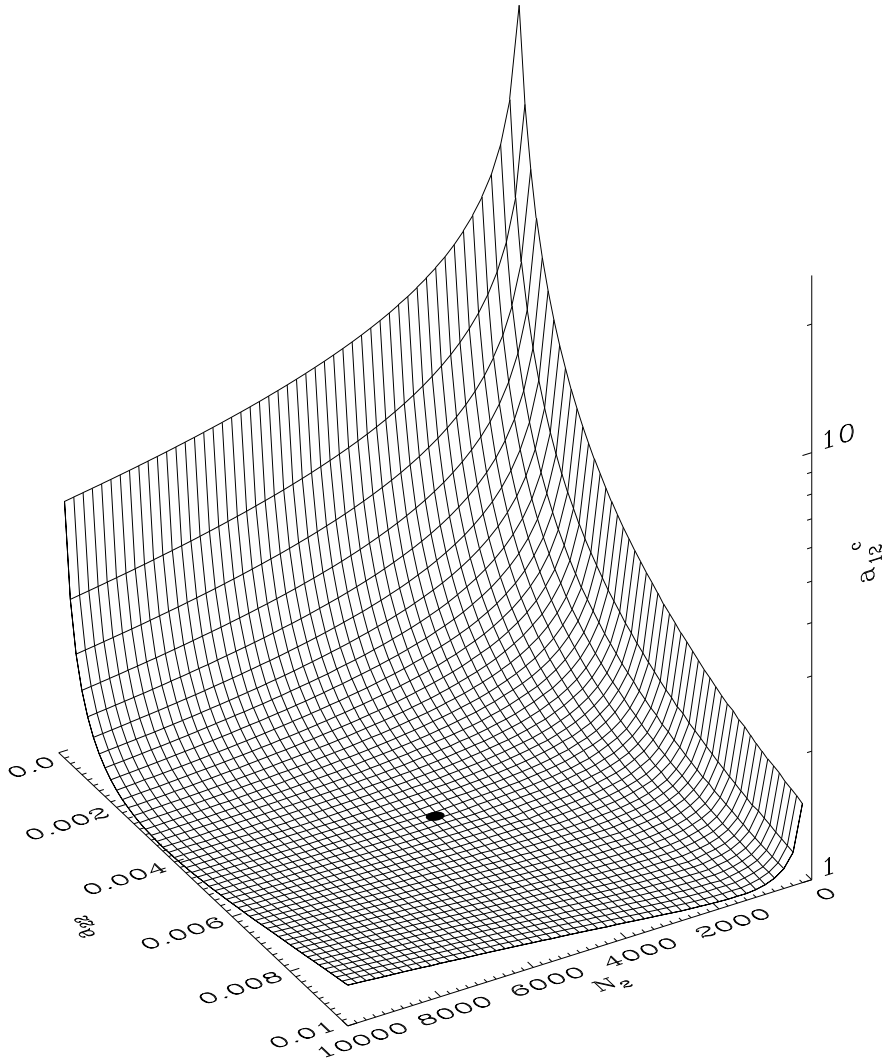

Figure 15. The critical interspecies scattering length for an attractive interspecies interaction determined variationally. N_1 and $\tilde{a}_{11}$ are fixed at 5000 and 0.005, respectively, and $\tilde{a}_{12}$ is scaled by the Thomas-Fermi result, $\tilde{a}_{12}^c=\sqrt{\tilde{a}_{11}\tilde{a}_{22}}$, Eq. (88). The filled circle marks the point at which $N_2=N_1$ and $\tilde{a}_{22}=\tilde{a}_{11}$.

although the multi-component generalization of these results is straightforward as well. Since the subtle details and variety of derivations carry over more or less intact from the discussion in Sec. 3.3, only the basic steps in the two component generalization of the time-independent derivation are included here.

The energies determined from Eq. (85) yield an approximate single particle excitation spectrum of the condensate. In general, however, this approximation will be quite poor [12]. An improved spectrum can be obtained using the RPA which for single condensates has proven successful in describing experimentally measured zero temperature excitation energies [11, 12]. The RPA has been shown to be largely equivalent to the Bogoliubov approximation [12, 18] and to give essentially the same numerical results [12]. The RPA is based upon determining an operator $\hat{O}^\dagger$ such that approximate excited states of the system can be determined from

$$\hat{O}_\nu^\dagger \left|\Phi_0^{\mathrm{RPA}}\right\rangle = \left|\Phi_\nu^{\mathrm{RPA}}\right\rangle,$$

where $\left|\Phi_0^{\mathrm{RPA}}\right\rangle$ is the RPA approximation to the exact ground state of the system. The heart of the RPA approximation lies in limiting the operator $\hat{O}$ to include only single particle excitations. If one makes the further "quasi-boson approximation" in which the RPA ground state is replaced by the Hartree-Fock ground state, $|N_1; N_2\rangle$, then the operators $\hat{O}$ can be written in terms of another set of operators defined as

$$\hat{C}_p^\dagger = \frac{\hat{c}_p^\dagger \hat{c}_0}{\sqrt{N_1}} \quad \text{and} \quad \hat{D}_p^\dagger = \frac{\hat{d}_p^\dagger \hat{d}_0}{\sqrt{N_2}}.$$

To approximately order N_i^{-1}, these operators also satisfy boson commutation relations [12]. Physically, they create single particle excitations from the Hartree-Fock ground state in one or the other of the atomic species. The explicit form for the operator $\hat{O}_\nu^\dagger$ in terms of these operators is

$$\hat{O}_\nu^\dagger = \sum_{p\neq 0} X_{p\nu}\hat{C}_p^\dagger - Y_{p\nu}\hat{C}_p + \sum_{p\neq 0} U_{p\nu}\hat{D}_p^\dagger - V_{p\nu}\hat{D}_p. \tag{91}$$

It must be remembered that the index p in the first sum refers to the single particle orbitals $\{\psi_i\}$ while in the second sum p refers to the set $\{\phi_j\}$. Requiring the $\hat{O}_\nu$ to also satisfy boson

commutation relations leads to the orthonormality condition

$$\sum_{p\neq 0} X^*_{p\nu'}X_{p\nu} - Y^*_{p\nu'}Y_{p\nu} + \sum_{p\neq 0} U^*_{p\nu'}U_{p\nu} - V^*_{p\nu'}V_{p\nu} = \delta_{\nu'\nu}.$$

The quasi-boson RPA approximation to the excited state energy of the entire system can thus be written as

$$E_\nu - E_0 = \frac{\left\langle N_1; N_2 \left| [\hat{O}_\nu, [\hat{H}, \hat{O}^\dagger_\nu]] \right| N_1; N_2 \right\rangle}{\left\langle N_1; N_2 \left| [\hat{O}_\nu, \hat{O}^\dagger_\nu] \right| N_1; N_2 \right\rangle}. \tag{92}$$

The equations for X, Y, U, and V are derived by taking variations of Eq. (92) with respect to their complex conjugates. Since approximations have been made in deriving Eq. (92), however, the energies obtained are not Rayleigh-Ritz variational approximations to the exact energies of the system. Up to this point, the single particle basis implicit in the above equations could have been either the quasi-Hartree-Fock or the Hartree-Fock basis, but from this point on I assume that it is the former. Defining the coefficient matrices

$$\begin{aligned} L_{qp} &= \frac{N_1-1}{2\hbar} \left\langle \psi_q\psi_0 \left| \overline{V}_{11} \right| \psi_p\psi_0 \right\rangle \\ M_{qp} &= \frac{N_2-1}{2\hbar} \left\langle \phi_q\phi_0 \left| \overline{V}_{22} \right| \phi_p\phi_0 \right\rangle \\ N_{qp} &= \frac{\sqrt{N_1N_2}}{\hbar} \left\langle \psi_q\phi_0 \left| \overline{V}_{12} \right| \psi_0\phi_p \right\rangle \end{aligned}$$

and recalling the simplification afforded by the pseudopotential approximation Eq. (82), the RPA equations for the double condensate system can be summarized in matrix form as

$$\begin{pmatrix} \Omega_1+\mathbf{L} & \mathbf{L} & \mathbf{N} & \mathbf{N} \\ \mathbf{L} & \Omega_1+\mathbf{L} & \mathbf{N} & \mathbf{N} \\ \mathbf{N}^T & \mathbf{N}^T & \Omega_2+\mathbf{M} & \mathbf{M} \\ \mathbf{N}^T & \mathbf{N}^T & \mathbf{M} & \Omega_2+\mathbf{M} \end{pmatrix} \begin{pmatrix} X_\nu \\ Y_\nu \\ U_\nu \\ V_\nu \end{pmatrix} = \omega_\nu \begin{pmatrix} X_\nu \\ -Y_\nu \\ U_\nu \\ -V_\nu \end{pmatrix}. \tag{93}$$

The entries of the diagonal matrices Ω_i are just the excitation energies of the basis states, $\hbar\Omega_{iq} = \varepsilon_{iq} - \varepsilon_{i0}$, and $\hbar\omega_\nu = E_\nu - E_0$ is the excitation energy of the system as a whole. In the limit $\mathbf{N} \to 0$ ($a_{12} \to 0$), these equations reduce to single condensate RPA equations for each species Eq. (42) [12].

Equations (93) can be approximately solved in the Tamm-Dancoff approximation (see Sec. 3.4) by setting $Y_{p\nu}$ and $V_{p\nu}$ to zero in Eq. (91). The resulting matrix equation is

$$\begin{pmatrix} \Omega_1+\mathbf{L} & \mathbf{N} \\ \mathbf{N}^T & \Omega_2+\mathbf{M} \end{pmatrix} \begin{pmatrix} X_\nu \\ U_\nu \end{pmatrix} = \omega_\nu \begin{pmatrix} X_\nu \\ U_\nu \end{pmatrix}.$$

Through the coupling matrix $\mathbf{N}$ the Tamm-Dancoff approximation for two component systems incorporates correlations between the excited states of species $|1\rangle$ and species $|2\rangle$ that was not included in the Hartree-Fock equations, Eq. (86). The source of this difference from single component condensates can be traced to the definition of the operator $\hat{O}^\dagger$ in the Tamm-Dancoff approximation,

$$\hat{O}^\dagger_\nu = \sum_{p\neq 0} X_{p\nu}\hat{C}^\dagger_p + \sum_{p\neq 0} U_{p\nu}\hat{D}^\dagger_p.$$

This operator creates an excitation that is a linear combination of single excitations of species $|1\rangle$ and species $|2\rangle$. Such an excitation cannot be labeled by a single set of occupation numbers in terms of the sets $\{\psi_i\}$ and $\{\phi_j\}$ and thus is not consistent with the Hartree-Fock *ansatz* of a single completely symmetric independent particle wave function. The Hartree-Fock equations, Eqs. (86), can, however, be recovered from the Tamm-Dancoff equations by setting $\mathbf{N}$ to zero.

4.4 JILA baseball trap results

The experiment of Myatt *et al.* [87] opened the way for an interesting new direction in BEC experiments by demonstrating that it is possible to simultaneously trap and condense two spin states of ^{87}Rb within a single trap. More general combinations of species require a more elaborate experimental apparatus. At the very least, another set of lasers would be needed that match the transition frequency of the second species. In principle, though, these remain feasible experiments. Two component condensates provide a rich range of ground state structures because there are so many adjustable parameters — the trapping frequencies, the number of atoms in each state, and the scattering lengths. For any given system, these parameters will not be completely independent, but the range of possibilities is still enormous.

4.4.1 ^{85}Rb+^{87}Rb. One interesting question is whether it is possible to "stabilize" the ground state of a Bose gas whose interactions are attractive through the injection of a second species into the trap. It was shown in Sec. 3.2 that the strength parameter α must be larger than some critical value α_c=−0.57497 in order for the Hartree-Fock ground state of atoms in an isotropic trap to be stable. Since α=$(N-1)a_{sc}/\beta$ where β=$\sqrt{\hbar/m\omega}$, it follows that in order to increase the number of atoms that the ground state will support before collapsing, either $|a_{sc}|$ or ω must be decreased. In an anisotropic trap, there is an additional parameter λ that can be used to increase the critical number. From Fig. 2, it is clear that values of λ smaller than about 0.5 (which corresponds to a more nearly one-dimensional trap) favor larger numbers of atoms in the ground state. It is not possible to change the scattering length appreciably at these densities merely by the addition of another species to the trap, but the curvature of the effective potential seen by the metastable state can be changed through the mean field interaction as can its aspect ratio. Consider, for instance, a collection of ^{85}Rb atoms (negative a_{sc} [96, 97]) together with ^{87}Rb atoms (positive a_{sc} [86, 85, 91]) in the baseball trap of the Myatt *et al.* experiment. The frequencies of this trap can be reduced to as low as 12×6×12 Hz [98], which leads to a maximum number of about 113 ^{85}Rb atoms, using α_c from Fig. 2, with λ=0.5. Unfortunately, the detection of so few atoms is a challenging, although achievable, experimental task [98]. Any increase in the maximum number of ^{85}Rb atoms would greatly increase the attractiveness of BEC experiments with this isotope.

This section considers one of the fifteen possible combinations of trapped spin states for the rubidium mixed isotope system: the $|3,3\rangle$ state of ^{85}Rb and the $|2,2\rangle$ state of ^{87}Rb. This is the only combination for which the centers of the effective harmonic trapping potentials coincide. That is, for any particular spin state, the combined effects of gravity and the harmonic trapping potential lead to an effective harmonic trapping potential whose zero is displaced by an amount $-g/\omega_z^2$ where g is the acceleration due to gravity and ω_z is the trap frequency in the direction parallel to gravity. This result comes directly from a consideration of the potential

energies as follows:

$$\frac{1}{2}m\omega_z^2 z^2 - mgz = \frac{1}{2}m\omega_z^2\left(z - \frac{g}{\omega_z^2}\right)^2 - \frac{1}{2}m\frac{g^2}{\omega_z^2}.$$

The last term on the right hand side is simply a constant energy offset and has no physical effect. Since the atoms are trapped by the interaction of their magnetic moment with an applied magnetic field, ω_z in the above expression is proportional to the square root of the product of the g factor and the total angular momentum projection M_F. Thus, the effective trapping frequency for a particular spin state is reduced from ω_z by the square root of this product. This product turns out to be unity for both the $|3,3\rangle$ and $|2,2\rangle$ spin states, whereby the two trapping potentials share a common zero. For the other spin state combinations, the differential sag in such a weak trap is large enough that the states no longer overlap for the numbers of atoms in present experiments. Thus, only the combination $|3,3\rangle+|2,2\rangle$ takes advantage of the larger critical number for a weak trap *and* allows for the possibility of stabilization.

Choosing length and energy units, $\beta=\sqrt{\hbar/m\omega}$ and $\hbar\omega$, respectively, for convenient values of m and ω, the Hartree-Fock equations, Eq. (85), rescale as

$$\begin{aligned}\left(\tilde{h}_1 + 4\pi(N_1-1)\tilde{a}_{11}\left|\psi_0(\tilde{\mathbf{x}})\right|^2 + 2\pi\frac{m_1}{\mu}N_2\tilde{a}_{12}\left|\phi_0(\tilde{\mathbf{x}})\right|^2\right)\psi_0(\tilde{\mathbf{x}}) &= \tilde{\varepsilon}_1\psi_0(\tilde{\mathbf{x}}) \\ \left(\tilde{h}_2 + 2\pi\frac{m_2}{\mu}N_1\tilde{a}_{12}\left|\psi_0(\tilde{\mathbf{x}})\right|^2 + 4\pi(N_2-1)\tilde{a}_{22}\left|\phi_0(\tilde{\mathbf{x}})\right|^2\right)\phi_0(\tilde{\mathbf{x}}) &= \tilde{\varepsilon}_2\phi_0(\tilde{\mathbf{x}}).\end{aligned} \tag{94}$$

A tilde denotes a quantity scaled by either the energy or length unit except for the orbital energies $\tilde{\varepsilon}_1$ and $\tilde{\varepsilon}_2$, which include an additional mass factor,

$$\tilde{\varepsilon}_i = \frac{m_i}{m}\frac{\varepsilon_i}{\hbar\omega}.$$

The one-body operators $\tilde{h}_i$ include the kinetic and trapping potential energy as follows:

$$\tilde{h}_i = -\frac{1}{2}\tilde{\nabla}^2 + \frac{1}{2}\left(\tilde{\omega}_{ix}^2\tilde{x}^2 + \tilde{\omega}_{iy}^2\tilde{y}^2 + \tilde{\omega}_{iz}^2\left(\tilde{z}-\tilde{z}_{i0}\right)^2\right).$$

The trap frequencies also contain an additional mass factor,

$$\tilde{\omega}_{i\alpha} = \frac{m_i}{m}\frac{\omega_{i\alpha}}{\omega}. \tag{95}$$

In the one-body harmonic potential energy expression apparent in $\tilde{h}_i$, $\tilde{z}_{i0}$ is the scaled displacement of the trap center due to gravity.

The present calculations are carried out for the baseball trap with ω_{ix}=ω_{iz}=12 Hz and ω_{iy}=6 Hz [98], which results in a vertical displacement of the trap centers of z_{i0}=−1.7 mm relative to a gravity-free frame. Here, I use the label "1" for the $|3,3\rangle$ state and "2" for the $|2,2\rangle$ state. Scattering lengths for this system are taken from Burke *et al.* [97]. The scattering lengths for processes involving ^{85}Rb have a relatively large uncertainty, but the following are close to the most likely values: a_{11}=−400 a.u., a_{12}=210 a.u., and a_{22}=109.1 a.u. To find the maximum number of ^{85}Rb atoms N_1 possible for these parameters, Eqs. (94) have been solved with N_2=10^5 using the method of steepest descents (see App. D and Ref. [49]) with a finite difference representation of the wave functions. The method of steepest descents (in this context) amounts to propagating the time-dependent Hartree-Fock equations in imaginary time. In other words, $\tilde{\varepsilon}_i$ in Eq. (94) is replaced by $\partial/\partial\tau$, and the equations are solved for the normalized orbital $\psi_0(\tilde{\mathbf{x}})$=$\psi_0(\tilde{\mathbf{x}}, \tau\to\infty)$ where $\tau = it$. With these solutions, all zero temperature condensate properties of interest can be calculated. Moreover, these solutions can be used as the initial state for the time-dependent version of Eq. (94) (replace $\tilde{\varepsilon}_i$ in Eq. (94) by $i\partial/\partial\tilde{t}$) without the trapping potentials to simulate the expansion of the condensates typically necessary experimentally to measure the number density.

Figure 16 shows the orbital energies $\varepsilon_1/\hbar\omega$ (solid line) and $\varepsilon_2/\hbar\omega$ (dashed line) as functions of N_1. Notice that the orbital energy of the $|2,2\rangle$ state exhibits little change over this range of N_1. This insensitivity to the presence of the ^{85}Rb atoms is reasonable since there are 10^5 ^{87}Rb atoms but at most couple hundred ^{85}Rb atoms. The orbital energy of the $|3,3\rangle$ state decreases rapidly as N_1 increases, however, as Fig. 4 demonstrated for the case of single a condensate with an attractive interaction. Moreover, the asymptote is reached at around 215 atoms, or almost twice the variational estimate of 113 for the critical number. Unfortunately, the orbital wave functions in Fig. 17 show that the stabilization in this case is an almost trivial result. The upper plot shows a cut of the $|3,3\rangle$ orbital wave function in the x=0 plane.

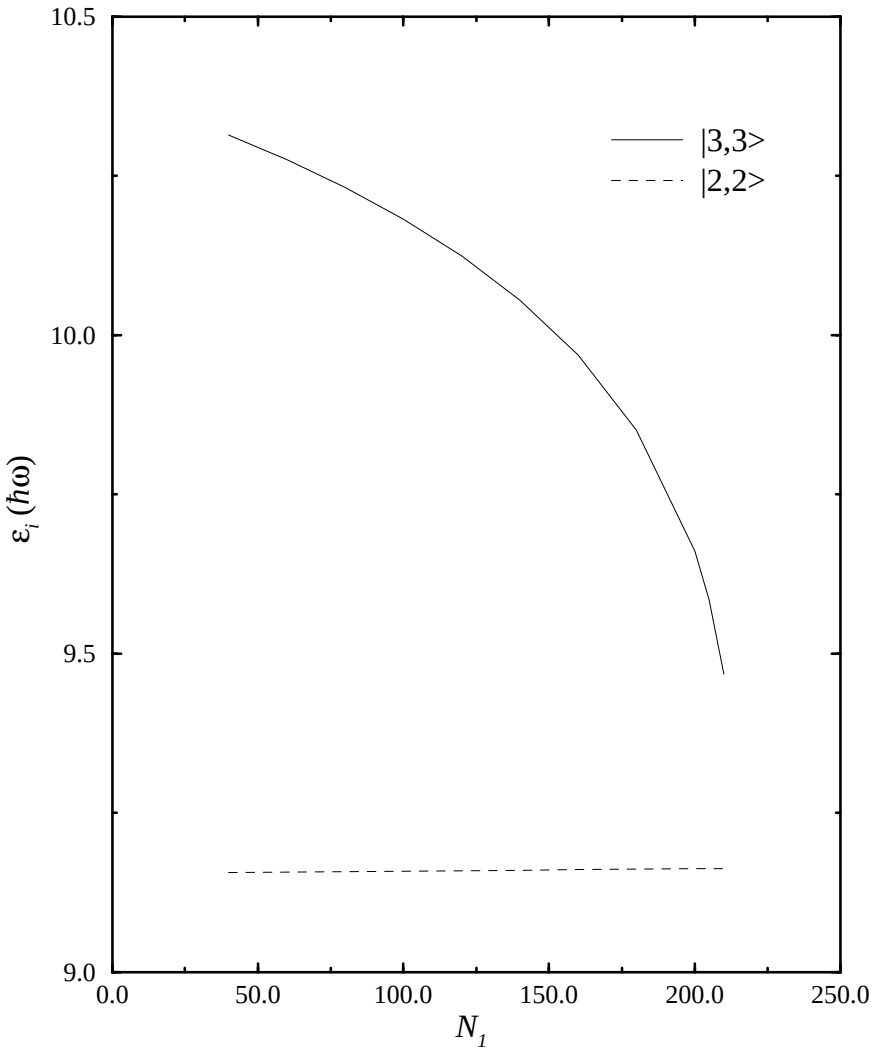

Figure 16. The orbitals energies $\varepsilon_i/\hbar\omega$ for mixed rubidium isotopes with ω=2π 12 Hz. The solid line marks the $|3,3\rangle$ state of ^{85}Rb; and the dashed line, the $|2,2\rangle$ state of ^{87}Rb.

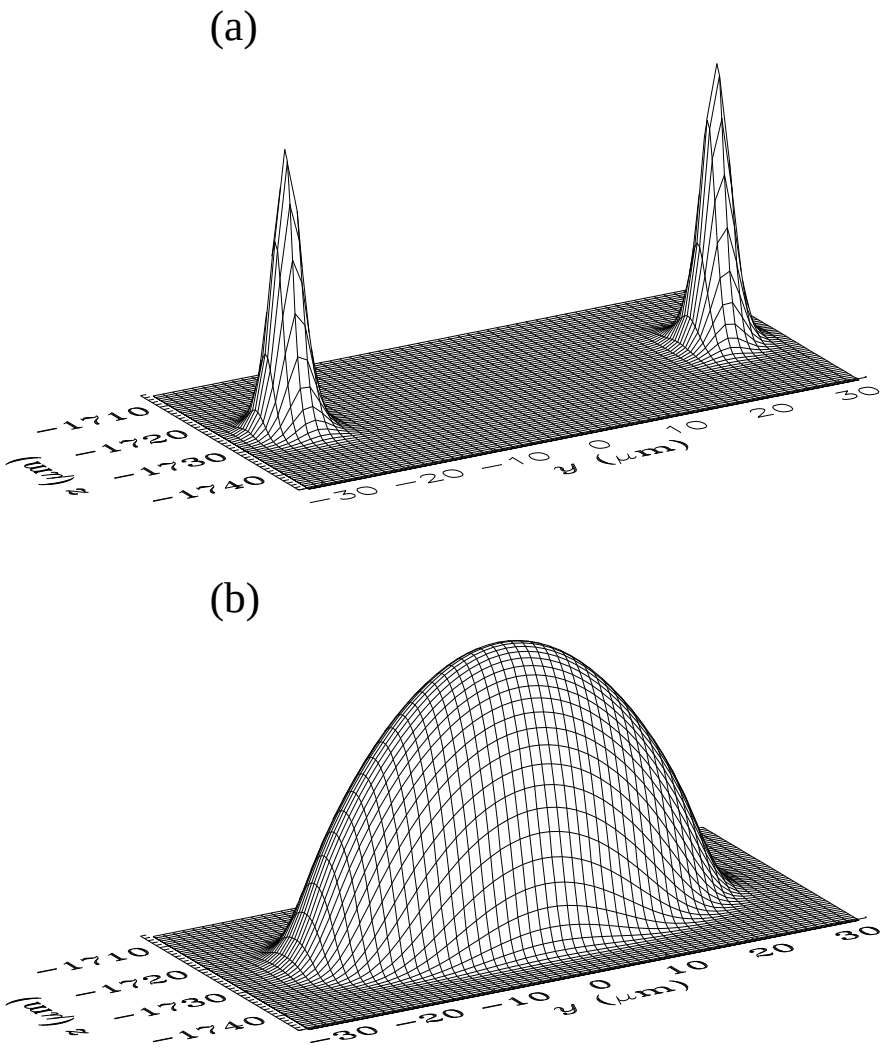

Figure 17. The single particle densities $|\psi_0(\mathbf{x})|^2$ and $|\phi_0(\mathbf{x})|^2$ for ^{85}Rb+^{87}Rb in the JILA baseball trap. The parameters are as follows: N_1=10^5, N_2=200, a_{11}=−400 a.u., a_{12}=210 a.u., a_{22}=109.1 a.u., ω_x=ω_z=2π 12 Hz, and ω_y=2π 6 Hz. The densities are plotted in the x=0 plane: (a) the $|3,3\rangle$ state of ^{85}Rb and (b) the $|2,2\rangle$ state of ^{87}Rb, shown in separate figures for clarity.

The minimum energy configuration of the system turns out to occur when the ^{85}Rb atoms are displaced to the ends of the ^{87}Rb condensate in the weaker trap direction. The ^{85}Rb atoms are localized within the exceptionally shallow potential wells near the classical turning points (similar wells are just barely visible in Fig. 7 for an isotropic trap). This localization effect is enhanced by the slightly weaker ^{85}Rb trapping potential due to the mass factors in the effective frequencies [see Eq. (95)]. In effect, *two* ^{85}Rb condensates now appear, each with about the critical number of atoms and separated by nearly 60 μm. When the Hartree-Fock equation for a single component ^{85}Rb condensate is solved numerically to determine the critical number, one finds that a more accurate estimate of the critical number is closer to 95 than the variational value of 113. These calculations suggest that there is indeed stabilization due to the presence of the ^{87}Rb, but only at about the 10% level.

4.4.2 ^{87}Rb. Another interesting question is whether the Hartree-Fock equations, Eq. (85), accurately describe the two component system. For a condensate that consists of a single species, the Hartree-Fock equation has proven remarkably accurate for predicting ground state properties. Unfortunately, very few quantitative experimental results exist to date for a two component system. Accordingly, this section focuses on the experimental configuration of Myatt *et al.* [87] for the ^{87}Rb system $|2,2\rangle+|1,-1\rangle$. The solution of the Hartree-Fock equations, Eq. (94), is carried out for the fully three-dimensional geometry of the experiment, again using the method of steepest descents with a finite difference representation of the two orbitals.

Figure 18 shows the single particle probability densities $|\psi_0(\mathbf{x})|^2$ and $|\phi_0(\mathbf{x})|^2$ for N_1=N_2=10^5 and ν_{2x}=ν_{2z}=400 Hz, ν_{2y}=11 Hz. These parameters correspond to the JILA baseball trap in which overlapping condensates have recently been observed [87]. Note that the z direction is parallel to gravity. Approximately 1.5 μm of the distance between the centers of the states along the z axis is caused by gravitationally induced sag; the remaining 0.5 μm arises from the repulsive interaction U_{12} between the atoms in the two condensates. The ^{87}Rb singlet potential has been adjusted such that its scattering length is 89.3 a.u. which, in turn, fixes two of the three scattering lengths to a_{11}=108.8 a.u. and a_{12}=108.0 a.u. — the third

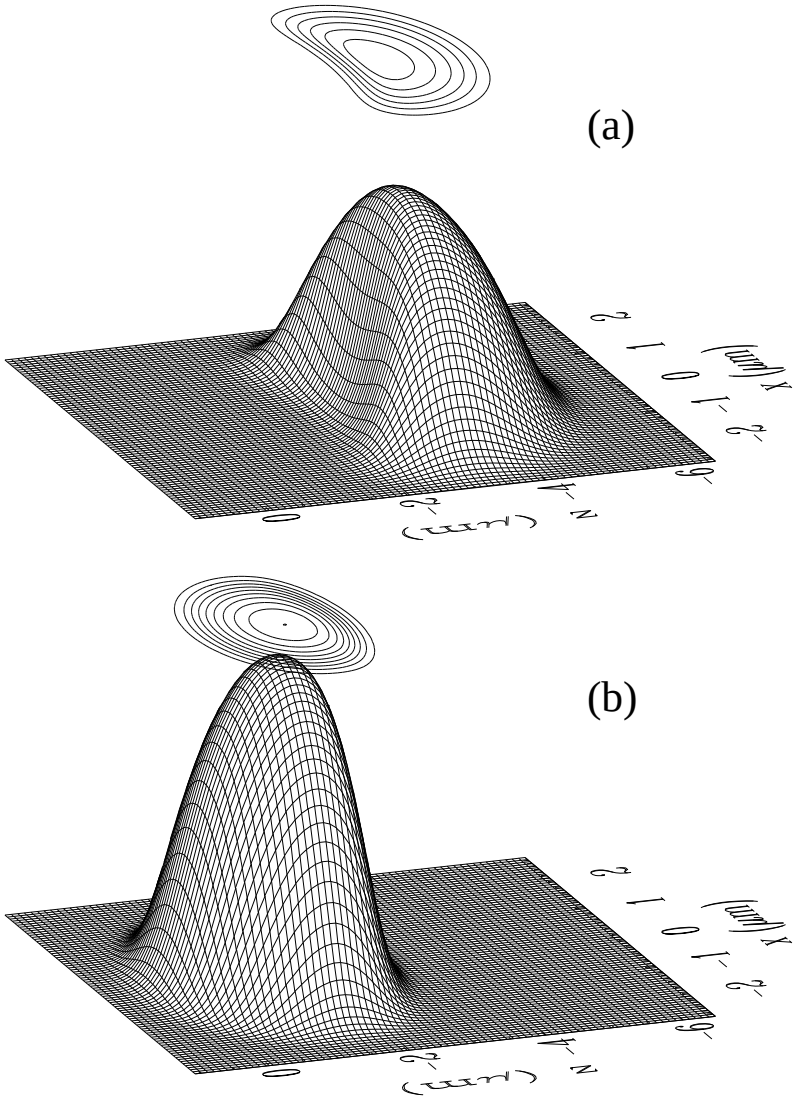

Figure 18. The single particle densities $|\psi_0(\mathbf{x})|^2$ and $|\phi_0(\mathbf{x})|^2$ for ^{87}Rb $|2,2\rangle + |1,-1\rangle$ in the JILA baseball trap. The parameters are as follows: N_1=N_2=10^5, a_{11}=108.8 a.u., a_{12}=108.0 a.u., a_{22}=109.1 a.u., ω_x=ω_z=$2\pi\,400$ Hz, and ω_y=$2\pi\,11$ Hz. The densities are plotted in the y=0 plane: (a) $|1,-1\rangle$ and (b) $|2,2\rangle$, shown in separate figures for clarity. Note that the z axis increases from right to left. The $|2,2\rangle$ is more tightly confined and is therefore closer to the nominal trap center, z=0. This figure adapted from Ref. [93].

scattering length a_{22} is purely triplet in character and has the value 109.1(10) a.u. [85, 86]. This choice leads to a spin exchange decay rate (the rate at which atoms are lost from the trap due to inelastic collisions between atoms in different spin states) of 2.15×10^{-14} cm^3/s [86] which is consistent with the measured value of $2.2(9)\times10^{-14}$ cm^3/s [87]. If one arbitrarily varies the singlet scattering length, then the calculated spin exchange rate changes by four orders of magnitude *via* a remarkable suppression mechanism [86]; its variation within the limits set by the experimental rate, however, amounts to no more than a 2% change in either a_{11} or a_{12}.

Figure 18 shows how the more tightly confined $|2,2\rangle$ state pushes the $|1,-1\rangle$ state out of its way. Furthermore, for this value of a_{12}, the overlap $\int d^3x\,|\psi_1|^2\,|\psi_2|^2$ between the two condensates is an order of magnitude smaller than either $\int d^3x\,|\psi_1|^4$ or $\int d^3x\,|\psi_2|^4$. These quantities, when multiplied by $N(=N_1=N_2)$ and the appropriate rate constant, can be used to estimate the lifetime of the condensate, assuming exponential decay caused by spin exchange collisions. The overlap of the states shown in Fig. 18 leads to a lifetime of 6 s for each condensate if spin exchange were the only loss mechanism. It should be emphasized that the Thomas-Fermi approximation badly underestimates this overlap, yielding instead an inflated lifetime of 450 s.

In reality, spin exchange competes with other loss processes such as dipolar relaxation (the dominant inelastic two-body loss process for like atoms) and three-body recombination. For the conditions of Fig. 18 relevant to the recent JILA experiment [87], the lifetimes due to dipolar loss alone are 2 s and 16 s for the $|2,2\rangle$ and the $|1,-1\rangle$ states, respectively, assuming dipolar loss rates of 3×10^{-15} cm^3/s for the $|2,2\rangle$ state and 6×10^{-16} cm^3/s for the $|1,-1\rangle$ state [99]. If I further assume a three-body recombination loss rate of 4×10^{-30} cm^6/s [100] and consider only collisions between like atoms, then the lifetimes due to this process alone are 8 s and 19 s for the $|2,2\rangle$ and the $|1,-1\rangle$ states, respectively. The density factors weighting the rates for three-body recombination between *unlike* atoms are smaller by a factor of at least 30 due to the small overlap of the associated wave functions and so can cause at most a 10% decrease in these estimates, assuming that the rates are comparable to the like-atom recombination rate. This means that we have an interesting situation in which the lifetime of each species is limited by

a different process, although the dominance of each particular mechanism is not overwhelming.

Figure 19a shows the single particle energies for each hyperfine state along with the result in the limit $a_{12}\rightarrow 0$ [49, 62, 12]. The effectively repulsive interspecies interaction boosts the single particle energies above their $a_{12}=0$ values as can be seen in Fig. 19a. Figure 19b shows the expectation value of z for each hyperfine state as a function of particle number. The behavior is qualitatively as expected: for smaller numbers of atoms, the values nearly coincide with the gravity displaced trap centers, while for larger numbers of atoms the mutual repulsion of the atoms in each hyperfine state forces the condensates farther apart. The separation of the condensates cannot currently be extracted from a direct *in situ* measurement, but their separation after some period of expansion can be measured. The calculated separation of 60 μm after 20 ms resulting from the time-dependent solution of Eq. (76) can thus be compared with the experimental result of 70-80 μm [101] following expansion.

In addition to the above example that applies directly to ^{87}Rb experiments, other values of scattering lengths — which might be realized for other atoms — can provide insight into qualitatively different experiments. The behavior of the two condensates as a function of a_{12} is particularly interesting in view of the predicted instability for a single condensate with negative scattering length within the mean field approximation (see Sec. 3.2). For a double condensate with positive a_{11} and a_{22}, one can utilize the Thomas-Fermi approximation [which neglects the kinetic energy in Eq. (76)] to calculate a critical value of $|a_{12}|$ (see Sec. 4.2). Beyond this critical value, the condensates cannot coexist [see Eq. (89)],

$$|a_{12}^c| \approx \sqrt{a_{11}a_{22}}$$

since $m_1=m_2$. The coexistence is prohibited in two different ways, depending on the sign of a_{12}. For $a_{12}\leq -a_{12}^c$, the attraction between the condensates overwhelms the repulsive interactions within each condensate, causing their collapse. For $a_{12}\geq +a_{12}^c$, the mutual repulsion of the two condensates dominates, and the two condensates no longer overlap at all within the Thomas-Fermi approximation. It is interesting to note that this critical behavior is still exhibited by the

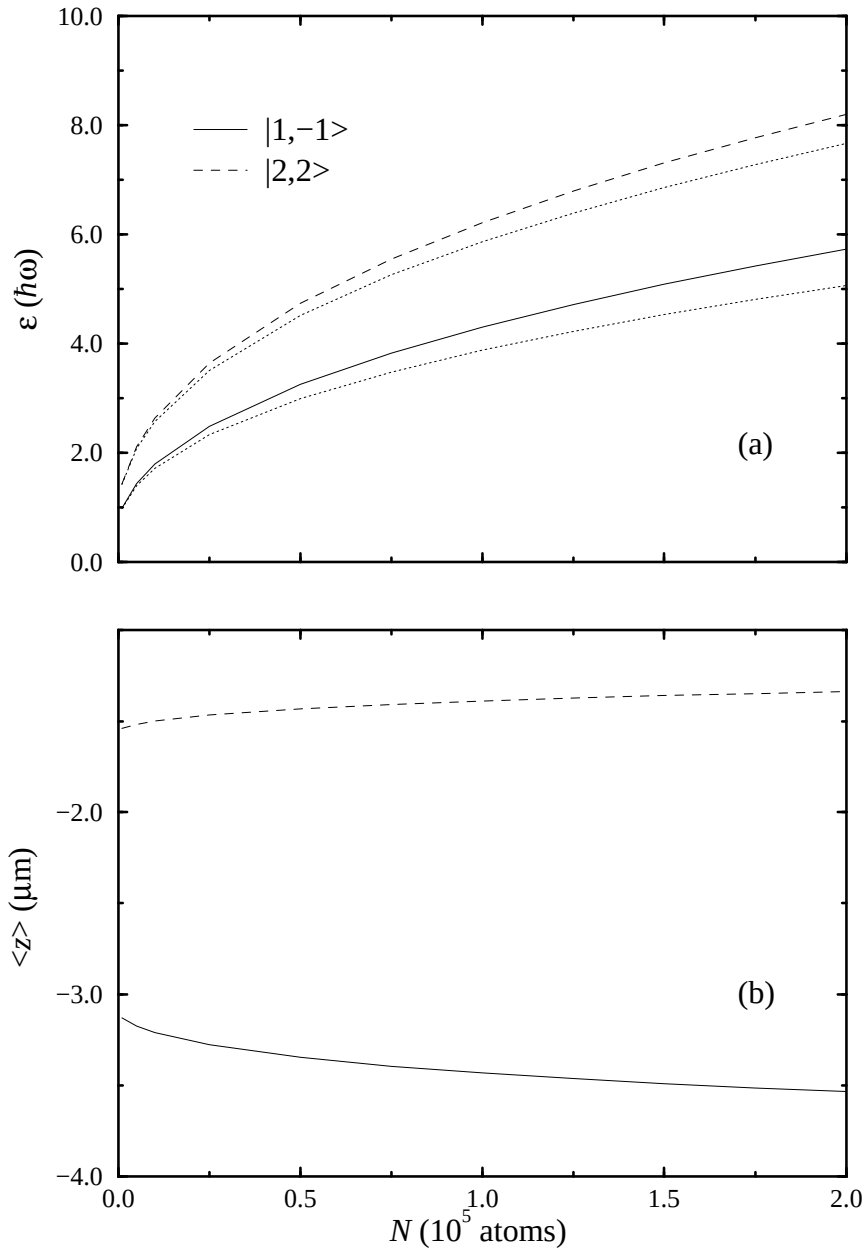

Figure 19. The orbital energies and average positions for ^{87}Rb $|2,2\rangle$+$|1,-1\rangle$ in the JILA baseball trap. The parameters are as in Fig. 18 save for the numbers of atoms. (a) The orbital energies as a function of N=N_1=N_2. (b) The expectation value of z for each cloud. In both (a) and (b), the solid lines correspond to the $|1,-1\rangle$ state; and the dashed lines, to the $|2,2\rangle$ state. In (a), the dotted lines are the single particle energies for condensates with vanishing interspecies interactions (a_{12}=0). This figure adapted from Ref. [93].

more complete Hartree-Fock solutions. Of course, with the kinetic energy retained in the coupled equations, the condensates still overlap by a nonzero but negligible amount for $a_{12} \geq +a_{12}^c$. The single particle energies, for instance, display this critical behavior. Near $-a_{12}^c$, they decrease rapidly as the mean field each experiences due to the other deepens in accordance with the increasing dominance of the interspecies attraction relative to same species repulsion. As $a_{12} \rightarrow +a_{12}^c$, the energies approach equilibrium values since the overlap decreases as a_{12} increases at just the rate required to keep the interaction energy essentially constant.

Figure 20 shows the expectation value of z for each species as a function of a_{12}. Figure 21 shows the lifetimes due to dipolar loss and spin exchange processes, also as functions of a_{12}. I have set $N_1 = N_2 = 10^5$ atoms, a_{11}=108.8 a.u., and a_{22}=109.1 a.u. (which gives a_{12}^c=109.0 a.u.) for these calculations. At $-a_{12}^c$, the attraction has pulled the centers of the condensates together, greatly increasing their density overlap. As a consequence, the spin exchange lifetime has shrunk to tens of milliseconds while the dipolar lifetime of each species has remained on the order of seconds. As a_{12} increases, the condensates move farther from each other and live longer. Finally, at $+a_{12}^c$, the mean field has reached its maximum effectiveness, and the condensate centers are essentially stationary with respect to further increases in a_{12}. At the same time, the lifetimes have increased for both states, with dipolar losses dominating the $|2, 2\rangle$ decay rate and spin exchange dominating the $|1, -1\rangle$ decay rate. The physical value of the scattering length a_{12}=108.0 a.u. is quite near the critical value and is indicated in the figure. The 2% variations in a_{12} that are possible owing to the uncertainty in the ^{87}Rb singlet scattering length will not affect these conclusions.

4.5 ^{87}Rb TOP trap results

In this section, I shift my focus from the baseball trap configuration of the previous section to the time orbiting potential (TOP) trap, because even with the gravitational shift of the effective trapping potential for each species, the system possesses cylindrical symmetry. The geometry of a double condensate in the TOP trap can be visualized as two pancakes lying on

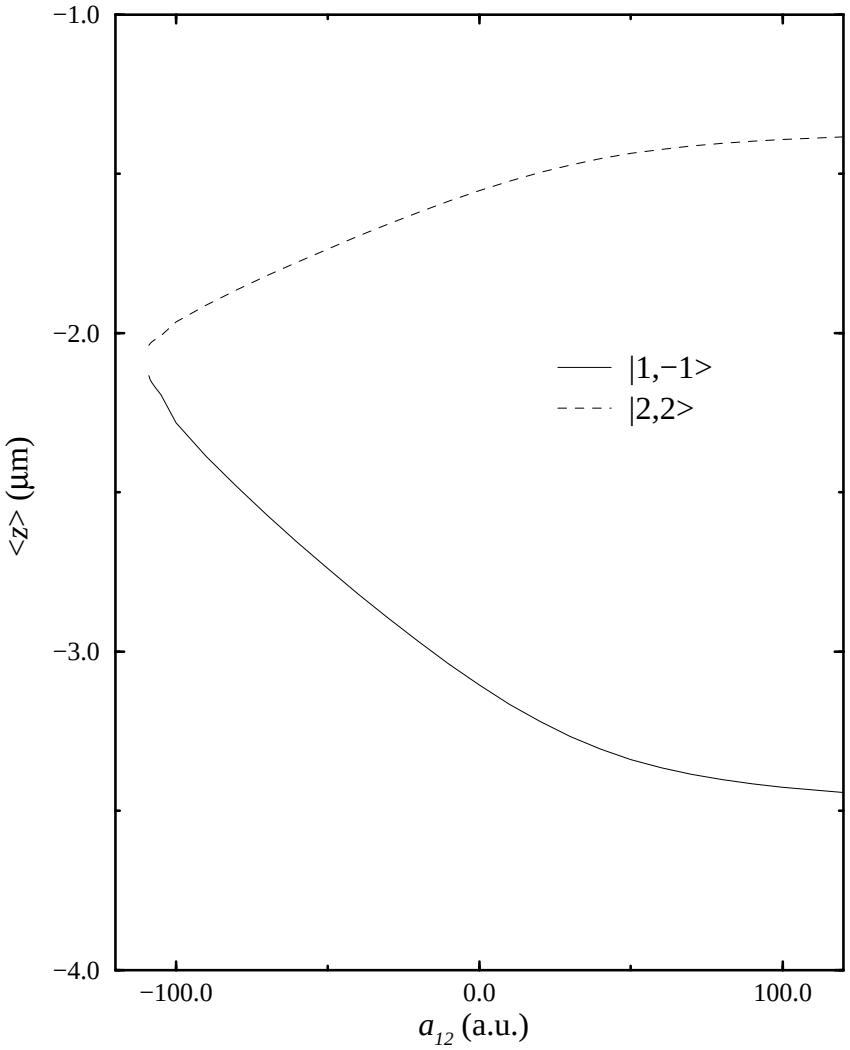

Figure 20. The expectation value of z for the $|2,2\rangle$ and $|1,-1\rangle$ hyperfine states of ^{87}Rb in the JILA baseball trap as a function of a_{12}. The parameters are as in Fig. 18 except for a_{12}. The solid line corresponds to the $|1,-1\rangle$ state; and the dashed line, to the $|2,2\rangle$ state. This figure adapted from Ref. [93].

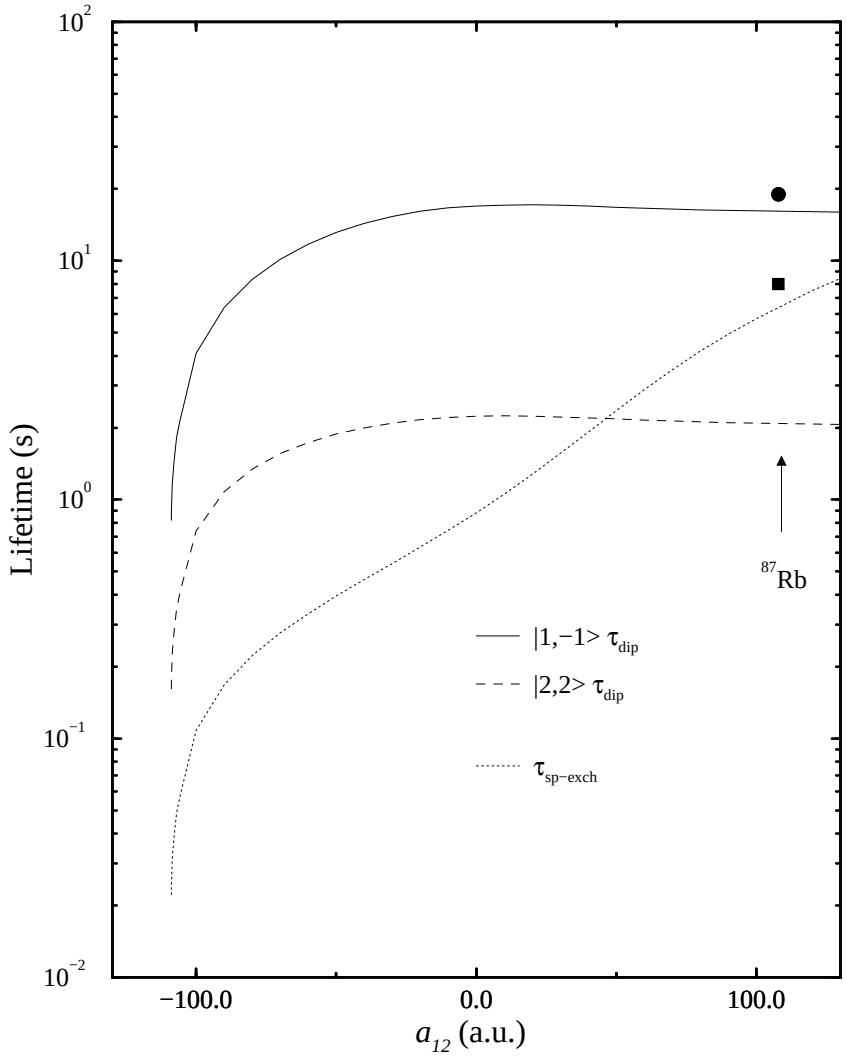

Figure 21. The lifetimes of the $|2,2\rangle$ and $|1,-1\rangle$ states of ^{87}Rb due to dipolar relaxation, τ_{dip}, and spin exchange, $\tau_{sp-exch}$, as a function of a_{12}. The parameters are as in Fig. 18 except for a_{12}. The thick solid line corresponds to the dipolar relaxation lifetime of the $|1,-1\rangle$ state; and the dashed line, to the $|2,2\rangle$ state. The dotted line represents the spin exchange lifetime of either species. The arrow marks the calculated value of a_{12} for ^{87}Rb, and the solid square and circle mark the lifetimes due to three-body recombination for this value of a_{12} for the $|2,2\rangle$ and $|1,-1\rangle$ states, respectively. This figure adapted from Ref. [93].

top of one another whereas the picture for the experiment of Myatt *et al.* resembles two parallel, horizontal cigars, one of which lies on top of the other. Computations for the TOP trap can thus be reduced to two dimensions which greatly facilitates exploration of various parameter combinations. In addition, the results retain direct physical relevance to experiment.

I have solved both the Hartree-Fock equations, Eq. (85), and the RPA equations, Eq. (93), for a wide range of parameters relevant to trapping ^{87}Rb in the JILA TOP trap. As a practical experimental matter, excitations of a double condensate can be created and measured just as for single condensates. That is, one can perturb the trapping potential by adding a harmonic driving field of the appropriate symmetry to reach the desired final state. The effective trapping potential for both species will be modulated at the same frequency, and the density of one or both of the species [87] can then be observed as a function of time [9, 10]. It may turn out, however, that one species or the other can respond with a larger amplitude for a given excitation frequency — a situation discussed in more detail in Sec. 4.5.1 below.

In a given trap, the ground and excited states of single condensates can be characterized by one parameter encompassing particle number, scattering length, and one of the trap frequencies. In the same trap, the five parameters for a double condensate — the number of atoms of each species plus the three scattering lengths — cannot similarly be reduced to such a useful parameter (or set of parameters). This makes general properties more difficult to ascertain, but it also allows for much richer possibilities for the dynamics of both the ground and excited states.

The remainder of this chapter uses the notation $|1\rangle \equiv |1,-1\rangle$ and $|2\rangle$ for either $|2,2\rangle$ (Sec. 4.5.1) or $|2,1\rangle$ (Sec. 4.5.2).

4.5.1 $|2,2\rangle+|1,-1\rangle$. A small portion of the available parameter space for the $|1,-1\rangle$ and $|2,2\rangle$ hyperfine states has been explored for two cases: (*i*) fixed scattering lengths and equal numbers in each hyperfine state as a function of the number of particles; and (*ii*) fixed intraspecies scattering lengths and a fixed, equal number of atoms in each state as a function of interspecies scattering length. For both cases, the trap frequencies are taken to be $\omega_{2\rho} = 2\pi$ 133

Hz (ω_{2z}=$\sqrt{8}\omega 2\rho$ and $\omega_{1\alpha}$=$\omega_{2\alpha}/\sqrt{2}$), which gives for the displacements of the effective harmonic trapping potentials z_{10}=-3.51 μm and z_{20}=-1.75 μm.

In the first case, the scattering lengths are fixed at their physical values for the $|2,2\rangle$ and $|1,-1\rangle$ hyperfine states of ^{87}Rb. From Burke *et al.* [86] (see also [91, 92]), these are a_{11}=108.8 a.u., a_{22}=109.1 a.u., and a_{12}=108.0 a.u. In addition, the number of atoms in each species was taken to be equal, N_1=N_2=N, as was approximately the case experimentally [87]. The properties of the ground state have previously been discussed for this case in Ref. [93] for the parameters of the Myatt *et al.* experiment, and I find no significant qualitative differences for the TOP trap aside from its different geometry. Consequently, my discussion here concentrates on the excited state properties.

Because the TOP trap retains cylindrical symmetry even for the double condensate system, the projection of the total angular momentum on the symmetry axis M is a good quantum number. Figure 22 shows several of the lowest RPA excitation frequencies for M=0, 1, and 2 with the frequency axis scaled by $\omega_{2\rho}$=2π 133 Hz. To aid in the classification of the states and to show the effects of the interaction of the two condensates, the figure includes the RPA excitation frequencies for uncoupled condensates, a_{12}=0. Note that the excitation frequencies differ significantly from the uncoupled frequencies for essentially all of the states shown. It should also be noted that the uncoupled frequencies for the largest number of atoms reported here, N=5×10^5, agree well with the analytical results available in the hydrodynamic limit [19, 22]. For some of the higher lying excitations though, it appears that the hydrodynamic limit has not yet been reached by N=5×10^5 where the numerical frequencies exceed the analytical frequencies by about 5%. The numerical results remain uncertain to within a few percent, however, due to basis set truncation of the RPA equations; this makes a definitive assessment difficult.

It happens that ω_{1z}=$\omega_{2\rho}$ and $2\omega_{1\rho}$=ω_{2z} for the $|1,-1\rangle$ and $|2,2\rangle$ hyperfine states in the TOP trap. These "accidentally" commensurate frequencies appear to ideally encourage simultaneous excitations of collective modes in both species, through the possibility of resonant

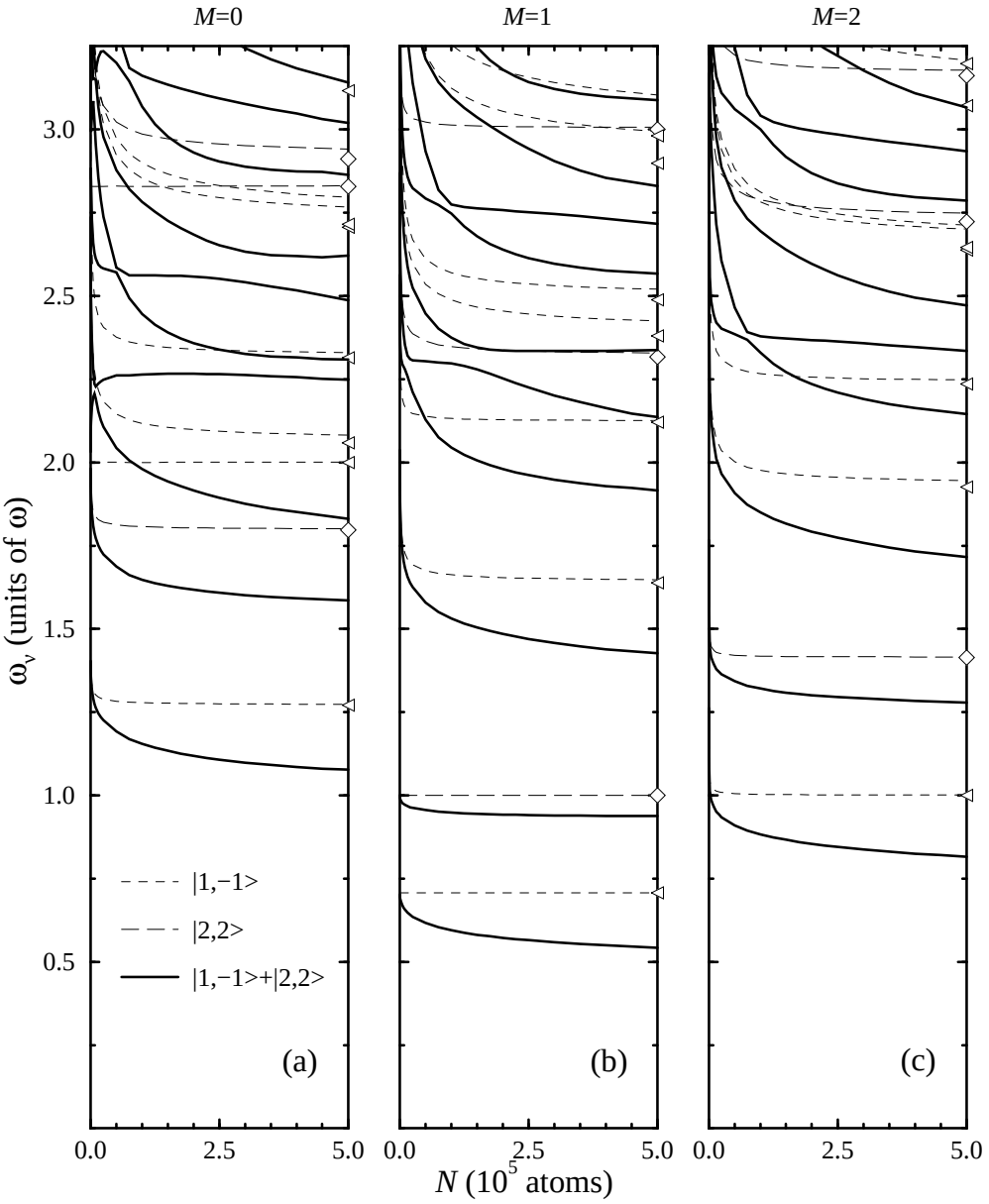

Figure 22. The RPA excitation frequencies for the ^{87}Rb $|2,2\rangle$+$|1,-1\rangle$ system in a TOP trap as a function of N=N_1=N_2. The scattering lengths used are a_{11}=108.8 a.u., a_{22}=109.1 a.u., and a_{12}=108.0 a.u. [86]. In (a) the M=0 spectrum is shown; in (b), the M=1 spectrum; and in (c), the M=2 spectrum. The coupled condensate frequencies are indicated by the heavy solid lines, while the uncoupled frequencies are indicated by the thin dashed and long-dashed lines for the $|1,-1\rangle$ and $|2,2\rangle$ states, respectively. The symbols at the right hand side of each plot indicate the frequencies in the hydrodynamic limit [22]: triangles for $|1,-1\rangle$ and diamonds for $|2,2\rangle$. This figure adapted from Ref. [102].

energy transfer between the condensates. The mean field quickly removes this degeneracy, however, thus making it an implausible mechanism for the generation of simultaneous modes.

The lowest two frequencies for each M in Fig. 22 arise primarily from the response of one or the other of the atomic species. That this is the case can be seen more clearly by considering oscillations in the expectation value of the number density for the singly excited time-dependent wave function

$$|\Psi(t)\rangle = \alpha\,|N_1; N_2\rangle + \beta e^{-i\omega_\nu t}\left|\Phi_\nu^{\mathrm{RPA}}\right\rangle.$$

This form of the wave function applies, for instance, after some period of driving the condensate although it will more generally also have multiply excited state contributions. The observable most often measured experimentally is the number density, and for double condensates the number density of each species can be measured separately. Thus, one revealing quantity is the expectation value of the species-specific number density operator

$$\hat{n}_1(\mathbf{x}) = \sum_{\alpha\beta} \hat{c}_\alpha^\dagger \hat{c}_\beta\, \psi_\alpha^*(\mathbf{x})\psi_\beta(\mathbf{x})$$

($\hat{n}_2(\mathbf{x})$ has the same form with $\hat{c}\to\hat{d}$ and $\psi\to\phi$). Experimentally, the total number density can also be measured, while theoretically it is calculated as the expectation value of $\hat{n}=\hat{n}_1+\hat{n}_2$. For the above wave function, the expectation value is thus

$$\begin{aligned}\langle\Psi(t)\,|\hat{n}_1(\mathbf{x})|\,\Psi(t)\rangle &= |\alpha|^2\,\langle N_1; N_2\,|\hat{n}_1(\mathbf{x})|\,N_1; N_2\rangle + |\beta|^2\,\left\langle\Phi_\nu^{\mathrm{RPA}}\,|\hat{n}_1(\mathbf{x})|\,\Phi_\nu^{\mathrm{RPA}}\right\rangle \\ &\quad +2\mathrm{Re}\left[\alpha^*\beta e^{-i\omega_\nu t}\left\langle N_1; N_2\,|\hat{n}_1(\mathbf{x})|\,\Phi_\nu^{\mathrm{RPA}}\right\rangle\right].\end{aligned}$$

Since the oscillation in the experimentally measured width is entirely due to the cross term in this expression (and to its analogue when multiple excitations are present), the quantity

$$\Delta\langle\hat{n}_i(\mathbf{x})\rangle = \left\langle N_1; N_2\,|\hat{n}_i(\mathbf{x})|\,\Phi_\nu^{\mathrm{RPA}}\right\rangle \quad i=1,2 \tag{96}$$

provides a convenient way to visualize the qualitative behavior of a given excited state. I show in Fig. 23 the density oscillation, Eq. (96), weighted by $\sqrt{N_i}$ for each species, for the two

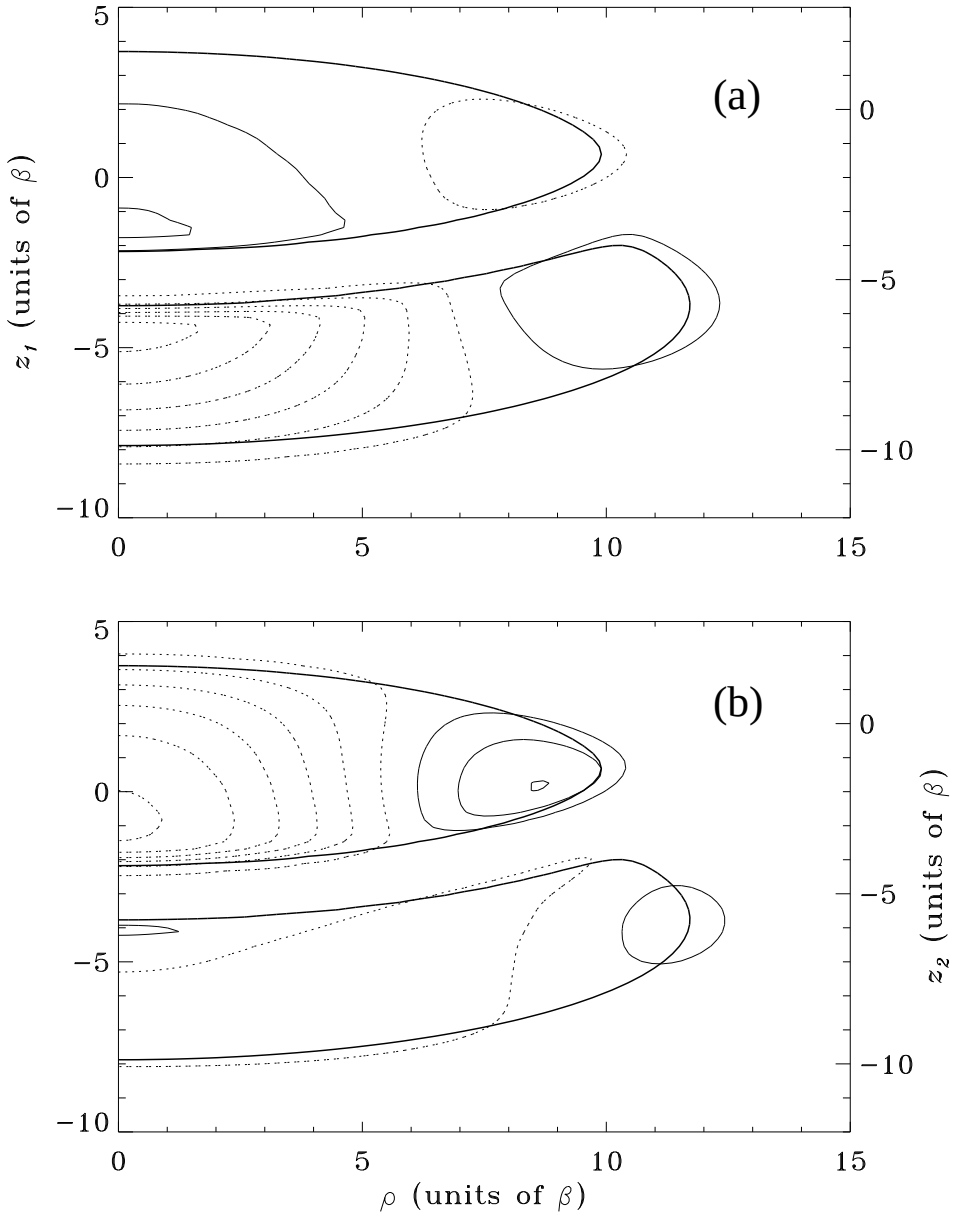

Figure 23. The density oscillation [see Eq. (96)] for the lowest two excitations of the $|2,2\rangle+|1,-1\rangle$ ^{87}Rb system in a TOP trap with N_1=N_2=5×10^5, a_{11}=108.8 a.u., a_{22}=109.1 a.u., and a_{12}=108.0 a.u.: (a) ν=1 and (b) ν=2. The contours are evenly spaced with negative values indicated by dotted lines and positive by solid lines. The heavy solid line marks the extent of the ground state at the level of the lowest positive contour (see Fig. 24). Note that the z-axis has been shifted for the upper ($|2,2\rangle$) state according to the right hand axes. With $\omega_{2\rho}$=2π 133 Hz, β= 0.935 μm. This figure adapted from Ref. [102].

lowest M=0 states. It is plotted in the ρz-plane with the z-axis of the $|2,2\rangle$ state (the upper condensate in the figure) shifted upward (to make each separate condensate more clearly visible in the figure) according to the axis on the right hand side of the plot. Unshifted, the two densities overlap by about one-half oscillator unit along the entire length of their interface as can be seen in the ground state number density in Fig. 24. In both figures, the density contour lines are equally spaced, and the heavy contours indicate the extent of the ground state at the level of the lowest positive contour. In Fig. 23a, it can be seen that the $|1,-1\rangle$ state (the lower condensate in the figure) responds much more strongly to the driving frequency than the $|2,2\rangle$ state. In Fig. 23b, just the opposite is apparent. The same is also approximately true for the lowest two excitations of both the M=1 and M=2 symmetries. Because of the distribution of negative and positive density oscillations — these are the dotted and solid contours in Fig. 23, respectively — excitations of the lowest two states are seen to cause oscillations of the clouds that are almost entirely radial.

Higher in the spectra in Fig. 22, several avoided crossings can be seen as the excitations that are primarily in the z direction get pushed higher with increasing N by the larger mean field. At N=1 the third excited state, for instance, converges to the $(n_{1\rho}, n_{1z}; n_{2\rho}, n_{2z})$=(0,1;0,0) harmonic oscillator state. As N increases, its excitation frequency rapidly increases until it reaches an avoided crossing with the state with $(n_{1\rho}, n_{1z}; n_{2\rho}, n_{2z})$=(2,0;0,0) character. After the crossing, the third excited state is mostly this ρ excitation while the fourth excited state carries the n_{1z} excitation. Finally, at N=500000, the fourth excited state is mostly $(n_{1\rho}, n_{1z}; n_{2\rho}, n_{2z})$=(0,1;1,0) in character with a large admixture of $(n_{1\rho}, n_{1z})$=(1,0) where the quantum numbers $n_{i\rho}$ and n_{iz} now count nodes along each coordinate for the nonseparable Hartree-Fock wave functions. It is useful at this point to recall the stacked pancake geometry of the TOP trap in which the z axis is the symmetry axis of the system. The higher energetic cost for excitations along this direction as N increases is physically reasonable since each condensate sees an increasingly hard wall due to the mean field of the other condensate. On the other hand, the trend for the excitations in the radial direction is just the opposite. Again,

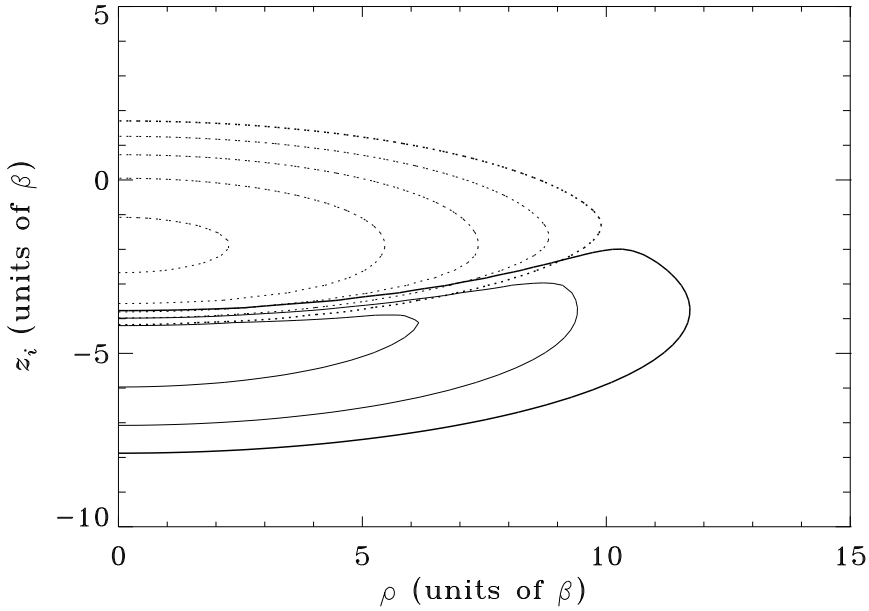

Figure 24. The ground state densities $|\psi_0(\mathbf{x})|^2$ and $|\phi_0(\mathbf{x})|^2$ for the $|2,2\rangle$+$|1,-1\rangle$ states of ^{87}Rb in a TOP trap. The parameters are as follows: N_1=N_2=5×10^5, a_{11}=108.8 a.u., a_{22}=109.1 a.u., a_{12}=108.0 a.u., ω_z= $\sqrt{8}\,\omega_\rho$, and ω_ρ=2π 133 Hz. The solid line corresponds to the $|1,-1\rangle$ state and the dotted to $|2,2\rangle$. The heavy lines are identical to those in Fig. 23 and Fig. 25. This figure adapted from Ref. [102].

this is physically reasonable since the condensates grow larger in this dimension as N increases, thus increasing the longest wavelength supported by the system. This is especially true for the $|1,-1\rangle$ condensate as it tends to lengthen by wrapping around the $|2,2\rangle$ condensate. The state which corresponds to the $(n_{1\rho}, n_{1z}; n_{2\rho}, n_{2z})$=(3,0;0,0) harmonic oscillator state with an excitation energy of 4.2 $\hbar\omega_{2\rho}$, for example, drops from the ninth excited state at N=1 to the fifth at N=500000 with an excitation frequency of ω_5=2.3 $\omega_{2\rho}$. For the uncoupled condensates, it drops to only the seventh excited state (counting both condensates) with an excitation frequency of ω_7=2.8 $\omega_{2\rho}$.

Nearly all of the states above ν=2 exhibit a simultaneous response of both condensates to driving. The ratio of the peak amplitudes for each ranges from about 2 to unity. The more interesting case of approximately equal response is exhibited in Fig. 25. The sixth and seventh excited M=0 states are shown; similar examples could be drawn from both the M=1 and M=2 symmetries. For ν=6, Fig. 25a, the radial and axial motions are coupled — albeit weakly — in a manner such that the total time-dependent density appears to transfer from the $|2,2\rangle$ state to the $|1,-1\rangle$ state along z and to a lesser extent along ρ for each. For ν=7, Fig. 25b, the coupling of radial and axial motions is stronger. This suggests that the density sloshes in phase along z for both species while also expanding and contracting in ρ.

In the second case considered, the numbers of atoms in each species are taken to be N_1=N_2=10^5, and the scattering lengths a_{11} and a_{22} are chosen to be 108.8 a.u. and 109.1 a.u., respectively; the interspecies scattering length a_{12} has been left free to vary. This might not be easily realized experimentally for the present choice of atomic species, but will almost certainly be attainable for some combination of atoms. It is likely, in fact, that the entire range of interspecies scattering lengths could be explored by tuning the molecular interaction potentials with an external field [103, 104].

Section 4.4.2 (see also Ref. [93]) briefly discussed some of the ground state properties as a function of a_{12} for the Myatt *et al.* experiment [87]. Here, I expand on that discussion, focusing on the TOP trap geometry. Figure 26 displays the ground state orbital energies.

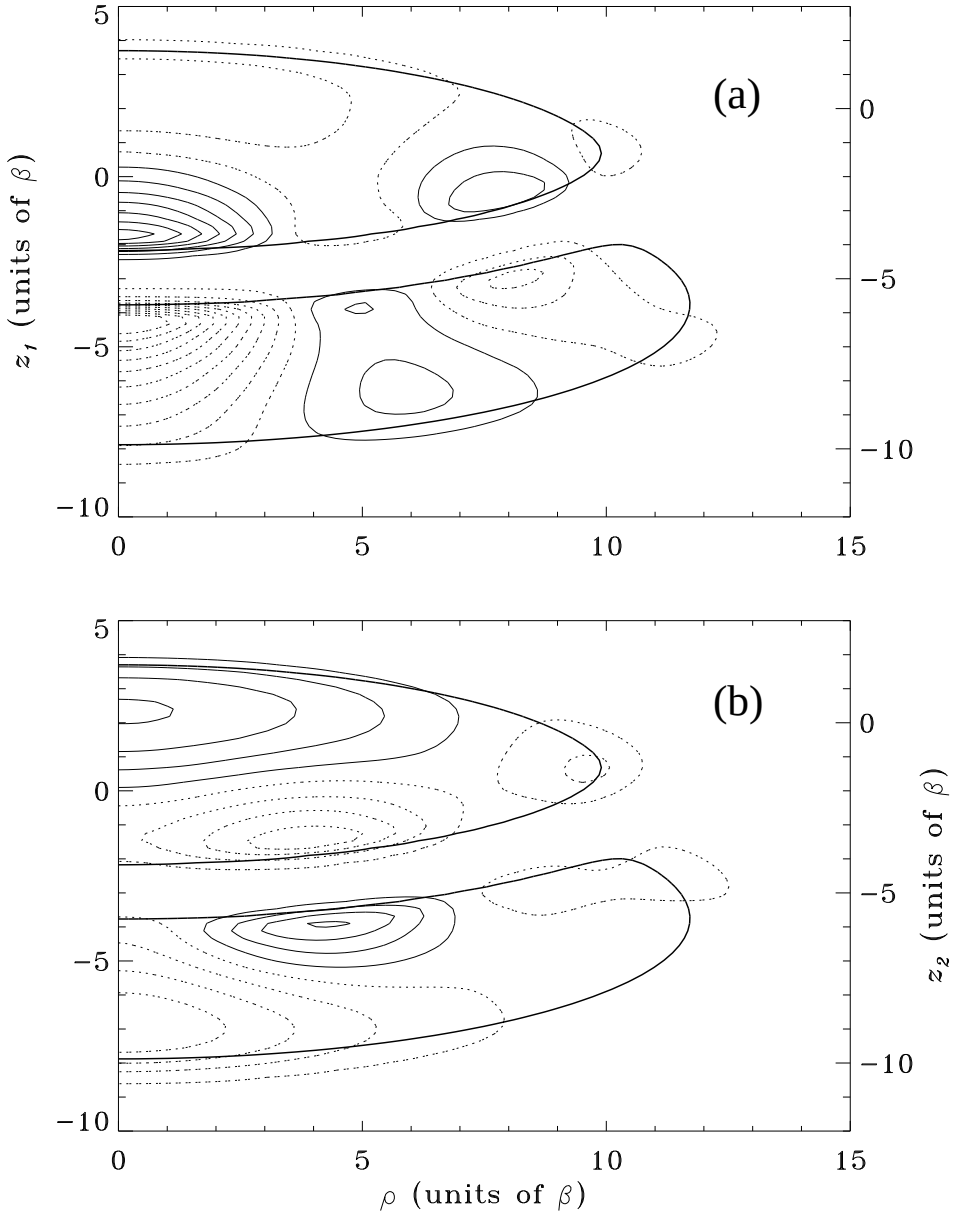

Figure 25. The density oscillation [see Eq. (96)] for ^{87}Rb $|2,2\rangle+|1,-1\rangle$ in a TOP trap. The parameters are N_1=N_2=5×10^5, a_{11}=108.8 a.u., a_{22}=109.1 a.u., and a_{12}=108.0 a.u.. In (a) ν=6 is shown; and in (b),ν=7. The contours are evenly spaced with negative values indicated by dotted lines and positive by solid lines. The heavy solid line marks the extent of the ground state at the level of the lowest positive contour (see Fig. 24). Note that the z-axis has been shifted for the upper ($|2,2\rangle$) state according to the right hand axes. This figure adapted from Ref. [102].

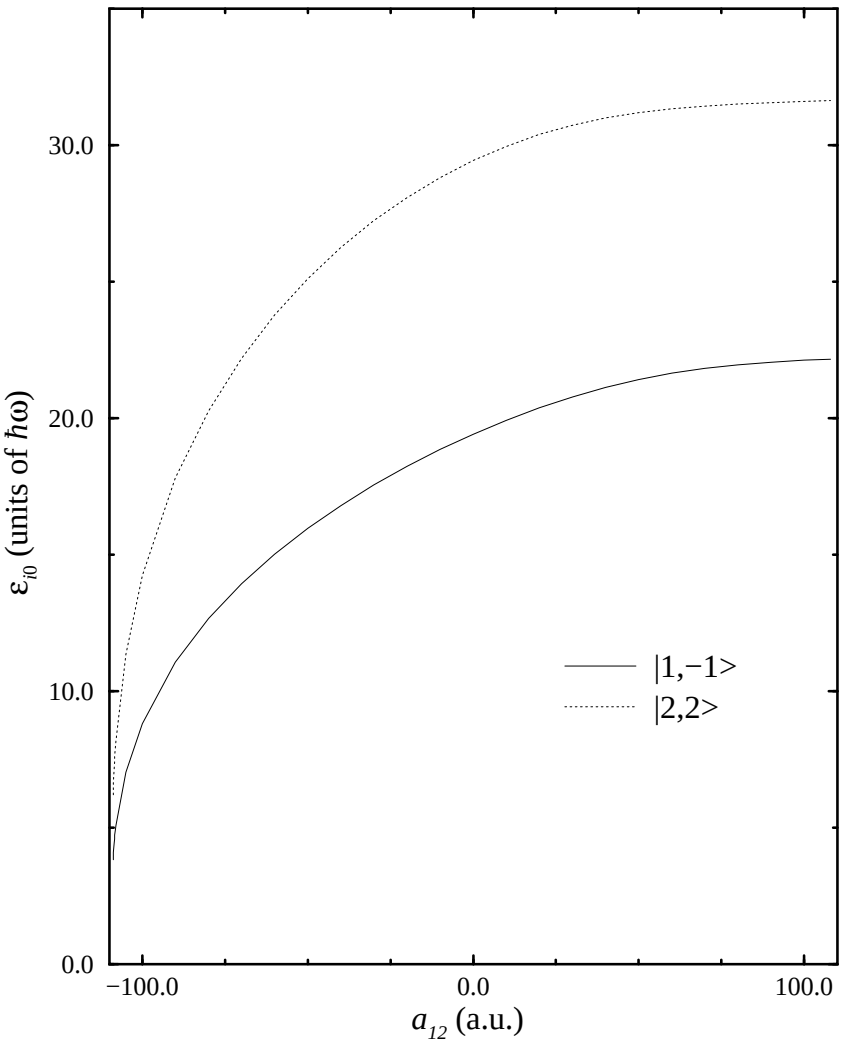

Figure 26. The ground orbital energies for the $|2,2\rangle+|1,-1\rangle$ ^{87}Rb system in a TOP trap as a function of interspecies scattering length. The remaining parameters are as follows: N_1=N_2=10^5, a_{11}=108.8 a.u., and a_{22}=109.1 a.u. The solid line corresponds to the $|1,-1\rangle$ state and the dotted to $|2,2\rangle$. This figure adapted from Ref. [102].

For an interspecies scattering length approaching the critical value $a_{12}\approx-110$ a.u., the orbital energies grow rapidly smaller. In the Thomas-Fermi approximation, double condensates with $a_{12}\leq-a_{12}^c=-\sqrt{a_{11}a_{22}}$ are in fact unstable (for the present parameters a_{12}^c=109.0 a.u.; see Sec. 4.2 for details). Ground state instabilities are typically expected to appear in the RPA excitation spectrum as an excitation frequency that becomes identically zero for some value of a parameter such as a_{12} [30, 53, 69]. Such behavior was explicitly demonstrated by Dodd *et al.* [30] for a single condensate of ^{7}Li. The excitation frequencies in Fig. 27, however, remain strictly positive, and show no tendency towards zero at the critical value of the interspecies scattering length. It follows that the instability expected for the double condensate differs in character from the single condensate instability. The Hartree-Fock approach combined with a RPA analysis shows the symptoms of an instability, but the only information they provide in this case is that the presumed Hartree-Fock ground state is a poor approximation to the true ground state. They give little indication how to improve the approximate Hartree-Fock state used. The desired improvements should build on either deeper physical insight or superior numerical algorithms. For the time being, these questions are being explored from a different perspective [105].

The qualitative behavior of the excitation frequencies as functions of a_{12} can be understood in terms of the change in the size of the condensate. As a_{12} increases from zero, the situation is essentially as described above for increasing N — the ρ-excitation frequencies decrease while the frequencies in z increase. As a_{12} decreases from zero, though, the condensates get steadily smaller, which forces the excitation frequencies higher in energy for both ρ and z excitations. That this is the case can be seen in Fig. 27, with only a few exceptions. Generally speaking, then, it follows that excitations predominantly in the z direction increase in frequency as $|a_{12}|$ increases, while excitations primarily in the ρ direction decrease as a_{12} increases from the value $-a_{12}^c$.

Figure 28 shows the contours of the ground state density for a_{12}=−108.0 a.u. With an interspecies scattering length this large in magnitude, the mean field experienced by an atom of one species due to the atoms in the other species becomes comparable to the atom's

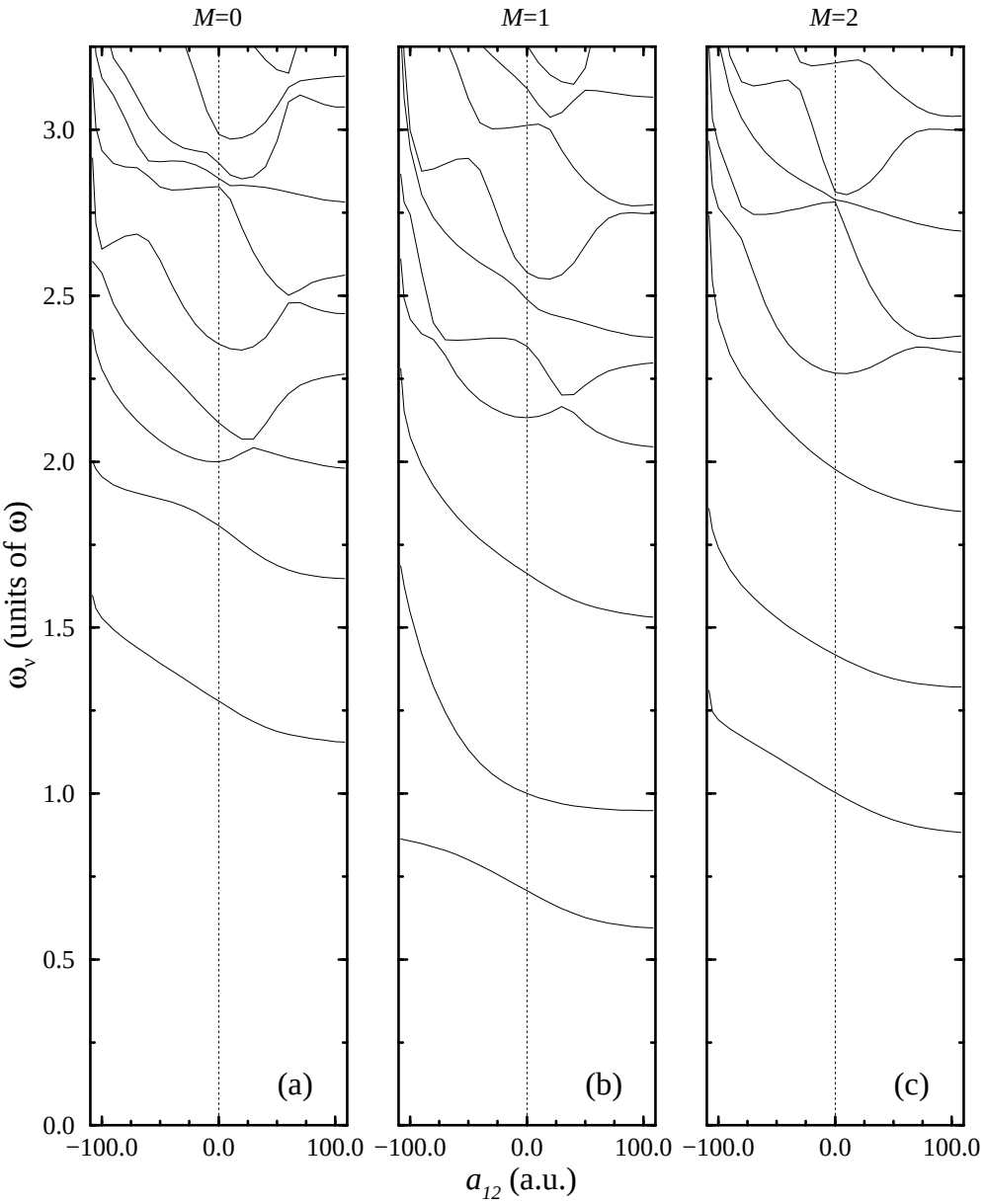

Figure 27. The RPA excitation frequencies for ^{87}Rb $|2,2\rangle$+$|1,-1\rangle$ in a TOP trap as a function of a_{12}. The remaining parameters are as follows: a_{11}=108.8 a.u., a_{22}=109.1 a.u., and N_1=N_2=10^5. In (a) the M=0 spectrum is shown; in (b), the M=1 spectrum ; and in (c), the M=2 spectrum. This figure adapted from Ref. [102].

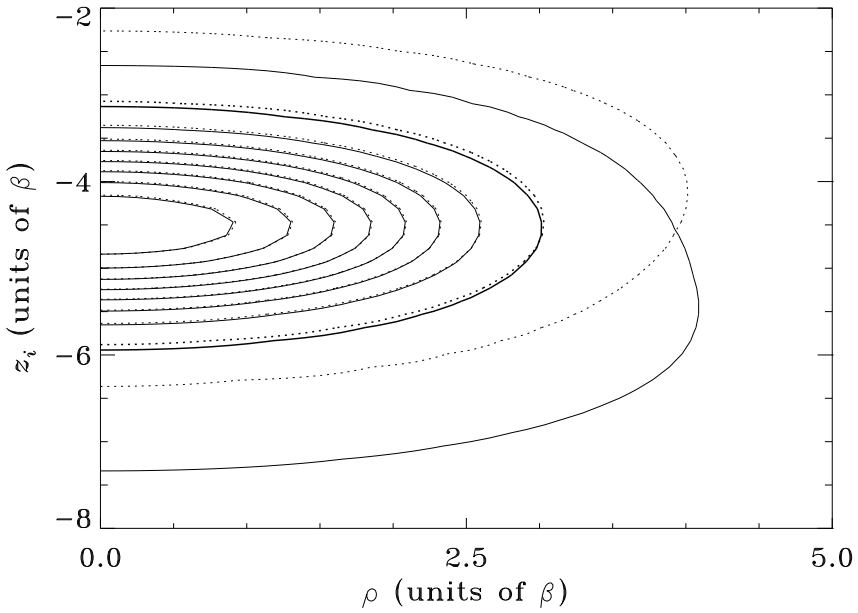

Figure 28. The ground state densities $|\psi_0(\mathbf{x})|^2$ and $|\phi_0(\mathbf{x})|^2$ for the $|2,2\rangle$ and $|1,-1\rangle$ states of ^{87}Rb. The parameters are N_1=N_2=10^5, a_{11}=108.8 a.u., a_{22}=109.1 a.u., and a_{12}=−108.0 a.u. The solid line corresponds to the $|1,-1\rangle$ state and the dotted to $|2,2\rangle$. The heavy lines are identical to those in Fig. 29. This figure adapted from Ref. [102].

interaction with its own species. The attraction is great enough, in fact, to overcome the gravitationally induced separation, and consequently the condensates lie almost completely on top of one another. Each of the condensates essentially coincide above the first contour in Fig. 28. And, given that the uncoupled condensates are about 12×4.5 ($\rho\times z$) oscillator units (FWHM) and 10×3.5 oscillator units for the $|1,-1\rangle$ and $|2,2\rangle$ states, respectively, the condensates in Fig. 28 are much smaller, as expected from the qualitative discussion above for the behavior of the excitation frequencies.

The density oscillations $\Delta\langle\hat{n}_i(\mathbf{x})\rangle$ for the first and third M=0 excited states are presented in Figure 29. These correspond to the ground state in Fig. 28. In this configuration, the two species behave like a single species condensate. This is manifested in both Fig. 29a and Fig. 29b (the $|2,2\rangle$ state has been shifted upward as for Figs. 23 and 29; also, compare Fig. 28) since the amplitude and topology of each condensate's response matches almost completely. Experimentally, the density variations should still be measurable independently and would show purely radial breathing for the first excited state and purely axial sloshing for the third.

4.5.2 $|2,1\rangle+|1,-1\rangle$**.** In this section, I consider the situation in which the $|2,1\rangle$ and $|1,-1\rangle$ hyperfine states of ^{87}Rb are contained within the same TOP trap. This case is fundamentally different from that considered in the last section for one reason — the magnetic moments of both the $|2,1\rangle$ state and the $|1,-1\rangle$ state are the same. The geometry of the system thus simplifies considerably since both the sag due to gravity and the trap frequency are also the same for both states. The former implies a higher spatial symmetry as well since the Hamiltonian is now invariant upon reflection through z=0. Further, because of the large spatial overlap of the two atomic clouds, the effects of the interspecies interactions will prove to be considerably more dramatic than in Sec. 4.5.1.

Specifically, I choose N_1=N_2=10^5 and take both intraspecies scattering lengths to have the same value, a_{ii}=107.0 a.u., which is approximately true within present uncertainties. With all parameters equal, the ground state orbital wave functions are identical as shown in Fig. 30 for a_{12}=107 a.u. As in Sec. 4.2, the coupled Hartree-Fock equations in this case reduce to a

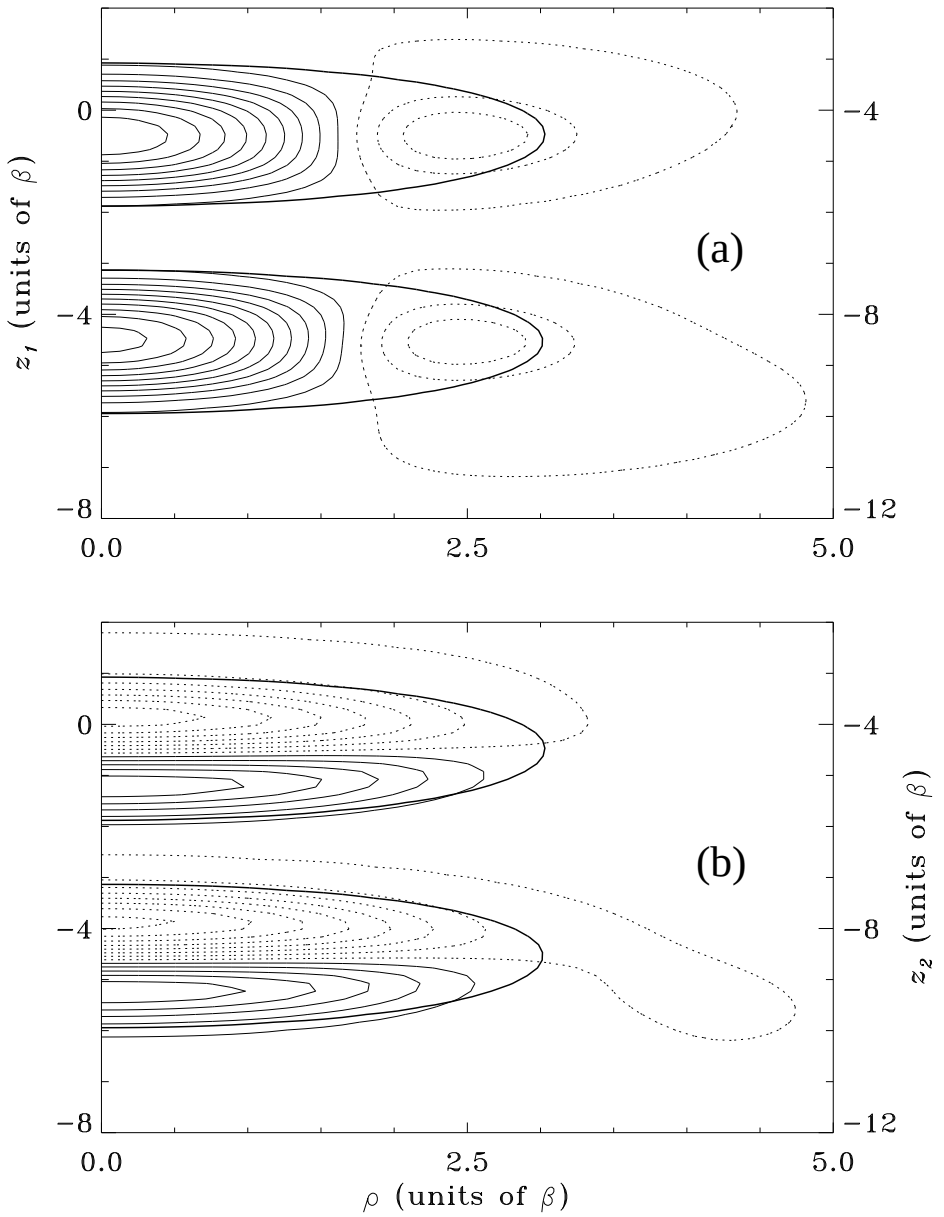

Figure 29. The density oscillation [see Eq. (96)] for the ^{87}Rb $|2,2\rangle + |1,-1\rangle$ system with N_1=N_2=5×10^5, a_{11}=108.8 a.u., a_{22}=109.1 a.u., and a_{12}=−108.0 a.u.. In (a) ν=1 is shown; and in (b), ν=3. The contours are evenly spaced with negative values indicated by dotted lines and positive by solid lines. The heavy solid line marks the extent of the ground state at the level of the lowest positive contour (see Fig. 28). Note that the z-axis has been shifted for the upper $|2,2\rangle$ state according to the right hand axes. This figure adapted from Ref. [102].

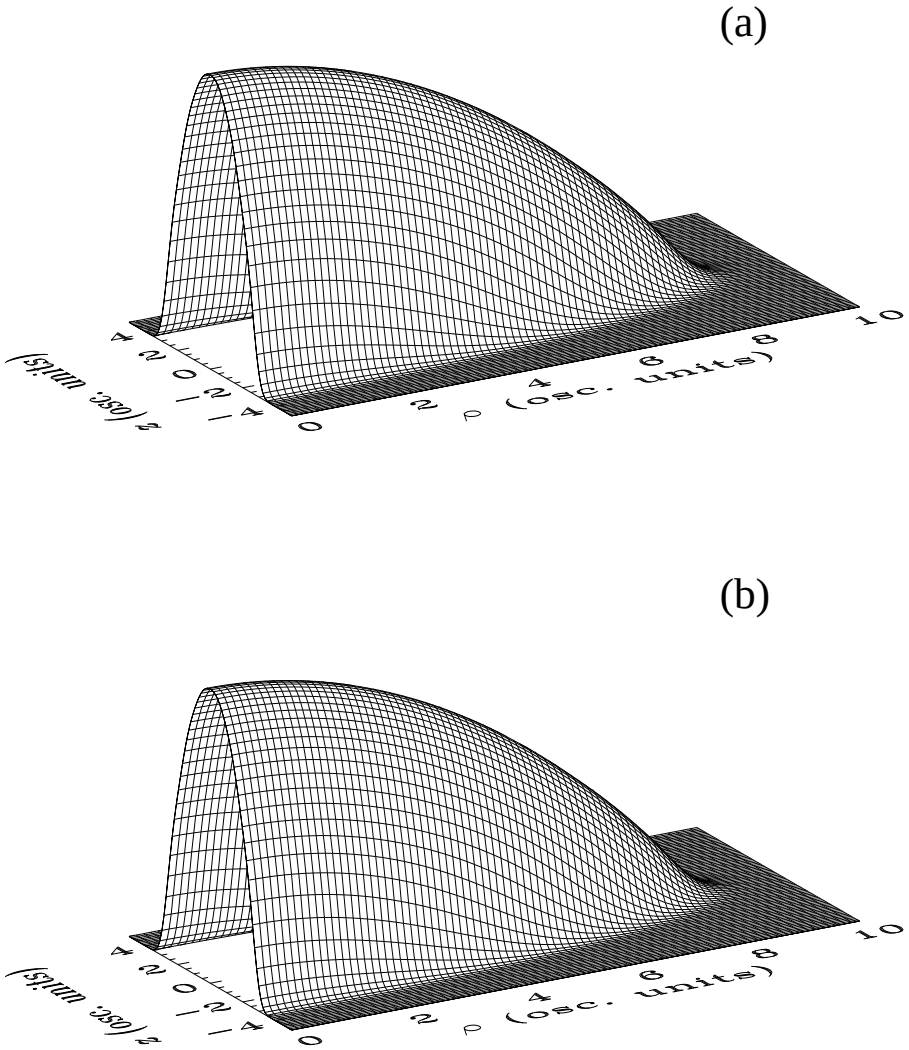

Figure 30. The single particle densities $|\psi_0(\mathbf{x})|^2$ and $|\phi_0(\mathbf{x})|^2$ in the ρz plane for the ^{87}Rb $|2,1\rangle + |1,-1\rangle$ system in a TOP trap. The parameters are as follows: N_1=N_2=10^5 and a_{11}=a_{22}=a_{12}=107 a.u. The $|1,-1\rangle$ state is shown in (a) and the $|2,1\rangle$ state in (b). Note that the wave functions are identical and that 1 osc. unit=β=0.935 μm.

single component equation with an effective scattering length of $a_{11}+a_{12}$.

The RPA equations, however, do not reduce to a single component equation. Such a reduction would not account for the twofold degeneracy in the a_{12}=0 excited state spectrum. Equation (93) does take it into account, and the results for the present system are shown in Fig. 31 as a function of a_{12}. The degeneracy at a_{12}=0 is evident as is the splitting of this degeneracy for $a_{12}\neq 0$. Generally speaking, each degenerate level is split into one mode that decreases roughly linearly in a_{12} and one mode that is essentially unaffected by changes in a_{12}. More precisely, it is affected by changes in a_{12} in the same way that the ground state is such that the excitation frequency is unaffected. This behavior can be qualitatively understood using a simple two state model that amounts to degenerate perturbation theory for the a_{12}=0 states. Consider, then, the Hamiltonian in this degenerate 2×2 space. In the quasi-Hartree-Fock basis, it can be written generally as

$$H = \begin{pmatrix} E_p & \gamma_p a_{12} \\ \gamma_p a_{12} & E_p \end{pmatrix}$$

where E_p is the total energy of the state under question and γ_p is a real positive constant originating from the two-body interspecies interaction. It is real because of my phase convention, and it is positive because I impose the same phase convention on the orbitals for both species. The latter follows since the interaction matrix elements reduce to an integral over four orbital wave functions in the pseudopotential approximation: the ground state and p-th excited state of one species and the ground state and p-th excited state of the other. Since the integrand is the product of the square of two functions, this integral (and thus γ_p) is positive definite. Diagonalizing the above Hamiltonian is straightforward, and the result is

$$E_{p-} = E_p - \gamma_p a_{12} \qquad |p-\rangle = \frac{1}{\sqrt{2}}\left(|N_1-1,1_p;N_2\rangle - |N_1;N_2-1,1_p\rangle\right) \tag{97}$$

$$E_{p+} = E_p + \gamma_p a_{12} \qquad |p+\rangle = \frac{1}{\sqrt{2}}\left(|N_1-1,1_p;N_2\rangle + |N_1;N_2-1,1_p\rangle\right). \tag{98}$$

The ground state energy will also be corrected to first order in a_{12} by the amount $\gamma_0 a_{12}$ where γ_0 is the integral of the fourth power of the ground state orbital wave function. To first order

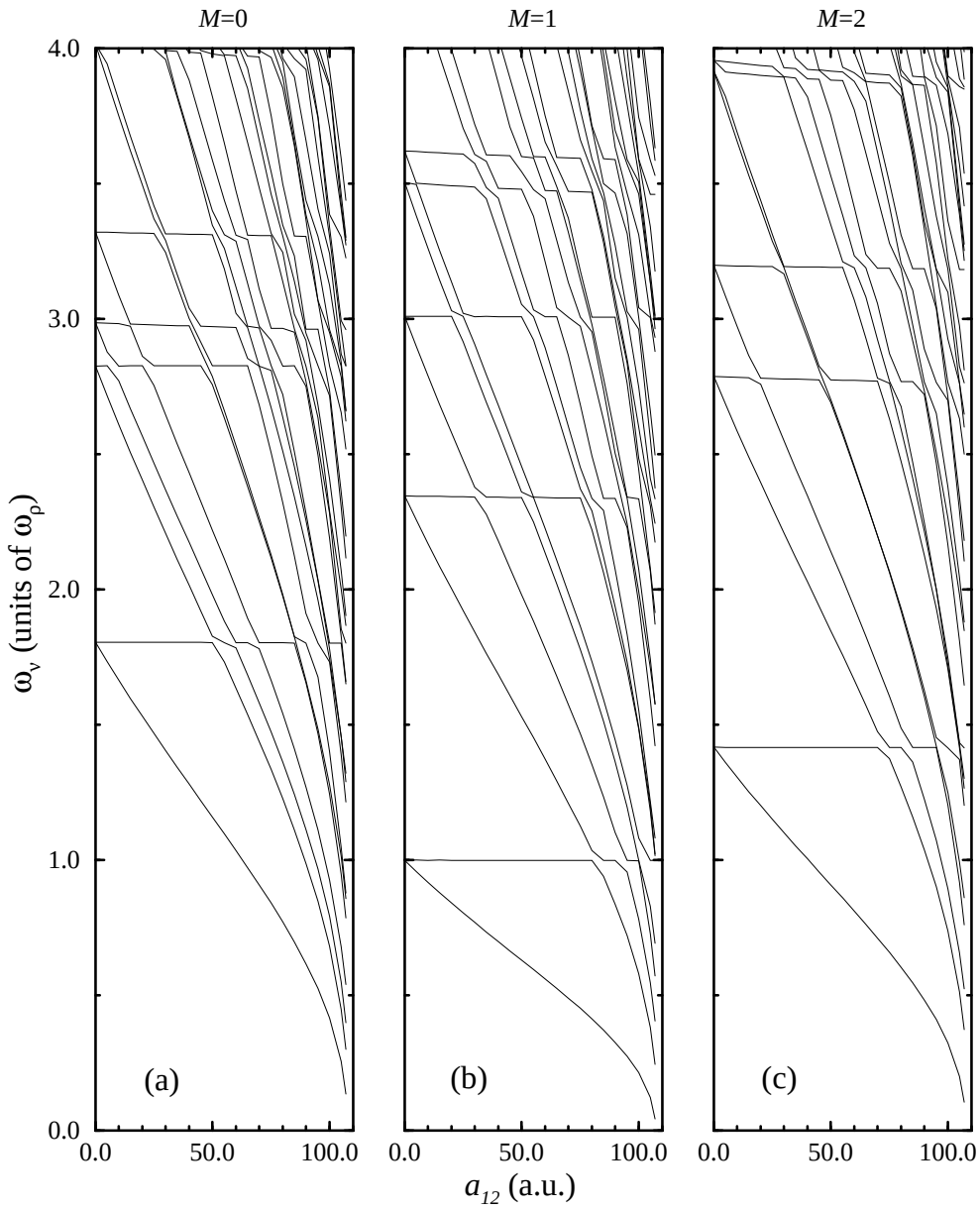

Figure 31. The RPA excitation frequencies for ^{87}Rb $|1,-1\rangle+|2,1\rangle$ in a TOP trap as a function of a_{12}. The parameters are a_{11}=a_{22}=107 a.u., and N_1=N_2=10^5. In (a) the M=0 spectrum is shown; in (b), the M=1 spectrum; and in (c), the M=2 spectrum.

in the interspecies scattering length, then, the excitation frequencies are

$$\hbar\omega_p^{\pm} = \hbar\omega_p + (\pm\gamma_p - \gamma_0)\, a_{12}.$$

Since γ_0 is approximately equal to γ_p or larger, $\hbar\omega_p^+$ will at most decrease slightly with increasing a_{12}; $\hbar\omega_p^-$, on the other hand, decreases linearly with a_{12} with a slope of approximately $2\gamma_p$. The states $|p\pm\rangle$ are in fact the eigenstates of the spin exchange operator (which commutes with the interspecies interaction). An examination of the full RPA solution vectors reveals precisely the same behavior as this simple two-state model. Because both the z-parity and the spin exchange are exact symmetries, the states labeled by these quantum numbers are not coupled so that the curve crossings in Fig. 31 are real rather than avoided as shown in the figure.

At values of a_{12} larger than about 100 a.u., it can be seen that the excitation frequencies are approaching zero with every indication of reaching it. Since both a_{11} and a_{22} have the value 107 a.u. in the present example, the critical value of a_{12} is also 107 a.u. It was stated in the discussion in Sec. 4.4.2 that for interspecies scattering lengths larger than the critical value that the two species completely separate spatially. It stands to reason that the excitation spectrum will show different behavior for $a_{12} \geq a_{12}^c$. It is this regime that is examined in detail in the next section.

4.6 Spatial symmetry breaking

It was shown in the last section that the RPA excitation spectrum for a double condensate gives indications that the Hartree-Fock ground state is unstable for a_{12} greater than the critical value. Since a recent calculation has shown that this could be the case for a physical system [106], it is important to understand the implications of the standard Hartree-Fock and random phase approximations in this case. It is known [88, 93, 94, 95] that for interspecies scattering lengths larger than the geometric mean of the intraspecies scattering lengths that the two components completely expel each other.

This so-called phase separation is shown in Figs. 32-34. I have chosen to use the TOP

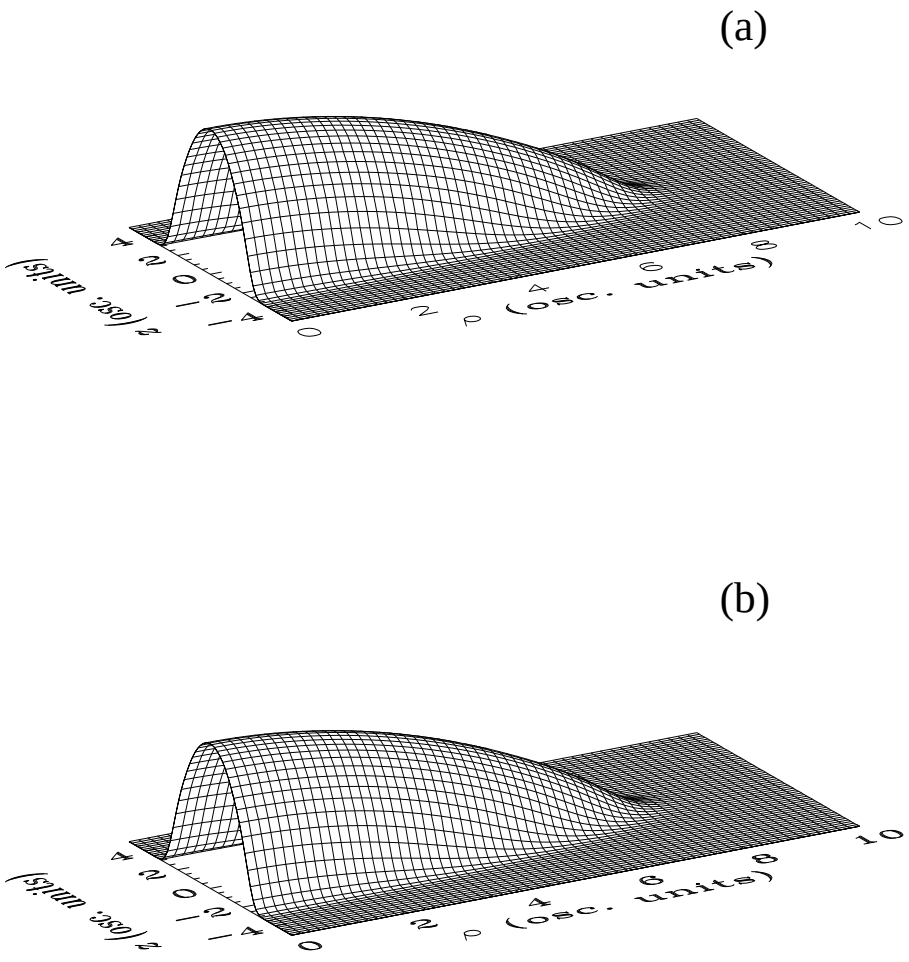

Figure 32. The single particle densities $|\psi_0(\mathbf{x})|^2$ and $|\phi_0(\mathbf{x})|^2$ in the ρz plane for the $|1,-1\rangle$ and $|2,1\rangle$ states of ^{87}Rb in a TOP trap. The parameters are as follows: N_1=10^5, N_2=5000 and a_{11}=a_{22}=a_{12}=107 a.u. The $|1,-1\rangle$ state is shown in (a) and the $|2,1\rangle$ state in (b). Note that the wave functions are identical and that 1 osc. unit=β=0.935 μm.

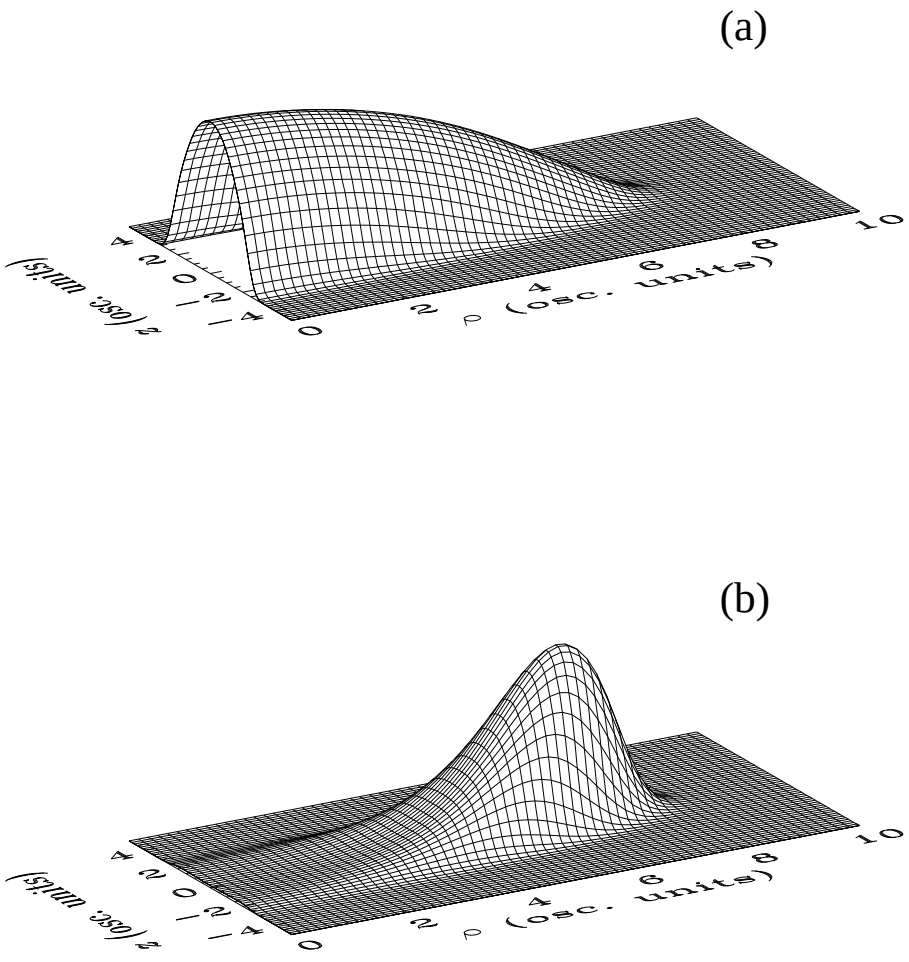

Figure 33. The single particle densities $|\psi_0(\mathbf{x})|^2$ and $|\phi_0(\mathbf{x})|^2$ in the ρz plane for the $|1,-1\rangle$ and $|2,1\rangle$ states of ^{87}Rb in a TOP trap. The parameters are as follows: N_1=10^5, N_2=5000, a_{11}=a_{22}=107 a.u., and a_{12}=110 a.u. The $|1,-1\rangle$ state is shown in (a) and the $|2,1\rangle$ state in (b). Note that the vertical scale is the same used in Fig. 32 and that 1 osc. unit=β=0.935 μm.

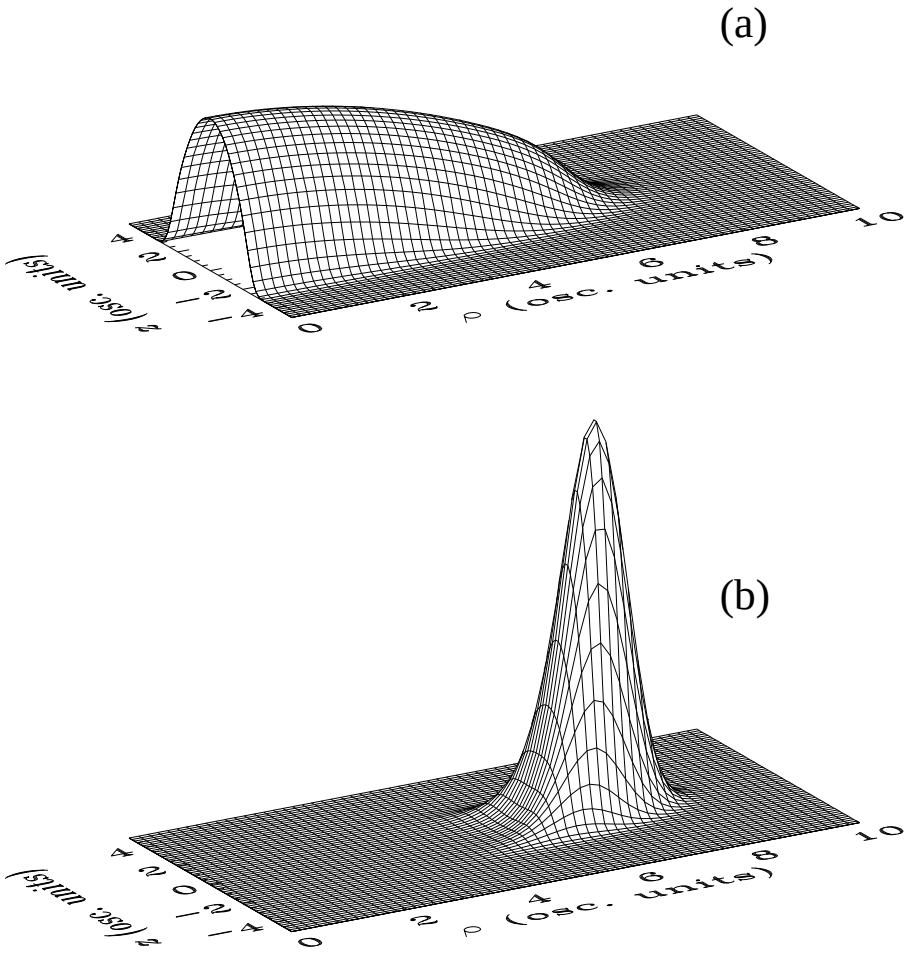

Figure 34. The single particle densities $|\psi_0(\mathbf{x})|^2$ and $|\phi_0(\mathbf{x})|^2$ in the ρz plane for the $|1,-1\rangle$ and $|2,1\rangle$ states of ^{87}Rb in a TOP trap. The parameters are as follows: N_1=10^5, N_2=5000, a_{11}=a_{22}=107 a.u., and a_{12}=130 a.u. The $|1,-1\rangle$ state is shown in (a) and the $|2,1\rangle$ state in (b). Note that the vertical scale is the same used in Figs. 32 and 33 and that 1 osc. unit=β=0.935 μm.

trap frequency ratio $\omega_z/\omega_\rho=\sqrt{8}$ with $\omega_\rho=2\pi\,133$ Hz. The $|1,-1\rangle$ state has $N_1=10^5$ atoms; and the $|2,1\rangle$ state, $N_2=5000$ atoms. The intraspecies scattering lengths are both fixed at 107 a.u. The difference in the apparent height of the wave functions for the two states is due to the fact that the probability densities are plotted on the same scale for each orbital; and, since there are more atoms in the $|1,-1\rangle$ state, it appears shorter and broader than the $|2,1\rangle$ state. For $a_{12}\leq a_{12}^c$ there is little qualitative difference between the wave functions for one value of a_{12} and the wave functions for another value of a_{12}. The orbital wave function for the $|2,1\rangle$ state gets shorter and broader as a_{12} increases from zero until at $a_{12}=107$ a.u. it is identical to the orbital for the $|1,-1\rangle$ state (see Fig. 32). For a_{12} just above a_{12}^c, the situation is quite different and is shown in Fig. 33. The combination of the greater interspecies repulsion and the smaller number of $|2,1\rangle$ atoms forces the bulk of the $|2,1\rangle$ wave function to the end of the $|1,-1\rangle$ wave function in the weaker trap direction ρ. By the time a_{12} is only 10% larger than a_{12}^c, the wave functions are essentially mutually exclusive. This effect, then, would seem to be what is predicted to occur above a_{12}^c. It would be an especially interesting condensate configuration with the $|2,1\rangle$ condensate forming a ring around the $|1,-1\rangle$ state (remember that the plots in Figs. 32-34 are in the ρz plane and must be rotated about the z axis to completely visualize the state).

Figure 35 shows the RPA spectrum for the ten lowest excited states of M=0, 1, and 2. The a_{12}=0 limit shows the splitting due to the differing numbers in each state save for the lowest M=1 excitation and the second lowest M=0 excitation. Both of these states are simply center of mass modes with excitation frequencies equal to ω_ρ and ω_z, respectively. It is also apparent in the figure that the lowest M=1 and M=2 modes go to zero at a_{12}^c. The shaded regions for larger a_{12} indicate the imaginary part of the excitation frequency (see Sec. 4.2). It follows that the Hartree-Fock ground states shown in Figs. 32-34 are not the optimal states within the Hartree-Fock *ansatz* (see Sec. 4.1). The degeneracy (*i.e.* zero excitation frequency) of the M=1 and M=2 excited modes with the ground state indicate that the improved Hartree-Fock ground state should include nonzero m's. Calculations by Öhberg and Stenholm [38] indicate that the spatial configuration of such a Hartree-Fock ground state is likely to show the two

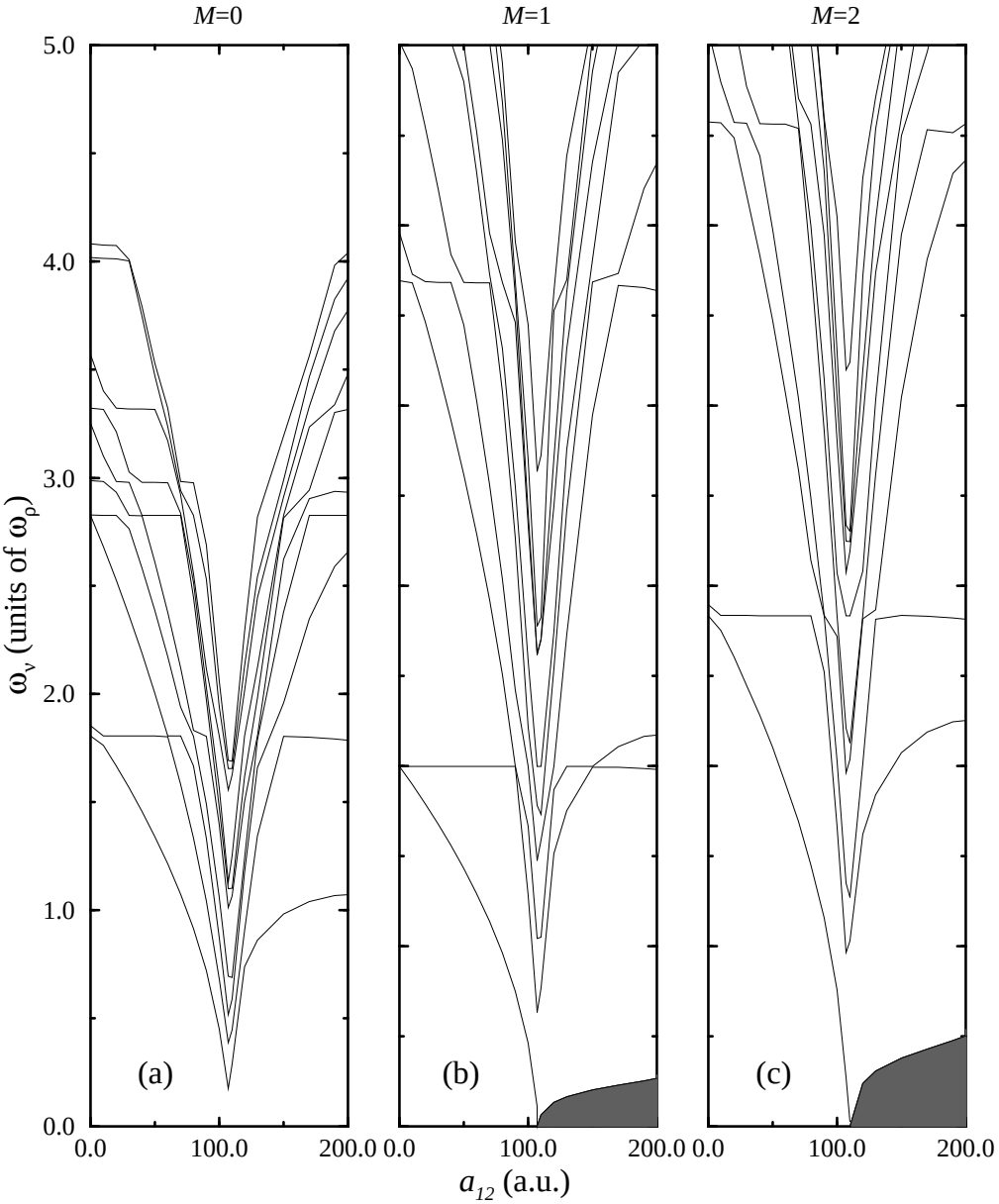

Figure 35. The RPA excitation frequencies for the $|1,-1\rangle$ and $|2,1\rangle$ states of ^{87}Rb in a TOP trap as a function of a_{12}. The parameters are as follows: a_{11}=a_{22}=107 a.u., N_1=10^5 and N_2=5000. In (a) the M=0 spectrum is shown; in (b), the M=1 spectrum; and in (c), the M=2 spectrum. The shaded regions for larger a_{12} indicate the imaginary part of the excitation frequency (see Sec. 4.2).

species localized side-by-side in the xy plane. The implication, then, is that the best Hartree-Fock ground state is not an eigenstate of L_z even though the true many-body ground energy eigenstate must be. In other words, the best Hartree-Fock solution breaks the spatial symmetry of the trap and thus breaks a symmetry of the Hamiltonian. It is apparently common to find such a circumstance when calculating the Hartree-Fock ground states of nuclei [66]. In the present case, it would be necessary to carry out a fully three-dimensional calculation (in order to account for m-mixing) to determine the ground state. While this calculation is possible, a systematic study is nonetheless more easily accomplished in a lower dimensional configuration.

To study spatial symmetry breaking, I have chosen to "invert" the TOP trap frequencies. That is, I take $\omega_z/\omega_\rho=1/\sqrt{8}$. Thus, the trap remains cylindrically symmetric with the weaker trapping now along the z axis. Any spatial symmetry breaking will occur along the weaker trap direction, so that I can expect m to be a good quantum number for the Hartree-Fock ground state for all a_{12}. The resulting calculation is two dimensional which is a clear advantage over the three dimensional case above. I should point out again that a fully three dimensional calculation is possible (see Secs. 4.4.1 and 4.4.2 and Ref. [93]), merely time consuming — especially for exploratory studies such as this. For the other parameters of the system, I choose the symmetric $N_1=N_2=10^5$ and $a_{11}=a_{22}=107.0$ a.u.

Figure 36 shows both the orbital and total energies for the ground state of the system as a function of a_{12}. For $a_{12}\geq a_{12}^c$ the symmetry breaking solution (the dashed line) is clearly lower in energy than the symmetry preserving solution (the solid line). Note that the symmetry being broken here is z-parity (reflection through the z=0 plane). The wave functions are identical in the symmetry preserving configuration, while in the symmetry breaking configuration they mutually expel each other. The symmetry preserving ground state orbital wave functions for a_{12}=107 a.u. are displayed in Fig. 37. They are, in fact, little different for other a_{12} in any way relevant to the present discussion. In Figs. 38-40, I show the symmetry breaking solutions over a range of a_{12}. Note that while these solutions are not identical, because of the symmetry in the parameters it is true that $\psi_0(x,y,-z)=\phi_0(x,y,z)$. The transition between the two extremes

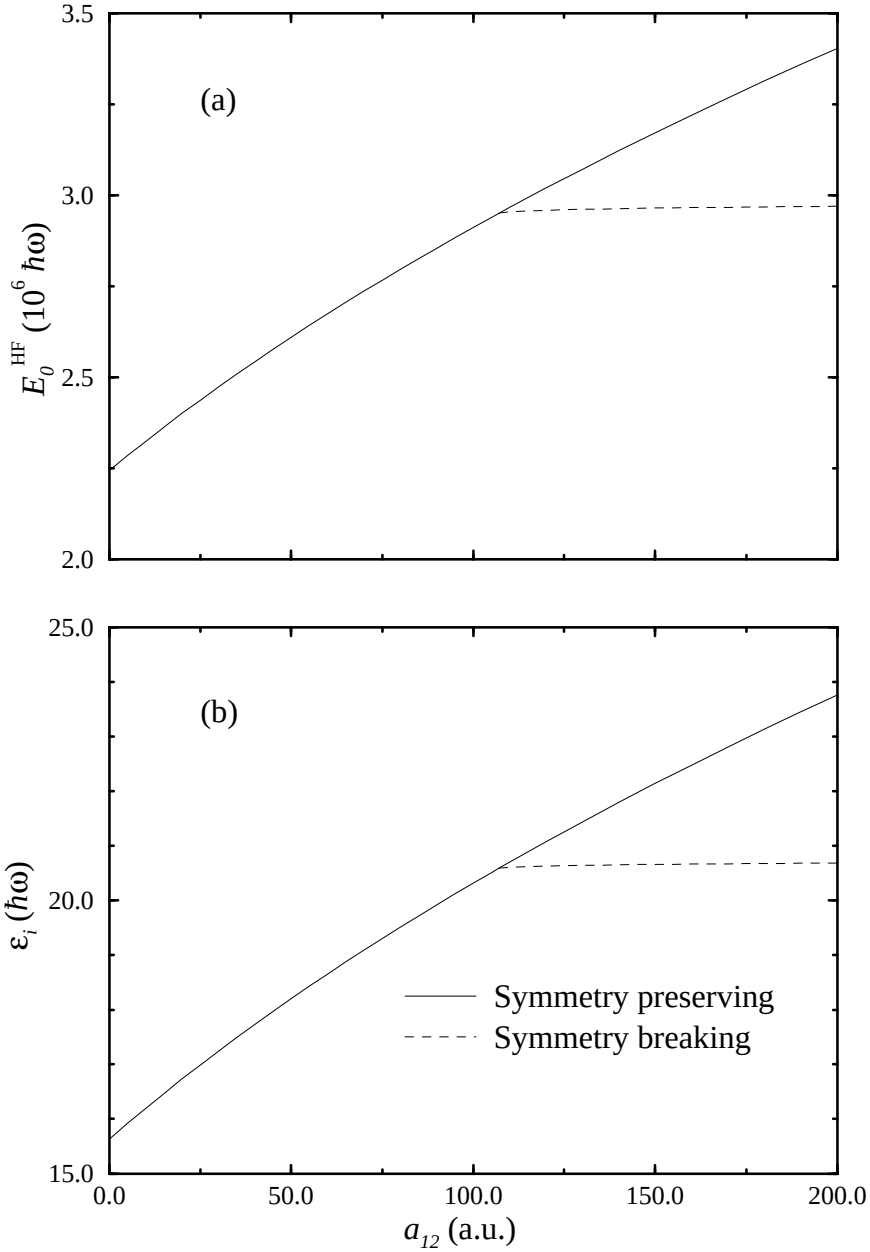

Figure 36. The Hartree-Fock ground state energies for ^{87}Rb $|1,-1\rangle+|2,1\rangle$ in an "inverted" TOP trap a function of interspecies scattering length. In (a) the total energy is shown; and in (b), the orbital energy. The solid line corresponds to the symmetry preserving solution; and the dashed, to the symmetry breaking solution. The frequencies are $\omega_z/\omega_\rho=1/\sqrt{8}$ with $\omega_\rho=2\pi\,376.2$ Hz. The remaining parameters are $a_{11}=a_{22}=107$ a.u. and $N_1=N_2=10^5$.

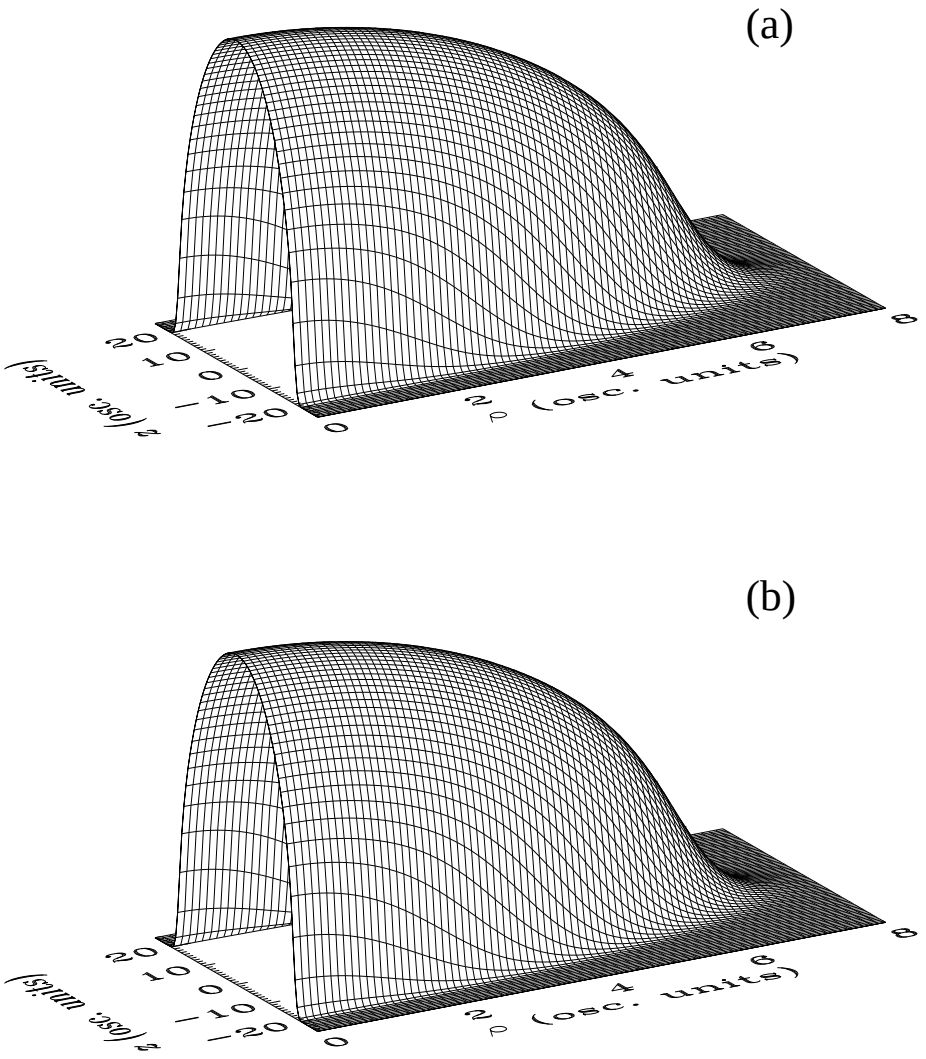

Figure 37. The single particle densities $|\psi_0(\mathbf{x})|^2$ and $|\phi_0(\mathbf{x})|^2$ in the ρz plane for for ^{87}Rb $|1,-1\rangle+|2,1\rangle$ in an "inverted" TOP trap. The parameters are as follows: N_1=N_2=10^5, a_{11}=a_{22}=107 a.u., and a_{12}=107 a.u., and ω_z/ω_ρ=$1/\sqrt{8}$ with ω_ρ=2π 376.2 Hz. The $|1,-1\rangle$ state is shown in (a) and the $|2,1\rangle$ state in (b). Note that 1 osc. unit=β=0.556 μm.

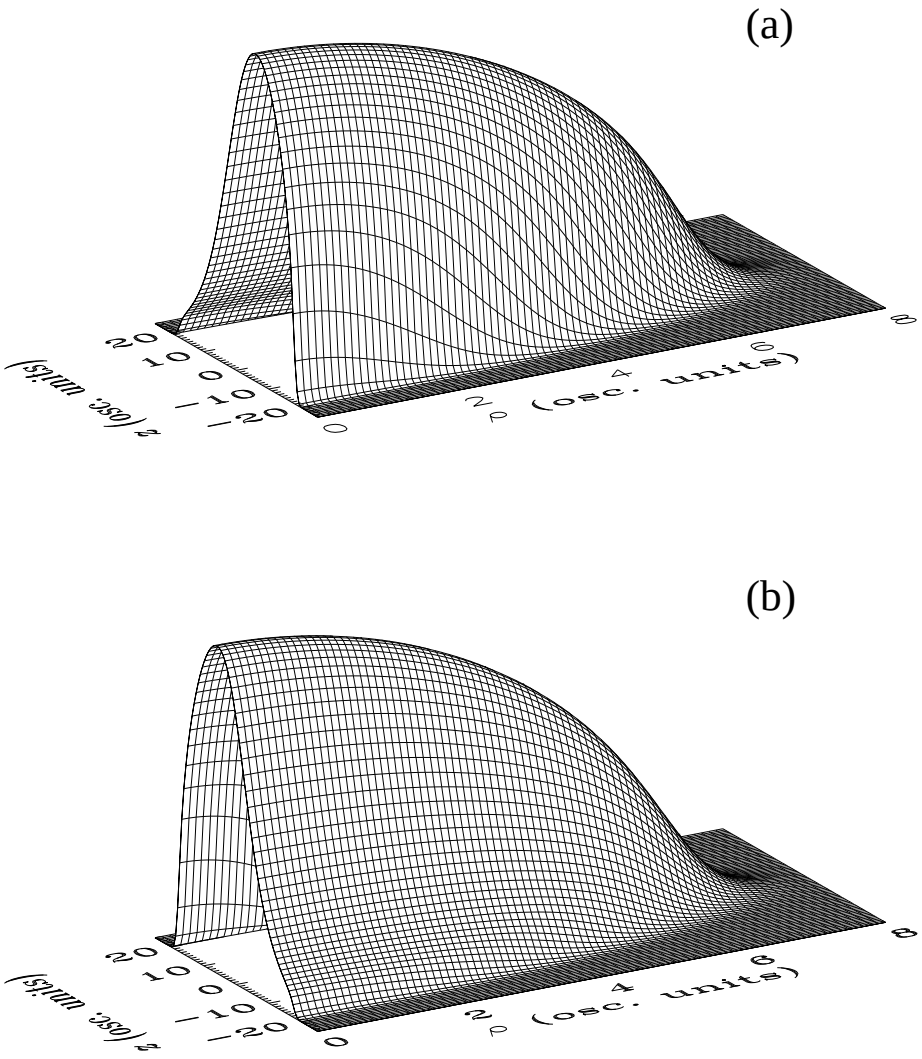

Figure 38. The single particle densities $|\psi_0(\mathbf{x})|^2$ and $|\phi_0(\mathbf{x})|^2$ in the ρz plane for for ^{87}Rb $|1,-1\rangle+|2,1\rangle$ in an "inverted" TOP trap. The parameters are as follows: N_1=N_2=10^5, a_{11}=a_{22}=107 a.u., and a_{12}=107.1 a.u., and ω_z/ω_ρ=$1/\sqrt{8}$ with ω_ρ=2π 376.2 Hz. The $|1,-1\rangle$ state is shown in (a) and the $|2,1\rangle$ state in (b). Note that 1 osc. unit=β=0.556 μm.

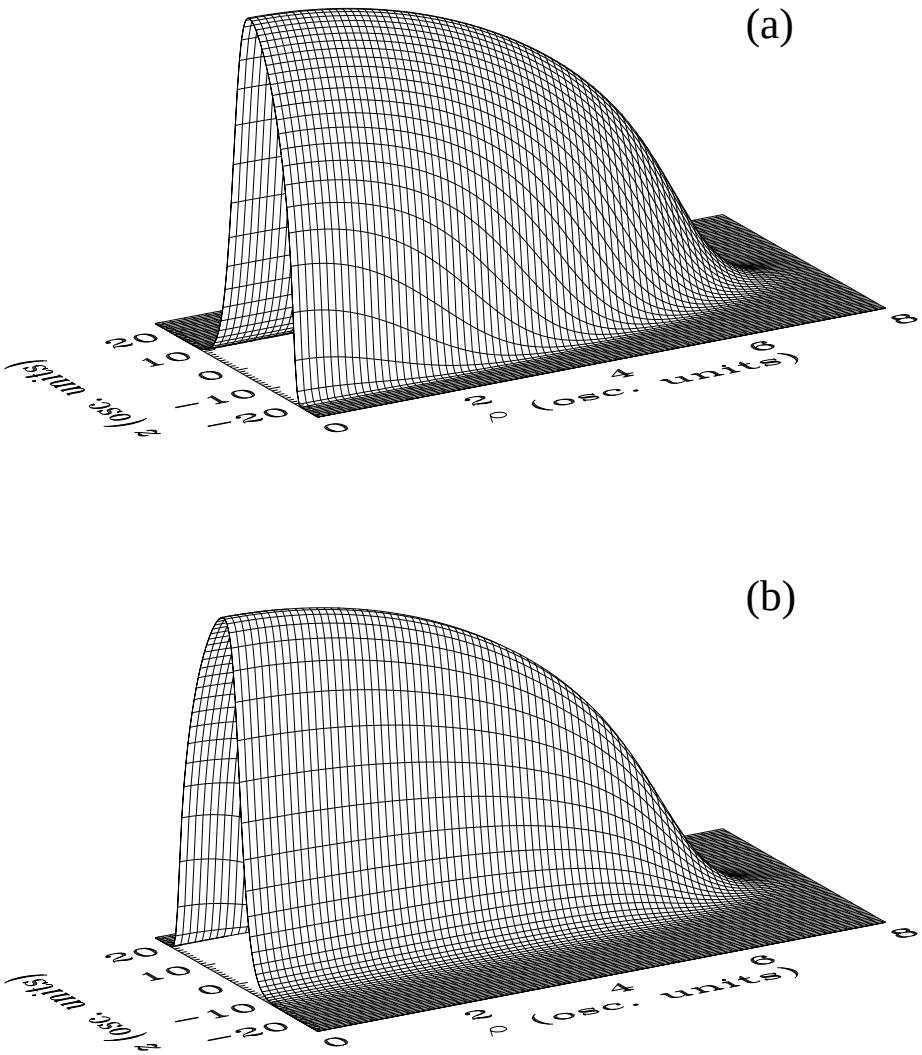

Figure 39. The single particle densities $|\psi_0(\mathbf{x})|^2$ and $|\phi_0(\mathbf{x})|^2$ in the ρz plane for for ^{87}Rb $|1,-1\rangle+|2,1\rangle$ in an "inverted" TOP trap. The parameters are as follows: N_1=N_2=10^5, a_{11}=a_{22}=107 a.u., and a_{12}=107.5 a.u., and ω_z/ω_ρ=$1/\sqrt{8}$ with ω_ρ=2π 376.2 Hz. The $|1,-1\rangle$ state is shown in (a) and the $|2,1\rangle$ state in (b). Note that 1 osc. unit=β=0.556 μm.

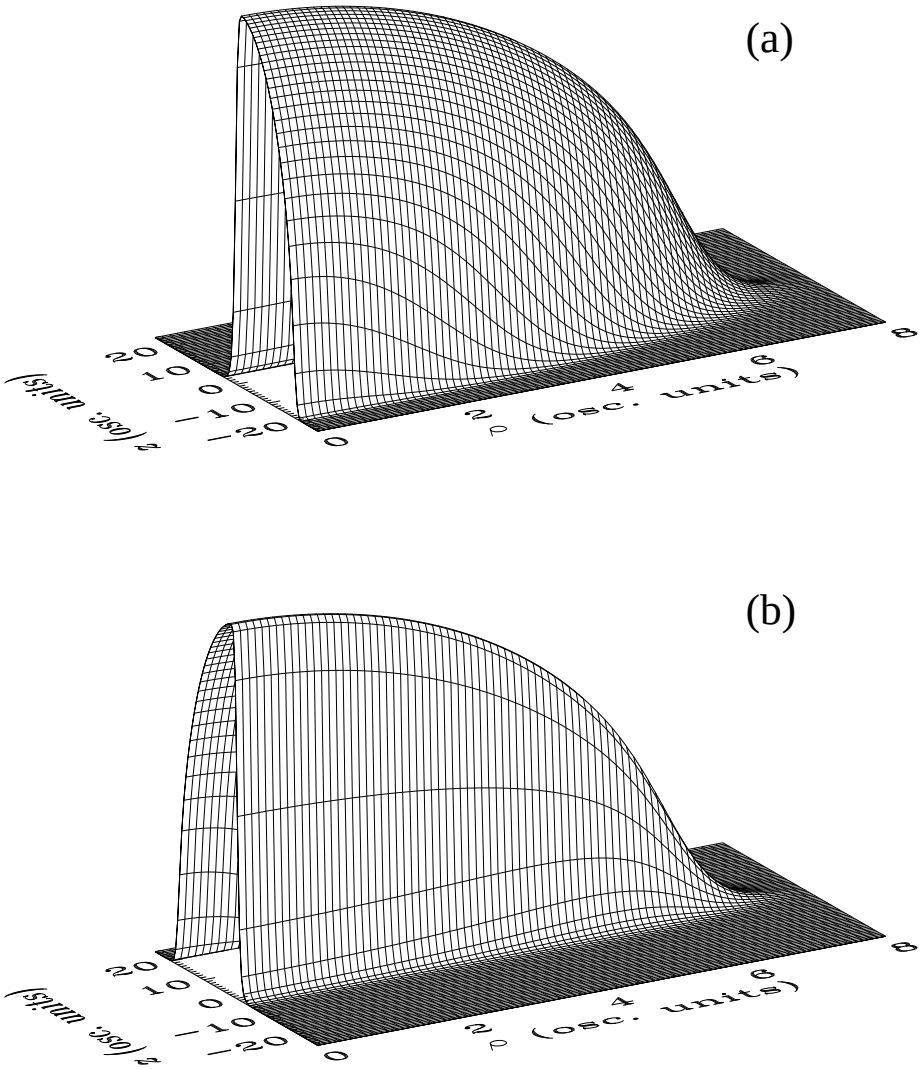

Figure 40. The single particle densities $|\psi_0(\mathbf{x})|^2$ and $|\phi_0(\mathbf{x})|^2$ in the ρz plane for for ^{87}Rb $|1,-1\rangle+|2,1\rangle$ in an "inverted" TOP trap. The parameters are as follows: N_1=N_2=10^5, a_{11}=a_{22}=107 a.u., a_{12}=115 a.u., and ω_z/ω_ρ=$1/\sqrt{8}$ with ω_ρ=2π 376.2 Hz. The $|1,-1\rangle$ state is shown in (a) and the $|2,1\rangle$ state in (b). Note that 1 osc. unit=β=0.556 μm.

again occurs over a range of a_{12} up to about 10% above a_{12}^c. From Figs. 38-40, in fact, it appears to largely happen within a few atomic units of a_{12}^c. A different quantification of this transition is shown in Fig. 41. It shows the expectation value of z for each orbital as a function of a_{12}, and reemphasizes the abrupt nature of the transition. Numerically, the final arrangement — which species is localized at positive z and which at negative — is determined by the initial conditions of the calculation. Physically, the Hartree-Fock ground state is degenerate with the state for which z is replaced by $-z$. It is precisely this degeneracy that can be utilized to construct a many-body state which *is* an eigenstate of total z-parity. The total z-parity operator, Π_z, will be diagonalized in the degenerate subspace of the many-body Hartree-Fock wave functions. The result will be an approximate energy eigenstate and an exact z-parity eigenstate. Explicitly, if $\Phi_0^{\mathrm{HF}}(\mathbf{x}_1, \ldots, \mathbf{x}_{N_1+N_2})$ is the configuration space representation of $|N_1; N_2\rangle$, then it is degenerate with $\Pi_z \Phi_0^{\mathrm{HF}}(\mathbf{x}_1, \ldots, \mathbf{x}_{N_1+N_2})$. The eigenstates of Π_z can be constructed from Φ_0^{HF} $\Pi_z \Phi_0^{\mathrm{HF}}$ as follows:

$$\Phi_0^{\pm}(\mathbf{x}_1, \ldots, \mathbf{x}_{N_1+N_2}) = \mathcal{N}_{\pm} \left[\Phi_0^{\mathrm{HF}}(\mathbf{x}_1, \ldots, \mathbf{x}_{N_1+N_2}) \pm \Pi_z \, \Phi_0^{\mathrm{HF}}(\mathbf{x}_1, \ldots, \mathbf{x}_{N_1+N_2}) \right]$$

where $\mathcal{N}_{\pm}$ is the normalization constant

$$\mathcal{N}_{\pm}^{-2} = 2 \left[1 \pm \left\langle \Pi_z \Phi_0^{\mathrm{HF}} \mid \Phi_0^{\mathrm{HF}} \right\rangle \right].$$

Since these are only approximate energy eigenstates, the expectation values $E_0^{\pm}$ of the Hamiltonian for $\Phi_0^{\pm}$ will not be the same even though the Hartree-Fock states shared a common energy expectation value E_0^{HF}. The improved estimate of the ground state energy will be the lower of the two energies

$$E_0^{\pm} = 2\mathcal{N}_{\pm}^2 \left[E_0^{\mathrm{HF}} \pm \left\langle \Pi_z \Phi_0^{\mathrm{HF}} \left| H \right| \Phi_0^{\mathrm{HF}} \right\rangle \right].$$

So, the fact that the Hartree-Fock solution itself is not an eigenstate of total z-parity should not be a concern since the wave functions $\Phi_0^{\pm}$ above are eigenstates of total z-parity but are not expressible in terms of a *single* completely symmetric independent particle wave

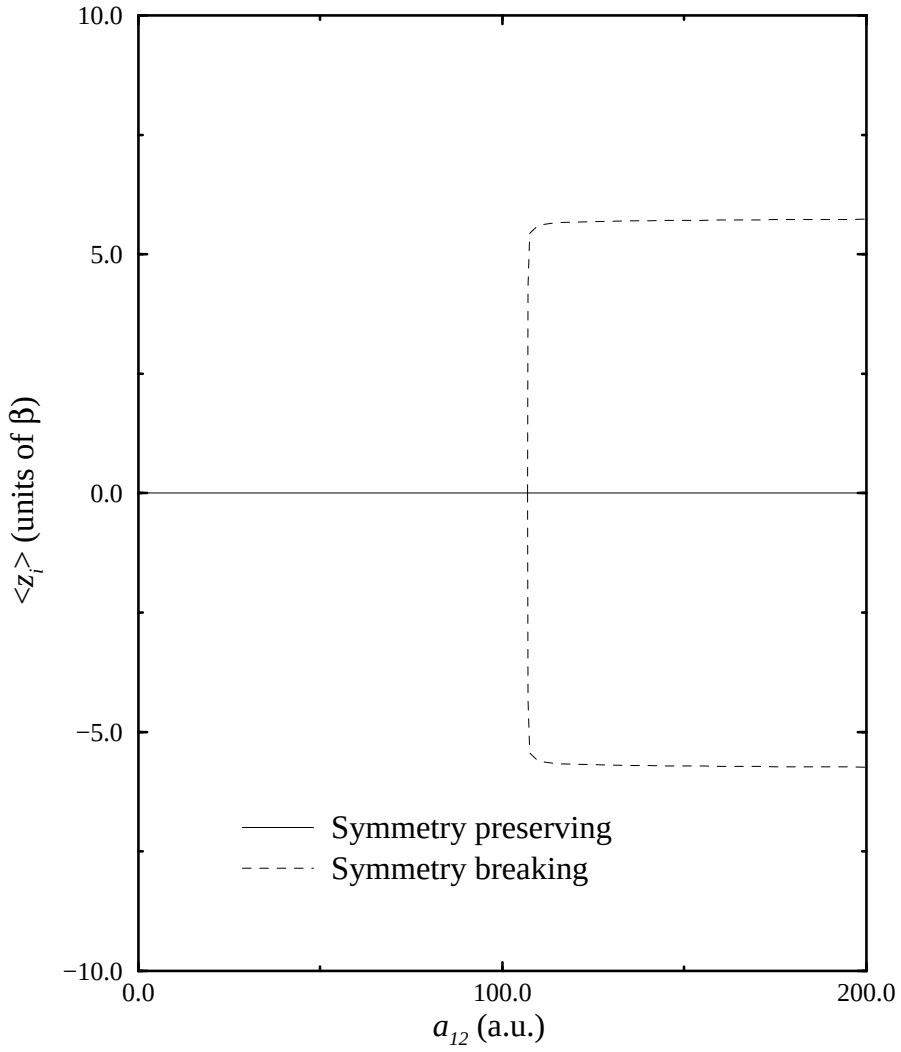

Figure 41. The expectation value of z for the $|1,-1\rangle$ and $|2,1\rangle$ hyperfine states of ^{87}Rb in an "inverted" TOP trap as a function of interspecies scattering length. The solid line corresponds to the symmetry preserving solution; and the dashed, to the symmetry breaking solution. The frequencies are $\omega_z/\omega_\rho = 1/\sqrt{8}$ with $\omega_\rho = 2\pi\, 376.2$ Hz. The remaining parameters are $a_{11}=a_{22}=107$ a.u. and $N_1=N_2=10^5$.

function. This example underscores the fact that it is the many-body wave function from which any physics should be extracted rather than the orbitals taken by themselves.

To complete this study of symmetry breaking, I show the excitation spectrum as a function of a_{12} in Fig. 42. Below a_{12}^c, the ground state is the symmetry preserving Hartree-Fock ground state, while above a_{12}^c it is the symmetry breaking solution. The qualitative features present in Fig. 31 are visible here as well. The states decreasing with a_{12} are the difference combinations, Eq. (97), of $|1,-1\rangle$ and $|2,1\rangle$ orbitals, and the states unaffected by changes in a_{12} are the sum combinations, Eq. (98). The frequencies above a_{12}^c are not converged numerically even including 1000 orbitals for each species. Typically, convergence to several digits can be achieved for double condensate spectra with approximately 200 orbitals per species. I include in Table 3 the convergence of the lowest 5 states with respect to the number of orbitals at a_{12}=214.0 a.u. It is worth noting that the sum combinations are converged to 3-4 digits by N_{basis}=1000.

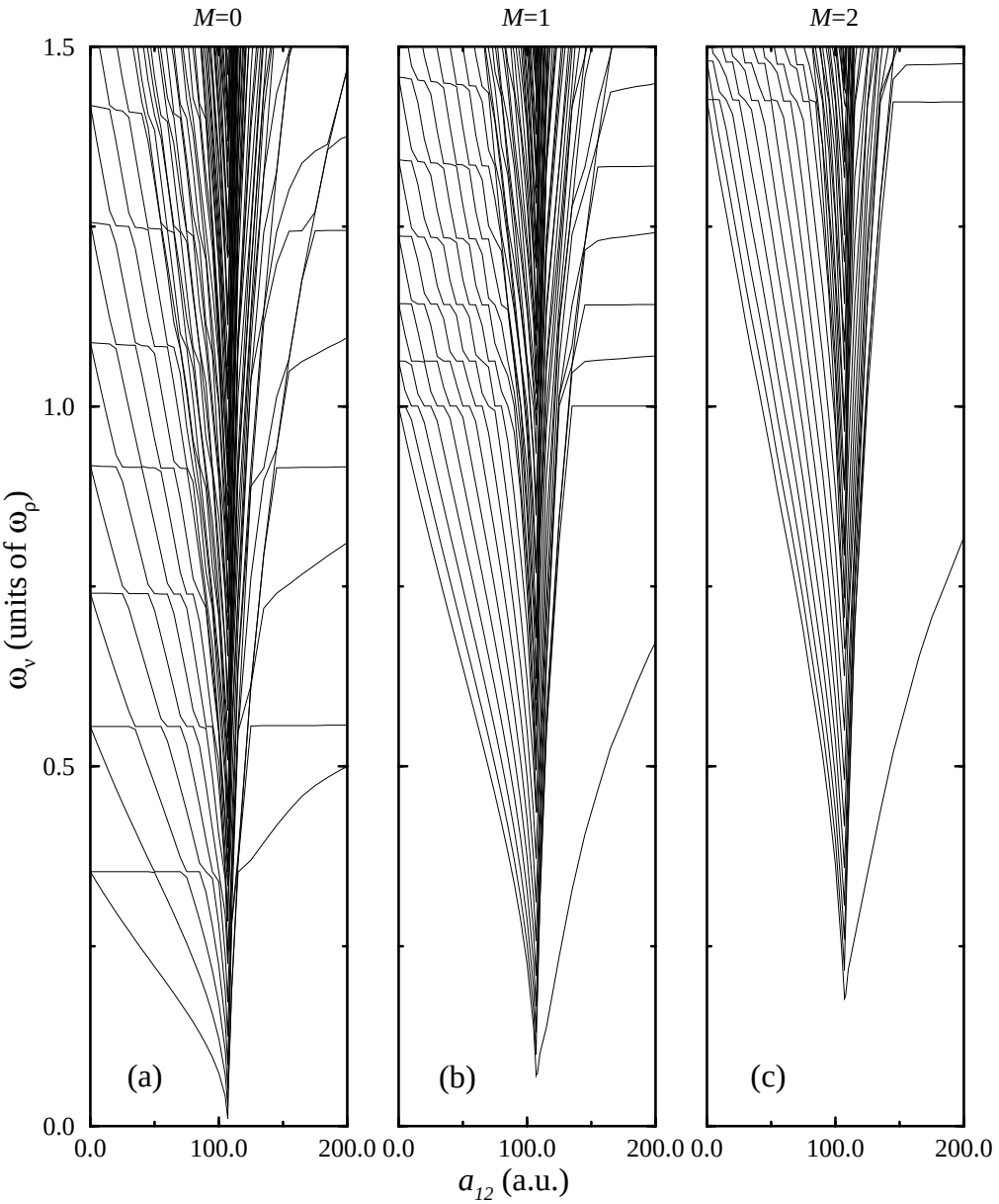

Figure 42. The RPA excitation frequencies for ^{87}Rb $|1,-1\rangle+|2,1\rangle$ in an "inverted" TOP trap as a function of a_{12}. The parameters are as follows: a_{11}=a_{22}=107 a.u., N_1=N_2=10^5. In (a) the M=0 spectrum is shown; in (b), the M=1 spectrum; and in (c), the M=2 spectrum. Note that for $a_{12}\geq a_{12}^c$ the results are not numerically converged (see Table 3).

Table 3. The convergence of the M=0 RPA spectrum for ^{87}Rb $|1,-1\rangle+|2,1\rangle$ in an "inverted" TOP trap with respect to the size of the quasi-Hartree-Fock single particle orbital basis. The trap frequencies are $\omega_z/\omega_\rho=1/\sqrt{8}$ with $\omega_\rho=2\pi\,376.2$ Hz. The remaining parameters are $N_1=N_2=10^5$, $a_{11}=a_{22}=107$ a.u. and $a_{12}=214$ a.u.

N_{basis}	$\tilde{\omega}_1$	$\tilde{\omega}_2$	$\tilde{\omega}_3$	$\tilde{\omega}_4$	$\tilde{\omega}_5$
100	0.535952	0.558283	0.873789	0.918471	1.17154
200	0.510728	0.557391	0.826916	0.916328	1.11030
400	0.465326	0.556036	0.774843	0.914234	1.07068
500	0.450096	0.556002	0.764073	0.914180	1.06142
700	0.428718	0.555953	0.751460	0.914101	1.03819
800	0.420635	0.555938	0.746923	0.914079	1.01849
900	0.413195	0.555926	0.743079	0.914062	0.998340
1000	0.406836	0.555917	0.739864	0.914049	0.972103

CHAPTER 5

SUMMARY

This dissertation has developed a comprehensive theory for interacting bosons at zero temperature. As stressed throughout, many similarities exist between the present approach and the standard Bogoliubov theory. At the same time, a number of subtle, pedagogical differences between the theories arise. These differences stem from a fundamental shift in viewpoint. Bogoliubov theory was conceived of to treat essentially infinite systems, systems with Avogadro's number of particles. In the case of alkali atom Bose-Einstein experiments, it is being applied to large but finite systems. The condensate in Bogoliubov theory possesses an indefinite number of particles, but in some sense it represents the ground state of a many-boson system. I take the view that the ground state, as well as every other pure quantum state, of the many-boson system has a fixed number of particles whose energy eigenstates can be calculated directly. I apply techniques designed for finite and modest sized systems to a finite but large system. Both theories are thus being applied in a new regime for which they were not specifically intended. While the qualitative differences are large, the quantitative results at the present level of approximation have proven to be negligible for the systems studied experimentally to date. In one of the few available examples where the present theory can be compared with experiment, it accurately reproduces the observed excitation frequencies to the within a few percent and is virtually identical to the Bogoliubov spectrum.

I have adapted the Hartree-Fock, random phase, and configuration interaction approximations to describe systems of interacting bosons, and have shown that such systems can be treated accurately and efficiently within a particle number conserving approximation. In fact, the resulting approximations are remarkably similar to those made in the standard Bogoliubov

approach and lead to largely the same equations. A key conclusion is that a system of interacting bosons can be treated in a manner analogous to that used to describe the electronic states of atoms. The hope is that the knowledge and intuition that have been gained from the extensive study of the atomic structure problem will ultimately lead to a deeper understanding of the quantum mechanical states of interacting, trapped atoms.

In the course of this work, several phenomena have been studied using both the Hartree-Fock approximation and the random phase approximation. The resulting analysis of the stability criteria for single and double condensates has improved on results available in the literature in both cases. The double condensate ground state configurations have been explored for various hyperfine and isotopic combinations of rubidium in fully three-dimensional geometries for realistic numbers of atoms. Random phase approximation excitation spectra were also calculated for both single and double condensates, also for realistic experimental parameters. Many of these predictions have not yet been tested experimentally, nor is there any other theoretical treatment with which comparisons can be made. A systematic study of spatial symmetry breaking has also been conducted, at the Hartree-Fock level of approximation for the ground state of double condensates. I have further proposed a resolution of this apparent "problem", which shows how the symmetry of the Hamiltonian can be restored for the many-body ground state in a relatively simple manner.

Several new approaches and problems have also been proposed in this dissertation. The simple implementation of a self-consistent random phase approximation, for instance, which would allow for a more complete study of the importance of ground state correlations, was discussed in Sec. 3.3.2. Based on the anisotropic trap results presented in Sec. 3.7, we now understand better that ground state correlations must be included in some approximation in order to obtain agreement with the experimental excitation spectrum. To assess the accuracy of a theory solely by its comparison with experiment is both dangerous and unsatisfying. In the absence of a better calculation, however, it is difficult to judge with certainty the accuracy of the random phase approximation on a purely theoretical basis. A self-consistent random

phase approximation study could provide such an estimate since it removes the quasi-boson approximation discussed in Sec. 3.3.1.

The proposed solution of the time-dependent Hartree-Fock equations for a double condensate system with an indefinite number of particles in each state also appears to be ripe for further theoretical and experimental study. An experiment that could be modeled by this approach is one in which atoms are driven by an external field from one trapped state to another. This configuration immediately suggests interesting interference that might be studied, analogous to the experiment of Andrews *et al.* [107]. Section 3.4 described an implementation of the configuration interaction approach familiar from atomic and chemical structure calculations. This formulation, which is in principle "exact" and can be improved systematically, is based on the direct expansion and diagonalization using the complete set of many-body basis functions constructed from Hartree-Fock orbitals. This method includes effects not accounted for within the random phase (or Bogoliubov) approximation. The resulting energy eigenstates can thus be used to calculate any desired property of the time-independent, unperturbed system. In the context of spatial symmetry breaking discussed in Sec. 4.6, a theoretical description that goes beyond the effective one-body, mean field picture is required, apparently, for the first time for an alkali atom condensate. Given the very real possibility that a physical combination of rubidium hyperfine states exists in this symmetry breaking regime, further experimental and theoretical studies of this phenomenon are of increasing interest.

BIBLIOGRAPHY

[1] M.H. Anderson, J.R. Ensher, M.R. Matthews, C.E. Wieman, and E.A. Cornell, Science **269**, 198 (1995).

[2] K.B. Davis, M.O. Mewes, M.R. Andrews, N.J. van Druten, D.D. Durfee, D.M. Kim, and W. Ketterle, Phys. Rev. Lett. **75**, 3969 (1995).

[3] C.C. Bradley, C.A. Sackett, J.J. Tollett, and R.G. Hulet, Phys. Rev. Lett. **75**, 1687 (1995); R.G. Hulet, C.C. Bradley, C.A. Sackett, and J.J. Tollett, Bull. Am. Phys. Soc. **41**, 1130 (1996).

[4] D.J. Han, R. Wynar, P. Courteille, and D. Heinzen, *Proceedings of the 1997 CLEO/QELS Conference* (1997).

[5] L.V. Hau, B. Busch, C. Liu, Z. Dutton, M.M. Burns, and J.A. Golovchenko, *Proceedings of the XX International Conference on the Physics of Electronic and Atomic Collisions* Ed. F. Aumayr, G. Betz, and H.P. Winter (1997).

[6] B. Anderson, M. Kasevich, *et al.*, `http://amo.phy.gasou.edu:80/bec.html`.

[7] U. Ernst, F. Schreck, J. Schuster, A. Marte, and G. Rempe, `http://quantum-optics.physik.uni-konstanz.de/cgi-bin/rempe`.

[8] S.N. Bose, Z. Phys. **26**, 178 (1924); A. Einstein, Sitzungsber. Kgl. Preuss. Akad. Wiss. **1924**, 261 (1924); *ibid.* **1925**, 3 (1925).

[9] D.S. Jin, J.R. Ensher, M.R. Matthews, C.E. Wieman, and E.A. Cornell, Phys. Rev. Lett **77**, 420 (1996).

[10] M.O. Mewes, M.R. Andrews, N.J. van Druten, D.M. Kurn, D.S. Durfee, C.G. Townsend, and W. Ketterle, Phys. Rev. Lett. **77**, 988 (1996).

[11] M. Edwards, P.A. Ruprecht, K. Burnett, R.J. Dodd, and C.W. Clark, Phys. Rev. Lett. **77**, 1671 (1996).

[12] B.D. Esry, Phys. Rev. A **55**, 1147 (1997).

[13] T.L. Ho and V.B. Shenoy, Phys. Rev. Lett. **77**, 3276 (1996).

[14] N. Bogoliubov, J. Phys. USSR **11**, 23 (1947).

[15] P. Nozières, *Bose-Einstein Condensate* Ed. A. Griffin, D.W. Snoke, and S. Stringari, (Cambridge University Press, Cambridge, 1995), p. 15).

[16] A. Griffin, *Excitations in a Bose-Condensed Liquid* (Cambridge University Press, Cambridge, 1993).

[17] C.W. Gardiner, Phys. Rev. A **56**, 1414 (1997).

[18] A. Mann, Phys. Rev. A **4**, 750 (1971).

[19] S. Stringari, Phys. Rev. Lett. **77**, 2360 (1996).

[20] F. Dalfovo, S. Giorgini, M. Guilleumas, L. Pitaevskii, and S. Stringari, Phys. Rev. A (in press).

[21] W.C. Wu and A. Griffin, Phys. Rev. A **54**, 4204 (1997).

[22] M. Fliesser, A. Csordás, P. Szépfalusy, and R. Graham, Phys. Rev. A **56**, R2533 (1997).

[23] P. Öhberg, E.L. Surkov, I. Tittonen, S. Stenholm, M. Wilkens, and G.V. Shlyapnikov, cond-mat/9705006 (preprint).

[24] R. Graham and D. Walls, cond-mat/9611111 (preprint).

[25] H.T.C. Stoof, J. Stat. Phys. **87**, 1353 (1997).

[26] M Bijlsma and H.T.C. Stoof, Phys. Rev. A **55**, 498 (1997).

[27] V.M. Perez-Garcia, H. Michinel, J.I. Cirac, M. Lewenstein, P. Zoller, Phys. Rev. A **56**, 1424 (1997).

[28] A.L. Fetter, J. Low Temp. Phys. **106**, 643 (1997).

[29] Th. Busch, J. I. Cirac, V. M. Perez-Garcia, and P. Zoller, Phys. Rev. A **56**, 2978 (1997).

[30] R.J. Dodd, M. Edwards, C.J. Williams, C.W. Clark, M.J. Holland, P.A. Ruprecht, and K. Burnett, Phys. Rev. A **54**, 661 (1996).

[31] R.J. Dodd, K. Burnett, M. Edwards, and C.W. Clark, Phys. Rev. A **56**, 587 (1997).

[32] L. You, W. Hoston, M. Lewenstein, and K. Huang, Phys. Rev. A **55**, R1581 (1997).

[33] P. Öhberg and S. Stenholm, J. Phys. B **30**, 2749 (1997).

[34] D.A.W. Hutchinson, E. Zaremba, and A. Griffin, Phys. Rev. Lett. **78**, 1842 (1997).

[35] R.J. Dodd, M. Edwards, C.W. Clark, and K. Burnett, cond-mat/9708139 (preprint).

[36] M. Houbiers, H.T.C. Stoof, and E.A. Cornell, Phys. Rev. A **56**, 2041 (1997).

[37] S. Giorgini, L. Pitaevskii, and S. Stringari, Phys. Rev. A **54**, 4633 (1996).

[38] P. Öhberg and S. Stenholm, cond-mat/9708110 (preprint).

[39] M. Holland, J. Williams, and J. Cooper, Phys. Rev. A, **55**, 3670, (1997).

[40] C. W. Gardiner, P. Zoller, R. J. Ballagh, and M. J. Davis, Phys. Rev. Lett. **79**, 1793 (1997).

[41] Y. Castin and J. Dalibard, Phys. Rev. A **55**, 4330 (1997).

[42] J. Javanainen and S.M. Yoo, Phys. Rev. Lett. **76**, 161 (1996).

[43] T. Wong, M.J. Collett and D.F. Walls, Phys. Rev. A **54**, R3718 (1996).

[44] A.L. Fetter and J.D. Walecka, *Quantum Theory of Many-Particle Systems* (McGraw-Hill, New York, 1971).

[45] P. Ring and P. Schuck, *The Nuclear Many-Body Problem* (Springer, New York, 1980).

[46] D. Bohm and D. Pines, Phys. Rev. **92**, 609 (1953).

[47] K. Huang, *Statistical Mechanics* (Wiley, New York, 1963); K. Huang and C.N. Yang, Phys. Rev. **105**, 767 (1957).

[48] D.J. Thouless, *The Quantum Mechanics of Many-Body Systems* (Academic Press, New York, 1972).

[49] F. Dalfovo and S. Stringari, Phys. Rev. A **53**, 2477 (1996).

[50] J.D. Jackson, *Classical Electrodynamics, Second Edition* (Wiley, New York, 1975), p. 45.

[51] H. Goldstein, *Classical Mechanics, Second Edition* (Addison Wesley, Reading, Massachusetts, 1980), p. 11.

[52] M. Lewenstein and L. You, Phys. Rev. Lett. **77**, 3489 (1996).

[53] A. deShalit and H. Feshbach, *Theoretical Nuclear Physics Volume 1: Nuclear Structure* (Wiley, New York, 1974).

[54] P.W. Anderson, *Basic Notions of Condensed Matter Physics* (Benjamin/Cummings, Menlo Park, California, 1984).

[55] V.L. Ginzburg and L.P. Pitaevskii, Zh. Eksp. Teor. Fiz. **34**, 1240 (1958) [Sov. Phys. JETP **7**, 858 (1958)]; E.P. Gross, J. Math. Phys. **4**, 195 (1963).

[56] W.C. Wu and A. Griffin, Phys. Rev. A **54**, 4204 (1996).

[57] M. Marinescu and A.F. Starace, Phys. Rev. A **56**, 570 (1997).

[58] K.G. Singh and D.S. Rokhsar, Phys. Rev. Lett. **77**, 1667 (1996).

[59] A.L. Fetter, Phys. Rev. A **53**, 4245 (1996).

[60] B.D. Esry and C.H. Greene, Bull. Am. Phys. Soc. **41**, 1137 (1996).

[61] R.D. Cowan, *The Theory of Atomic Structure and Spectra* (University of California Press, Berkeley, 1981), Chap. 13.

[62] M. Edwards and K. Burnett, Phys. Rev. A **51**, 1382 (1995).

[63] T. Koopmans, Physica **1**, 104 (1933).

[64] L. Brillouin, Actual. Sci. Ind. **71**, (1933); L. Brillouin, Actual. Sci. Ind. **159**, (1934);

[65] P.A. Ruprecht, M.J. Holland, K. Burnett, M. Edwards, Phys. Rev. A **51**, 4704 (1995).

[66] D.J. Rowe, *Nuclear Collective Motion: Models and Theory* (Methuen and Company, London, 1970).

[67] W. Ledermann and S. Vasda, Eds., *Handbook of Applicable Mathematics* (Wiley, New York, 1980), p. 436.

[68] G. Baym and C.J. Pethick, Phys. Rev. Lett. **76**, 6 (1996).

[69] D.J. Thouless, Nucl. Phys. **21**, 225 (1960).

[70] D.J. Thouless, Nucl. Phys. **22**, 78 (1961).

[71] A. Omont, J. Phys. (Paris) **38**, 1343 (1977).

[72] W. Lenz, Z. Physik **56**, 778 (1929).

[73] E. Fermi, Nuovo Cimento **11**, 157 (1934).

[74] N.P. Proukakis, K. Burnett, and H.T.C. Stoof, cond-mat/9703199 (preprint).

[75] K.A. Brueckner and C.A. Levinson, Phys. Rev. **98**, 1445 (1955).

[76] K.A. Brueckner and K. Sawada, Phys. Rev. **106**, 1117 (1957).

[77] J. Goldstone, Proc. Roy. Soc. (London) **A239**, 267 (1957).

[78] P.M. Morse and H. Feshbach, *Methods of Theoretical Physics: Part II* (McGraw-Hill, New York, 1953), p. 1671.

[79] G. Herzberg, *Molecular Spectra and Molecular Structure: Vol. I* (van Nostrand, Toronto, 1950).

[80] B.M. Axilrod and E. Teller, J. Chem. Phys. **11**, 299 (1943).

[81] M. Marinescu and A.F. Starace, Phys. Rev. A **55**, 2067 (1997).

[82] Z. Zhen and J. Macek, Phys. Rev. A **38**, 1193 (1988).

[83] W. Ketterle, BEC '97.

[84] P.A. Ruprecht, M. Edwards, K. Burnett, and C.W. Clark, Phys. Rev. A **54**, 4178 (1996).

[85] H.M.J.M. Boesten, C.C. Tsai, J.R. Gardner, D.J. Heinzen, and B.J. Verhaar, Phys. Rev. A **55**, 636 (1997).

[86] J.P. Burke Jr., J.L. Bohn, B.D. Esry, and C.H. Greene, Phys. Rev. A **55**, R2519 (1997).

[87] C.J. Myatt, E.A. Burt, R.W. Ghrist, E.A. Cornell, and C.E. Wieman, Phys. Rev. Lett. **78**, 586 (1997).

[88] E. Timmermans, cond-mat/9709301 (preprint).

[89] M.O. Mewes, M.R. Andrews, D.M. Kurn, D.S. Durfee, C.G. Townsend, and W. Ketterle, Phys. Rev. Lett. **78**, 582 (1997).

[90] R.J. Ballagh, K. Burnett, and T.F. Scott, Phys. Rev. Lett. **78**, 1607 (1997).

[91] P.S. Julienne, F.H. Mies, E. Tiesinga, and C.J. Williams, Phys. Rev. Lett. **78**, 1880 (1997).

[92] S.J.J.M.F. Kokkelmans, H.M.J.M. Boesten, and B.J. Verhaar, Phys. Rev. A **55**, 636 (1997).

[93] B.D. Esry, C.H. Greene, J.P. Burke Jr., and J.L. Bohn, Phys. Rev. Lett. **78**, 3594 (1997).

[94] E.D. Siggia and A.E. Ruckenstein, Phys. Rev. Lett. **44**, 1423 (1980).

[95] A.F. Andreev and E.P. Bashkin, Zh. Eksp. Teor. Fiz. **69**, 319 (1975) [Sov. Phys. JETP **7**, 698 (1958)].

[96] C.C. Tsai, R.S. Freeland, J.M. Vogels, H.M.J.M. Boesten, D.J. Heinzen, and B.J. Verhaar, Phys. Rev. Lett. **79**, 1245 (1997).

[97] J.P. Burke Jr., J.L. Bohn, B.D. Esry, and C.H. Greene, Phys. Rev. A (submitted).

[98] E. Burt, R. Ghrist, and C.E. Wieman (private communication).

[99] F. Mies, *et al.*, J. Res. Natl. Inst. Stand. Technol. **101**, 521 (1996); C.J. Myatt, E.A. Burt, R.W. Ghrist, E.A. Cornell, and C.E. Wieman, private communication, the experimental dipolar loss rate for $|1,-1\rangle+|1,-1\rangle$, 6×10^{-16} cm^3/s, is an upper bound.

[100] A.J. Moerdijk, H.M.J.M. Boesten, and B.J. Verhaar, Phys. Rev. A **53**, 916 (1996).

[101] C.J. Myatt, Ph.D. Thesis, University of Colorado, 1997.

[102] B.D. Esry and C.H. Greene, Phys. Rev. A (submitted).

[103] J.L. Bohn and P.S. Julienne, Phys. Rev. A **56**, 1486 (1997).

[104] J.M. Vogels, C.C. Tsai, R.S. Freeland, S.J.J.M.F. Kokkelmans, B.J. Verhaar, and D.J. Heinzen, Phys. Rev. A **56**, R1067 (1997).

[105] J.L. Bohn, B.D. Esry, and C.H. Greene (unpublished).

[106] J.P. Burke Jr., (private communication).

[107] M.R. Andrews, C.G. Townsend, H.J. Miesner, D.S. Durfee, D.M. Kurn, and W. Ketterle, Science **275**, 637 (1997).

[108] C.D. Lin, Phys. Rep. **257**, 1 (1995).

[109] Y. Zhou, C.D. Lin, and J. Shertzer, J. Phys. B **26**, 3937 (1993).

[110] J. Avery, *Hyperspherical Harmonics: Applications in Quantum Theory* (Kluwer, Boston, 1989).

[111] J. Macek, J. Phys. B **1**, 831 (1968).

[112] U. Fano, Physics Today **29**, 32 (1976).

[113] B.D. Esry, Chris H. Greene, Y. Zhou, and C.D. Lin, J. Phys. B **29**, L51 (1996).

[114] B.D. Esry, C.D. Lin, and C.H. Greene, Phys. Rev. A **54**, 394 (1996).

[115] R. Lehoucq, K. Maschhoff, D. Sorensen, and C. Yang, `http://www.caam.rice.edu/software/ARPACK/indexold.html`.

[116] J.K. Cullum and R.A. Willoughby, *Lanczos algorithms for large symmetric eigenvalue computations* (Birkhauser, Boston, 1985).

[117] A. Starace and G.L. Webster, Phys. Rev. A **19** 1629 (1979).

[118] J.A. Fleck, J.R. Morris, and M.D. Feit, Appl. Phys. **10**, 129 (1976).

[119] H. De Raedt, Comp. Phys. Rep. **7**, 1 (1987).

[120] C. de Boor, *A Practical Guide to Splines* (Springer, New York, 1978).

[121] C. de Boor, `pppack`, `http://netlib.bell-labs.com/netlib`.

[122] W.H. Press, S.A. Teukolsky, W.T. Vetterling, and B.P. Flannery, *Numerical Recipes, Second Edition* (Cambridge, Cambridge, 1992), p. 844.

APPENDIX A

ADIABATIC HYPERSPHERICAL APPROACH

In this appendix, I specialize the adiabatic hyperspherical method [108, 109, 110, 111]. to solve the Schrödinger equation for three identical, interacting particles in an isotropic harmonic trapping potential.

If the particle coordinates are defined as in Fig. 43, then the Schrödinger equation in the laboratory frame is given by

$$\left[-\frac{1}{2m}\left(\nabla^2_{\mathbf{r}_1}+\nabla^2_{\mathbf{r}_2}+\nabla^2_{\mathbf{r}_3}\right)+\frac{1}{2}m\omega^2\left(r_1^2+r_2^2+r_3^2\right)+\sum_{i<j}V(r_{ij})\right]\Psi(\mathbf{r}_1,\mathbf{r}_2,\mathbf{r}_3)=E\Psi(\mathbf{r}_1,\mathbf{r}_2,\mathbf{r}_3)$$

assuming the particles interact *via* the two body potential $V(r)$. This equation is written in atomic units (e=m_e=$\hbar$=1), m is the mass of the particles, and ω is the frequency of the trap. This equation can be transformed to the coordinates of the center of mass $\mathbf{X}$ plus Jacobi coordinates for the internal motion $\boldsymbol{\rho}_1$ and $\boldsymbol{\rho}_2$.

Jacobi coordinates are a set of internal coordinates for which the many body Laplacian remains uncoupled, *i.e.* there are no mixed derivatives as there are for any other choice of internal coordinates. In an atom, for instance, the electron coordinates are usually defined relative to the position of the nucleus. This choice leads to dot products between different electron momenta — the "mass polarization" terms — that are usually included only perturbatively, if at all. Hylleraas coordinates are another relatively common choice of coordinates that lead to mixed derivatives in the Laplacian. In this case, however, the mixed derivatives cannot be accurately neglected to zeroth order as can the mass polarization terms. One set of Jacobi coordinates is generated by first using the position of one particle relative to another, then successively connecting each additional particle to the center of mass of the previous subsystem.

The coordinates of the center of mass and the Jacobi coordinates are related to the

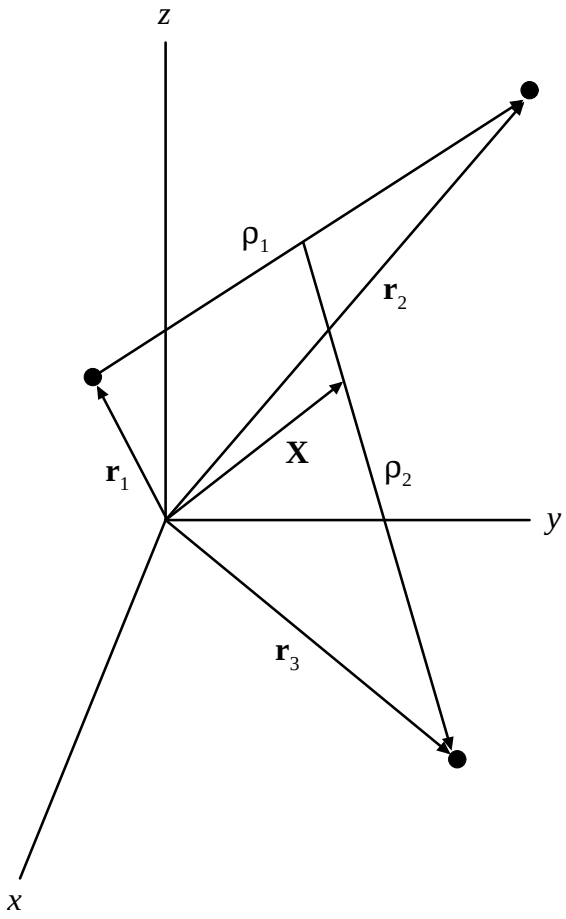

Figure 43. The laboratory frame coordinates $\mathbf{r}_1$, $\mathbf{r}_2$, and $\mathbf{r}_3$; the center of mass coordinate $\mathbf{X}$; and the Jacobi coordinates $\boldsymbol{\rho}_1$ and $\boldsymbol{\rho}_2$.

lab frame coordinates by the transformation

$$\begin{aligned}
\mathbf{X} &= \frac{1}{3}(\mathbf{r}_1 + \mathbf{r}_2 + \mathbf{r}_3) \\
\boldsymbol{\rho}_1 &= \mathbf{r}_2 - \mathbf{r}_1 \\
\boldsymbol{\rho}_2 &= \mathbf{r}_3 - \frac{1}{2}(\mathbf{r}_1 + \mathbf{r}_1)
\end{aligned}$$

and the lab frame coordinates back to them by the inverse transformation

$$\begin{aligned}
\mathbf{r}_1 &= \mathbf{X} - \frac{1}{2}\boldsymbol{\rho}_1 - \frac{1}{3}\boldsymbol{\rho}_2 \\
\mathbf{r}_2 &= \mathbf{X} + \frac{1}{2}\boldsymbol{\rho}_1 - \frac{1}{3}\boldsymbol{\rho}_2 \\
\mathbf{r}_3 &= \mathbf{X} + \frac{2}{3}\boldsymbol{\rho}_2.
\end{aligned}$$

In terms of ($\mathbf{X}$,$\boldsymbol{\rho}_1$,$\boldsymbol{\rho}_2$), the Schrödinger equation is written

$$\left[H_{\rm CM} + H_{\boldsymbol{\rho}_1} + H_{\boldsymbol{\rho}_2} + \sum_{i<j} V(\boldsymbol{\rho}_1, \boldsymbol{\rho}_2) \right] \Psi(\mathbf{X}, \boldsymbol{\rho}_1, \boldsymbol{\rho}_2) = E\, \Psi(\mathbf{X}, \boldsymbol{\rho}_1, \boldsymbol{\rho}_2).$$

The oscillator Hamiltonians are simply

$$\begin{aligned}
H_{\rm CM} &= -\frac{1}{2M}\nabla^2_{\rm CM} + \frac{1}{2}M\omega^2 X^2 \\
H_{\boldsymbol{\rho}_1} &= -\frac{1}{2\mu_1}\nabla^2_{\boldsymbol{\rho}_1} + \frac{1}{2}\mu_1\omega^2\rho_1^2 \\
H_{\boldsymbol{\rho}_2} &= -\frac{1}{2\mu_2}\nabla^2_{\boldsymbol{\rho}_2} + \frac{1}{2}\mu_2\omega^2\rho_2^2
\end{aligned}$$

with X=|$\mathbf{X}$|, ρ_1=|$\boldsymbol{\rho}_1$|, and ρ_2=|$\boldsymbol{\rho}_2$|. I have also defined the mass factors

$$M = 3m \quad \mu_1 = \frac{m}{2} \quad \mu_2 = \frac{2m}{3}.$$

The interaction $V(\boldsymbol{\rho}_1, \boldsymbol{\rho}_2)$ depends only on the internal coordinates so that the motion of the center of mass can be separated from the internal motion in the Schrödinger equation. This separation is accomplished by writing the wave function as

$$\Psi(\mathbf{X}, \boldsymbol{\rho}_1, \boldsymbol{\rho}_2) = \varphi(\mathbf{X})\, \psi(\boldsymbol{\rho}_1, \boldsymbol{\rho}_2).$$

The equation for the motion of the center of mass is then just the simple harmonic oscillator equation

$$\left[-\frac{1}{2M}\nabla^2_{\rm CM} + \frac{1}{2}M\omega^2 X^2\right]\varphi(\mathbf{X}) = E_{\rm CM}\varphi(\mathbf{X}).$$

The energy eigenvalues are thus $E_{\rm CM}=(n+\frac{3}{2})\,\omega$, $n=0,1,2,\ldots$; and the eigenstates are the isotropic oscillator solutions.

Defining mass-weighted hyperspherical coordinates [108] as

$$\mu R^2 = \mu_1\rho_1^2 + \mu_2\rho_2^2, \qquad 0 \le R < \infty,$$

$$\tan\phi = \sqrt{\frac{\mu_2}{\mu_1}}\frac{\rho_2}{\rho_1}, \qquad 0 \le \phi \le \frac{\pi}{4},$$

and

$$\cos\theta = \frac{\boldsymbol{\rho}_1\cdot\boldsymbol{\rho}_2}{\rho_1\rho_2}, \qquad 0 \le \theta \le \frac{\pi}{2},$$

the Schrödinger equation for the internal motion is

$$\left[-\frac{1}{2\mu}\frac{1}{R^5}\frac{\partial}{\partial R}\left(R^5\frac{\partial}{\partial R}\right) + \frac{\Lambda^2}{2\mu R^2} + V(R,\Omega)\right]\psi(\boldsymbol{\rho}_1,\boldsymbol{\rho}_2) = E_{\rm INT}\psi(\boldsymbol{\rho}_1,\boldsymbol{\rho}_2). \tag{99}$$

In these expressions, μ is an arbitrary scaling factor for which a convenient choice is $\mu=\mu_1$. In Eq. 99, Ω is shorthand for the set of angles $\{\phi,\theta,\hat{\boldsymbol{\rho}}_1,\hat{\boldsymbol{\rho}}_2\}$, $E_{\rm INT}=E-E_{\rm CM}$ is the internal energy, and Λ^2 is the "grand angular momentum" operator [108, 112]:

$$\Lambda^2 = -\frac{1}{\sin^2\phi\cos^2\phi}\frac{\partial}{\partial\phi}\left(\sin^2\phi\cos^2\phi\frac{\partial}{\partial\phi}\right) + \frac{\boldsymbol{\ell}_1^2}{\cos^2\phi} + \frac{\boldsymbol{\ell}_2^2}{\sin^2\phi}.$$

The operators $\boldsymbol{\ell}_1^2$ and $\boldsymbol{\ell}_2^2$ are the orbital angular momentum operators associated with the Jacobi vectors $\boldsymbol{\rho}_1$ and $\boldsymbol{\rho}_2$, respectively, and depend on their spherical polar angles $\hat{\boldsymbol{\rho}}_1$ and $\hat{\boldsymbol{\rho}}_2$.

In the center of mass system, at any given instant the three particles define a plane. In general, three Euler angles can be used to describe the orientation of this plane in space; and three internal coordinates, to describe the motion in the plane. But, since I only consider zero total orbital angular momentum, the Euler angle dependence drops out (the rotation function is simply a constant). The Schrödinger equation then involves only the three internal coordinates

R, ϕ, and θ (in atomic units) [108, 109, 112],

$$\left(-\frac{1}{2\mu}\frac{\partial^2}{\partial R^2}+\frac{\Lambda^2-\frac{1}{4}}{2\mu R^2}+V(R,\phi,\theta)\right)\psi(R,\phi,\theta)=E_{\rm INT}\psi(R,\phi,\theta). \tag{100}$$

In terms of (R,ϕ,θ) the grand angular momentum operator is

$$\Lambda^2=-\frac{\partial^2}{\partial\phi^2}-\frac{1}{\sin^2\phi\cos^2\phi\sin\theta}\frac{\partial}{\partial\theta}\left(\sin\theta\frac{\partial}{\partial\theta}\right).$$

Note that the wave function $\psi(R,\phi,\theta)$ is rescaled by a factor $R^{5/2}\sin\phi\cos\phi$ in order to eliminate first derivatives from the kinetic energy operator. The rescaled wave function must be square integrable for a bound state, and it must obey the boundary conditions

$$\psi(0,\phi,\theta)=0,$$

$$\psi(R,0,\theta)=\psi(R,\frac{\pi}{2},\theta)=0,$$

and

$$\left.\frac{\partial\psi}{\partial\theta}\right|_{\theta=0}=\left.\frac{\partial\psi}{\partial\theta}\right|_{\theta=\pi}=0.$$

In the adiabatic approach, R is treated initially as a fixed parameter and the remaining eigenvalue equation

$$\left(\frac{\Lambda^2-\frac{1}{4}}{2\mu R^2}+V(R,\phi,\theta)\right)\Phi_\nu(R;\phi,\theta)=U_\nu(R)\Phi_\nu(R;\phi,\theta)\qquad\nu=1,2,3,\ldots \tag{101}$$

solved for the adiabatic potential $U_\nu(R)$ and channel functions $\Phi_\nu(R;\phi,\theta)$. From the definitions of the coordinates, the qualitative interpretation of the hyperspherical coordinates is that R gives the overall size of the three-body system; ϕ, the radial correlation; and θ, the angular correlation. Further, R is completely symmetric under particle permutations. It follows that the channel functions contain all of the identical particle symmetries as well as all of the correlations in the system. Because of this, the channel functions display much of the physical content of the total wave function, and can often be used to obtain a qualitative understanding of the dynamics.

I typically solve Eq. (101) using a local function expansion such as the basis splines, see App. C and Refs. [109, 113, 114], thus determining the adiabatic potential curves $U_\nu(R)$

and the set of orthonormal channel functions $\Phi_\nu(R;\phi,\theta)$ that depend parametrically on R. The local function expansion approach leads to large matrices (on the order of thousands) of which less than about 20% of the entries are non-zero. These large sparse matrices can be diagonalized on workstations by using the `arpack` package publicly available on the world wide web [115] which is based upon the Lanczos algorithm [116]. This provides an efficient means of obtaining the lowest eigenvalues and eigenvectors (potential curves and channel functions) of the adiabatic equation, Eq. (101).

The exact solution to the Schrödinger equation can be found by writing

$$\psi(R,\phi,\theta) = \sum_\nu F_\nu(R)\Phi_\nu(R;\phi,\theta),$$

substituting in Eq. (100), and solving the resulting set of coupled differential equations in R. The adiabatic solution is obtained by neglecting the coupling between different channels arising from the nonvanishing derivatives of the channel functions with respect to R. The Schrödinger equation in this approximation reduces to

$$\left(-\frac{1}{2\mu}\frac{d^2}{dR^2} + U_\nu(R) + W_{\nu\nu}(R)\right) F_{\nu n}(R) = E_{\nu n}F_{\nu n}(R) \tag{102}$$

where

$$W_{\nu\nu}(R) = -\frac{1}{2\mu}\left\langle \Phi_\nu(R)\left|\frac{\partial^2}{\partial R^2}\right|\Phi_\nu(R)\right\rangle.$$

The quantum numbers ν and n label the channel and energy eigenstate within a channel, respectively. Equation (102) is a one-dimensional radial Schrödinger equation with an effective hyperradial potential $U_\nu(R)+W_{\nu\nu}(R)$ that determines the three-body spectrum in the adiabatic approximation. It can be shown [117] that the ground state energy obtained by solving Eq. (102) is an upper bound to the true ground state energy. This can be simply understood from the fact this approach is equivalent to assuming a variational trial wave function of the form

$$\psi^t_{\nu n}(R,\phi,\theta) = F_{\nu n}(R)\Phi_\nu(R;\phi,\theta).$$

The variational principle then guarantees that the energy thus obtained is an upper bound to the true ground state energy. A further approximation may be made in Eq. (102) by which a lower

bound to the ground state energy can also be determined [117]. One need only neglect $W_{\nu\nu}(R)$. This corresponds to the familiar Born-Oppenheimer approximation. The energy calculated variationally, however, is often much closer to the actual energy than is the lower bound.

A principal advantage of the adiabatic hyperspherical method is simplification in interpretation afforded by the reduction of a multidimensional problem to a one dimensional problem with a set of effective potentials [108]. These potential curves provide a great deal of qualitative as well as quantitative information about the dynamics of the system and often give a convenient and useful classification scheme [108]. The adiabatic hyperspherical method provides a framework within which one can often sketch semi-quantitative potential curves for more general cases without resorting to numerical calculations.

APPENDIX B

GENERAL MANY-BODY HAMILTONIAN MATRIX ELEMENT

The general Hamiltonian matrix element in an independent particle basis is:

$$
\begin{aligned}
\left\langle \mathbf{n}' \left| \hat{H} \right| \mathbf{n} \right\rangle &= \sum_j n_j \left\langle j \left| H_0 \right| j \right\rangle + \frac{n_j(n_j-1)}{2} \left\langle jj \left| V \right| jj \right\rangle \\
&+ \sum_{j<k} n_j n_k \left\langle jk \left| \overline{V} \right| jk \right\rangle \\
&+ \sum_{j\neq k} \sqrt{(n_j+1)n_k} \left\langle j \left| H_0 \right| k \right\rangle \delta_{n_j+1,n'_j} \delta_{n_k-1,n'_k} \\
&+ 2 \sum_{j<k\neq l<m} \sqrt{(n_j+1)(n_k+1)n_l n_m} \left\langle jk \left| V \right| lm \right\rangle \delta_{n_j+1,n'_j} \delta_{n_k+1,n'_k} \delta_{n_l-1,n'_l} \delta_{n_m-1,n'_m} \\
&+ \sum_{j<k\neq l} \sqrt{(n_j+1)(n_k+1)n_l(n_l-1)} \left\langle jk \left| V \right| ll \right\rangle \delta_{n_j+1,n'_j} \delta_{n_k+1,n'_k} \delta_{n_l-2,n'_l} \\
&+ \sum_{j\neq k} \sqrt{(n_j+1)n_k(n_k-1)^2} \left\langle jk \left| V \right| kk \right\rangle \delta_{n_j+1,n'_j} \delta_{n_k-1,n'_k} \\
&+ \frac{1}{2} \sum_{j\neq k} \sqrt{(n_j+1)(n_j+2)n_k(n_k-1)} \left\langle jj \left| V \right| kk \right\rangle \delta_{n_j+2,n'_j} \delta_{n_k-2,n'_k} \\
&+ \sum_{j\neq k<l} \sqrt{(n_j+1)(n_j+2)n_k n_l} \left\langle jj \left| V \right| kl \right\rangle \delta_{n_j+2,n'_j} \delta_{n_k-1,n'_k} \delta_{n_l-1,n'_l} \\
&+ \sum_{j\neq k} \sqrt{n_j^2(n_j+1)n_k} \left\langle jj \left| V \right| jk \right\rangle \delta_{n_j+1,n'_j} \delta_{n_k-1,n'_k} \\
&+ \sum_{j\neq k\neq l} \sqrt{(n_j+1)n_k^2 n_l} \left\langle jk \left| \overline{V} \right| kl \right\rangle \delta_{n_j+1,n'_j} \delta_{n_k,n'_k} \delta_{n_l-1,n'_l}.
\end{aligned}
$$

APPENDIX C

BASIS SPLINES

Most problems in atomic physics involve the solution of either the time-dependent or time-independent Schrödinger equation. Often, it is a nonseparable problem in two or more dimensions. An efficient means of solving multidimensional partial differential equations that is easily adaptable to different coordinate systems is thus an indispensable tool for the theoretical atomic physicist. In this appendix, I describe one method, the basis splines expansion, that meets the above criteria.

The basic idea of the basis splines expansion method is to approximate an unknown wave function by a linear combination of locally defined polynomials. These polynomials are "local" in the sense that they are nonzero only over some finite region. Further, they are generated piecewise from a given mesh under continuity constraints at the mesh points on both the function and its derivatives. For instance, if the splines are chosen to be piecewise kth order polynomials in each interval, then the spline is continuous as are all its derivatives up to the $(k-1)$th — thus the name splines. I will not discuss the construction of the basis splines and the exceptions to the continuity conditions here, rather I refer the reader to the text by de Boor, *A Practical Guide to Splines* [120]. This text also contains many formal mathematical properties of basis splines that will not be directly relevant to the discussion in this appendix. In fact, the numerical construction of the basis splines themselves is most easily accomplished by downloading the FORTRAN routines described in de Boor's book from `netlib` [121]. Figure 44 shows the 5th order basis splines $u_n(x)$ generated from the 11 point mesh, linearly distributed from 0 to 5. The spline with the thick line in Fig. 44 is identically zero for $x \leq 1.0$ and for $x \geq 4.0$. Similarly, the function to its left is nonzero only for $0.5 \leq x \leq 3.5$; the function to the left of this

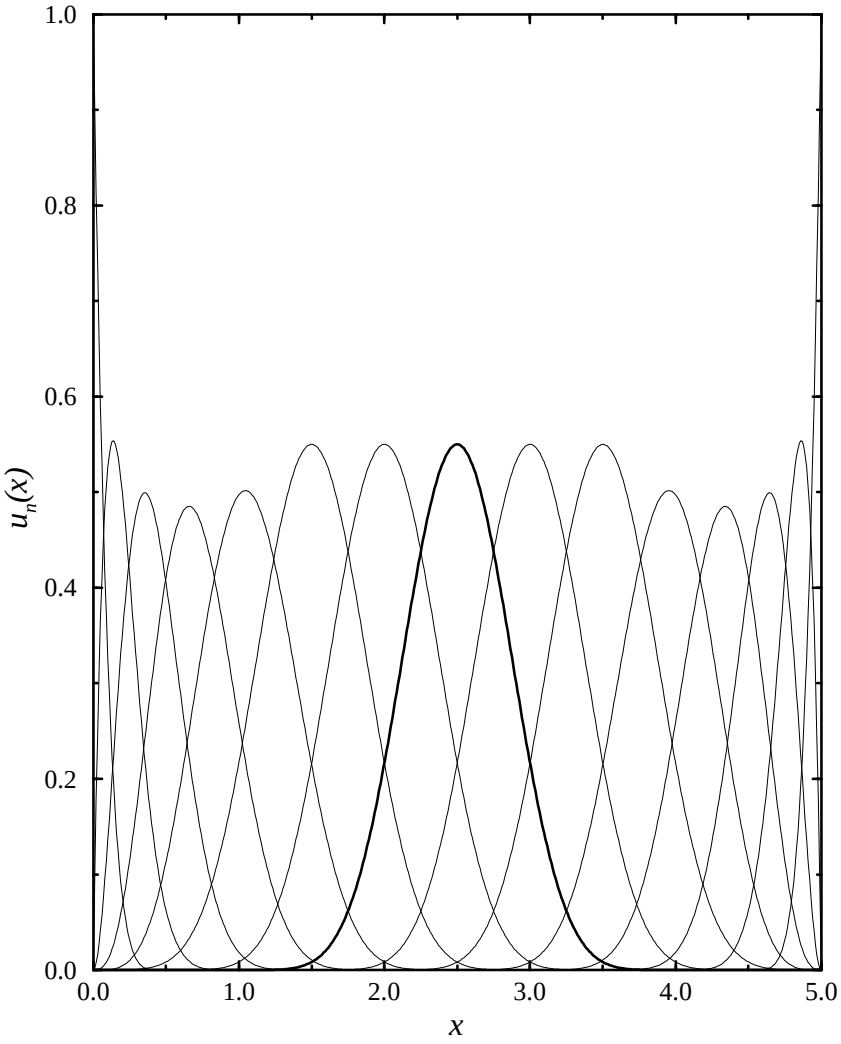

Figure 44. The basis splines $u_n(x)$ on a linear mesh. The thick solid line denotes the spline that is nonzero only for $1.0 \leq x \leq 4.0$.

one is nonzero only for $0.0 \leq x \leq 3.0$. This pattern repeats until the last function at the left end of the mesh is nonzero only for $0.5 \leq x \leq 0.5$.

Note that I use the convention that in the call to de Boor's subroutine to calculate the basis spline functions, the endpoints of the interval are repeated k times (k=5 in the case of the figure). There is some freedom in choosing the splines at the ends of the mesh, the subtleties of which are discussed in detail in the *Guide*. The convention I have chosen proves convenient in imposing boundary conditions since it produces a set of splines in which only one spline is nonzero on a boundary and only two have a nonzero first derivative. To force a function to zero at the left boundary, for instance, the first spline should be excluded from the expansion of the wave function. To force a function to have zero derivative on the same boundary, the first two splines should be replaced in the expansion by their sum. More general boundary conditions can be handled in a similar manner.

For the purposes of solving the Schrödinger equation, the basis splines can simply be regarded as a set of functions on which to expand the wave function. In two dimensions, one writes, for instance,

$$\psi(x,y) = \sum_{l,m}^{L,M} c_{lm} u_l(x) v_m(y). \tag{103}$$

The wave function is thus characterized by the LM expansion coefficients c_{lm} describing its dependence on the sets of basis spline functions $\{u_l\}$ and $\{v_m\}$. The upper limits of the sum in this expansion are determined by the number of mesh points, the order of the polynomials, and the boundary conditions. If N_x and N_y are the number of mesh points in each direction and k is the order of the polynomial (assumed to be the same for each coordinate), then $L=N_x+k-1$ and $M=N_y+k-1$. These limits are reduced by one for every condition placed on $\psi(x,y)$ at the corresponding boundary. If, for example, the wave function is forced to vanish on every boundary, then $L=N_x+k-3$ and $M=N_y+k-3$. Because the expansion is a simple product of one-dimensional spline sets, one such limit is needed for each dimension in the problem. These results are not limited to the Cartesian coordinates used in this example.

I will only discuss the details of the solution of the time-independent Schrödinger equation since they largely carry over to the solution of the time-dependent equation (see also App. D). Substituting $\psi(x,y)$ from Eq. (103) into the two-dimensional Schrödinger equation

$$H(x,y)\psi(x,y) = E\psi(x,y) \tag{104}$$

and projecting out $u_{l'}(x)v_{m'}(y)$ gives the matrix equation

$$\mathbf{Hc} = E\mathbf{Sc} \tag{105}$$

if the two indices l and m are mapped into the single index i. Two straightforward mappings are

$$i = (l-1)M + m \text{ and } i = (m-1)L + l.$$

The choice of mapping has a direct impact on the efficiency of the numerical solution of Eq. (105) and will be discussed below. The Hamiltonian matrix $\mathbf{H}$ is defined as

$$H_{i'i} = \int dx \int dy\, u_{l'}(x)v_{m'}(y)H(x,y)u_l(x)v_m(y); \tag{106}$$

and the overlap matrix $\mathbf{S}$, as

$$S_{i'i} = \int dx \int dy\, u_{l'}(x)v_{m'}(y)u_l(x)v_m(y). \tag{107}$$

Since these integrals must be evaluated numerically, it is advantageous to split the two-dimensional integrations into a product of one-dimensional integrations where possible. The kinetic energy and overlap matrix elements usually separate into one-dimensional integrals. For general potentials this will typically not be possible, however, and the two-dimensional integrations must be performed. Since the expansion functions are polynomials of finite order k, the overlap matrix can, in principle, be evaluated exactly using a Gaussian quadrature with $k+1$ points in each interval of the mesh [122]. (Recall that Gaussian quadrature exactly integrates polynomials of up to degree $2k-1$ with k quadrature points. Of course, on a computer "exact" means to within the machine precision.) The kinetic energy terms can also be exactly calculated

(de Boor's subroutine can return derivatives of the basis splines as well as the spline itself), but the potential will generally not be a simple polynomial. For a converged calculation, the mesh will be dense enough, *i.e.* the intervals small enough, that the potential can be well approximated by a polynomial in every interval. In this case, Gaussian quadrature will return matrix elements with machine precision accuracy if care is taken to increase the number of quadrature points to somewhat more than $k+1$ to account for the approximate local polynomial nature of the potential.

The efficient numerical solution of Eq. (105) requires a knowledge of the structure of the Hamiltonian and overlap matrices. To this end, consider Fig. 45. It shows the nonzero structure of a fifth order basis spline matrix generated for a two-dimensional grid with 10×8 points. The wave function is forced to be zero on the boundaries so that the matrix dimension is 120. Besides its sparseness, a key feature of the matrix is its bandedness. The fact that it is banded derives from the localization of the basis splines. That is, each spline only overlaps the nearest k splines. This property is also called finite support. Banded matrices offer the benefit of reduced storage requirements compared to full matrices as well as more favorable scaling of the CPU time with matrix dimension. Thus, it is important to characterize the band width and to reduce it to whatever extent possible. It turns out that for any number of dimensions $d\geq2$ the half band width H_d, the number of nonzero diagonals above the main diagonal including the main diagonal, can be determined from the recursion relation

$$H_d = N_d\,(H_{d-1}-1) + k + 1 \tag{108}$$

where N_d is the number of splines for the dth coordinate. The recursive series is started with the one-dimensional result, $H_1=k+1$. For two dimensions, Eq. (108) gives $H_2=N_2k+k+1$; and for three, $H_3=N_2N_3k+N_3k+1$. In Eq. (108) it has been assumed that the expansion coefficients labeled by $l_1, l_2, \ldots, l_d$ have been mapped into a single index i as follows:

$$i = (l_1-1)\,N_2\cdots N_d + (l_2-1)\,N_3\cdots N_d + \ldots + (l_{d-1}-1)\,N_d + l_d.$$

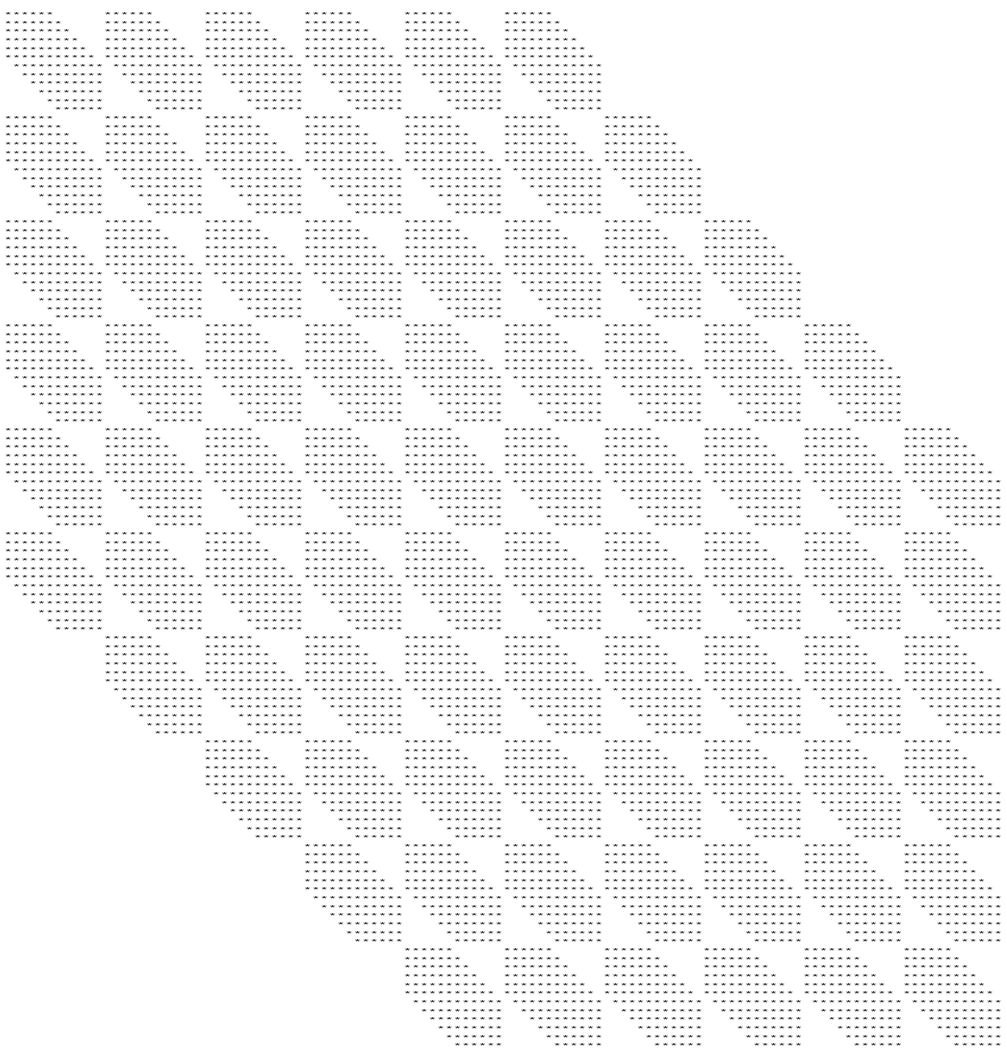

Figure 45. The structure of the matrices **H** and **S** for a two-dimensional Schrödinger equation with N_x=10 and N_y=8. The asterisks denote locations of nonzero matrix elements.

Because there is the freedom to choose which coordinate corresponds to a given index l_j, Eq. (108) can be used to minimize the half band width by choosing the optimal ordering in the mapping. After some consideration, it can be seen that the optimal ordering is the one which satisfies

$$N_1 \geq N_2 \geq N_3 \geq \cdots \geq N_{d-1} \geq N_d.$$

For instance, in the two-dimensional example shown in Fig. 45, the mapping is $i=(m-1)\,N_x+l$ so that $N_2=N_x$ in the calculation of the half band width H_2. Since $N_x=12$, the resulting half band width is $H_2=66$. Had I instead used $N_2=N_y=10$, the half band width would have been 55, and the mapping would change to $i=(l-1)\,N_y+m$.

The benefits of the sparse, banded structure of the matrices in Eq. (105) can then be gained in the numerical solution of Eq. (105) through the use of routines from `arpack` [115]. `Arpack` is a robust set of matrix eigenvalue routines that are specifically designed for large sparse systems of equations. It employs a variant of the Lanczos algorithm [116] that for some cases needs only to compute the action of the matrix on a vector. Such powerful numerical tools make the basis splines solution of a three-dimensional linear Schrödinger equation feasible in some cases.

Case Study. I discuss below the details of the basis spline solution of the anisotropic harmonic oscillator equation for $m=0$.

$$\left[-\frac{1}{2\rho}\frac{\partial}{\partial\rho}\left(\rho\frac{\partial}{\partial\rho}\right)-\frac{1}{2}\frac{\partial^2}{\partial z^2}+\frac{1}{2}\left(\rho^2+\lambda^2 z^2\right)\right]\psi(\rho,z)=E\psi(\rho,z) \tag{109}$$

In this equation, λ is the anisotropy parameter ω_z/ω_ρ. The exact solutions of this equation are well known to be

$$E_{n_\rho n_z}=2n_\rho+1+\left(n_z+\frac{1}{2}\right)\lambda.$$

The choice $\lambda=2$ yields the simple result that all of the energies are integers. Table 4 shows the CPU time on a 400 MHz Digital Equipment Corporation Alpha workstation, the percent of the matrix elements that are nonzero, and the lowest three energies as a function of $N_\rho=N_z$ (the

Table 4. The convergence of the eigenenergies for an anisotropic oscillator with ω_z=2ω_ρ using the basis spline expansion method. Convergence is tested with respect to the number of mesh points in each direction with the constraint N_ρ=N_z. The exact results are E_{00}=2, E_{10}=4, and E_{02}=6.

N_ρ	CPU time (seconds)	% nonzero	E_{00}	E_{10}	E_{02}
5	0.04	83.35	2.0071 6362 2457	4.2085 3251 0254	6.2264 0918 2362
10	0.14	46.08	2.0001 7578 9632	4.0001 3436 5722	6.0001 9470 4113
15	0.35	27.52	2.0000 0116 1596	4.0000 3793 6458	6.0001 1698 4161
20	0.96	18.07	2.0000 0003 8924	4.0000 0133 3879	6.0000 0204 8286
25	1.93	12.72	2.0000 0000 2535	4.0000 0007 8053	6.0000 0014 2948
30	4.09	9.43	2.0000 0000 0290	4.0000 0000 8118	6.0000 0001 6483
35	6.53	7.26	2.0000 0000 0049	4.0000 0000 1290	6.0000 0000 2761
40	8.52	5.76	2.0000 0000 0011	4.0000 0000 0275	6.0000 0000 0607
45	12.32	4.68	2.0000 0000 0003	4.0000 0000 0072	6.0000 0000 0163
50	17.43	3.87	2.0000 0000 0000	4.0000 0000 0022	6.0000 0000 0051
55	23.13	3.26	2.0000 0000 0000	4.0000 0000 0008	6.0000 0000 0018
60	31.29	2.78	2.0000 0000 0000	4.0000 0000 0003	6.0000 0000 0007

calculation of the lowest ten energies, however, is included in the CPU time). The boundaries of the grid are fixed at 0 and 10 in ρ and at 0 and 7.07 in z for all entries. The mesh, then, is simply made finer as N_ρ increases. Since the lower boundary in z is at zero and I have imposed the boundary condition that the derivative vanishes there, all of the states obtained are of even z-parity (forcing the wave function to be zero at z=0 yields the odd z-parity states). At the upper boundary in both coordinates, the wave function is forced to vanish; and at ρ=0, no boundary conditions are imposed. To evaluate the necessary matrix elements, a 12 point Gauss-Legendre quadrature is used in each interval. Since the splines are fifth order, twelve points are more than sufficient to obtain matrix elements accurate to within machine precision. Note that in this simple example, all matrix elements can be reduced to one-dimensional integrals. The CPU time quoted in the second column of Table 4 can thus be regarded as a best case estimate.

The matrix dimension scales quadratically with N_ρ since I have taken N_z=N_ρ. The largest matrix diagonalized in this example is 3906×3906. Notice that the CPU time scales approximately quadratically with N_ρ which means that it scales linearly with the matrix dimension. This scaling is much more favorable than the N^3 scaling of direct diagonalization. This is not a completely valid comparison, though, since the direct diagonalization yields all of the eigenvalues rather than just the lowest few. Experience has shown that the additional dependence of the CPU time on the number of eigenvalues sought can be expected to be roughly linear when using the `arpack` routines.

APPENDIX D

SOLVING THE HARTREE-FOCK EQUATION

The first and possibly most difficult technical problem in carrying out calculations for realistic zero temperature alkali gas condensates is the solution of the Hartree-Fock equation. This is especially true given the anisotropic traps typically used and the large number of atoms trapped. Including more than one component complicates the task even further. I present in this appendix two methods for solving the Hartree-Fock equations. The first is a straightforward iterative diagonalization scheme that works only moderately well. The second, imaginary time propagation, is a less obvious scheme that converges in nearly every case in which there is a solution.

D.1 Iterative diagonalization

One of the first methods that comes to mind for solving the nonlinear equation

$$\left[H_0(\mathbf{x}) + \alpha \left|\psi(\mathbf{x})\right|^2\right] \psi(\mathbf{x}) = \varepsilon \psi(\mathbf{x}) \tag{110}$$

is to make a guess at $\psi(\mathbf{x})$, substitute it into the above equation, and solve for a new $\psi(\mathbf{x})$ [61]. This process must be iterated until the above equation is satisfied to within some tolerance. Stated another way, $\psi(\mathbf{x})$ must be self-consistent. If the iteration number i is denoted as a subscript on $\psi(\mathbf{x})$ and ε, then the iterative diagonalization procedure is summarized as

$$\left[H_0(\mathbf{x}) + \alpha \left|\psi_{i-1}(\mathbf{x})\right|^2\right] \psi_i(\mathbf{x}) = \varepsilon_i \psi_i(\mathbf{x}). \tag{111}$$

Note that at every step this is a linear equation for $\psi_i(\mathbf{x})$ and can thus be solved by standard basis or local polynomial expansion methods (see App. C).

As it turns out, the wave function updating strategy in Eq. (111) fails quickly as α is increased. One such failure mode is shown in Fig. 46 for an α of 561.4. I have used the case

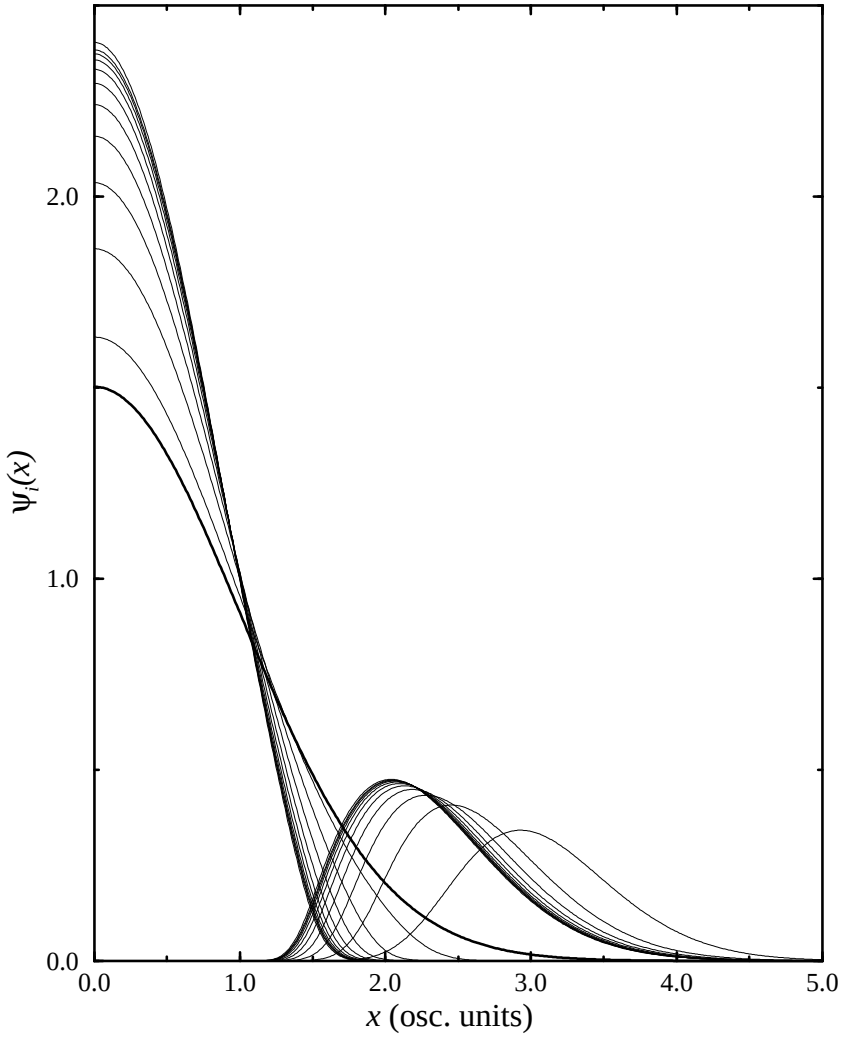

Figure 46. The wave function $\psi_i(\mathbf{x})$ for successive iterations i for α=561.4 in an isotropic trap. The thick line is the initial guess — the harmonic oscillator ground state.

of an isotropic harmonic trap and expanded the wave function on a set of B-splines (see App. C). The initial guess, shown in the figure as a thick solid line, is the solution of the harmonic oscillator equation $H_0(\mathbf{x})\psi_0(\mathbf{x})=\varepsilon_0\psi_0(\mathbf{x})$. Successive iterations alternately converge to different functions. It is easy to understand the difficulty. The mean field term resulting from the initial guess forms a large barrier in the middle of the harmonic trapping potential forcing the next solution into the well around it. The following iteration finds an effective potential with a well in the middle so that the solution is again localized near the center of the trap. The process repeats until each localized function is well converged as shown in the figure. Unfortunately, neither is a solution of Eq. (110). This type of convergence failure can be alleviated but not completely remedied by choosing a better updating strategy. Cowan [61], for instance, suggests the following scheme for the *i-th* guess:

$$\psi_i(\mathbf{x}) = (1-\gamma)\,\psi_{i-2}(\mathbf{x}) + \gamma\,\psi_{i-1}(\mathbf{x})$$

with $0.001 \leq \gamma \leq 0.5$. This iteration can stall for a few to several steps without converging further, or can fail to converge altogether for γ too large. This difficulty is overcome by making an adaptive reduction of γ as the solution is iterated. For small values of the nonlinear parameter α, I have had success using the harmonic oscillator ground state as the initial guess and beginning the iteration with larger values of γ. For large values of α, I have used the Thomas-Fermi solution [49], Eq. (12), and began with smaller values of γ.

D.2 Imaginary time propagation

I detail in this section the method of imaginary time propagation (ITP), a robust, general method of calculating the lowest state of a given symmetry for the non-relativistic Schrödinger equation. It applies equally well to the linear and to the nonlinear Schrödinger equation and adeptly handles multidimensional problems. Further, ITP works well for the coupled equations arising in the multi-component analysis, Eq. (76). It has been pointed out [49] that propagation in imaginary time is equivalent to the steepest descents method of

minimizing a function. In the present case, the function being minimized is the total energy of the system.

Since the method is most simply presented in terms of the linear Schrödinger equation, I will develop the method for the linear equation and leave consideration of the modifications necessary for the solution of the Hartree-Fock equation until the end of the section. The essential step lies in rewriting the time-dependent Schrödinger equation as a diffusion equation with the replacement $\tau = it$, or

$$-\frac{\partial}{\partial\tau}\psi(\mathbf{x},\tau) = H\psi(\mathbf{x},\tau) \tag{112}$$

where H is the Hamiltonian of the system. Propagation of this equation in imaginary time τ given some initial condition $\psi(\mathbf{x},0)$ yields a method that converges exponentially to the lowest energy eigenstate of the system which overlaps $\psi(\mathbf{x},0)$. This result is most easily illustrated by considering the general solution of Eq. (112)

$$\psi(\mathbf{x},\tau) = \sum_n a_n e^{-E_n\tau}\phi_n(\mathbf{x})$$

where E_n and $\phi_n(\mathbf{x})$ are the eigenenergies and eigenfunctions of H, respectively, and $a_n = \langle\phi_n|\,\psi(0)\rangle$. As $\tau\to\infty$, only the state with the lowest energy remains so that in this limit $\psi(\mathbf{x},\tau)\to\phi_0(\mathbf{x})$. The exponential convergence is evident from the above expression since the amplitudes of the higher states decay exponentially with τ more rapidly than the ground state amplitude decays. When implementing this procedure for a linear Schrödinger equation, it is advisable to renormalize the wave function at each step to keep the amplitudes within a reasonable numerical range. For a nonlinear Schrödinger equation, it is imperative to renormalize the wave function since otherwise at each step the effective α in Eq. (110) is changing with the normalization.

Typically, one is interested in only the ground state of the system, but the method will allow the determination of an excited state, say $\phi_m(\mathbf{x})$, as well if $a_n = 0$ for $n < m$. In practice, one first finds the ground state and then all excited states with an energy lower than the one of interest and projects them out of the initial wave function. This projection will

have to be repeated occasionally throughout the calculation due to contamination of the wave function through numerical errors such as roundoff. Alternatively, if the state of interest is the lowest of a given symmetry, then the initial state can simply be chosen to have the appropriate symmetry. Barring numerical errors that destroy the symmetry, the wave function will converge to the desired state. For instance, the symmetry preserving state above a_{12}^c in Sec. 4.6 was determined in this manner by choosing an initial state symmetric in z.

The task is thus reduced to solving for the imaginary time evolution of $\psi(\mathbf{x}, \tau)$. Numerically, the evolution is broken up into short intervals δ over which the imaginary time evolution operator $\exp(-H\delta)$

$$\psi(\mathbf{x}, \tau + \delta) = e^{-H\delta}\psi(\mathbf{x}, \tau) \tag{113}$$

can be well approximated. At this point, the deciding factor in the efficiency of the algorithm is the choice of representation for $\psi(\mathbf{x}, \tau)$. In the following sections, I discuss two different representations, both of which fall under the category of a discrete representation of the wave function. In Sec. D.2.1, I discuss the finite differences approach. In cases where a Cartesian mesh can be used and only moderate accuracy is necessary, finite differencing is acceptable. In cases where non-Cartesian meshes are more appropriate or high accuracy is needed, basis splines are the better choice. I discuss in Sec. D.2.2 the application of basis splines to solving Eq. (112), and assume all of the results of App. C. Finite differences tend to be most useful for the three-dimensional double condensate calculation, for instance, because the basis splines are prohibitively slow. The utility of both representations stems from the sparseness of the matrix representing the action of the evolution operator. Even two-dimensional problems would scarcely be feasible were the matrices not sparse.

D.2.1 Finite differences. The essence of finite differences lies in the approximation of the wave function on a lattice of points

$$\psi_{ijk} = \psi(x_i, y_j, z_k).$$

Typically, the lattice is an evenly spaced Cartesian mesh. The imaginary time evolution operator can be represented to a very good approximation by using $H = T + V$ to write the split operator form [118]

$$e^{-H\delta} = e^{-V\frac{\delta}{2}} e^{-T\delta} e^{-V\frac{\delta}{2}} + \mathcal{O}(\delta^3).$$

Since $V(\mathbf{x})$ is a local operator on the lattice, $e^{-V\frac{\delta}{2}}$ is diagonal and is easily evaluated as the matrix with $e^{-V(\mathbf{x}_i)\frac{\delta}{2}}$ along the diagonal. The exponential of the kinetic energy operator can be greatly simplified by noting that the kinetic energy operator for each coordinate, T_i, commutes with the kinetic energy operator of all of the other coordinates. Thus, in three dimensions,

$$e^{-T\delta} = e^{-(T_x+T_y+T_z)\delta} = e^{-T_x\delta} e^{-T_y\delta} e^{-T_z\delta}.$$

The action of the exponential of the three-dimensional kinetic energy operator has thus been reduced to the action of three exponentials of one-dimensional kinetic energy operators. The simplest approximation for the one-dimensional kinetic energy on the lattice is the three-point finite difference form

$$\frac{\partial^2 \psi_i}{\partial x^2} = \frac{\psi_{i-1} - 2\psi_i + \psi_{i+1}}{\Delta x^2} + \mathcal{O}(\Delta x^2).$$

The approximation implicit in this form is that the wave function is linear between lattice points. The action of a single exponential of a one-dimensional kinetic energy operator is thus represented by the exponential of a tridiagonal matrix. This can, in turn, be reduced to 2×2 matrix-vector multiplications by recognizing that [119]

$$T = \begin{pmatrix} 0 & T_{12} & 0 & 0 & \cdots \\ T_{21} & 0 & T_{23} & 0 & \cdots \\ 0 & T_{32} & 0 & T_{34} & \cdots \\ 0 & 0 & T_{43} & 0 & \ddots \\ \vdots & \vdots & \vdots & \ddots & \ddots \end{pmatrix}$$

$$= \begin{pmatrix} \begin{pmatrix} 0 & T_{12} \\ T_{21} & 0 \end{pmatrix} & \begin{matrix} 0 & 0 \\ 0 & 0 \end{matrix} & \cdots \\ \begin{matrix} 0 & 0 \\ 0 & 0 \end{matrix} & \begin{pmatrix} 0 & T_{34} \\ T_{43} & 0 \end{pmatrix} & \cdots \\ \vdots & \vdots & \ddots \end{pmatrix} + \begin{pmatrix} 0 & \begin{matrix} 0 & 0 \end{matrix} & 0 & \cdots \\ 0 & \begin{pmatrix} 0 & T_{23} \\ T_{32} & 0 \end{pmatrix} & 0 & \cdots \\ 0 & & & \\ \begin{matrix} 0 \\ 0 \end{matrix} & \begin{matrix} 0 & 0 \end{matrix} & \begin{matrix} 0 \\ 0 \end{matrix} & \cdots \\ \vdots & \vdots & \vdots & \ddots \end{pmatrix}$$

where the diagonal elements have been included with the potential energy. Labeling the two matrices on the right hand side T^A and T^B, the action of the exponential of the kinetic energy operator in one dimension can be split again

$$e^{-T\delta} = e^{-T^A \frac{\delta}{2}} e^{-T^B \delta} e^{-T^A \frac{\delta}{2}} + \mathcal{O}(\delta^3).$$

Noting that T^A and T^B are 2×2 block diagonal matrices, all that is required to compute the effect of the kinetic energy is the matrix exponentiation of 2×2 matrices. (The exponential of a 2×2 block diagonal matrix is the matrix of the exponentials of the 2×2 matrices.) For one 2×2 matrix, this can be evaluated analytically:

$$\exp \begin{pmatrix} 0 & -\lambda \\ -\lambda & 0 \end{pmatrix} = \begin{pmatrix} \cosh \lambda & -\sinh \lambda \\ -\sinh \lambda & \cosh \lambda \end{pmatrix}.$$

An equally accurate alternative to this approach is to simply use the Taylor expansion of $e^{-T\delta}$ to second order in δ. Upon performing an operation count, however, the latter method requires $12N$ floating point operations where N is the number of lattice points, while breaking the problem down to 2×2 matrix-vector products requires $9N$ floating point operations.

For a given choice of δ and Δx, this is a clear prescription for propagating an initial wave function in imaginary time. Since our lattice solution is a variational trial wave function, the variational principle ensures that the energy will be an upper bound to the true energy, and in the limits $\delta \to 0$, $\Delta x \to 0$, and $\tau \to \infty$ it should be the exact energy. None of these limits is achievable in practice, but the first two can be approximated by performing the calculation for several values of δ and Δx and extrapolating to the limit. The last limit reduces to the question

of when to halt the propagation. Two straightforward choices are as follows: stopping when the energy expectation value, $\langle\psi(\tau)|\, H\, |\psi(\tau)\rangle$, changes from τ to $\tau+\delta$ by less than some small tolerance ϵ (10^{-8} is a typical choice); and stopping when the variance of the energy expectation value, $\langle\psi(\tau)|\, (H-\langle H\rangle)^2\, |\psi(\tau)\rangle$, is zero to within some small tolerance. Both conditions are satisfied exactly by an eigenstate. I use the first condition largely because of its simplicity.

The method outlined above finds the ground state of a many dimensional Schrödinger equation in a time which is proportional to the total number of lattice points. This is the most favorable scaling one can expect to find. Additionally, the method presented here is optimal in its memory requirements since only the wave function at the current time need be stored. For two and three dimensions, it is extremely important to traverse the wave function array in an efficient manner (*i.e.* such that the array elements are retrieved sequentially from memory). Otherwise, the memory access time can overwhelm the actual computational time.

It is worth noting that the nonlinearity of the Hartree-Fock equations in the pseudopotential approximation pose no particular problems in finite differences. The mean field merely contributes to the local effective potential.

D.2.2 Basis splines. The wave function can also be represented using basis splines (see App. C). In this case, the appropriate form for the imaginary time evolution operator, Eq. (113), is the Cayley form [122]. It can be simply obtained from Eq. (113) by multiplying both sides by $\exp(H\delta/2)$ and expanding to first order in δ,

$$\left(I+\frac{\delta}{2}H\right)\psi(\mathbf{x},\tau+\delta)=\left(I-\frac{\delta}{2}H\right)\psi(\mathbf{x},\tau) \tag{114}$$

where I is the identity operator. Multiplying both sides of this equation by the inverse of the operator on the left hand side gives

$$\psi(\mathbf{x},\tau+\delta)=\frac{I-\frac{\delta}{2}H}{I+\frac{\delta}{2}H}\psi(\mathbf{x},\tau).$$

Comparing with Eq. (113) shows that the approximate evolution operator is

$$e^{-H\delta}\approx\frac{I-\frac{\delta}{2}H}{I+\frac{\delta}{2}H}.$$

This relation is not directly useful. In practice, Eq. (114) is solved directly for $\psi(\mathbf{x}, \tau+\delta)$ since efficient routines exist for the solution of systems of linear equations. Equation (114) is also known as the Crank-Nicholson method and as the implicit method.

In a basis splines (or any nonorthogonal) representation in which the wave function is

$$\psi(\mathbf{x}, \tau) = \sum_{n=0}^{N} c_n(\tau) u_n(\mathbf{x}),$$

Eq. (112) is written

$$-\frac{\partial}{\partial \tau}\mathbf{S}\mathbf{c}(\tau) = \mathbf{H}\mathbf{c}(\tau). \tag{115}$$

The matrix $\mathbf{S}$ in this expression is just the τ-independent overlap matrix defined in Eq. (107). The Hamiltonian matrix $\mathbf{H}$ is similarly defined in Eq. (106). The presence of an overlap matrix rather than the identity modifies Eq. (114) by the simple replacement of the identity operator by the overlap matrix. This can be explicitly shown by assuming a Cholesky decomposition of $\mathbf{S}$, $\mathbf{S}$=$\mathbf{L}\mathbf{L}^T$, and eliminating the overlap in Eq. (115). The system of equations to be solved, then, is

$$\left(\mathbf{S} + \frac{\delta}{2}\mathbf{H}\right)\mathbf{c}(\tau+\delta) = \left(\mathbf{S} - \frac{\delta}{2}\mathbf{H}\right)\mathbf{c}(\tau).$$

If $\mathbf{H}$ depends on $\mathbf{c}$ as in the Hartree-Fock equations, then $\mathbf{c}(\tau)$ is used to calculate $\mathbf{H}$ on both sides of this equation. For the basis splines, the coefficient matrix on the left hand side is a banded matrix, making it especially efficient to solve. In fact, in solving the Hartree-Fock equations, the time devoted to solving this linear system is only a small fraction of the overall computation time especially for two- and three-dimensional problems. The largest fraction by far is spent in numerically integrating over the nonlinear term which must be done at every time step. The cost in three-dimensions is prohibitive enough to make three-dimensional basis spline solutions of the Hartree-Fock equation impractical.

Case study. I discuss in detail the basis splines solution of the Hartree-Fock equation for a particular case: a single ^{87}Rb $|2,2\rangle$ condensate (a_{sc}=109.1 au.) with 10^5 atoms in a TOP trap. The trap frequencies are ω_z=2π 376.18081 Hz and ω_ρ=2π 133 Hz. The mesh is taken to

be evenly spaced in both ξ=ρ/β and η=z/β where β=$\sqrt{\hbar/m\omega_\rho}$. For ξ, there are 29 points between 0.0 to 14, inclusive, in increments of 0.5; for η, there are also 29 points between 0.0 to 8.4, inclusive, in increments of 0.3. I choose the boundary conditions at ξ=0 to be free although a zero derivative boundary condition would also work; at ξ=14, I force the wave function to zero. In the η direction, I choose a zero derivative boundary condition at η=0 and a zero function boundary condition at η=8.4. The resulting matrix is 992×992 with a band width of 331. For the initial condition, I simply set all coefficients not eliminated by boundary conditions equal. This wave function is shown in Fig. 47a. Within 10 steps, the relative change in the orbital energy has been reduced to 0.1. The corresponding wave function is shown in Fig. 47b. The wave functions for longer times do not differ visibly from the one shown in Fig. 47b. The detailed results at every 10 steps (δ=0.01) until the magnitude of the relative change in the orbital energy is less than 10^{-8} is shown in Table 5. Note that the orbital energy has a minimum around τ=10, but that the total energy monotonically decreases with τ in accordance with the variational principle. The total energy is minimized by the Hartree-Fock solution, not the orbital energy. Also, the total energy converged to the first eight digits much more quickly than the orbital energy. The entire calculation took about 8 Mb of memory and approximately 20 minutes on a 333 MHz Digital Equipment Corporation Alpha workstation.

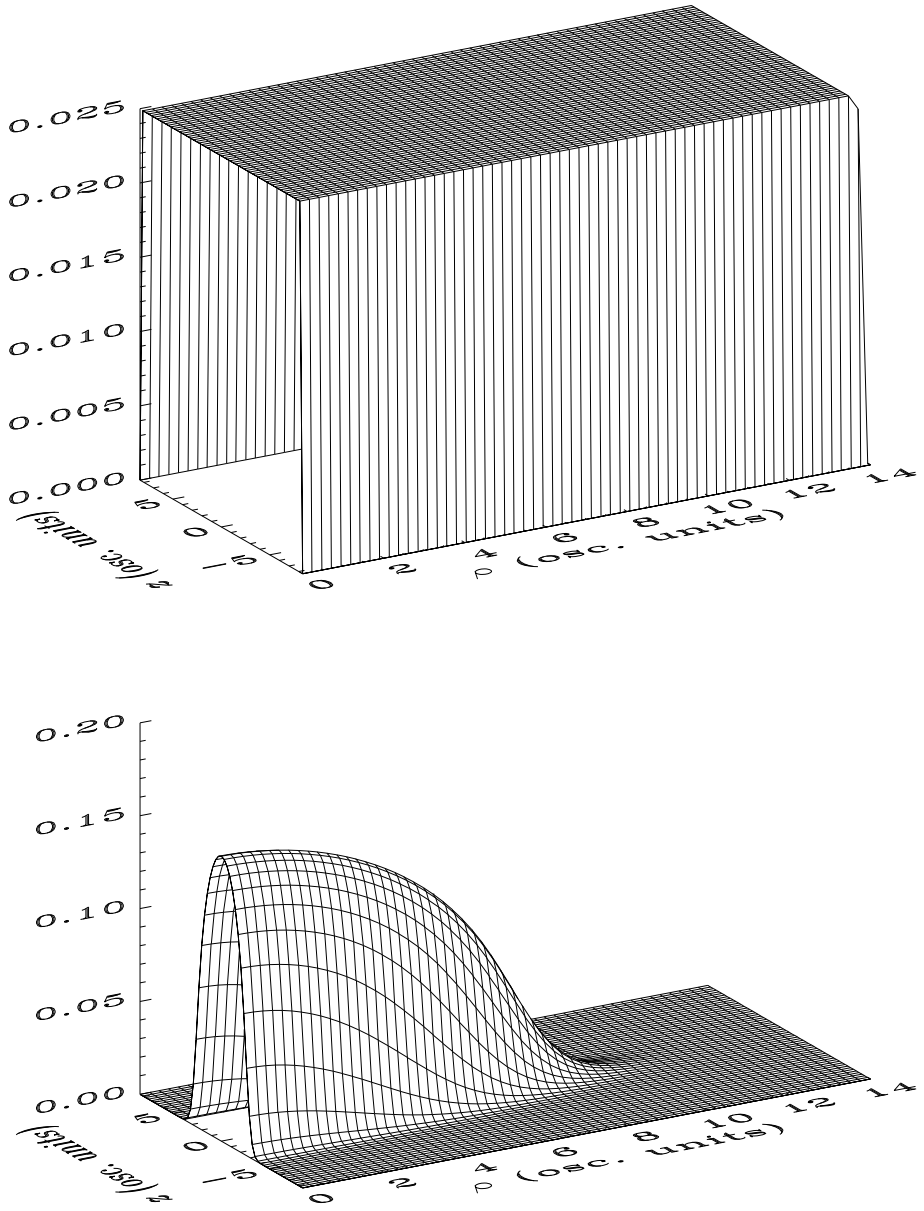

Figure 47. The ground state orbital wave function $\psi_0(\mathbf{x})$ in the ρz plane: (a) τ=0 and (b) τ=10. Note that 1 osc. unit=0.935 μm.

Table 5. The total and orbital energies as a function of τ for a typical imaginary time propagation calculation. The trap is a TOP trap with ω_ρ=2π 133 Hz, containing 10^5 ^{87}Rb atoms in the $|2,2\rangle$ hyperfine state (a_{sc}=109.1 a.u.). The last column is the relative change in the orbital energy.

τ (units of δ)	$E_0^{\rm HF}$ (osc. units)	ε_0 (osc. units)	$(\varepsilon_\tau - \varepsilon_{\tau-10})/\varepsilon_{\tau-10}$
0	14196727.2	142.348797	1.000000000
10	2151926.6	28.826073	0.797496896
20	2119253.4	29.184588	-0.012437173
30	2116105.5	29.319753	-0.004631404
40	2115527.2	29.378243	-0.001994893
50	2115384.5	29.405900	-0.000941419
60	2115342.7	29.419802	-0.000472742
70	2115329.0	29.427137	-0.000249318
80	2115324.3	29.431159	-0.000136685
90	2115322.7	29.433430	-0.000077185
100	2115322.0	29.434742	-0.000044547
110	2115321.8	29.435510	-0.000026118
120	2115321.7	29.435966	-0.000015487
130	2115321.7	29.436239	-0.000009258
140	2115321.7	29.436403	-0.000005566
150	2115321.7	29.436502	-0.000003361
160	2115321.7	29.436562	-0.000002036
170	2115321.7	29.436598	-0.000001236
180	2115321.7	29.436620	-0.000000751
190	2115321.7	29.436634	-0.000000457
200	2115321.7	29.436642	-0.000000278
210	2115321.7	29.436647	-0.000000170
220	2115321.7	29.436650	-0.000000103
230	2115321.7	29.436652	-0.000000063
240	2115321.7	29.436653	-0.000000038
250	2115321.7	29.436654	-0.000000023
260	2115321.7	29.436654	-0.000000014
270	2115321.7	29.436654	-0.000000008

APPENDIX E

RELATED PUBLICATIONS

- "Effective potentials for Bose-Einstein condensates," J.L. Bohn, B.D. Esry, and C.H. Greene, Phys. Rev. A (submitted).
- "Low-lying excitations of double Bose-Einstein condensates," B.D. Esry and C.H. Greene, Phys. Rev. A (submitted) (1997).
- "Prospects for mixed-isotope Bose-Einstein condensates in rubidium," J.P. Burke Jr., J.L. Bohn, B.D. Esry, and C.H. Greene, Phys. Rev. A (submitted) (1997).
- "Hartree-Fock theory for double condensates," B.D. Esry, C.H. Greene, J.P. Burke Jr., and J.L. Bohn, Phys. Rev. Lett. **78**, 3594 (1997).
- "Impact of the ^{87}Rb singlet scattering length on suppressing inelastic collisions," J.P. Burke Jr., J.L. Bohn, B.D. Esry, and C.H. Greene, Phys. Rev. A **55**, R2519 (1997).
- "Hartree-Fock theory for Bose-Einstein condensates and the inclusion of correlation effects," B.D. Esry, Phys. Rev. A **55**, 1147 (1997).
- "Adiabatic hyperspherical study of the helium trimer," B.D. Esry, C.D. Lin, and C.H. Greene, Phys. Rev. A **54**, 394 (1996).
- "Role of the scattering length in three-boson dynamics and Bose-Einstein condensation," B.D. Esry, C.H. Greene, Y. Zhou, and C.D. Lin, J. Phys. B **29**, L51 (1996).